ORNL-3676
UC-34 – Physics
TID-4500 (33rd ed.)

SOLID STATE DIVISION

ANNUAL PROGRESS REPORT

FOR PERIOD ENDING MAY 31, 1964

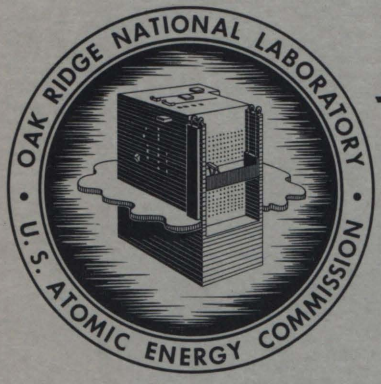

OAK RIDGE NATIONAL LABORATORY
operated by
UNION CARBIDE CORPORATION
for the
U.S. ATOMIC ENERGY COMMISSION

Printed in USA. Price $3.00. Available from the Clearinghouse for Federal Scientific and Technical Information, National Bureau of Standards, U.S. Department of Commerce, Springfield, Virginia

ORNL-3676

Contract No. W-7405-eng-26

SOLID STATE DIVISION

ANNUAL PROGRESS REPORT

For Period Ending May 31, 1964

D. S. Billington, Director
J. H. Crawford, Jr., Associate Director
M. K. Wilkinson, Associate Director

OCTOBER 1964

OAK RIDGE NATIONAL LABORATORY
Oak Ridge, Tennessee
operated by
UNION CARBIDE CORPORATION
for the
U. S. ATOMIC ENERGY COMMISSION

Table of Contents and Summary

Note: In the key-word entries under the titles, E = experimental, T = theoretical, E/T = experiment supported by theory.

PART I. THEORY

1. STUDIES OF THE MOVEMENT OF ENERGETIC ATOMS IN AND FROM SOLIDS

2. CALCULATIONS OF PROPERTIES OF COLOR CENTERS IN IONIC CRYSTALS

3. MOLECULAR THEORY

4. THEORY OF METALS

5. RADIATION DAMAGE THEORY

A computer program has been written for determining the defect concentration during irradiation for the case in which the defects may annihilate by pair recombination or by diffusion to fixed sinks. Calculations made with this program have been used as a basis for analyzing the effects of radiation-enhanced diffusion in Cu-Al alloys.

The problem considered is that of the annihilation of mechanically unstable vacancy-interstitial pairs formed in a displacement cascade. The amount of such self-anneal is calculated using a time-dependent absorption description in terms of multiparticle density functions. The importance of this general method lies in the possibility of including spatial correlations of pairs of defects.

Theoretical studies of isochronal or "pulse" annealing have been stimulated by the excellent experimental work of R. R. Coltman, C. E. Klabunde, and co-workers. The ultimate goal is the explanation of annealing peaks observed during warm-up after low-temperature recoil damage of cadmium in terms of activation energies, orders of kinetics, and basic defect processes.

The Mott scattering series has been used to numerically calculate atomic displacement cross sections by fast electrons for 18 elements selected to span the atomic table. Several atomic displacement thresholds were used, together with electron energies ranging up to 10 Mev.

Some analytical aspects of a set of equations pertinent to radiation-enhanced diffusion are discussed.

PART II. CRYSTAL PHYSICS

6. X-RAY DIFFRACTION

7. ELECTRON MICROSCOPY

8. SPIN RESONANCE

9. SUPERCONDUCTIVITY AND LOW-TEMPERATURE PHYSICS

10. NEUTRON SCATTERING

The construction of the Triple-Axis Neutron Spectrometer Facility for the HN-4 beam hole at the ORR has been completed, and it is currently being assembled for operation. In addition to conventional neutron-scattering experiments of interest to solid state physics, the HN-4 facility was designed for inelastic neutron-scattering studies at various temperatures and applied magnetic fields.

PART III. METALS

11. INVESTIGATIONS OF METAL SURFACES

F. W. Young, Jr., L. D. Hulett, L. H. Jenkins, U. Bertocci, and J. R. Savage

Over a period of months, no differences in electrochemical equilibrium potentials could be measured, nor were preferential orientations developed on any surface. It was concluded that no orientation was thermodynamically more stable than any other.

Pits and facets developed on surfaces undergoing very slow reaction were examined, and some postulates concerning the nucleation and motion of steps on variously oriented surfaces were made.

Initial high slopes in potential vs current curves in systems also corroding at a very low rate lead to false conclusions concerning equilibrium potentials between orientations.

A detailed description of ledges and pits formed on the surface undergoing dissolution and their motion is presented. A unified explanation involving kinematic mechanistics is advanced.

Potentials at zero current density for different orientations differed mainly because of kinetic parameters. Faceting due to either chemical or electrochemical processes was not found to be different. Preliminary differential capacitance measurements are discussed.

Differences and similarities to chloride solutions are discussed.

Abstract of paper to be submitted for publication in the *Journal of Applied Physics*.

Abstract of paper submitted for publication in the *Journal of Applied Physics* (June 1964).

12. LOW-TEMPERATURE IRRADIATION STUDIES

R. R. Coltman, J. K. Redman, C. E. Klabunde, and G. F. Fielder

The new low-temperature irradiation facility located at the BSR is completed and is operating routinely. The development of modifications to improve the reliability and capability of the system is under way.

By use of a new temperature-measuring technique, complete detailed isochronal recovery of (n,γ) damage in Cd is studied as a function of initial damage concentration.

13. ELASTICITY AND ANELASTICITY STUDIES

The Bordoni internal friction relaxation peak in deformed copper was found to be reduced considerably in height by fast-neutron irradiation, presumably through pinning of dislocations by radiation defects. Annealing at 400°C, which is known to eliminate defect pinning points, restored the peak to its original height. It is concluded that point defects play no role in the relaxation process.

Abstract of paper submitted for publication in the *Journal of Applied Physics*.

An anelasticity apparatus has been developed for which the sample can be a copper crystal oriented for etch pit observations of dislocation distribution. The sample is vibrated in flexure and its size is such that it can be made with existing equipment for producing crystals of very low dislocation density.

In attempts to obtain third-order elastic constants of crystals by measuring distortion generated in high-amplitude sound waves, difficulties may occur if the attenuation is too high. It is shown that in the case of pure copper, where the dislocation attenuation is appreciable, the anticipated improvement in observation of the second harmonic can be obtained by irradiating so as to pin the dislocations.

A highly sensitive, broad-band capacitance microphone detector has been built so as to make possible absolute measurements of displacement amplitude and harmonic distortion in ultrasonic waves in crystals.

14. Ar^+ ION BOMBARDMENT OF METAL SURFACES

A. L. Southern

Abstract of paper to be presented at and published in the Twelfth Annual Conference on Mass Spectrometry and Allied Topics, Montreal, Canada, June 7–12, 1964.

Two new types of atom-ejection-pattern collectors were used. Ejection patterns and yield measurements were made for the three low-index planes of gold, and comparisons were made with earlier results on Cu and Al. Recent studies have been interpreted in terms of focusing collision chains in Cd, Zn, and Mg. The sputtering yield is reported for the (0001) and $(10\bar{1}0)$ planes of Zn.

PART IV. NONMETALS

15. INSULATING CRYSTALS

A study of *F*-center and V_k-center production by ionizing radiation in KCl is in progress. Results show that lead impurity causes the rate of production and the limiting V_k-center concentration to be increased. Lead also increases the *F* colorability. Heating of lead-doped samples prior to irradiation also affects the V_k- and *F*-center production. However, the way in which these changes in coloring properties take place is not yet clear.

The shape of the *K*-band in KCl has been examined in detail at low temperatures. There is no evidence of a doublet structure, and the *K*-band is distinctly non-Gaussian.

Abstract of paper submitted for publication in the *Physical Review*.

After long irradiation the *F*-center concentration in KCl at room temperature no longer continues to grow. A study of this limiting value has shown that it is a function of temperature and radiation intensity. Moreover, limited results suggest that the rate of approach to steady state is also dependent upon temperature.

16. SEMICONDUCTOR STUDIES

The radiation response of germanium and silicon to fast neutrons over a wide range of energy has been determined for both monoenergetic neutrons and neutrons of known spectral distribution. Germanium is much more sensitive to the effect of disordered regions than is silicon, as is expected from differences in band structure of these two materials.

The studies of the annealing properties of ^{60}Co gamma-irradiated germanium have been continued, using a broader range of impurity concentrations and two different impurity types. The isochronal anneals show two annealing stages: a low-temperature stage (stage A) between 289 and 380°K and a high-temperature stage (stage B) between 390 and 450°K.

Abstract of paper to be published in August 1964 issue of the *Physical Review.*

CdS and CdTe were irradiated with ^{60}Co gamma rays, ^{137}Cs gamma rays, and thermal neutrons. Observed and theoretical damage rates are compared.

PART V. RADIATION METALLURGY

17. RADIATION METALLURGY

The relative kinetics of the resistivity change of first and second runs for Cu–15 at. % Al were analyzed. The kinetics of the resistivity change for an interrupted irradiation were also treated. The results suggest that interstitials, rather than vacancies, are responsible for enhancement of diffusion in this alloy.

The effect of prior cold working to 0 to 54% reduction in area on the rate of short-range ordering during irradiation at 100°C was determined for Cu–15 at. % Al. The decrease in ordering rate with increasing amounts of cold work is interpreted in terms of the introduction of sinks for radiation-produced point defects.

21. PURE MATERIALS PROGRAM

Two essentially nondestructive methods are discussed for obtaining estimates of the amount of Pb in "pure" KCl single crystals down to concentrations below 1 Pb atom per 10^9 K sites. These methods may be used to replace the expensive and time-consuming atomic absorption spectroscopy technique.

PUBLICATIONS, PAPERS, AND SEMINARS

Part I. Theory

D. K. Holmes

1. Studies of the Movement of Energetic Atoms in and from Solids

CHANNELING AND THE DISPLACEMENT CASCADE

(particle radiation damage in crystals; atomic scattering; T)

O. S. Oen M. T. Robinson

In a recent paper we described a modified Kinchin and Pease cascade model to show how channeling of energetic atoms could substantially reduce the expected number of displaced atoms in a cascade. In that paper it was assumed that the atoms emerging from a binary collision would be equally likely to be channeled. Further, it was assumed that channeled atoms subsequently dissipated all their energy in subthreshold collisions. The above formalism has been extended to allow the moving atom and the struck lattice atom to have unequal channeling probabilities following a collision. This should be more realistic, since it is expected to be more difficult for an atom to become channeled starting from a lattice position than starting from an arbitrary position which, in general, is closer to a channeling axis. This has been borne out by our computer range calculations. In addition, the present formalism provides for the use of atomic scattering functions other than that of the hard-core approximation.

If $P_1(E)$ and $P_2(E)$ are the channeling probabilities of lattice atom and striking atom, respectively, the average number of displacements is given by the following pair of integral equations:

$$\nu_1(E) = P_1(E) + [1 - P_1(E)] \left[\int_{E_d}^{E} \nu_1(T)\, K(E, T)\, dT + \int_{0}^{E-E_d} \nu_2(E - T)\, K(E, T)\, dT \right] \tag{1}$$

$$\nu_2(E) = P_2(E) + [1 - P_2(E)] \left[\int_{E_d}^{E} \nu_1(T)\, K(E, T)\, dT + \int_{0}^{E-E_d} \nu_2(E - T)\, K(E, T)\, dT \right]$$

for $E \geq 2E_d$; $\nu_1(E) = \nu_2(E) = 1$ for $E < 2E_d$. Here E_d is the displacement energy, $\nu_1(E)$ is the average number of displacements produced by a primary originating from a lattice site with an energy E, and $\nu_2(E)$ is the analogous quantity for a primary beginning at a nonlattice position. The quantity $K(E, T)$ is the probability that a primary of energy E will transfer an energy T to the struck atom. For hard-core scattering $K(E, T)$ is equal to $1/E$. Solutions of the above integral equations have been found for several specific cases. The simplest case occurs for hard-core scattering and equal channeling probabilities (i.e., $P_1 = P_2 =$ constant). For that case Eqs. (1) reduce to a

single integral equation; the solution has been discussed in our previous paper.[1] The next simplest case occurs for hard-core scattering but with P_1 and P_2 taken as unequal constants (in energy). For this case

$$\nu_1(E) = \frac{1}{1 - P_1 - P_2} \times \left[(1 - P_2) \left(\frac{E}{2E_d} \right)^{1-P_1-P_2} - P_1 \right] . \quad (2)$$

The expression for $\nu_2(E)$ is obtained from Eq. (2) simply by the interchange of P_1 and P_2. It is seen that the above expression is very similar in form to that found previously and reduces to it for the special case of $P_1 = P_2$. General scattering functions represented by a series of Legendre polynomials have been studied to see how they affect the average number of displacements when channeling is included. It is found that for equal channeling probabilities the inclusion of only the odd polynomials in any arbitrary manner gives results which are identical to hard-core scattering. Since a number of the features of forward scattering can be represented using only the odd polynomials, this result indicates that the average number of displacements is relatively insensitive to the scattering function unless a highly peaked scattering law as used by Sigmund[2] is assumed.

The role of channeling in displacement cascades has not been experimentally established at present; however, as given in Eq. (2), $\nu(E)$ has the correct energy dependence to account for at least part of the difference between theory and experiment with respect to number of displacements. The reduction in the number of displacements is critically dependent upon the channeling probability, and the experimental value of this parameter is not known. Our computer calculations suggest that it is smaller than that needed to remove the entire discrepancy. It would be very useful to try to determine experimentally the channeling probability and also to test the assumption that channeled atoms produce few or no displacements.

[1] O. S. Oen and M. T. Robinson, *Appl. Phys. Letters* 2, 83 (1963).

[2] P. Sigmund, *Phys. Letters* 6, 251 (1963).

THEORY OF THE SPUTTERING EJECTION PATTERN[3]

(particle radiation damage in crystals; atomic scattering; T)

M. T. Robinson

The angular distribution of the material ejected from a monocrystal during ion bombardment, when recorded on a suitable collector, consists of a series of spots and streaks, together with a background which, although continuous, displays symmetry related to that of the crystal. As a guide to the interpretation of these ejection patterns, studies have been made of a much simplified numerical model, employing Monte Carlo methods on a CDC 1604-A computer. The solid is regarded as a crystalline array of impenetrable spheres, with a particular crystallographic surface exposed. An isotopic source of primary atoms, located at a selected lattice site, generates cascades of displaced atoms, some of which are ejected from the crystal. Angular distributions of the ejected atoms have been computed for a variety of different surfaces of fcc and hcp crystals. The effects of the depth and initial energy of the source and of the sizes of the atomic spheres have been studied.

In this model, fcc crystals show Silsbee focusing along $\langle 110 \rangle$ rows and assisted focusing along $\langle 100 \rangle$ and $\langle 111 \rangle$ rows. Atoms ejected by $\langle 100 \rangle$ sequences are deposited close to the $\langle 100 \rangle$ poles of the pattern only for crystal surfaces near {100}. Otherwise, the incompleteness of the final ring of assisting atoms causes these sequences to be ejected closer to the surface normal than expected. Hexagonal close-packed crystals show the expected Silsbee focusing along $\langle 11\bar{2}0 \rangle$ rows, but evidence has also been obtained for a mixed focusing process along rows approximately parallel to $\langle 10\bar{1}1 \rangle$, which appears to be responsible for the experimental patterns from $\langle 0001 \rangle$ crystals of Zn and Cd. Additionally, the model shows very sharp spots approximating to $\langle 13\bar{4}5 \rangle$, associated

[3] Abstract of a paper to be presented at Symposium on Atomic Collision Cascades, AERE, Harwell, England, July 13–17, 1964.

not with a focusing mechanism but with a minimum-energy-loss principle.

COMPUTER STUDIES OF THE SLOWING DOWN OF ENERGETIC ATOMS IN CRYSTALS[4]

(particle radiation damage; 1–10 kev Cu in fcc, bcc, and diamond-structure crystals; atomic scattering; T)

M. T. Robinson O. S. Oen

The slowing down of 1- to 10-kev copper atoms in fcc, bcc, and diamond-structure crystals has been investigated by high-speed digital computer techniques, using exponentially screened Coulomb and Born-Mayer potentials to describe the interatomic repulsion. The ranges of these atoms prove to be strongly dependent on their initial directions of motion, the order of ranges being

fcc [011] > [001] > [111] ≈ isotropic,

bcc [111] > [001] > [011] > isotropic,

diamond [011] > [001] ≈ [111] > isotropic.

This orientation dependence of the range, which has also been observed experimentally, is a consequence of the tendency of the lattice to focus moving particles into channels bordered by relatively closely packed atomic rows. Inclusion of zero-point vibrations reduces the degree of channeling, but does not modify the order of ranges for fcc. The experimental evidence for channeling and some of its implications for radiation damage theory are discussed.

MONTE CARLO RANGE CALCULATIONS FOR A THOMAS-FERMI POTENTIAL[5]

(particle radiation damage in solids; atomic scattering; 1–100 kev; T)

O. S. Oen M. T. Robinson

Our earlier Monte Carlo calculations of the ranges of atoms having energies from 1 to 100 kev, slowing down in a random solid through binary elastic collisions, have been extended by using a Thomas-Fermi potential to represent the interaction between the moving atom and a lattice atom. The screening radius of the potential is that derived by Firsov. The calculations have been made for a wide variety of target-to-projectile mass ratios. Except for the highest energies, the calculated ranges are considerably shorter than those found previously using the exponentially screened Coulomb potential. Most of the experimental range data lie between the range curves calculated for these two potentials, although the Thomas-Fermi potential gives somewhat better overall agreement. The shapes of the calculated range distributions give close agreement with those found by experiment in amorphous solids. Average ranges calculated by integrating the reciprocal of the stopping power agree fairly well with these Monte Carlo calculations, especially when the mass of the slowing-down atom is large compared with that of a lattice atom.

TRUNCATED MATCHING POTENTIALS IN THE CLASSICAL THEORY OF ELASTIC ATOMIC SCATTERING[6]

(particle radiation damage; atomic scattering; T)

Christian Lehmann[7] M. T. Robinson

Atomic collisions in the radiation damage of solids can be described by repulsive potentials for which the scattering integrals cannot generally be evaluated in closed form. However, the evaluation becomes possible when the actual interatomic potential is replaced by certain truncated power potentials which match the actual potential in value and in slope at the minimum distance. The usefulness and accuracy of such matching potentials are discussed, and numerical examples are given for the scattering angle, the "time integral," and the energy transfer in the cases of an exponential potential and of an exponentially screened Coulomb potential. The agreement with the exact numerical solutions is surprisingly good.

---

[4]Abstract of published paper: *Phys. Rev.* **132**, 2385 (1963).

[5]Abstract of paper to be published in the August 1964 issue of the *Journal of Applied Physics*.

[6]Abstract of published paper: *Phys. Rev.* **134**, A37 (1964).

[7]Present address: KFA-Werkstoffinstitut, Jülich, Germany.

2. Calculations of Properties of Color Centers in Ionic Crystals

THE *F* CENTER

(wave functions of electronic states; T)

R. F. Wood H. W. Joy[1]

The work on the excited states of the *F* center using the linear combination of atomic orbitals (LCAO) method described in the previous report has been extended and, for the time being, concluded. The results have been reported in *Physical Review Letters.*[2] The most important conclusion reached was that the *K* band is due to transitions which are forbidden in a rigid, undistorted lattice. It was suggested that interactions of the *F*-center electron with the phonon field lift this forbiddenness.

Calculations are now being carried out on the excited states using the vacancy-centered method in the point-ion approximation. In the vacancy-centered method the radial part of the *F*-center wave function is expressed as a sum of terms of the form $r^n e^{-\beta_n r}$, where *n* is an integer and *r* is the distance of the electron from the center of the vacancy. This is in contrast to the LCAO method, in which the wave function is expressed as a linear combination of atomic orbitals centered on the neighboring ions. In the point-ion approximation, the electronic structure of all ions is neglected, and the ions are represented by point charges. Preliminary results indicate qualitative agreement with the LCAO calculations.

A paper, *On the Theory of the Absorption and Emission of the F Center in Alkali Halide Crystals,*[3] has been accepted for publication in the *Physical Review.* The abstract follows:

"The absorption and emission processes of the *F* center and their relationship to each other are treated using a model which contains many of the features of an exact treatment. The calculations are based on a formulation in which the total energy of the crystal in the ground and excited states is expressed as a function of the variational parameters in the *F*-center wave functions and of the displacements of the neighboring ions. The *F* electron is treated quantum mechanically, but classical ionic crystal theory is used for all other terms in the total energy. A modified method of steepest descents is used to minimize the total energy. The electronic structure of the outer shells of the first nearest neighbor ions is taken into account in detail in the expression for the energy of the *F*-center electron. Simple, one-parameter, vacancy-centered wave functions are used to describe the *F* electron. A large Stokes shift is obtained in all crystals. The distortions are small in the ground state, but, in the relaxed excited state, they are of the order of 10 percent of the nearest neighbor distance and have a pronounced asymmetry."

THE *M* CENTER

(color centers; alkali halides; wave functions of electronic states; T)

Axel Meyer R. F. Wood

Some of the work on the *M* center was described in the previous report. A paper, *Electronic Structure of the M Center in LiCl and LiF,*[4] which covers the *M*-center work, has been published, and the abstract follows:

[1] Metals and Ceramics Division.

[2] R. F. Wood, *Phys. Rev. Letters* 11, 202 (1963).

[3] Paper submitted to the *Physical Review.*

[4] Axel Meyer and R. F. Wood, *Phys. Rev.* 133, A1436 (1964).

"Experimental work of the past few years has fairly conclusively established that the *M* center in alkali halides consists of two *F* centers bound together at neighboring halide sites. Using this model, the wave functions and energy levels of the *M* center in LiCl and LiF are calculated in the Heitler-London approximation. The *F* electron wave functions used in the calculations are of the vacancy-centered type. The finite extension of the neighboring alkali ions is treated, but all other ions are considered to be point charges. The results of the calculations show that there is a transition energy which corresponds closely to the observed M_1 band. In addition, there are numerous possibilities for other transitions, all giving energies which cluster in the vicinity of the main *F*-band energy. The results for the M_1 band follow the empirical Ivey relationship quite well."

At the time the calculations described in the above abstract were carried out, there was little interest in the triplet states of the *M* center. Recently, however, the spin resonance work of Seidel[5] and the temporary bleaching results of Schneider and Caspari[6] have focused attention on the triplet states. We have investigated these states using the results of our singlet calculations, with appropriate modifications. The results indicate that the singlet and triplet ground levels lie very close together and that the triplet state is much less stable than the singlet state. A paper on the triplet levels has been accepted for publication in *Solid State Communications*.

THE MOLLWO-IVEY RELATIONSHIP

(color centers; alkali halides; absorption spectrum vs interionic distance; T)

R. F. Wood

Many color centers in alkali halides obey the empirical Mollwo-Ivey relationship, which is of the form $\nu R^n = K$, where ν is the frequency of the absorbed light, R is the interionic distance, and n and K are adjustable parameters. In the course of carrying out some of the calculations described above, it was observed that the interionic distance seemed to be serving as a scale parameter when going from one crystal to another. Starting with this observation, it has been shown that the transition energies of both the *F* and *M* centers can be expressed as a series in inverse powers of R, that is,

$$E_T = C_1 R^{-1} + C_2 R^{-2} + C_3 R^{-3} \ldots .$$

Using the data for LiCl to calculate the coefficients, an expression has been obtained for the *F* and *M* centers which gives quite close agreement with experiment. A paper on these results has been prepared for publication.

---

[5]H. Seidel, *Phys. Letters* **7**, 27 (1963).

[6]I. Schneider and M. E. Caspari, *Phys. Rev.* **133**, A1193 (1964).

3. Molecular Theory

QUANTUM MECHANICAL STUDIES OF BIOLOGICAL MOLECULES

(photosynthesis; E)

R. F. Wood W. Bertsch[1] M. Kamrin[1]

A program has been started to apply simple quantum mechanical calculations to certain molecules of interest in photosynthesis. These molecules act as poisons to the photosynthetic process, and if their mode of action can be understood, some insight into photosynthesis itself may be gained. The type of calculation used is semiempirical and, at best, can only be used to obtain correlations among groups of molecules. A rigorous quantum mechanical calculation of the electronic structure of even the simplest molecules of biological interest is still a long way off. Nevertheless, the calculations of the type we are doing have proved to be useful in other areas of biology.[2] Preliminary results indicate a very definite and unexpected correlation with the charge density on the No. 2 position in the carbon ring of the molecules.

---

[1]Biology Division.

[2]B. Pullman and A. Pullman, *Quantum Biochemistry*, Interscience, New York, 1963.

4. Theory of Metals

THE PSEUDOPOTENTIAL IN METALLIC LITHIUM

(scattering of conduction electrons by ionic cores; T)

Axel Meyer W. H. Young

Fundamental to the study of the properties of metals in any phase of matter are the details of the scattering of conduction electrons by ionic cores. The electrical transport properties of both pure and imperfect metals are quite clearly affected, but many others are also. Thus, a collection of scattering centers will change the Fermi surface and density of states of the free-electron gas, thereby influencing such properties as the specific heat and the magnetic susceptibility. In addition, in some cases at least, ionic coupling takes place almost entirely indirectly via the valence electrons, thus determining such characteristics as force constants, phonon spectra, energies of formation, and interaction between defects.

The basic problem of the interaction of the conduction electrons with the ions can be broken down into two parts. First, beginning with the work of Phillips and Kleinman[1] and Antončík,[2] it has become clear that in any problem in which electrons scatter from ions, the real situation of an electron moving in a deep Hartree field and satisfying core orthogonality requirements can be replaced by that of a particle in a rather modest (operator) pseudopotential but without the above Pauli conditions. Thus we see that the exclusion principle has been simulated by a repulsive (operator) potential. The second part of the problem is specific to metals and concerns the screening of the bare pseudopotential referred to above. So far, linear screening[3] has been used exclusively at this point in the rather small amount of quantitative theoretical work published on metals.

Our present work is directed toward calculating and then applying the pseudopotential for lithium as a function of the density of the material. We have used the Austin[4] bare pseudopotential and have screened, using Harrison's techniques,[3] to obtain a final l-dependent potential

$$U = \begin{cases} U_H + U_S + U_R & (l = 0) \\ U_H + U_S & (l \neq 0) \end{cases} \qquad (1)$$

for lithium at its melting point. (The Hartree approximation has been used throughout; we intend next to incorporate core-valence exchange.) In Eq. (1), U_S is the screening potential associated with the Hartree field U_H. The screened field thus obtained is the same for all $l \neq 0$ and is shown in Fig. 4.1. On the other hand, U_R is an operator arising from the presence of the two 1s electrons. Its effect on any s wave, ϕ, is defined by[4]

$$U_R\phi = -\left\langle \Psi \mid U_H \mid \phi \right\rangle \Psi \ , \qquad (2)$$

where we have taken Ψ to be the well-known[5] Slater 1s function for lithium. Since U_H is negative, we see the repulsive nature of U_R.

We are in the process of solving the Schrödinger equations defined by Eq. (1) for electrons at the Fermi surface, chiefly, at the moment, in order to find the physically important phase shifts. If, now, ϕ denotes the final self-consistent s wave

[1] J. C. Phillips and L. Kleinman, *Phys. Rev.* **116**, 287 (1959).

[2] E. Antončík, *J. Phys. Chem. Solids* **10**, 314 (1959).

[3] W. A. Harrison, *Phys. Rev.* **129**, 2503, 2512 (1962).

[4] B. J. Austin, V. Heine, and L. J. Sham, *Phys. Rev.* **127**, 276 (1962).

[5] N. F. Mott and I. N. Sneddon, *Wave Mechanics and Its Applications*, p. 144, Clarendon, Oxford, 1948.

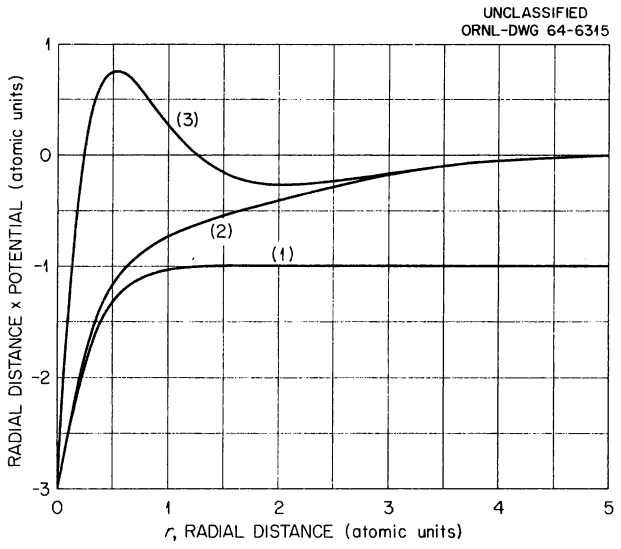

Fig. 4.1. Pseudopotential for Metallic Lithium at Its Melting Point. (1) rU_H, where U_H is the Hartree field of the bare ion; (2) $r(U_H + U_S)$, where U_S is the field of the conduction electrons screening the ion; and (3) $r(U_H + U_S + \phi^{-1} U_R \phi)$, with $\phi = 1$. The second factor is the estimate of the scattering potential for s electrons at the Fermi surface indicated in the text [see Eq. (3) and subsequent remarks].

thus obtained, we may write the total potential (for this class of electrons only) in the spatial form

$$U_H + U_S + \phi^{-1} U_R \phi \ , \qquad (3)$$

which can, therefore, be plotted graphically. At the time of writing, ϕ has not been found; but it can be estimated crudely, as Cohen and Heine[6] have pointed out, but putting $\phi = 1$ in (3). The reason for this is that the net pseudopotential is expected to be, and a posteriori is found to be, small in an average sort of way. Thus we might expect to roughly represent ϕ over the small region of the core [outside which, by Eq. (2), its behavior is unimportant] by the corresponding s wave for a zero potential. This estimate of (3) is shown in Fig. 4.1.

These results may be compared with the qualitative anticipations in the review of Sham and Ziman[7] (see their Fig. 4), where further applications for pseudopotentials are discussed. A more complete description of this work will be given upon completion of the calculations now in progress.

[6]M. H. Cohen and V. Heine, *Phys. Rev.* **122**, 1821 (1961).

[7]L. J. Sham and J. M. Ziman, *Solid State Phys.* **15**, 221 (1963).

ON THE ELECTRICAL RESISTIVITY OF ALKALI VAPOURS AT HIGH DENSITIES[8]

(MHD generator fluid; T)

W. H. Young

Highly compressed alkali vapours are being considered as a working fluid in MHD generators. Some estimates have therefore been made of the expected resistivities at the relevant temperatures of a few thousand degrees.

Mott has reasoned that the transition to the metallic phase should be quite sharp and has estimated this critical density for H. More phenomenologically, Miller has examined the existing data for Hg and found the onset of the high-conductivity phase to correspond to that r_s given by the free atom radius defined to include all but 0.1 electron. Moreover, the latter criterion gives Mott's result for H. In this way the critical r_s values for Li, Na, K, Rb, and Cs are found to be 5.35, 6.5, 8.7, 9, and 10 a_0, respectively, where a_0 is the Bohr radius.

In the free-electron region the Ziman liquid-metal theory applies. The electron-ion pseudopotential is simulated by a square well of depth $\frac{2}{3}E_F$ and range r_s (this effectively limits us to Na), while the ion-ion potential is taken to be that of hard spheres, the long-range tails which are significant at lower temperatures being now unimportant. In this way, the resistivity of Na is estimated to be

$$\rho = 31(r_s/a_0)\, C(\sigma/r_s)\ \mu\Omega\text{cm} \ ,$$

where σ, estimated to be 4.5 a_0, is the diameter of the ion, and C is an ion correlation factor taking values between 1 and 0 as its argument varies between gas and solid limits. In the physically important interval (0.9, 1.4) it can be well represented by

$$C(\sigma/r_s) = 1.6 - 1.1(\sigma/r_s) \ .$$

[8]Abstract of published paper: *Phys. Letters* **8**, 253 (1964).

THEORY OF COERCIVE FORCE FOR RANDOMLY DISTRIBUTED LATTICE DEFECTS AND PRECIPITATIONS[9]

(ferromagnetic materials; T)

H.-D. Dietze

In this paper a theory of the coercive force of ferromagnetic materials, caused by the motion of domain walls, is developed. The obstacles for the motion of a wall are assumed to have a small range of the force as compared with the mean distances between obstacles and to have interaction potentials which are additive. It is shown that the curvatures of the walls are very important and that the displacement resulting from this curvature is mostly not small compared with the distances of obstacles. For a random distribution of obstacles a formula for the coercive force is derived.

[9]Abstract of published paper: *Phys. Kondens. Materie* 2, 117 (1964).

THEORY OF INELASTIC NEUTRON SCATTERING OF METALLIC ELECTRONS IN ONE-ELECTRON APPROXIMATION[10]

(Fermi surface; electron mass tensor; T)

H.-D. Dietze

The cross section is studied for the inelastic magnetic scattering of epithermal neutrons by electrons in a metal where the states for the electrons are described by band theory. If the ratio between the wave number of the electrons and the wave number of the incoming neutrons is small compared with unity but not smaller than the mass ratio between electron and neutron, it is possible to calculate the cross section in the vicinity of certain scattering angles more closely. By such experiments one could obtain some information about the diameter of the Fermi surface and the mass tensor of the electrons.

[10]Abstract of a paper submitted for publication in *Physik der Kondensierten Materie*.

5. Radiation Damage Theory

NUMERICAL CALCULATION IN THE THEORY OF RADIATION-ENHANCED DIFFUSION

J. H. Barrett E. J. Lee

Various workers[1-3] have developed approximate analytical expressions describing the radiation enhancement of diffusion. They have assumed that the irradiation-produced defects are subject to annihilation during the irradiation by diffusion to fixed sinks and by interstitial-vacancy pair recombination. These analytical solutions are very useful, but there are limits to the range of their validity. In order to solve this problem for any conditions of irradiation, a computer program for numerical integration of the differential equations involved was written. The appropriate differential equations are

$$\frac{dv}{dt} = K - \beta\nu_v(v - v_0) - \gamma\nu_i vi \,, \qquad (1)$$

$$\frac{di}{dt} = K - \beta\nu_i i - \gamma\nu_i vi \,, \qquad (2)$$

where v and i are the vacancy and interstitial concentrations per lattice site, v_0 is the thermal equilibrium vacancy concentration per lattice site, K is the defect production rate per lattice site, $\beta = \alpha\lambda^2$, α is approximately the dislocation density, λ is the jump distance of a defect, the ν's [$= \nu_0 \exp(-M/kT)$] are the jump frequencies of the defects, and γ is the reduced cross section of vacancies for interstitial capture. If r_0 is the interstitial-vacancy distance within which recombination is a certainty and a is the lattice constant, γ is given by $8\pi r_0/a$. This form is based on diffusion into a spherical sink of very small size.[4] In previous work[1-3] γ has been taken as unity. Use of the present form instead has a significant effect on the results of the calculations.

It is generally accepted that interstitials move more freely than do vacancies. On this basis it is to be expected that the interstitial concentration will rise to a quasi-steady state comparatively quickly. This will be followed by a slower approach of both concentrations to a final steady state, the time scale of this slower process being determined by the more slowly moving vacancies. Experience gained from the behavior of the analytical solutions was used in choosing the interval size for the computer calculations. To observe the initial rapid rise of i, the time interval chosen was

$$\Delta t_i = 0.1\nu_i^{-1}\left[(\beta + v_0/2)^2 + \gamma K/\nu_i\right]^{-1/2} . \qquad (3)$$

This time interval was used for about twice the length of time that it took for i to reach a maximum. After this length of time a longer time interval was chosen in order to proceed more rapidly toward the final steady state. If the enhanced diffusion due to vacancies was being studied, the new interval chosen was

$$\Delta t_2 = (0.01 J_i/\beta\nu_v) \cdot \text{lesser of}\left(1, \beta\gamma^{1/2}\nu_v^{1/2}K^{-1/2}\right) . \qquad (4)$$

[1] W. M. Lomer, *Diffusion Coefficients in Copper Under Fast Neutron Irradiation*, AERE-T/R-1540 (December 1954).

[2] G. J. Dienes and A. C. Damask, *J. Appl. Phys.* **29**, 1713 (1958).

[3] M. S. Wechsler *et al.*, *Solid State Div. Ann. Progr. Rept. Aug. 31, 1962*, ORNL-3364, pp. 127–34; J. M. Williams *et al.*, *Solid State Div. Ann. Progr. Rept. May 31, 1963*, ORNL-3480, pp. 135–42.

[4] G. J. Dienes and G. H. Vineyard, *Radiation Effects in Solids*, p. 143, Interscience, New York, 1957.

If the enhanced diffusion due to interstitials was being studied, the new interval chosen was

$\Delta t_2 = 0.01\ J_i$/greater of

$$[\beta\nu_v,\ \nu_i i\ (\text{time of choosing } \Delta t_2)]\ . \quad (5)$$

The J's are the total number of defect jumps per lattice site that are to be accumulated during the calculation.

The first integration procedure used was a Runge-Kutta method. This method introduced numerical instability into the solution when using Δt_2 if Δt_2 was greater than about 20 times the value of Δt_1 given by Eq. (3). A predictor-corrector method was also tried. When this method was iterated in the most straightforward way, it failed to converge. This failure of convergence occurred under the same conditions for which the Runge-Kutta method was unstable. However, a special method of iteration was found which converged and was stable. The predictor formulas were

$$v_{n+1} = v_n + v_n' \Delta t\ , \quad (6)$$

$$i_{n+1} = i_n + i_n' \Delta t\ , \quad (7)$$

and the corrector formulas were

$$v_{n+1} = v_n + \frac{1}{2}\Delta t(v_n' + v_{n+1}')\ , \quad (8)$$

$$i_{n+1} = i_n + \frac{1}{2}\Delta t(i_n' + i_{n+1}')\ . \quad (9)$$

The iteration procedure was as follows: In Eq. (8), v_n and v_n' were fixed by the values at the previous point. Equation (1) was substituted for v_{n+1}'. During this substitution, i_{n+1} was assigned its best previously available value, but v_{n+1} was left as an unknown. The best previously available value was obtained from the predictor for the first iteration and from the last previous iteration for later ones. The equation obtained from this substitution of Eq. (1) in (8) was solved for v_{n+1}. Then Eqs. (2) and (9) were used in a similar way to obtain i_{n+1} and complete a cycle of iteration. The iteration was continued until some predetermined degree of convergence was achieved.

The program for the numerical integration also computed the accumulated number of defect jumps. The calculation could be terminated when the accumulated number of jumps by either type of defect reached some predetermined value J. This yielded $t(J)$.

The accuracy of the calculations was checked in three ways. First, the calculations were redone using values of Δt_1 and Δt_2 that were half those given by Eqs. (3) to (5). Second, numerical integration was performed with Δt_2 given by $\Delta t_2 = 10\ \Delta t$, rather than by using Eq. (4) or (5). This method was only possible for favorable cases and was lengthy even then. Third, the numerical integration was compared with the analytical approximation in certain cases where the latter was expected to be quite accurate. The results of all types of checks indicated that the numerical integration was always acceptably accurate.

During use of formulas other than (4) or (5) to choose Δt_2, it was found that dv/dt and di/dt underwent oscillations of large enough amplitude to cause changes in sign of these quantities. Such oscillations always reached a saturation amplitude. Equations (4) and (5) were evolved in order to reduce the amplitude of these oscillations. Use of these choices for Δt_2 caused the amplitude of the oscillations to be much smaller in magnitude than any of the terms on the right-hand sides of Eqs. (1) and (2). The checks of accuracy referred to in the previous paragraph confirmed that the oscillations did not cause any appreciable errors in the calculations.

Some results obtained by the integration method outlined above are shown in Figs. 5.1 and 5.2. The values of the various parameters in the theory have been chosen so as to give as good agreement as possible with experiments[3] on radiation-enhanced diffusion in the Cu–15 at. % Al alloy. The experimental results are shown along with the calculated curves. The experimentally measured quantity is $\tau_{1/2}$, the time for half completion of the resistivity decrease that occurs during irradiation. The points labeled first runs in the figures are experiments performed on previously unirradiated specimens; those labeled second runs are experiments performed on specimens which had been irradiated for a week or more and then annealed at 210°C. In order to compare the calculations with the experiments, it is necessary to assume that $\tau_{1/2}$ corresponds to some given number of defect jumps $J_{1/2}$. The values for the parameters that are the same in all these calculations are $K = 10^{-10}$ sec^{-1}; $\nu_{0v} = \nu_{0i} = 10^{14}$ sec^{-1}; $v_0 = 5$ exp (–1 ev/kT); and $\gamma = 25$. The values of the other parameters are indicated on the fig-

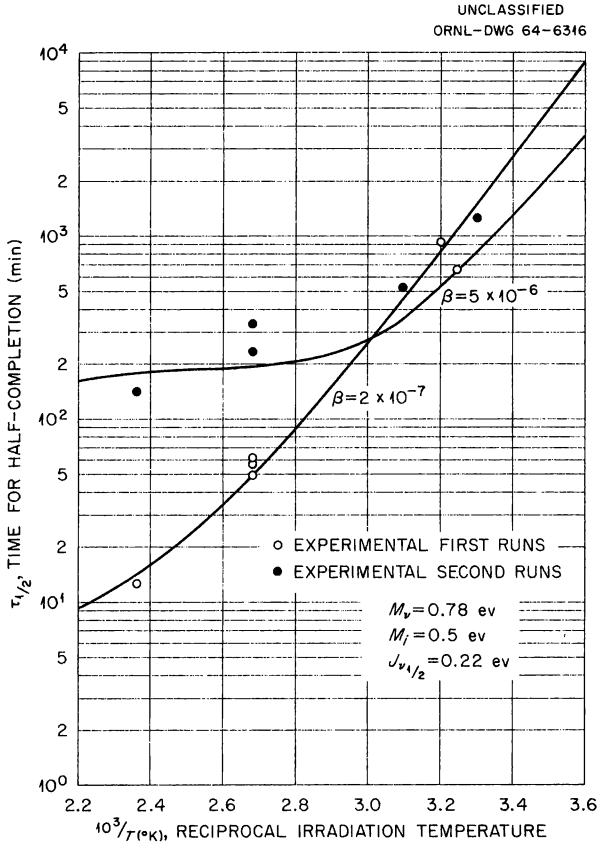

Fig. 5.1. Time for Half Completion of the Resistivity Decrease as a Function of the Reciprocal Irradiation Temperature for the Case in Which the Enhancement of Diffusion Is Due to Vacancy Motion.

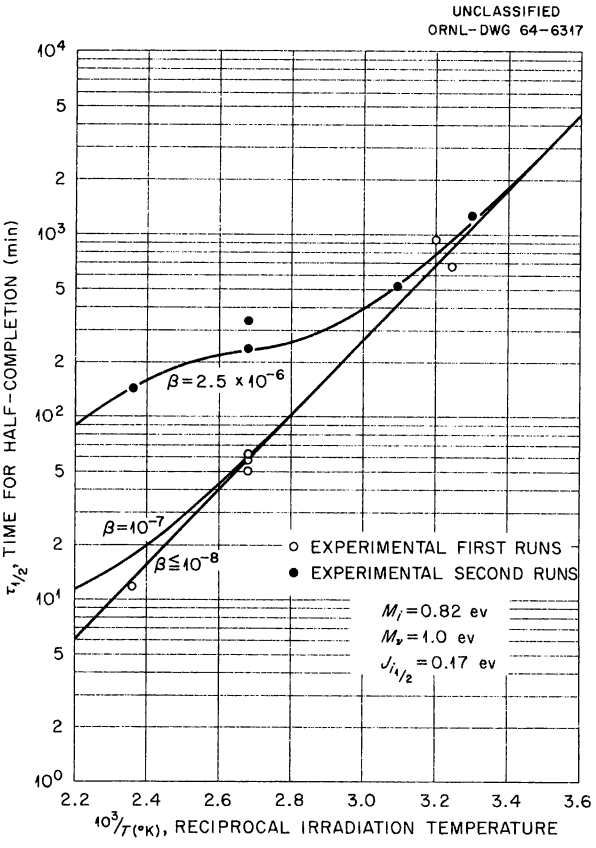

Fig. 5.2. Time for Half Completion of the Resistivity Decrease as a Function of the Reciprocal Irradiation Temperature for the Case in Which the Enhancement of Diffusion Is Due to Interstitialcy Motion.

ures. This value of γ was obtained by setting $r_0 = a$; it is as small a value as could be reasonably considered. This minimum choice was made to avoid overemphasizing the introduction of the factor γ.

DIFFUSIONLESS SELF-ANNEAL IN VACANCY-INTERSTITIAL CASCADES

K. Dettmann[5] D. K. Holmes G. Leibfried

Introduction

Primary displaced atoms of high energy in solids occurring in radiation damage produce cascades containing a large number of vacancy-interstitial pairs (Frenkel pairs) in a relatively small volume. The densities can be so large that annihilation of pairs takes place by purely static and attractive forces of short range between vacancies and interstitials without diffusive motion. If one considers one vacancy as fixed, then one has a certain number of mechanically unstable interstitial sites around that vacancy. The number of those sites can be quite large (50 to 100 in machine calculations for lattice models of copper[6] and iron[7]). For large numbers it is justified to describe this instability by an annealing volume v_a around the vacancy and to use continuous positions rather than lattice sites for the defects. If an interstitial is located in that volume around a vacancy, annihilation occurs due to mechanical instability

[5]Technische Hochschule, Aachen, Germany.

[6]J. B. Gibson *et al.*, *Phys. Rev.* **120**, 1229 (1960).

[7]C. Erginsoy, private communication.

alone. The shape of the volume depends on crystal symmetry, but in the following treatment it will be sufficient to consider a spherical volume $v_a = 4\pi R_a^3/3$ (i.e., a vacancy at $\mathbf{r}_v$ and an interstitial at $\mathbf{r}_i$ anneal if their distance $|\mathbf{r}_i - \mathbf{r}_v|$ is smaller than the annealing radius R_a). For large defect densities this effect of self-anneal can drastically reduce the number of defects in a displacement cascade as usually calculated.[8]

The starting point of such a calculation would then be the distribution of vacancies and interstitials being created in the first fast stage of the slowing down of the primary. The self-anneal is usually a much slower process occurring in a second, slower, stage for which the above distribution can serve as initial condition. It is convenient to describe the self-anneal by an absorption function $\sigma(\mathbf{r}_i - \mathbf{r}_v)$, where $\sigma\, dt$ is the probability of a pair anneal in the time dt for a given distance $\mathbf{r}_i - \mathbf{r}_v$. In the following we will only consider a particularly simple absorption function $\sigma(\mathbf{r}_i - \mathbf{r}_v) = \sigma_a p(\mathbf{r}_i - \mathbf{r}_v)$, where $p(\mathbf{r}_i - \mathbf{r}_v) = 1$ for $|\mathbf{r}_i - \mathbf{r}_v| < R_a$ and $p = 0$ for $|\mathbf{r}_i - \mathbf{r}_v| > R_a$. The annealing rate σ_a is then independent of the pair distance within the annealing volume. The average annealing time for one pair is $1/\sigma_a$ and should be of the order of about 10^{-13} sec, much longer than the development times for the cascades in the first fast stage.[6,7] The number of annihilations depends on time t, and the self-anneal corresponds to times $t\sigma_a \gg 1$ when the annealing process is practically completed. In this case the result cannot depend any more on the numerical value of σ_a. This time-dependent picture of self-anneal rests on a physical basis and uniquely determines the distribution once the initial conditions are known. It also has some mathematical advantages as compared with a static model.[9] Imagine a vacancy with two interstitials contained in v_a. Then, in the static model, one has to decide which interstitial anneals with the vacancy. For instance, one could assume that the smaller distance is decisive. Already this simple assumption is difficult to formulate even mathematically. In the time-dependent description, both anneal with a rate given by σ. The rates can be made dependent on distance through σ. Here, of course, it is assumed that the various annealing processes connecting more than two defects at the same time can be superimposed.

In view of the possible importance of this effect, it seems to be of interest to study the extent of such an anneal on a more general basis. In the following we will only consider the most simple initial configuration, namely, a random and homogeneous distribution of vacancies and interstitials, neglecting inhomogeneity (surface) and correlation effects in the displacement cascade.

Basic Equations

We will work here with density functions commonly employed in the theory of liquids and gases.[10] Position vectors of interstitials will be abbreviated by $\mathbf{r}_n = n$ and by $\mathbf{r}_n' = n'$ for vacancies. The single-particle densities are denoted by $\rho(1;;t)$ and $\rho(;1';t)$ for interstitials and vacancies respectively. Here $\rho(1;;t)\, d1$ means the average number of interstitials in the differential volume $(\mathbf{r}_1, d\mathbf{r}_1) = (1, d1)$ and correspondingly for the vacancies. The pair densities are denoted by $\rho(1,2;;t)$, $\rho(1;1';t)$, and $\rho(;1',2';t)$, where, for example, $\rho(1;1';t)\, d1\, d1'$ is the average number of vacancy-interstitial pairs, the interstitial being located on $(1, d1)$ and the vacancy in $(1', d1')$. The densities $\rho(1,2;;t)$ and $\rho(;1',2';t)$ refer correspondingly to interstitial and vacancy pairs. The triplet densities are given by $\rho(1,2,3;;t)$, $\rho(1,2;1';t)$, $\rho(1;1',2';t)$, and $\rho(;1',2',3';t)$, where, for example, $\rho(1,2;1';t)\, d1 d2 d1'$ is the average number of triplets, an interstitial pair being in $(1, d1)(2, d2)$ and a vacancy being in $(1', d1')$.

The basic equations of our problem are integro-differential equations connecting the various densities ($\dot{\rho}$ stands for $\partial\rho/\partial t$):

$$\dot{\rho}(1;;t) = \dot{\rho}(;1;t) = -\int \rho(1;1';t)\, \sigma(1;1')\, d1', \quad (1)$$

$$\dot{\rho}(1;1';t) = -\sigma(1;1')\, \rho(1;1') - \int \rho(1,2;1')\, \sigma(2;1') \times d2 - \int \rho(1;1',2')\, \sigma(1;2')\, d2', \quad (2)$$

$$\dot{\rho}(1,2;t) = -\int \rho(1,2;1')\, [\sigma(1;1') + \sigma(2;1';)]\, d1',$$
$$\dot{\rho}(;1',2';t) = -\int \rho(1;1',2')\, [\sigma(1;1') + \sigma(1;2')]\, d1. \quad (3)$$

[8] D. S. Billington and J. H. Crawford, Jr., *Radiation Damage in Solids*, Princeton University Press, Princeton, N.J., 1961.

[9] G. Leibfried and D. K. Holmes, *Solid State Div. Ann. Progr. Rept. May 31, 1963*, ORNL-3480, p. 6.

[10] J. O. Hirschfelder, *Molecular Theory of Gases and Liquids*, Wiley, New York, 1954.

Equation (1) describes the decrease of the single-particle densities due to pair annealing with the absorption rate σ. Equation (2) gives the decrease of the vacancy-interstitial pair density due to pair annealing and due to the anneal of one partner of the pair with another defect. Equation (3) shows the decrease of equal pair densities due to annealing with a third partner. The complete set consists in a hierarchy of equations connecting the time change of densities with densities of higher order.

If the correlation between particles is not too large, one can convert Eqs. (1) to (3) into a complete system by expressing the triplet densities in terms of the pair densities. This, also, is a procedure that is well known from the statistical theory of liquids and gases.[10,11] The simplest assumption is

$$\rho(1,2;1') \cong \frac{\rho(1,2;)\,\rho(1;1')\,\rho(2;1')}{\rho(1;)\,\rho(2;)\,\rho(;1')}\,;\ \rho(1;1',2') \cong \frac{\rho(1;1')\,\rho(1;2')\,\rho(;1',2')}{\rho(1;)\,\rho(;1')\,\rho(;2')}\,. \quad (4)$$

If one can regard like defects as uncorrelated, one has, with $\rho(1;2;) \cong \rho(1;)\,\rho(2;)$ and $\rho(;1',2') \cong \rho(;1')\,\rho(;2')$,

$$\rho(1,2;1') \cong \rho(1;1')\,\rho(2;1')/\rho(;1');\ \rho(1;1',2') \cong \rho(1;1')\,\rho(1;2')/\rho(1;)\,. \quad (4a)$$

In this case Eq. (4a) together with Eqs. (1) and (2) alone form a complete set; this is essentially Waite's assumption[11] in his diffusion-annealing treatment. Though no rigorous proof of these assumptions can be given at present, we will treat our annealing problem on that basis.

The initial conditions for $t = 0$ determine the problem uniquely. For a random, homogeneous initial distribution, they are with the initial single-particle densities $\rho(1;;t=0) = n_0$ and $\rho(;1';t=0) = n_0'$ independent of position:

$$\rho(1;1';0) = n_0 n_0';\ \rho(1,2;;0) = n_0^2;\ \rho(;1',2';0) = n_0'^2 \quad (5)$$

for the set of Eqs. (1) to (4) and

$$\rho(1;1';0) = n_0 n_0' \quad (5a)$$

for the set (1, 2, 4a).

[11] T. R. Waite, *Phys. Rev.* **107**, 463, 471 (1957).

Uncorrelated Like-Particle Densities

With the assumption of no correlation between like defects (Eqs. 1, 2, 4a, 5a), the single-particle densities $\rho(1;;t) = n(t)$ and $\rho(;1';t) = n'(t)$ cannot depend on position, and the pair density $\rho(1;1';t)$ can only depend on the distance $|\mathbf{r}_1 - \mathbf{r}_{1'}|$. Then one has

$$\dot{n} = \dot{n}' = -\,C(t) \text{ with } C(t) = -\int \rho(1;1';t)\,\sigma(1;1')\,d1'\,, \quad (1a)$$

$$\dot{\rho}(1;1';t) = -\,\sigma(1;1')\,\rho(1;1') - \rho(1;1') \times \left(\frac{1}{n} + \frac{1}{n'}\right) C(t)\,. \quad (2a)$$

Multiplying (2a) with $\sigma(1;1')$ and integrating over 1 or 1', one obtains [$\sigma^2(1;1') = \sigma_a \sigma(1;1')$ for constant absorption rate within v_a]

$$\dot{C} = -\,\sigma_a C - \left(\frac{1}{n} + \frac{1}{n'}\right) C^2 = C\left(-\sigma_a + \frac{d}{dt} \ln nn'\right) \quad (2b)$$

or

$$\frac{d}{dt} \ln \frac{C}{nn'} = -\sigma_a\,,$$

leading to

$$\frac{C}{nn'} = \frac{C_0}{n_0 n_0'} e^{-\sigma_a t} = \sigma_a v_a e^{-\sigma_a t}\,. \quad (6)$$

Equation (2a) has the solution

$$\rho(1;1';t) = \rho(1;1';0) \frac{nn'}{n_0 n_0'} e^{-\sigma(1;1')t} = nn' e^{-\sigma(1;1')t}\,. \quad (7)$$

Substituting Eq. (6) into (1a) and using $n - n' = n_0 - n_0'$ gives

$$\frac{d}{dt} \frac{1}{n_0 - n_0'} \ln \frac{n - n_0 + n_0'}{n} = -\sigma_a v_a e^{-\sigma_a t}$$

or (8)

$$\ln \frac{(n - n_0 + n_0')n_0}{nn_0'} = (n_0 - n_0')\,v_a(e^{-\sigma_a t} - 1)\,.$$

For complete anneal ($\sigma_a t \gg 1$), one has

$$1 + \frac{n_0' - n_0}{n_\infty} = \frac{n_0'}{n_0} e^{-(n_0 - n_0')v_a}$$

or

$$n_\infty = \frac{n_0' - n_0}{(n_0'/n_0)\, e^{-(n_0 - n_0')v_a} - 1} \tag{9}$$

For equal initial densities ($n_0 - n_0' \longrightarrow 0$ in Eq. 8), it is

$$\frac{d}{dt}\frac{1}{n} = \sigma_a v_a e^{-\sigma_a t}; \quad \frac{1}{n} - \frac{1}{n_0} = v_a(1 - e^{-\sigma_a t});$$

$$n_\infty = \frac{n_0}{1 + n_0 v_a} . \tag{10}$$

In Eq. (10) the result for n_∞ is identical with that obtained from Monte Carlo calculations[9] and leads to a saturation[12] value $n_\infty = 1/v_a$ for large initial densities $n_0 = n_0'$ corresponding to a saturated density of two defects per annealing volume. This agreement can serve to partly justify the drastic assumptions having been made to simplify the original equations.

Pair Correlation

Unfortunately, the above procedure cannot be used if one has initial correlations. This can be shown by an especially simple example using a random distribution of correlated pairs as initial state. We consider a volume V containing N Frenkel pairs. The initial distribution of the pair $\mathbf{r}_1, \mathbf{r}_1'$ is $f(|\mathbf{r}_1 - \mathbf{r}_1'|)/V = f(1;1')/V$, where $f(1;1')$ is normalized to unity ($\int f\, d1' = \int f\, d1 = 1$), and extends over a range that is small in comparison with the linear dimensions of V. Then the initial normalized probability distribution W in configuration space is

$$W(1, \ldots N; 1', \ldots N') = \frac{1}{V^N} f(1;1') \ldots f(N;N'). \tag{11}$$

The initial densities are given by ($d\tau = d1 \ldots dNd1' \ldots dN'$)

$$\rho_0(\mathbf{r};) = \int \sum_{j=1}^{N} \delta(\mathbf{r} - \mathbf{r}_j)\, W\, d\tau = \frac{N}{V}$$

$$= \rho_0(;\mathbf{r}') = n_0 = n_0' \tag{12}$$

and

$$\rho_0(\mathbf{r};\mathbf{r}') = \int \sum_{j=1}^{N} \sum_{j'=1}^{N} \delta(\mathbf{r} - \mathbf{r}_j)\, \delta(\mathbf{r}' - \mathbf{r}_{j'}')\, W\, d\tau$$

$$= \frac{N}{V} f(\mathbf{r};\mathbf{r}') + \frac{N(N-1)}{V^2} \cong n_0 f + n_0^2 . \tag{13}$$

If one again uses Eqs. (1, 2, 4*a*, and 5*a*), neglecting correlation between like particles,[13] one can use the same procedure as before except for another initial value for $C(t = 0) = C_0$,

$$C_0 = \int \sigma(\mathbf{r};\mathbf{r}')\, \rho_0(\mathbf{r};\mathbf{r}')\, d\mathbf{r}' = n_0 \sigma_a \int_{V_a} f(\mathbf{r};\mathbf{r}')\, d\mathbf{r}'$$

$$+ n_0^2 \sigma_a v_a . \tag{14}$$

This has the effect that v_a in Eq. (10) has to be replaced by $C_0/\sigma_a n_0^2 = \int f(\mathbf{r};\mathbf{r}')\, d\mathbf{r}'/n_0 + v_a$, leading to

$$n_\infty = \frac{n_0}{1 + \int_{V_a} f(\mathbf{r};\mathbf{r}')\, d\mathbf{r}' + n_0 v_a} . \tag{15}$$

This is a physically meaningless result. If $\int_{V_a} f\, d\mathbf{r}' = 1$, which means that the pairs are all contained in v_a, one has to expect 100% anneal ($n_\infty = 0$) for small $n_0 v_a$. Instead, one obtains $n_\infty = n_0/2$ for $n_0 v_a \ll 1$. What one would have to expect is that in Eq. (10) for n_∞ the initial density is replaced by $n_0(1 - \int_{V_a} f\, d\mathbf{r}')$, taking into account the anneal within the pairs already. How this problem can be handled with physically meaningful results has been shown by Waite.[11] In his treatment the defects are still identified, and one

[12] Such a saturation exists only for $n_0 = n_0'$; for $n_0 \neq n_0'$ and large initial concentrations the kind of defect with the lower initial concentration anneals out completely, as is to be expected.

[13] In the initial state (11), like defects are uncorrelated.

keeps track of the ones which are initially correlated, whereas here we have used a symmetrized theory with a symmetrized initial condition, Eq. (11). The symmetrization does not change the physical result, but the factorization of the triplet densities [Eqs. (4, 4*a*)] does not seem to be possible any more. The reasons for this behavior are not yet fully understood. It is certainly connected with the fact that during annealing the configuration space contains subspaces with different numbers of particles. It is easy to give examples with different defect numbers where the defects are uncorrelated and where nevertheless a decomposition like Eq. (4) is invalid.

The same kind of situation is presumably encountered when considering production. If the production rate P is the same for both defects and if they are produced uncorrelatedly, one obtains, with Eqs. (1, 2, 4*a*, and 5*a*),

$$\dot{n} = -C + P \quad \dot{\rho}(1;1';t) = -\rho(1;1')\left[\sigma(1;1') + \frac{2C}{n}\right] + 2nP, \quad \dot{C} = -C\left(\sigma_a + \frac{2C}{n}\right) + 2\sigma_a v_a n P \; . \tag{16}$$

The stationary value n_s for time-independent production ($\dot{n} = \dot{C} = 0$) is given by $\sigma_a + 2P/n_s = 2\sigma_a v_a n_s$ and is $n_s = \frac{1}{2} v_a$ for small production rates, $Pv_a/\sigma_a \ll 1$. One would expect, however, the value $1/v_a$ derived in Eq. (10) for large initial densities. Here also one presumably can employ the more elaborate treatment of Waite, keeping track of the correlation between vacancy-interstitial pairs created at the same time. The same, of course, holds true a fortiori for correlated pair production as in electron damage.

Influence of Like-Pair Correlation

We will discuss like-pair correlation only for equal initial densities [$n_0 = n_0'$, $n = n'$; $\rho(1,2;) = \rho(;1,2)$]. From Eqs. (1 to 5) one obtains

$$\dot{n} = -C \; , \tag{17a}$$

$$\dot{\rho}(1;1') = -\rho(1;1') \times \left[\sigma(1;1') + \frac{2}{n^3}\int \rho(1,2;)\,\rho(2;1')\,\sigma(2;1')\,d2\right] \; , \tag{17b}$$

$$\dot{\rho}(1,2;) = -\frac{2}{n^3}\,\rho(1,2;)\int \rho(2;1')\,\rho(1;1')\,\sigma(1;1')\,d1' \; . \tag{17c}$$

Multiplying (17*b*) with $\sigma(1;1')$ and integrating over $1'$ gives

$$\dot{C} = -\sigma_a C - \frac{2}{n^3}\int \rho(1,2;)\,\rho(1;1')\,\sigma(1;1') \times \rho(2;1')\,\sigma(2;1')\,d1'd2 \; . \tag{18}$$

Because of the σ factors, only relatively close distances $\mathbf{r}_1 - \mathbf{r}_2$ are contained in the integrand. For small initial densities, to which the following will be restricted, one can certainly assume that for these distances $\rho(1,2;)$ will only vary slowly so that $\rho(1,2;) \cong \rho(1,1;) = G(t)$, resulting in

$$\dot{C} = -C(\sigma_a + 2GC/n^3) \; . \tag{18a}$$

From (17*c*) with $1 = 2$, one obtains $\dot{G} = -2GD/n^3$ with

$$D = \int \rho^2(1;1')\,\sigma(1;1')\,d1' \; , \tag{19}$$

and using (17*b*) again one gets $\dot{D} = -2D(\sigma_a + 2GC/n^3)$. Comparison with (18*a*) shows that $C^2/D = C_0^2/D_0 = \sigma_a v_a$ is time independent,[14] and the equation for $\dot{G}$ becomes then

$$\dot{G} = -2GC^2/\sigma_a v_a n^3 \; . \tag{19a}$$

Equations (17*a*, 18*a*, and 19*a*) now form a complete set. It can be reduced to two equations by realizing that $n + v_a G - C/\sigma_a = n_0$ is independent of time, leaving only n and C as independent functions. The quantity $1/n + C/\sigma_a n^2 = 1/n_0 + v_a$, which is independent of time in the uncorrelated case ($G = n^2$), now is time dependent:

$$\frac{d}{dt}\left(\frac{1}{n} + \frac{C}{\sigma_a n^2}\right) = \frac{2C^2}{n^3\sigma_a}\left(1 - \frac{G}{n^2}\right) \; . \tag{20}$$

[14] This result means that $\rho(1;1')$ is constant in v_a.

To estimate the error introduced by like-pair correlation, one can substitute the solution (10) of zero order on the right-hand side of (20):

$$\frac{d}{dt}\left(\frac{1}{n}+\frac{C}{\sigma_a n^2}\right)=F(t);\ \frac{1}{n_\infty}-\frac{1}{n_0}-v_a$$

$$=\int_0^\infty F(t)\,dt=\Delta\leq 0\ , \quad (21)$$

$$(C_\infty=0)\ \text{with}\ F=\frac{2C^2}{n^4 v_a\sigma_a}\left(2-\frac{n}{n_0}-\frac{n_0}{n}\right)\leq 0\ .$$

According to (10) it is $C/n^2\sigma_a = v_a e^{-\sigma_a t}$ and $1/n = 1/n_0 + v_a - v_a e^{-\sigma_a t}$. Introducing $x(t) = n_0/n(t)$ as a new variable, one obtains

$$\frac{\Delta}{v_a}=-\frac{2}{(n_0 v_a)^2}\int_1^{1+n_0 v_a} dx\,(1+n_0 v_a-x)$$

$$\times\left(x+\frac{1}{x}-2\right), \quad (22)$$

$$\frac{\Delta}{v_a}=-\frac{2}{\alpha^2}\left[(1+\alpha)\ln(1+\alpha)-\alpha-\frac{\alpha^2}{2}+\frac{\alpha^3}{6}\right]$$

$$\cong -\frac{2}{\alpha^2}\left(\frac{\alpha^4}{12}-\frac{\alpha^5}{20}+\ldots\right)=-\frac{\alpha^2}{6}+\frac{\alpha^3}{10}+\ldots$$

with $\alpha = n_0 v_a$. Therefore, the anneal will be given by[15]

$$\frac{n_0}{n_\infty}=1+n_0 v_a-\frac{(n_0 v_a)^3}{6}\ . \quad (23)$$

The correction is negative, is only of third order, and shows that due to like-pair correlation the self-anneal is smaller than that given by (10). One also can see that a correlation between like pairs is built up. Because of $v_a G_\infty = n_0 - n_\infty$, one has $G_\infty/n_\infty^2 \cong 1 + \alpha - \alpha^3/3$. Thus G_∞ is larger than the square of the corresponding single-defect density.

[15]This result has been obtained also by K. Dettmann by expanding the solutions directly in powers of α.

Consequently, like defects tend to remain in clusters, thus lowering the effect of self-anneal. No attempt has been made to treat Eqs. (17*a*–c) for large $n_0 v_a$. But there are indications that the actual saturation value for large $n_0 v_a$ is only slightly above $1/v_a$, showing that as in Eq. (23) the influence of like-pair correlation is not very important even for $n_0 v_a \gg 1$. This has been dealt with by Dettmann,[15] who started with the probability distribution and did not use density functions and approximations like Eqs. (4 and 4*a*).

Also, one can convince oneself that the treatment given above replacing $\rho(1,2;)$ by its central value $\rho(1,1;)$ will overestimate the influence of like-pair correlation. To see this, let us assume that $\rho(1;1')$ is constant in v_a and equals n^2 outside,

$$\rho(1;1')=\frac{C}{\sigma_a v_a}p(1;1')+n^2[1-p(1;1')];$$

$$\frac{C}{\sigma_a v_a}=\int\rho(1;1')\,p(1;1')\,d1'\ , \quad (24)$$

where

$$p(1;1')=\sigma(1;1')/\sigma_a=\begin{pmatrix}1\\0\end{pmatrix}$$

for

$$|\mathbf{r}_1-\mathbf{r}_1'|\begin{pmatrix}<\\>\end{pmatrix}R_a \text{ and } p^2=p.$$

This behavior is that of the uncorrelated solution. Now let us assume the same behavior also for $\rho(1,2;)$:

$$\rho(1,2;)=G\,p(1;2)+n^2[1-p(1;2)];$$

$$G=\int\rho(1,2;)\,p(1;2)\,d2\ . \quad (24a)$$

With both these assumptions one obtains the following set of equations:

$$\dot{n}=-C\ , \quad (25a)$$

$$\dot{C}=-C\left(\sigma_a+\frac{2CG}{n^3}A+\frac{2C}{n}B\right), \quad (25b)$$

$$\dot{G}=-\frac{2GC}{n^3}\left(\frac{C}{\sigma_a v_a}A+n^2 B\right), \quad (25c)$$

with

$$A = \frac{1}{V_a^2} \int p(1,2)\, p(2,1')\, p(1',1)\, d2d1' \text{ and}$$

$$A + B = 1 . \quad (26)$$

The equations without like-pair correlation correspond to $A = 0$ and $B = 1$, whereas the above treatment results from $A = 1$ and $B = 0$. Equations (25*a*–*c*) describe therefore an intermediate case showing that the set (17*a*, 18*a*, and 19*a*) probably overestimates the influence of equal pair correlation. For the assumptions (24 and 24*a*), the actual value of $A = {}^{15}/_{32}$ is easily calculated. Whereas the assumption (24) is quite natural, (24*a*) gives a like-pair correlation length R_a of the same value as that of unlike pairs. Presumably the correlation length for $\rho(1,2;)$ will be smaller than R_a, say R_a^{lp}. One would then obtain again Eqs. (25) where $p(1,2)$ in the definition of A would be replaced by a corresponding function containing R_a^{lp}. This would lower the numerical value of A and would render a solution even closer to the uncorrelated case. An improvement could be obtained by considering a time-dependent R_a^{lp}, but this will not be discussed further.

THEORETICAL STUDIES OF ISOCHRONAL ANNEALING

D. K. Holmes

Until recently, isochronal annealing has been used in radiation damage work mostly as an experimental tool for surveying the annealing behavior over a broad temperature range. More precise knowledge of the kinetics and activation energies is usually obtained by combining the isochronal annealing results with isothermal annealing studies in the appropriate temperature ranges. However, the work of the Low-Temperature Irradiation Group on the isochronal annealing of cadmium after recoil damage[16] seems to justify closer attention to the possibility of direct quantitative analysis of isochronal data. This is principally due to the excellent temperature control and relatively close spacing of annealing temperatures achieved by this group, but is also due to the great range of damage concentration which can be obtained by the recoil method.

With this work in mind, theoretical studies of isochronal annealing have been started. For the initial effort, the pulse-annealing process is simulated by a continuous warm-up at a constant rate chosen to represent the average rate of the isochronal annealing. First, consider a concentration of defects which anneals out in a given temperature range with a unique activation energy. Suppose the kinetic equation is of the form

$$-\frac{df}{dt} = k_n f^n , \quad (1)$$

where f = the fraction of defects remaining at time t,

$$k_n = c_n e^{-E/kT} .$$

Choosing a linear relationship between temperature and time,

$$T = T_0 + \beta t ; \quad (2)$$

the time variation of f may be replaced by a temperature variation. Integrating Eq. (1) formally,

$$-\int_1^{f(T)} \frac{df'}{f'^n} = \frac{c_n}{\beta} \int_{T_0}^{T} e^{-E/kT'} dT' . \quad (3)$$

The integral on the right is related to an exponential integral:

$$\int_{T_0}^{T} e^{-E/kT'} dT' = \frac{E}{k} \int_{E/kT}^{E/kT_0} \frac{e^{-y}\, dy}{y^2} \quad (4)$$

$$\cong \frac{E}{k} \left[\left(\frac{e^{-y}}{y^2} \right) \left(1 - \frac{2}{y} + \frac{6}{y^2} - \frac{24}{y^3} + \cdots \right) \right]_{E/kT}^{E/kT_0}$$

The approximate form at the right in Eq. (4) holds for large values of the limits of the integral and is often acceptable in annealing studies.[17] Comparison with experimental results is best done through the derivative form, $-df/dT$, in which the separate processes appear as peaks. Some

[16] R. R. Coltman *et al.*, "Thermal Neutron Damage in Cadmium," Chap. 12, this report.

[17] Some aspects of Eqs. (3) and (4) have been considered by M. Balarin and A. Zetzsche, *Phys. Status Solidi* **2**, 1670 (1962).

simple peaks calculated on the basis of Eq. (3) are shown in Fig. 5.3. A first-order peak (n = 1) and two (broader) second-order peaks (n = 2) showing the shift in peak temperature as the initial defect concentration is increased are given. (The initial concentration enters into the constants, c_n, for all except first order, which is concentration independent.) There is also shown a comparison between pulse annealing (calculated) and continuous warm-up for a first-order process. It is clear that the two do not give identical results. This also is a warning for the experimentalists that different pulse-annealing programs may yield somewhat different results.

It may be important to study the pulse-annealing process itself rather than the continuous warm-up approximation. Coltman and Klabunde have used the property changes observed in successive pulses to calculate an effective activation energy under the assumption that the process is uniquely activated. To assess the validity of this procedure, it would be necessary to use (for the simple cases) Eq. (1) for a series of isothermal anneals at successively higher temperatures. As an example, a preliminary study of pulse annealing based on two independent first-order processes with different, but not widely separated, activation energies showed that the effective activation energy which would be obtained if the annealing were interpreted as resulting from a single process is considerably smaller than either of the two energies.

The theoretical studies are actually planned to cover a much broader area than that implied in Eq. (1), which treats only a single process. A complete investigation of annealing by warm-up after low-temperature irradiation must take into account the motions of both vacancies and interstitials and, further, must allow for mutual annihilation as well as trapping or annihilation at other sinks. Thus, Eq. (1) represents only a special case of a general situation involving several interdependent processes, each with its own activation energy. A first effort in this direction has been made in treating the following model. During irradiation, single vacancies and single

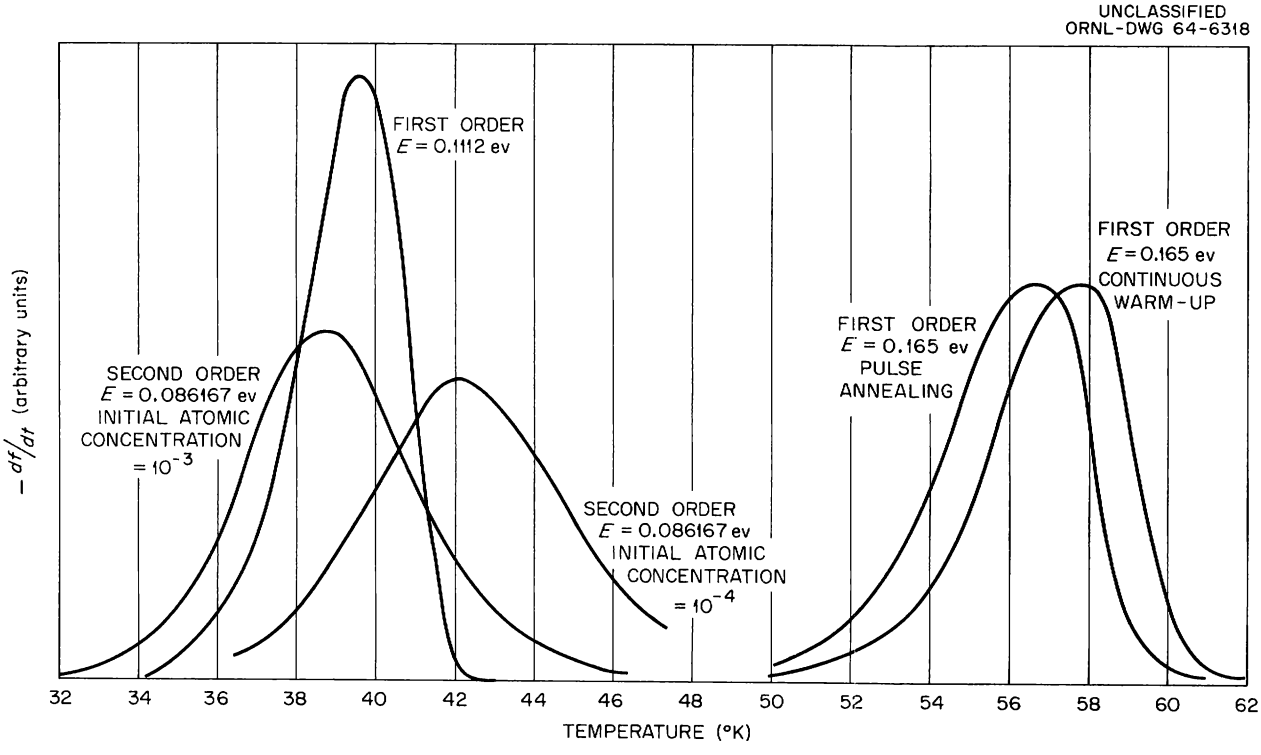

Fig. 5.3. Examples of Calculated Annealing Peaks Based on Single, Uniquely Activated Processes. (The atomic frequency factor is taken as 10^{12} for all these.) All are calculated on the continuous warm-up model, except for the one labeled "pulse annealing."

interstitials are formed in equal numbers. At the temperature of irradiation, interstitials are mobile (but vacancies are immobile) and diffuse either to annihilation or to traps. At the beginning of the warm-up there are two species of defects present in equal initial concentrations: single vacancies and interstitials in traps. As the temperature rises, a third species of defect occurs, single interstitials, which have "boiled off" the traps and are wandering either back to traps or to annihilation at vacancies. The following three equations govern the behavior of the system:

$$-\frac{dv}{dt} = \kappa_1 iv , \tag{5a}$$

$$\frac{di}{dt} = \kappa_0 n - \kappa_1 iv - \kappa_1 (N_0 - n) , \tag{5b}$$

$$\frac{dn}{dt} = -\kappa_0 n + \kappa_1 i(N_0 - n) , \tag{5c}$$

where

v = atomic concentration of vacancies,
i = atomic concentration of interstitials,
n = atomic concentration of trapped interstitials,
N_0 = atomic concentration of trapping sites for interstitials,
$\kappa_0 = c_0 e^{-E_0/kT}$ = rate at which interstitials are jumping from traps,
$\kappa_1 = c_1 e^{-E_1/kT}$ = jump rate for interstitials in the lattice.

The interest in this model is in the determination of the kinetic behavior, during warm-up, of the concentration of vacancies as the interstitials are released from traps at a temperature at which they are highly mobile ($E_0 > E_1$). Is it essentially a first-order process, because the release from traps is first order and the interstitials are effectively instantly annihilated upon release, or is it second order, because the interstitials and vacancies annihilate by pairs?

An attempt to handle these equations analytically (with the temperature taken as rising linearly with time) was not successful. An approximate solution for the free interstitial concentration at very low temperatures was found to be

$$i(T) \cong e^{-(E_0 - E_1)/kT} , \tag{6}$$

but it was not found possible to continue this process to temperatures of real interest. At present a program is being written for machine calculation of these equations. It is planned to use the experience gained from this set of equations to study a number of interesting annealing models including other atomistic processes such as clustering of defects. The ultimate goal of this calculational program is to discover a plausible model to explain the observations on the annealing of radiation damage in cadmium.

ELECTRON CROSS SECTIONS FOR ATOMIC DISPLACEMENTS

O. S. Oen

The calculational program outlined in a previous report[18] for computing the number of atomic displacements produced by elastic collisions between fast electrons and atomic nuclei has been completed and is being published as an ORNL report. The program was expanded beyond its original plan and now includes displacement cross sections for 18 different elements spanning the atomic table using both the Mott series and the conventional, but less accurate, McKinley-Feshbach formula. Cross sections for both the primary and the cascade using the Kinchin and Pease model were calculated using sharp displacement thresholds ranging from 10 to 50 ev in steps of 5 ev. Electron energies ranging from threshold to 10 Mev were used for each case. In addition, tables giving the differential cross section in steps of $7\frac{1}{2}^\circ$ for both the Mott series and the McKinley-Feshbach formula are included. Calculational difficulties which were finally traced to numerical round-off errors were encountered in using a computer operating with a 36-bit word. These difficulties were overcome by rewriting and running the program on a computer which uses a 48-bit word. The numerical results are probably accurate to within a few percent. They agree very closely with published calculations for those special cases which overlap. The calculations should be especially useful for estimating the errors associated with using the conventional McKinley-Feshbach formula for elements of high Z ($Z > 30$).

[18] O. S. Oen, *Solid State Div. Ann. Progr. Rept. Aug. 31, 1962*, ORNL-3364, p. 26.

FORMAL SOLUTION OF SOME EQUATIONS OF RADIATION-ENHANCED DIFFUSION

E. J. Lee

The equations considered by Barrett[19] may be written in general form as

$$\frac{dx}{dt} = a_1 - b_1 x - c_1 xy \,, \tag{1}$$

$$\frac{dy}{dt} = a_2 - b_2 y - c_2 xy \,, \tag{2}$$

where x and y = vacancy and interstitial concentrations, a_1 and a_2 = corresponding production rates, $b_1 x$ and $b_2 y$ = sink terms, $c_1 xy$ and $c_2 xy$ = recombination terms.

By differentiating (1) with respect to t and eliminating y and dy/dt from the resulting equation and (1) and (2), the following equation is obtained:

$$x\frac{d^2x}{dt^2} - \left(\frac{dx}{dt}\right)^2 + (a_1 + b_2 x + c_2 x^2)\frac{dx}{dt}$$

$$- a_1 b_2 x + (a_2 c_1 - a_1 c_2 + b_1 b_2)x^2 + b_1 c_2 x^3 = 0. \tag{3}$$

The system (1), (2) is thus decoupled.

The transformation $u = x/(dx/dt)$ reduces Eq. (3) to the first-order equation,

$$\frac{du}{dx} = Pu^2 + Qu^3 \,, \tag{4}$$

where

$$P = \frac{a_1}{x^2} + \frac{b_2}{x} + c_2 \tag{5}$$

and

$$Q = -\frac{a_1 b_2}{x^2} + \frac{a_2 c_1 - a_1 c_2 + b_1 b_2}{x} + b_1 c_2 \,. \tag{6}$$

Thus, if $u = u(x)$ is the solution of (4), the solution of (3) is

$$t = \int_{x_0}^{x} \frac{u(g)\,dg}{g} + t_0 \,, \tag{7}$$

and similarly, replacing x by y and interchanging subscripts in (5) and (6), the solution for y is

$$t = \int_{y_0}^{y} \frac{u(g)\,dg}{g} + t_0 \,. \tag{8}$$

This approach to the solution of (1), (2) was motivated by the hope of bypassing the difficulties at first encountered in the direct numerical solution. Equation (4) is a special case of Abel's equation,[20,21]

$$\frac{dv}{ds} = A_0 + A_1 v + A_2 v^2 + A_3 v^3 \,,$$

where the A's are functions of s. The analytical intractability of (1), (2) is made apparent by this relationship to an equation of known difficulty.

Solution of (1), (2) by this approach would involve the numerical solutions of (4) followed by numerical quadratures of (7), (8). This scheme has not been investigated, since the earlier problems with the direct numerical solution of (1), (2) were subsequently resolved.[19]

---

[19] J. H. Barrett, "Numerical Calculation in the Theory of Radiation-Enhanced Diffusion," this chapter.

[20] E. Kamke, *Differentialgleichungen, Lösungsmethoden und Lösungen*, vol. I, pp. 24–27, Akademische Verlagsgesellschaft, Geest und Portig K.-G., Leipzig, 1959.

[21] R. Liouville, *Acta Math.* **27**, 55 (1903).

Part II. Crystal Physics

M. K. Wilkinson

6. X-Ray Diffraction

AN INVESTIGATION OF TRANSMUTATION EFFECTS IN CRYSTALLINE SOLIDS[1]

(x-ray diffraction; electron diffraction; electron microscopy; single-crystal alloys)

M. C. Wittels[2] J. O. Stiegler[3]
F. A. Sherrill

X-ray diffraction, electron diffraction and microscopy, metallography, and thermal methods were utilized to study transmutation effects in a group of crystalline solids. Nearly homogeneous distributions of transmuted species were introduced into small single crystals of ^{197}Au, ^{107}Ag, and ^{115}In and powder samples of ^{193}Ir, $^{115}In_2O_3$, and $^{176}Lu_2O_3$. The crystals were irradiated in a thermal-neutron flux of 4.0×10^{14} neutrons cm^{-2} sec^{-1} at a temperature of ~85°C for periods of a few days to several months, so that considerable fractions of transmuted species were formed.

Small metal single-crystal spheres were converted to alloy single crystals in their solid-solution ranges at temperatures up to several hundred degrees below those required by normal laboratory methods in $Au_{0.82}Hg_{0.18}$, $Ag_{0.78}Cd_{0.22}$, and $In_{0.95}Sn_{0.05}$. A powder sample of ^{193}Ir was transformed into the solid-solution alloy $Ir_{0.68}Pt_{0.32}$, a high-temperature alloy, which would require a temperature in excess of 2000°C for its formation by laboratory methods.

The production of 22.5 at. % ^{198}Hg and ^{199}Hg in ^{197}Au through nuclear transmutation revealed the nucleation of Au_3Hg particles with the hcp structure, while the introduction of 29 at. % caused a recrystallization into two unidentified phases. Long-range order in single crystals of ^{115}In was completely destroyed when 14 at. % ^{116}Sn was introduced through nuclear transmutation.

Powder specimens of In_2O_3 enriched in ^{115}In were irradiated to produce concentrations of ^{116}Sn as high as 38 (metal) at. %, with the result that a new phase with a smaller fluorite structure was formed which contains oxygen vacancies. The original In_2O_3 structure was largely recovered upon annealing at 1200°C, and SnO_2 particles were precipitated. Powder samples of Lu_2O_3 containing ^{176}Lu were irradiated to produce 74 (metal) at. % ^{177}Hf, and the resultant material was cubic (fluorite) with a lattice parameter approximately one-half that of the original structure. This oxygen-deficient lattice was stable at temperatures up to 1200°C.

The results are considered in terms of the original crystal structures and known phase equilibrium systems, and possible future experiments are discussed.

ABSOLUTE INTENSITIES OF X RAYS ANOMALOUSLY DIFFRACTED THROUGH THICK COPPER CRYSTALS[4]

R. M. Nicklow F. W. Young, Jr.
F. A. Sherrill

Absolute integrated intensities of the x-ray beams "anomalously transmitted" through nearly perfect copper crystals have been measured for

[1]Abstract of published paper: *Phys. Status Solidi* 4, 533 (1964).

[2]Presently with the Metallurgy and Materials Branch, Division of Research, U.S. Atomic Energy Commission, Washington, D.C.

[3]Metals and Ceramics Division.

[4]Abstract of paper to be submitted to the *Physical Review*.

the (111) planes for values of μt ranging from 10 to 90. Results obtained for both the symmetric and the asymmetric Laue geometries are compared with theory. These comparisons yield a value of 0.960 ± 0.003 for the ratio $f''(111)/f''(000)$ and indicate that the crystals investigated have a high degree of perfection. The measurements were made with Mo $K\alpha$ radiation, using a double-crystal spectrometer arranged in the parallel condition and with the first crystal diffracting in the Bragg geometry. Measured profiles of the Bragg-Laue double-crystal rocking curves for μt = 10 and 90 are in semiquantitative agreement with the theory.

RADIATION DAMAGE EFFECTS IN NEARLY PERFECT COPPER CRYSTALS

(fast neutron irradiation; x-ray diffraction; E)

R. M. Nicklow F. W. Young, Jr.
F. A. Sherrill

In a previous investigation[4] it was noted that although the copper crystals examined were irradiated with 10^{17} fast neutrons/cm^2, they appeared to be very perfect with respect to their x-ray diffraction properties. These observations are quite different from some reported in the literature for polycrystalline and imperfect single-crystal metals[5,6] for comparable neutron radiation doses. Also, it is desirable to determine whether or not the value of ϵ obtained for copper from the previous measurements has been influenced by the irradiation dose of 10^{17} neutrons/cm^2 that the crystals received. Thus, we have started a study of the effects of neutron irradiation on the x-ray diffraction properties of nearly perfect copper crystals, and this report summarizes some initial results.

Peak Widths in Bragg Geometry

It has recently been reported[7] that the measured half-width of the (222) reflection of an unirradiated nearly perfect copper crystal, diffracting in the Bragg geometry, is ~3.0 sec, and this value agrees with theory. If thermal effects, based on a Debye characteristic temperature of 320°K, are considered, the theoretical half-width reported[7] earlier would be reduced from 3.6 sec to 3.2 sec.

Measurements of the half-width of the (222) Bragg reflection from a 1 × 1 × 0.125 cm copper crystal, which was sliced from the center of a 1 × 1 × 2 cm crystal that had been irradiated with 10^{17} fast neutrons/cm^2 (shielded from thermals), have also been made and again yield ~3.0 sec. Both the irradiation and half-width measurements were made at room temperature, and no annealing was performed. Subsequent irradiation of this crystal slice with 10^{19} fast neutrons/cm^2 did not significantly increase this half-width above ~3.0 sec. These results imply that the half-widths of Bragg reflections of nearly perfect copper crystals are not measurably influenced by the damage that results from fast-neutron irradiations $\leq 10^{19}$ neutrons/cm^2.

Anomalous Transmission in the Laue Geometry

Intensities. – In order to investigate the dependence of ϵ on radiation damage, the absolute integrated intensities of the (111) anomalously transmitted and diffracted x-ray beams from this copper crystal were measured after various treatments. Measurements were first made after the crystal had been irradiated with 10^{17} fast neutrons/cm^2 and were repeated after the crystal had been annealed at 200 and at 300°C. These annealings had no significant effect on the measured intensities. The crystal was then irradiated with 10^{19} neutrons/cm^2, and intensity measurements were made after each of the following annealings: (1) room temperature, (2) 1 hr at 200°C, (3) 1 hr at 350°C, and (4) 1 hr at 500°C. The results are summarized in Table 6.1, where t is the crystal thickness in the direction of the x-ray beam, and μ is the linear absorption coefficient.

The value for ϵ measured after irradiation of the crystal with 10^{17} neutrons/cm^2 agrees well with the average value 0.960 ± 0.003 obtained from previous measurements on other copper crystals which had received the same dose.[4] The two values shown for R_H and ϵ at 500°C correspond to two crystal orientations which were related to

[5]W. V. Cummings, *J. Phys. Soc. Japan* **18**, suppl. 3, 189 (1963).

[6]J. Auleytner, *J. Phys. Soc. Japan* **18**, suppl. 3, 194 (1963).

[7]M. C. Wittels, F. A. Sherrill, and F. W. Young, Jr., *Phys. Letters* **5**, 183 (1963).

Table 6.1. Radiation Damage Effect on ϵ Values

Dose (neutrons/cm^2)	Annealing Temperature (°C)	μt	R_H (rads)	ϵ
			$\times 10^{-7}$	
10^{17}	Room temp to 300	59.3	1.11	0.961
10^{19}	Room temp	47.5	0.60	0.935
10^{19}	200	44.7	1.20	0.945
10^{19}	350	39.6	1.56	0.943
10^{19}	500	38.8	3.58	0.963
10^{19}	500	38.8	4.26	0.968

each other by a 180° rotation about an axis perpendicular to the plane of incidence. Thus, these values should be equal. The fact that they are unequal is not understood at present.

In any event, it is clear that the damage produced in this copper crystal by irradiation with 10^{19} neutrons/cm^2 has a significant and easily detectable effect on ϵ. The effect measured is surprisingly small in view of the extensive damage such a radiation dose is thought to produce.[8] At 200 to 350°C, only some of the damage was annealed out. However, at 500°C the crystal was restored to a degree of perfection equal to at least that which existed after the 10^{17} neutrons/cm^2 irradiation. The significance of the result obtained after the 500°C anneal, that ϵ was larger than 0.960, is not clear in view of the peculiar dependence of R_H on crystal orientation and is a subject of continuing investigation. Thus, although an irradiation dose of 10^{19} neutrons/cm^2 produces a measurable effect on ϵ, as yet we have not definitely established whether an irradiation dose of 10^{17} neutrons/cm^2 produces any effect.

Peak Widths. — Few quantitative data concerning the dependence on radiation damage of the half-widths of the anomalously transmitted x-ray beams in copper have been obtained. Measurements made with a double-crystal spectrometer, using two copper crystals which were irradiated with 10^{17} neutrons/cm^2 and which were oriented in the Laue geometry and in the parallel condition, have yielded half-widths for the (111) anomalous beams which vary between 4.5 and 6.5 sec, depending on the thickness of the second crystal. Both the magnitudes of these half-widths and their dependence on sample thickness are in semiquantitative agreement with theory. The half-widths of the (111) anomalous beam, obtained from the sample which received a 10^{19} neutrons/cm^2 irradiation dose, were not carefully examined after the different annealing temperatures. However, the data obtained indicate that within our experiment accuracy the half-width was not significantly influenced by this irradiation.

[8] M. J. Makin, A. D. Whapham, and F. J. Minter, *Phil. Mag.* 7, 285 (1962).

DEFECT IMAGES IN BORRMANN BEAM X-RAY TOPOGRAPHS OF NEARLY PERFECT COPPER CRYSTALS

(E)

R. M. Nicklow F. W. Young, Jr.
F. A. Sherrill

The program of investigating copper crystals by x-ray techniques has been broadened to include several additional topics. Preliminary results of these experiments, which were initiated to provide information on the defects in copper, have shown very interesting effects; these experiments are briefly summarized.

Contrast effects, associated with the defect images, are observed in all x-ray topographs. In general, the dislocation images are lines of less intensity than the background in both the transmitted and diffracted Borrmann beams. However, some dislocation images are lines of greater intensity in one or the other Borrmann beam, and always such an image is reversed in contrast in the other beam. This effect is demonstrated in Fig. 6.1. Such images, which are generally associated with dislocations lying near the exit surface of the x rays, are being investigated as a function of crystal thickness and of wavelength and angle of incidence of the beam.

Plates cut from large copper crystals of dislocation density $\lesssim 10^3/cm^2$ contained small defects which apparently were dislocation loops that had resulted from clustering and collapse of excess vacancies during cooling. These defects were ~50 to 100 μ in diameter, and their density was about $10^6/cm^3$, as shown in Fig. 6.2*a*. When the plates were annealed, so that the surface could act as a sink for the vacancies, the defects vanished (Fig. 6.2*b*).

Two instruments for making Bragg topographs have been constructed during the past year. One is of the conventional Berg-Barrett type, and the second consists of a double-crystal spectrometer, which uses the technique of Bonse. The second apparatus is particularly sensitive in revealing dislocations in the vicinity of external surfaces.

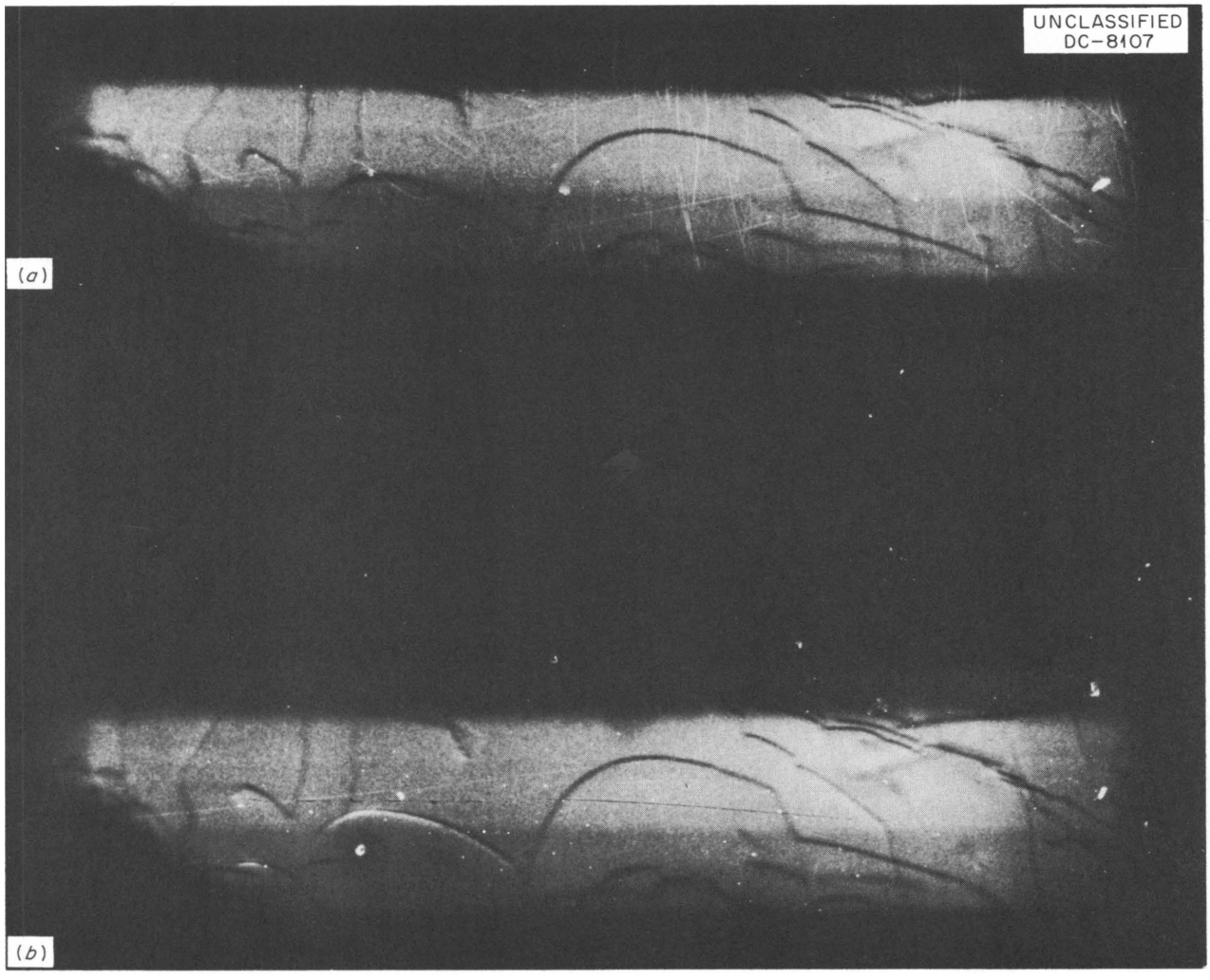

Fig. 6.1. Reverse Contrast in an X-Ray Topograph of a Copper Crystal. (*a*) Transmitted Borrmann beam. (*b*) Diffracted Borrmann beam.

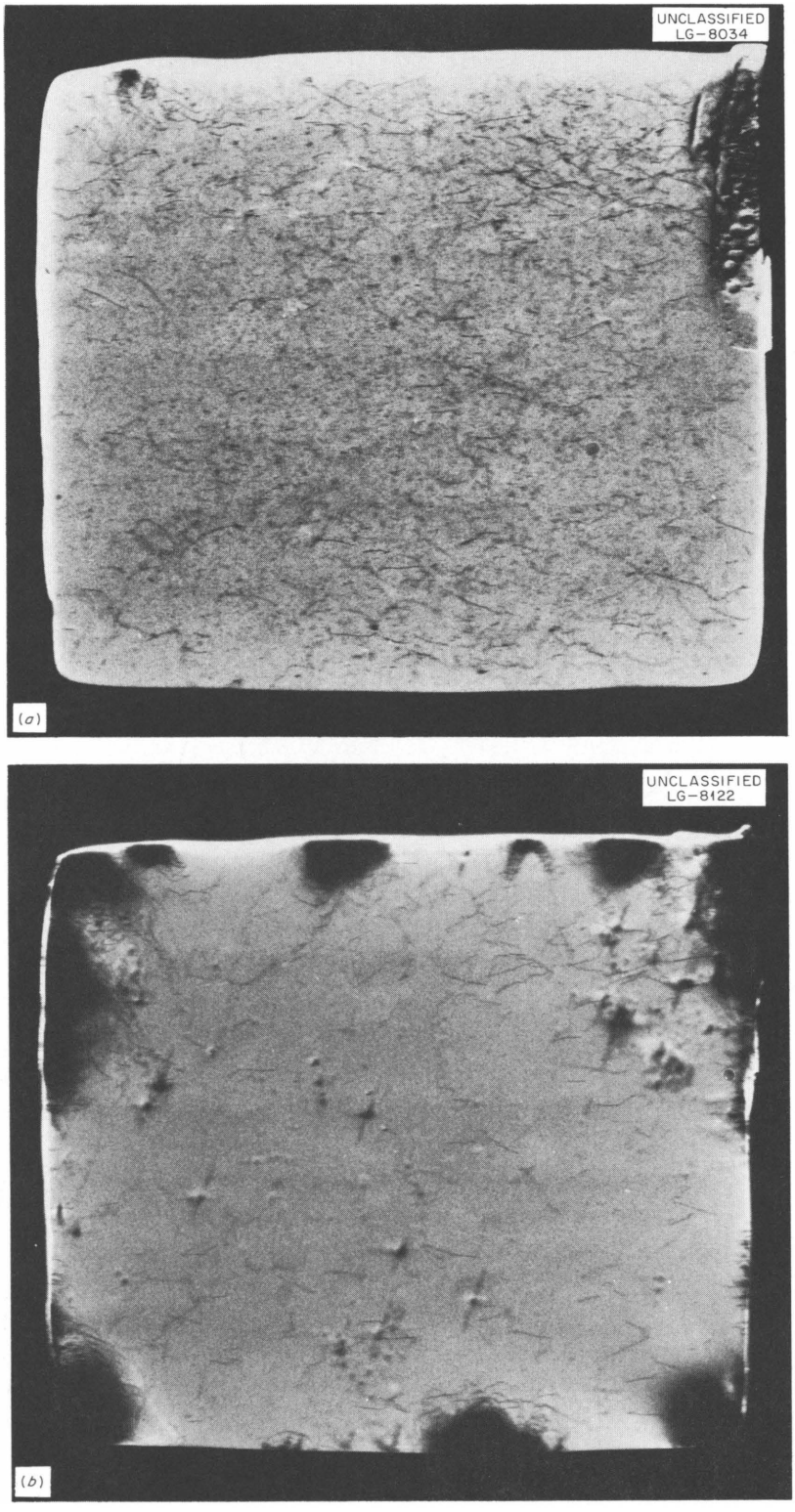

Fig. 6.2(*a*). X-Ray Topograph of a Copper Crystal Which Contains Large Dislocation Loops; (*b*) Same Crystal After Annealing.

7. Electron Microscopy

ELECTRON MICROSCOPE STUDIES OF FISSION FRAGMENT DAMAGE IN MOLYBDENUM TRIOXIDE[1]

(E)

T. S. Noggle

The damage caused by fission-fragment irradiation of molybdenum trioxide has been studied by high-resolution microscopy. Displacements of the 6.94-A fringes from (020) planes in the crystal in the vicinity of fission-fragment tracks indicate a decrease in volume of the disturbed region, while the absence of fringes in the tracks proper indicates modification of material. Dark-field observations confirm this latter point and suggest that the modified material is essentially amorphous. These results suggest that the observed damage arises primarily from thermal effects associated with the fission spike.

HIGH-RESOLUTION ELECTRON MICROSCOPY

(E)

T. S. Noggle

The studies on molybdenum trioxide have established the feasibility of high-resolution experiments on a more or less routine basis. Figures 7.1 and 7.2 are examples of (001) oriented MoO_3 crystals in which the 6.94-A fringes from (020) planes are resolved, and these figures illustrate the sensitivity for detection and identification of disturbances to the lattice. In Fig. 7.1, microprecipitates and dislocation dipoles present in the unirradiated material may be clearly seen and identified; whereas in Fig. 7.2, a fission track, which traverses a cleavage crack, is shown. Figure 7.1 serves to emphasize the importance of specimen preparation in studies of this type, because the background of structure in the material due to specimen-preparation procedures inhibits the identification of possible radiation-induced structures less prominent than the fission tracks.

The high-resolution technique is being extended to additional materials. An example of a promising system for radiation damage study is the ordered

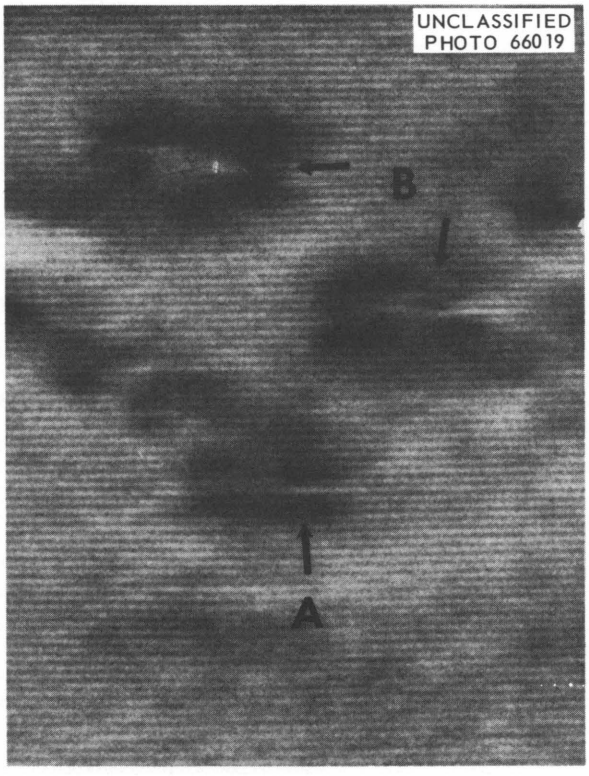

Fig. 7.1. Electron Micrograph of a Molybdenum Trioxide Crystal. Arrow labeled *A* indicates a coherent precipitate on the (010) planes in the crystals, while arrows labeled *B* indicate dislocation dipoles. 1,500,000X.

[1]Abstract of paper to be submitted for publication.

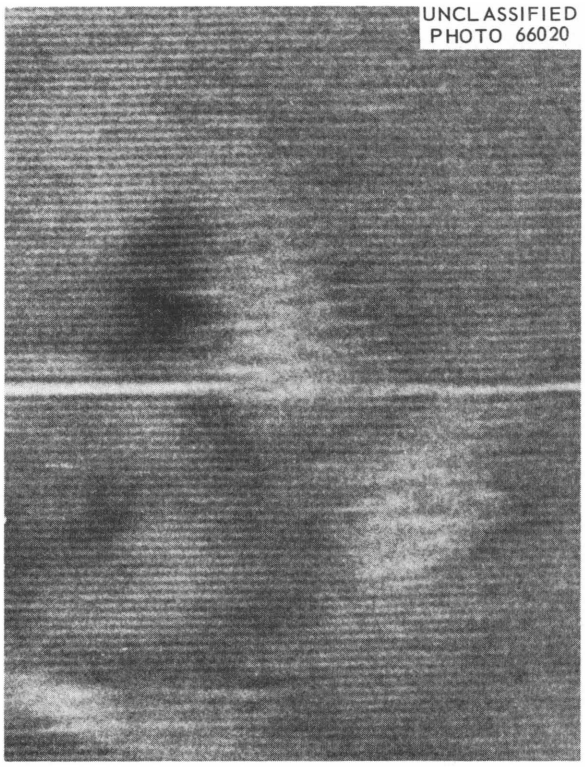

Fig. 7.2. Electron Micrograph of Fission-Fragment-Irradiated Molybdenum Trioxide Showing a Fission Fragment Track Which Has Made a Micro "Spot Weld" Across a Cleavage Crack. 1,500,000X.

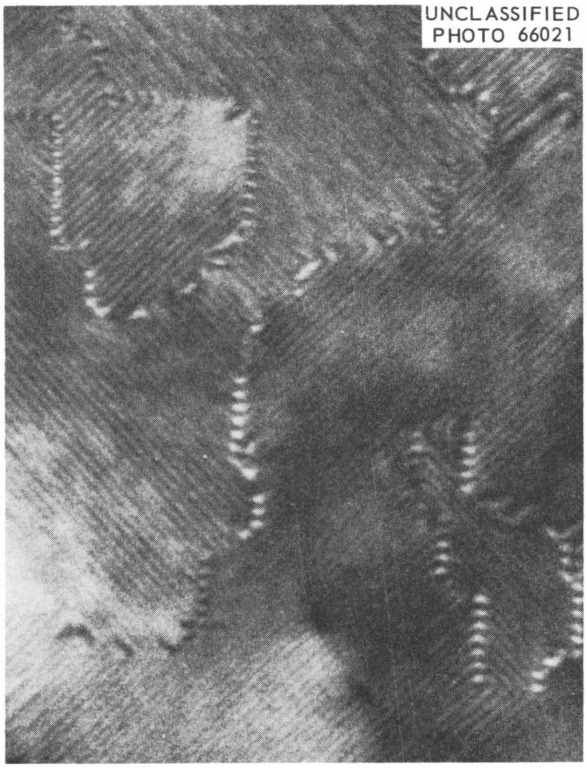

Fig. 7.3. Bright-Field Micrograph of Cu-Au II Showing the Regular Antiphase Structure of This Material. The periodicity of this structure is approximately 20 A. 600,000X.

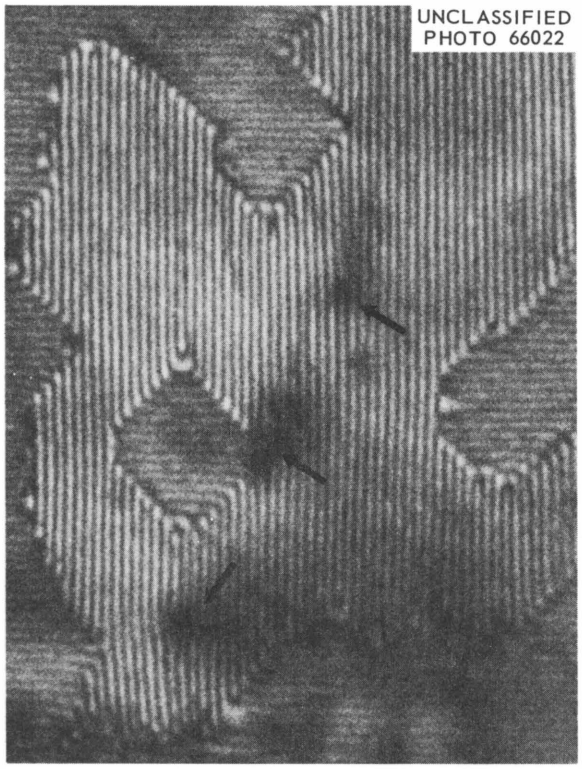

Fig. 7.4. Tilted-Beam Dark-Field Micrograph of Antiphase Domain Structure in Cu-Au II. Arrows indicate dislocation in film on which a boundary terminates. 600,000X.

alloy Cu-Au II, which has a regular antiphase domain structure that may be readily studied by high-resolution techniques.[2,3] Figures 7.3 and 7.4 show bright- and dark-field micrographs in which the approximate 20-A fringe patterns relate directly to the regular antiphase domain structure of this material.

PHONON SCATTERING BY THE *F*-CENTER ELECTRON[4]

(color centers; T)

Derek Walton

The scattering of phonons by the electron bound to the *F* center has been calculated by use of the conventional perturbation theory. The process is analogous to the scattering of light from an atom, with the electron making virtual transitions to an excited state. In this case the most important transitions are to a level lying above the first excited state. The scattering rate initially follows a Rayleigh law, being proportional to ω^4, where ω is the phonon frequency. However, as ω becomes larger than about half the Debye frequency, the scattering becomes weaker. By use of the results of this calculation it has been possible to account for most of the experimentally observed effect of *F* centers on the thermal conductivity.

---

[2]D. W. Pashley and A. E. B. Presland, *J. Inst. Metals* **87**, 419 (1959).

[3]A. B. Glossop and D. W. Pashley, *Proc. Roy. Soc. (London)* **A250**, 132 (1959).

[4]Abstract of paper to be published in the *Physical Review*.

8. Spin Resonance

RELATION BETWEEN E' CENTERS AND HYDROXYL BONDS IN SILICA[1]

(spin resonance; optical absorption; irradiation effects; E/T)

R. A. Weeks E. Lell[2]

The relation between the concentration of intrinsic paramagnetic states (the E' centers) of silica (silica glass) produced by irradiation and the concentration of OH^- ions in the silica was investigated by introducing OH^- ions into silica, initially free of these ions, in a controlled manner. Optical absorption and electron spin-resonance measurements were used to establish the relation. The results of the investigation showed that in synthetic silicas the concentration of E' centers varied linearly with the concentration of hydroxyl units, the sum of the concentrations of hydroxyl units and E' centers being constant. A "vacancy" model for the silica structure is proposed. In terms of this model the estimated saturation concentration of E' centers is of the same order as the concentration of "vacancies," $\sim 10^{20}/cm^3$. The saturation concentration of hydroxyl units is also $\sim 10^{20}/cm^3$. Silica made by fusing natural quartz crystals differs from the synthetic silica with respect to the optical bands and the electron spin-resonance spectra produced by irradiation. The effects of introducing hydroxyl units into natural quartz silica initially free of hydroxyl units are also different. These differences between natural quartz silica and synthetic silica are related to the models which have been suggested for the E' centers. The models suggested are in agreement with the results of other experiments.

[1]Abstract of published paper: *J. Appl. Phys.* **35**, 1932 (1964).

[2]Presently at Bausch & Lomb, Inc., Rochester, N. Y.

RARE-EARTH IONS IN THORIUM OXIDE: Yb^{3+} AND Er^{3+} [3]

(spin resonance; 2 to 4°K; E)

M. Abraham R. A. Weeks

The paramagnetic resonance spectra of Yb^{3+} and Er^{3+} in ThO_2 have been investigated at 10.5 kMc/sec over the temperature range 4 to 2°K. Sites of cubic symmetry as well as axial sites due to nearby charge compensation were observed. Both cubic spectra gave isotropic g values, with $g = 3.423 \pm 0.001$ for Yb^{3+} and $g = 6.752 + 0.005$ for Er^{3+}, and these values are in good agreement with the predicted values for Γ_7 doublets. Temperature variation showed that these were the lowest states. For either ion in dilute crystals, the line width was ≤ 0.5 gauss, and in heavily doped crystals the line width was 3 to 4 gauss. Nearby charge compensation in the Yb^{3+} case produces four sites of trigonal symmetry with [111] axes, while in the Er^{3+} case the preponderant axial site had tetragonal symmetry with three [100] axes. For Yb^{3+}, $g_{\parallel} = 4.772 \pm 0.002$ and $g_{\perp} = 2.724 \pm 0.001$, and one-third the trace of the g tensor was 3.406. For Er^{3+}, $g_{\parallel} = 3.462 \pm 0.003$ and $g_{\perp} = 7.624 \pm 0.005$, and one-third the trace of the g tensor was 6.24. The line widths obtained for the axial sites were broader than those for cubic sites and varied with angle. Evidence for macroscopic crystalline imperfections was also found.

[3]Abstract of paper to be submitted for publication.

ATOMIC HYDROGEN IN IRRADIATED QUARTZ[4]

(spin resonance; gamma and election irradiation; E/T)

R. A. Weeks M. Abraham

Room-temperature irradiation of synthetic quartz with $\sim 10^{18}$ electrons/cm^2 (1.5 Mev) followed by an irradiation with ^{60}Co gamma rays ($\sim 10^7$ r) at 78°K has produced a paramagnetic center which has been identified as atomic hydrogen. The hyperfine interaction constant (A = 1453 Mc) is larger than that for the free atom. In this respect it is similar to atomic hydrogen in CaF_2. The isotropic g = 2.0021 ± 0.005 was calculated from the Breit-Rabi equation. The line width of 0.1 gauss was presumed to be due to inhomogeneities of the laboratory magnetic field. This narrow line width permitted the observation of an anisotropy in the electron-proton hyperfine interaction of 0.75 gauss with an isotropic part of 521.3 gauss. An anisotropy of $g < 0.0002$ was also detected. Hyperfine interactions with nearby silicon sites occupied by ^{29}Si were utilized in constructing a tentative model of the center.

SPIN-1 STATES OF DEFECTS IN QUARTZ

(spin resonance; gamma and election irradiation; temperature dependence; E/T)

R. A. Weeks M. Abraham

The irradiation of quartz crystals (Clevite, General Electric, and Sawyer specimens) by electrons (1.5 Mev at 1.5 μa/cm^2 for 6 hr) followed by an irradiation with ^{60}Co gamma rays (10^7 r) at 78°K produced many lines centered at g = 2.002, in addition to the atomic hydrogen (discussed in the previous section), the E_1', E_2', E_4',[5,6] and "Al"[7] centers. These lines were not produced when the gamma-ray irradiation was made at ~300°K. A warm-up to 300°K after the 78°K irradiation reduced the intensity by $\sim \frac{1}{2}$, but when the specimens remained at 300°K for a week, there was no further decrease in the intensity. These lines disappeared when the specimens were irradiated with light from a 4-w mercury lamp at either 78 or 300°K.

These lines could be separated into three sets of lines with an intensity ratio of approximately 3:2:1. The orientation dependence of the most intense (intensity 3) set was measured for rotation of the magnetic field about a twofold crystal axis (Fig. 8.1) and a [100] crystal axis (Fig. 8.2). The curves in Fig. 8.1 for rotation about a twofold axis show that 6 lines were present in the spectrum of the set. The curves in Fig. 8.2 for rotation about a [100] crystal axis show that the 6-line set has become a 12-line set.

From the orientation dependence and the number of lines observed for the two different rotation axes, a spin Hamiltonian of the form

$$\mathcal{H} = \beta \vec{H} \cdot g \cdot \vec{S} + D[S_z^2 - \tfrac{1}{3} S(S+1)] + E(S_x^2 - S_y^2)$$

was used in fitting the curves. The values for the various terms were g = 2.002 ± 0.001, S = 1, D = 192.5 ± 0.5 gauss, and $E \approx 0.01\ D$; and there were six sites per unit cell for the paramagnetic center. The axis of one of the sites made an angle θ = 51° with respect to the [00.1] direction (the threefold axis) and an angle ϕ = 7° with respect to the [10.0] direction in the basal plane. The axes for the remaining five sites could be obtained by using the symmetry operators of the crystal, that is, a 120 and 240° rotation about the threefold axis plus reflections through the basal plane. The orientation of the E term relative to the crystal axes has not been determined, although the differences in the splitting when the field was perpendicular to the axes of each of the sites have given an estimate of its magnitude.

Jung and Newell[8] have observed paramagnetic states in silicon which are S = 1 states. In silicon these states result from an exchange interaction of two nearby $S = \frac{1}{2}$ states. They have shown that if two electrons forming the S = 1 state have their orbital centered on a particular silicon atom, the

[4]Abstract of paper submitted for publication.

[5]R. A. Weeks and C. M. Nelson, *J. Am. Ceram. Soc.* **43**, 401 (1960).

[6]R. A. Weeks, *Phys. Rev.* **130**, 570 (1963).

[7]J. H. E. Griffiths, J. Owen, and I. M. Ward, *Rep. Conf. Defects Crystalline Solids, London, 1954*, p. 81 (1955).

[8]W. Jung and G. S. Newell, *Phys. Rev.* **132**, 648 (1963).

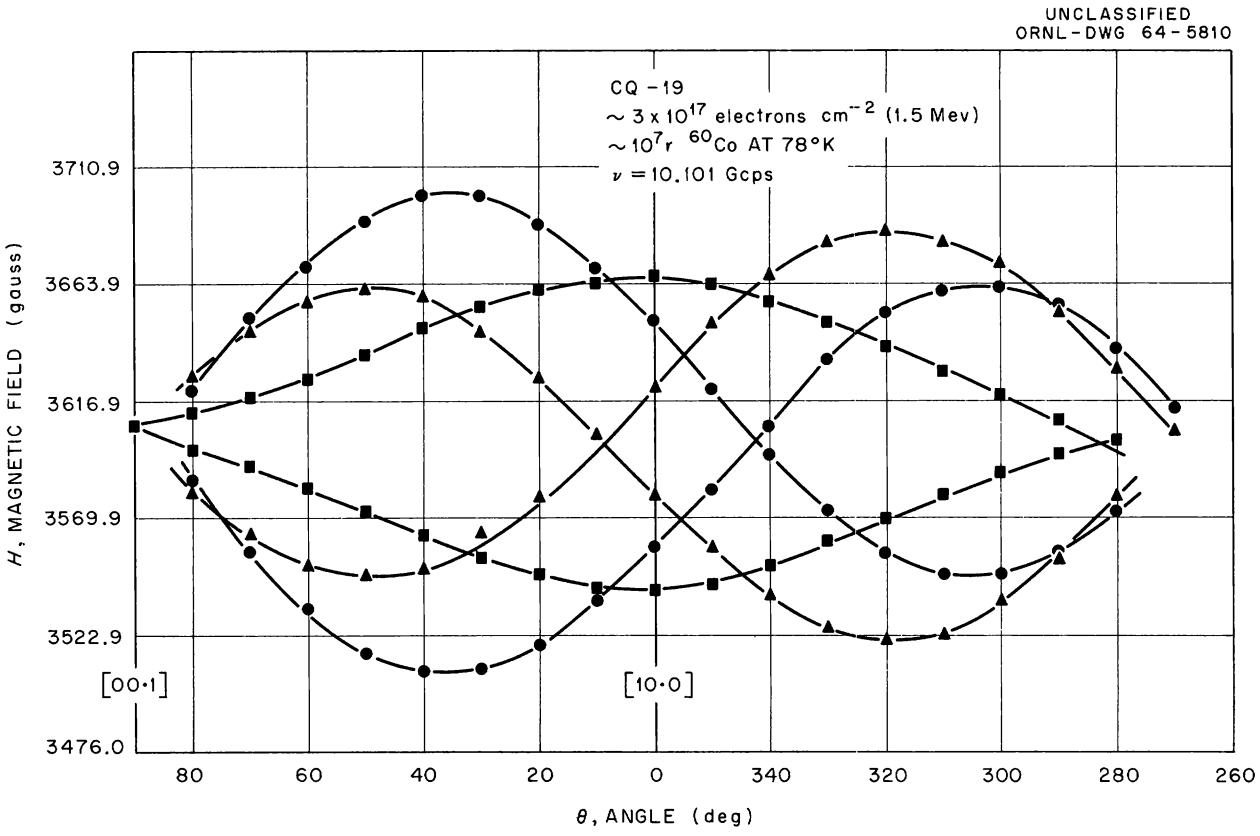

Fig. 8.1. Orientation Dependence of the Most Intense (Intensity 3) Set of Spin 1 Centers in Synthetic Quartz. The field was rotated about a crystal twofold axis. Each data point is the midpoint of two lines of equal intensity whose separation varied from 0 to 2 gauss. (This doubling of the lines for some angles is due to a small deviation of the crystal twofold axis from the rotation axis.) Each "line" was followed as the field was rotated.

magnitude of D is about 2000×10^{-4}/cm, while for two $S = \frac{1}{2}$ states on two nearby silicon atoms the D would be much smaller.

Since the quartz crystal is composed of tetrahedrally coordinated silicon ions, the estimates of Jung and Newell for silicon are applicable if the electrons forming the $S = 1$ state are in silicon orbitals. A comparison of the g (2.002) of the $S = 1$ states with the g (~2.001) of the $S = \frac{1}{2}$ states (E_1' and E_2' centers) shows that they are almost the same. The similarities of the g's lend support to the idea that silicon orbitals are involved. If we assume that the $S = 1$ state arises from a dipole-dipole interaction of two $S = \frac{1}{2}$ states on two silicon atoms, then an estimate of the magnitude of D for the nearest-neighbor silicon-silicon distance (~3.2 A) and the next-nearest-neighbor distance (~4.2 A) can be made. With a 3.2-A separation, $D \approx 600 \times 10^{-4}$/cm, and with a 4.2-A separation, $D \approx 200 \times 10^{-4}$/cm. This last value is in reasonable agreement with the value observed for the $S = 1$ state.

Although the available data obtained for the $S = 1$ states are not sufficient for a detailed model, several tentative conclusions can be drawn: (1) the $S = 1$ state is not associated with any of the known impurities in the quartz crystals; (2) the $S = 1$ state is the result of a dipole-dipole interaction of two nearby electrons in $S = \frac{1}{2}$ states; (3) these electrons are located in incomplete silicon orbitals on next-nearest-neighbor silicon ions; and (4) the necessity of electron bombardment followed by a low-temperature gamma-ray irradiation for the production of these centers indicates

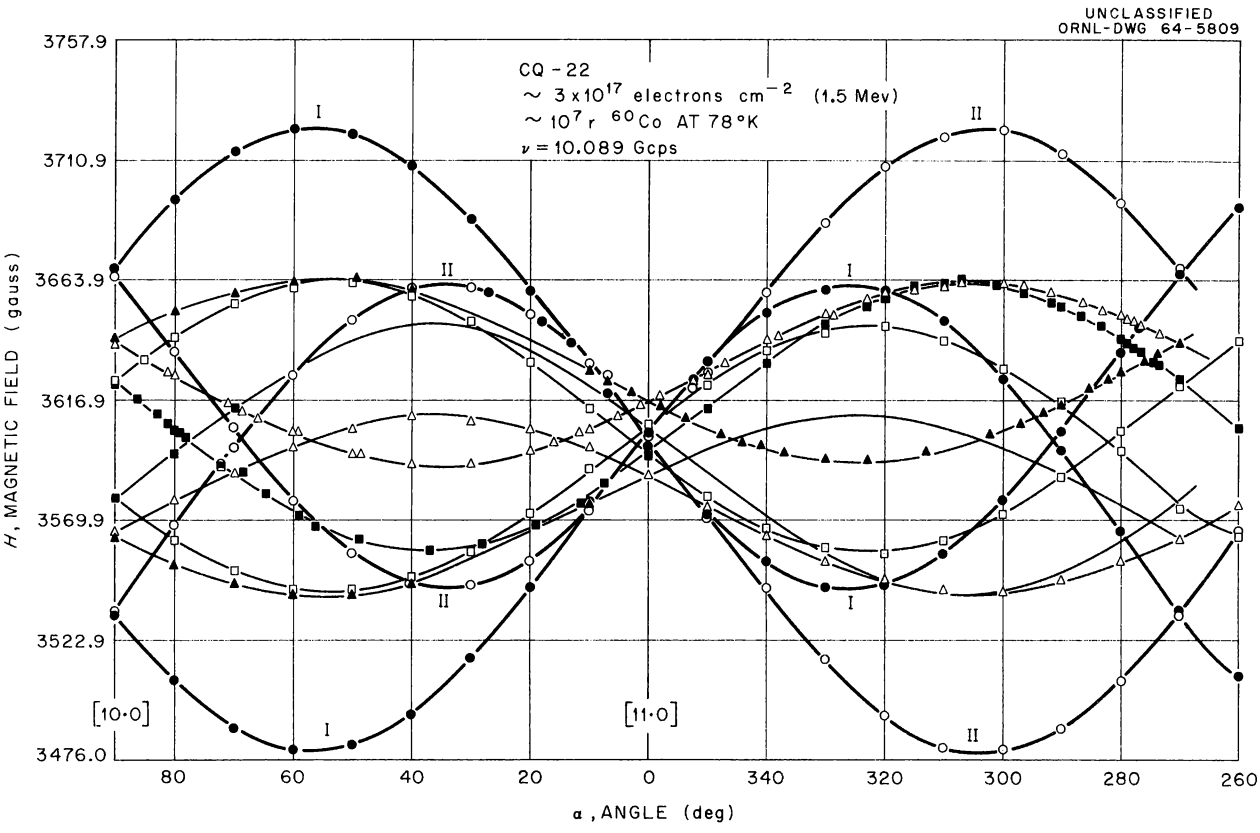

Fig. 8.2. Orientation Dependence of the Most Intense (Intensity 3) Set of Spin 1 Centers for Rotation About a [100] Crystal Axis. Two techniques were used in measuring the line positions: (1) each line was followed as the field was rotated, and its position was measured at each angle; and (2) at each angle, all the lines in the set were measured. The differences between the two sets of data were less than the random errors in each set. All curves are experimental curves. A good fit was obtained between curves I and II and curves that were calculated by assuming $D = 192.5$ gauss and $E \approx 0$.

that atom displacements are necessary and that the temperature-dependent distribution of electrons and holes in the available traps is metastable. If we assume that these conclusions are valid, the $S = 1$ center is, therefore, a different state of the E_1' center.

PARAMAGNETIC CENTERS IN GeO_2 GLASS PRODUCED BY ELECTRON AND GAMMA-RAY IRRADIATION[9]

(spin resonance; annealing effects; E)

R. A. Weeks T. Purcell

Paramagnetic centers produced in germanium dioxide glass by ^{137}Cs gamma rays and by 1.5-Mev electron irradiations at room temperature have been observed by electron spin-resonance techniques at ~78°K. The most intense line observed in both gamma and electron irradiations had a line shape characteristic of the powder pattern for a paramagnetic center with an axially symmetric g tensor. Assuming the center to be axially symmetric, then $g_\perp = 1.9957$ and $g_{||} = 2.0016$. The concentration of this center was measured as a function of increasing dose for both electron and gamma-ray irradiations. The concentration was a monotonically increasing function of dose in both cases. The maximum concentration achieved by electron irradiation was approximately 2.5×10^{18} centers/cm^3.

[9]Abstract of ORNL-3625; paper also to be submitted for publication.

On the basis of optical properties, the high spin concentration, and the estimated impurity content, it was assumed that this center was intrinsic to the GeO_2 glass. Similarities of this center to an intrinsic center, E_1', observed in silica, are discussed. A tentative model for the paramagnetic center in the GeO_2 glass is that of an electron trapped in an uncompleted germanium bonding orbital. Powdered crystals of the hexagonal and tetragonal phase were also irradiated under similar conditions. The similarity of the line shapes in the powdered crystals of the hexagonal phase and in the glass was interpreted as an indication that the randomly oriented GeO_4 tetragonal groups of the glass bore some relation to the hexagonal phase of the crystalline material.

Annealing of the electron-irradiated glass produced another center similar to the one observed after irradiation. The $g_{\parallel}$ value for these two centers was approximately the g value of the free electron; however, $g_{\perp}$ of the center produced by annealing was 2.0084. Other centers were also observed in the GeO_2 glass.

9. Superconductivity and Low-Temperature Physics

MAGNETIZATION STUDIES OF TYPE II SUPERCONDUCTORS

(Pb-Tl alloys; 4.2°K; E)

S. T. Sekula[1] R. H. Kernohan
P. G. Huray J. B. Sanders[2]

One of the characteristics of type I (soft) superconductors is the complete exclusion of magnetic flux up to a certain critical field. Beyond this value of field, magnetic flux penetrates the material completely. In type II superconductors, flux is at first excluded; but eventually it penetrates the material gradually, and penetration becomes complete at an upper critical field much higher than that found in type I superconductors. The last vestiges of superconducting current supposedly disappear at the upper critical field, H_{c2}.

We have studied the magnetization characteristics of a series of lead-rich Pb-Tl alloys fabricated by the Metals and Ceramics Division. These alloys are type II superconductors which bear a close analogy to the commercially important Nb-Zr and Nb_3Sn high-field superconductors. However, the temperatures, currents, and magnetic fields required for studying these Pb-Tl alloys are much more easily attained than those for the high-field superconductors.

Magnetization measurements of our alloy samples were made ballistically at 4.2°K. The samples were bundles of 20 cold-drawn wires, each 0.020 in. in diameter and 1 in. long. Typical magnetization curves for one of the alloys are shown in Fig. 9.1. It is a characteristic of cold-worked type II superconductors that the area under the solid curve (measured with increasing magnetic field) is larger and that there is a greater hysteresis effect than for the same material in the annealed condition. It may also be noted that the upper critical field, H_{c2}, is independent of the amount of annealing. On the other hand, the field of first flux penetration, H_{c1}, where the initial portion of the curve first deviates from a straight line, drops slightly for annealed samples. A third quantity, the thermodynamic critical field, H_c, is obtained by integrating under the solid curve; H_c is related to the difference in free energy between the normal and superconducting states.

The relationships between the above critical fields have been analyzed by Berlincourt and Hake[3] and by Goodman,[4] using the fundamental Ginzburg-Landau-Abrikosov-Gorkov theory. The ratio of the two critical fields is defined as

$$h_2 = H_{c2}/H_c = \sqrt{2K}\,. \tag{1}$$

However, K may be expressed as the sum of two terms,

$$K = K_0 + K_1\,. \tag{2}$$

The first term on the right, K_0, involves only the electronic structure of the pure metal. It is related to the parameters reserved for type I superconductors and is usually small compared with the second term, K_1. The latter term involves the electron mean free path and is given by Gorkov as

$$K_1 = \frac{e\rho_n\gamma^{1/2}}{\pi^3 k}\sqrt{\frac{21\zeta(3)}{2\pi}}, \tag{3}$$

[1]On leave of absence: Middle East Technical University, Ankara, Turkey.

[2]Co-op student from the University of Tennessee, Knoxville.

[3]T. G. Berlincourt and R. R. Hake, *Phys. Rev.* 131, 140 (1963).

[4]B. B. Goodman, *IBM J. Res. Develop.* 6, 63 (1962).

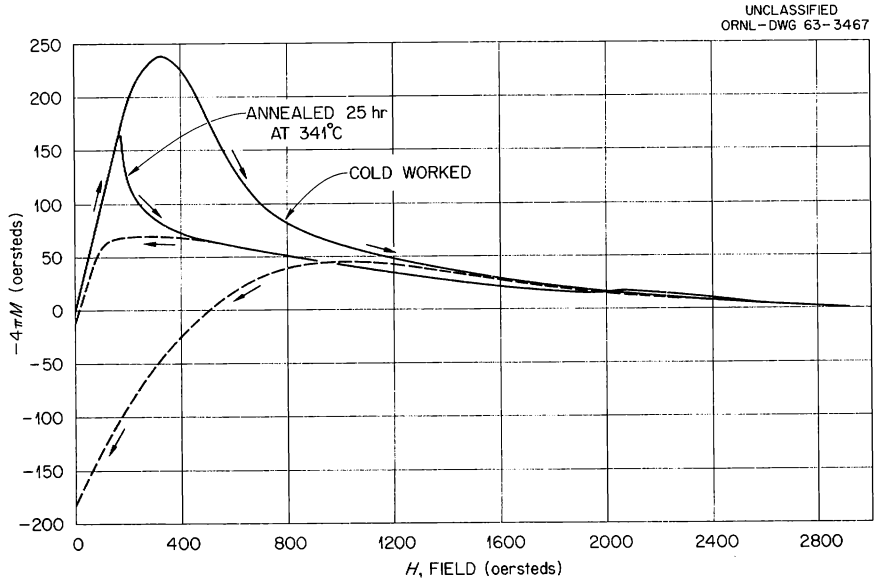

Fig. 9.1. Magnetization of Pb–27% Tl Alloy at 4.2°K.

where ρ_n is the normal-state resistivity, γ is the temperature coefficient of electronic specific heat per unit volume, and $\xi(3) = 1.202$. In practical units, Eq. (3) becomes

$$K_1 = 7.53 \times 10^3 \gamma^{1/2} \rho_n . \qquad (4)$$

It is estimated that for lead, $K_0 \cong 0.4$ and $\gamma = 1713$ ergs cm^{-3} deg^{-2}. Assuming that these values would be about the same for Pb-Tl alloys, we can combine expressions (1), (2), and (4) to obtain

$$H_{c2}/H_c = 0.56 + 0.44\rho_n , \qquad (5)$$

where ρ_n is in microhm-centimeters.

The critical fields obtained from our magnetization curves taken at 4.2°K of fully annealed specimens are given in Table 9.1 along with measured values of the critical temperature for each alloy and normal resistivity values measured just above these critical temperatures.

The agreement of our data with the theoretical value given by expression (5) is shown in Fig. 9.2 (for type II superconductors $H_{c2}/H_c > 1$). One of the important factors in the determination of H_c is the quality of anneal. All samples were annealed for 25 hr within 10°C of their melting points in a helium atmosphere. Another factor is the difficulty of determining H_{c2}, inasmuch as the

Table 9.1. Experimental Data on Pb-Tl Alloys

Thallium Content (%)	H_{c2} (oersteds)	H_c at 4.2°K (oersteds)	$\frac{H_{c2}}{H_c}$	ρ_n (microhm-cm)	T_c (°K)
0.7	590	533	1.11	0.35	7.03
5.3	1060	563	1.88	2.85	6.90
7.4	1205	550	2.19	4.06	6.89
16.8	2250	483	4.66	9.45	6.64
26.9	2900	450	6.44	14.9	6.31
49.0	2200	223	9.87	21.9	5.54

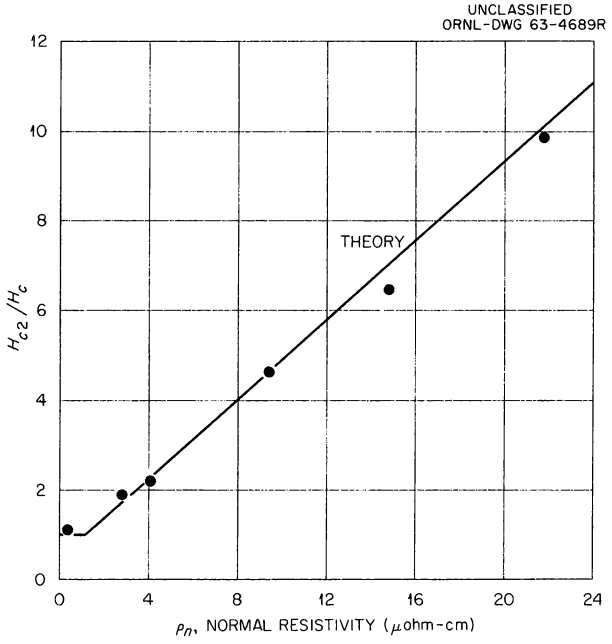

Fig. 9.2. Critical Field Ratio vs Normal Resistivity for Pb-Tl Alloys. Points are experimental results. Line is derived from the Ginsburg-Landau-Abrikosov-Gorkov theory.

magnetization curve approaches the axis asymptotically. However, the agreement of our results with theory is excellent and provides verification of the work done by Livingston[5] and by Bon Mardion, Goodman, and Lacaze[6] on other type II superconductors.

UPPER CRITICAL FIELDS IN TYPE II SUPERCONDUCTORS

(Pb-Tl alloys; E)

R. H. Kernohan P. G. Huray J. B. Sanders[2]

We have investigated the current-carrying capacity of 0.020-in.-diam wire specimens of the Pb-Tl alloys described in the previous section as a function of the longitudinal external magnetic field in order to study the upper critical fields in these alloys. A typical example of one of these experiments is shown in Fig. 9.3. The transition from the superconducting to the normal state was abrupt and sharp at currents above 1 or 2 amp (about 500 to 1000 amp/cm^2). However, at lower currents the transition was more gradual, and in order to attempt to establish an upper critical field, a value of 1% of the normal resistance was used as an arbitrary criterion to indicate the superconducting-to-normal transition point.

Extrapolation of the nearly vertical part of the curve in Fig. 9.3 yields a value of the upper critical field, H_{c2}, very nearly the same as that obtained by magnetization measurements (shown in Fig. 9.1 and Table 9.1) for Pb–27% Tl. The value of H_{c2} for all alloys determined from critical-current measurements agrees well with that determined from magnetic measurements. This can be seen by comparing the data in Table 9.2 with those in Table 9.1.

The critical current at zero field never exceeded the value which we measured for pure lead (68 amp). In nearly every alloy the critical-current curve was fairly flat at low values of field, and in some cases there was a slight peak in the value of the critical current at low values of field.

The gradual transition of superconducting alloys from zero resistance to normal resistance in specimens parallel to an external magnetic field greater than H_{c2} was observed by Druyvesteyn and van Oijen.[7] Whereas H_{c2} is the critical field at which

[5]J. D. Livingston, *Phys. Rev.* **129**, 1943 (1963).

[6]G. Bon Mardion, B. B. Goodman, and A. Lacaze, *Phys. Letters* **2**, 321 (1962).

[7]W. F. Druyvesteyn, D. J. van Oijen, and T. J. Berben, *Rev. Mod. Phys.* **36**, 58 (1964).

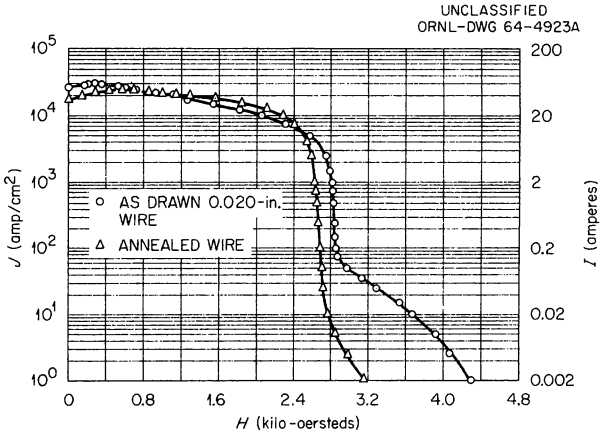

Fig. 9.3. Critical Current Density vs External Field for Pb–27% Tl Alloy at 4.2°K.

Table 9.2. Upper Critical Field for Pb-Tl Alloys at 4.2°K

Thallium Content (%)	H_{c2} (oersteds)	H_{c3} (oersteds)	H_{c3}/H_{c2}
0.7	530	775	1.46
5.3	1030	1782 ±22	1.730
7.4	1195	2043 ±15	1.710
16.8	2200	3740 ±17	1.700
26.9	2860	4810 ±15	1.682
49.0	2220	3710 ±33	1.667

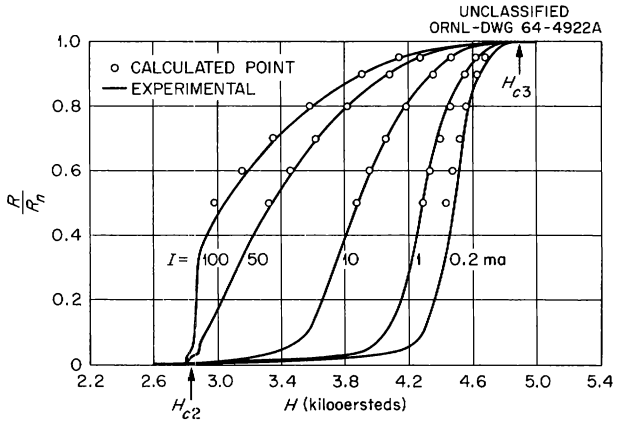

Fig. 9.4. Resistive Transition for Pb–27% Tl Alloys at 4.2°K. Wire diameter = 0.020 in.; R_n = 0.0245 ohm.

some trace of normal electrical resistance first appears, they postulated that H_{c3} may be defined as the upper critical field at which the last trace of superconductivity disappears. Saint-James and de Gennes[8] have shown that under certain limiting conditions a solution of the Ginzburg-Landau equation can be found that indicates the existence of a thin superconducting sheath near the surface of a sample which will be stable at fields greater than H_{c2}. The new upper critical field was calculated to be $H_{c3} = 1.695H_{c2}$ for ideal (defect-free) type II superconductors in which current flow was parallel to the magnetic field.

Our attention was next focused on the resistive transition from the superconducting to the normal state for the above series of Pb-Tl alloy wires. Instrumentation was devised to record the transition on an *X-Y* recorder, and the transition was measured for the wires as drawn and for the wires annealed within 10°C of their melting points. An example of the resistive transition at various currents for a typical well-annealed wire specimen is shown in Fig. 9.4. Values of H_{c3} could be estimated from the curves, but more consistent values were obtained by using an empirical equation of the form

$$H = \gamma \frac{1}{\text{slope}} + H_{c3} ,$$

where γ and H_{c3} are constants. Data for this equation were taken at constant R/R_n from the upper halves of the curves, and the resulting plot of these data yielded the values of H_{c3}. The values obtained in this way appear to be more consistent than values of H_{c2} that are merely estimated from magnetization curves or critical-current curves. The results for all the well-annealed Pb-Tl alloys are shown in Table 9.2; they indicate an H_{c3}/H_{c2} ratio very close to that predicted by Saint-James and de Gennes. The 0.7% Tl alloy is an exception and indeed may be so dilute that it may be considered almost a type I superconductor. Similar work by other authors has not approached this degree of accuracy.[9] It is interesting to note in Table 9.2 that as the thallium content of the annealed specimens increases, this ratio decreases. Our data are not sufficiently accurate to indicate that this is a significant trend. Resistive transition curves of the as-drawn wire samples did not indicate a very precise value for H_{c3}, and the H_{c3}/H_{c2} ratio ranged from 2 to 2.5.

Resistive transition curves between H_{c2} and H_{c3} were taken at different temperatures for the Pb–27% Tl wire specimen. The curves were all similar in shape to those in Fig. 9.4, and upon analysis they also gave H_{c3}/H_{c2} ratios in excellent agreement with theory. The results are given in Table 9.3. Many more curves than those

[8]D. Saint-James and P. G. de Gennes, *Phys. Letters* 7, 306 (1963).

[9]G. Bon Mardion, B. B. Goodman, and A. Lacaze, *Phys. Letters* 8, 15 (1964).

Table 9.3. Upper Critical Field Values for Annealed Pb–27% Tl Alloy

Measurement Temperature (°K)	H_{c2} (oersteds)	H_{c3} (oersteds)	H_{c3}/H_{c2}
5.00	1850	3106 ±15	1.679
4.20	2860	4810 ±15	1.682
3.20	3960	6746 ±30	1.704
2.18	4950	8339 ±22	1.685
1.77	5250	8900 ±45	1.695

shown in Fig. 9.4 were made at different currents (from 200 to 0.002 ma).

With these data on well-annealed materials, it was desirable to determine if an empirical expression could be found relating H_{c2}, H_{c3}, R/R_n, and I. Previous investigators[9,10] have pointed out that such a relationship has not yet been found; however, they have noticed an approximate relationship between the external field, H, and the cube root of the current. It was found that for any particular value of R/R_n greater than about 0.5, the field H could be expressed approximately as a function of current in the form $H = \beta(I^{1/3} + b) + H_{c3}$, where β and b are constants. Using this expression and the experimentally determined evidence that the constant β may be expressed as the $\frac{1}{n}$th power of the normalized resistance R/R_n in the form $1 - R/R_n = \omega\beta^n$, it was shown that

$$1 - R/R_n = a\left(\frac{H_{c3} - H}{I^{1/3} + b}\right)^n$$

could represent the shape of any one of the resistive transition curves for $R/R_n > 0.5$. One may normalize the scale of the magnetic field between H_{c2} and H_{c3} by the factor

$$h = \left(\frac{H_{c3} - H}{H_{c3} - H_{c2}}\right),$$

in which case the equation for the shape of the curves becomes

$$1 - R/R_n = \omega\left(\frac{h}{I^{1/3} + b}\right)^n,$$

where $\omega = a(H_{c3} - H_{c2})^n$. By use of the curves for the Pb–27% Tl alloy at different temperatures, the following values of constants were found: $n = 2.29 \pm 0.04$, $\omega = 24.16 \pm 0.38$, and $b = 0.465 \pm 0.018$ (I in milliamperes). The points shown in Fig. 9.4 were calculated from the equation with the above constants. The values of the constants for the other alloys measured at 4.2°K were also calculated. The exponent n was in the 2.1 to 2.5 range for all but one of the alloys. The other constants varied over a wider range and may be sensitive to the state of anneal and other parameters. It is obvious that the empirical equation developed above is inadequate to describe the complete physical picture.

EFFECT OF NEUTRON IRRADIATION ON MAGNETIC PROPERTIES OF Fe-Ni ALLOYS[11]

(annealing effects; E)

A. I. Schindler[12] R. H. Kernohan
J. Weertman[13]

Hysteresis loop measurements were conducted on several commercial Fe-Ni alloys during neutron irradiations at 90°K and at temperatures up to 175°C, in both zero and saturating magnetic fields. Isochronal annealing tests were also performed on the alloys after irradiation. The low-temperature irradiation results indicated that magnetic properties are affected, not by the point defects themselves, but by their motion and eventual disposition. The radiation-induced changes appeared in many ways similar to those observed in these alloys upon magnetic annealing.

Experiments on the alloys at temperatures from 70 to 175°C in a saturating magnetic field showed that the activation energy of the radiation-induced

[10]P. R. Doidge, *Phil. Trans. Roy. Soc. London* A248, 553 (1956).

[11]Abstract of paper to be published in the *Journal of Applied Physics*.

[12]U.S. Naval Research Laboratory, Washington, D.C.

[13]Northwestern University, Evanston, Ill.

process was 0.3 ev. In all cases the radiation-induced changes were annealed out at temperatures below the usual ordering temperature for Ni_3Fe. This recovery process appeared to be dependent upon the state of the magnetization of the sample.

HELIUM-3 CRYOSTAT FOR THERMAL CONDUCTIVITY MEASUREMENTS

Derek Walton

Introduction

During the past year a cryostat has been designed and constructed for the measurement of thermal conductivities in the range from 0.3 to 4.2°K. The purpose of these measurements is the study of the effect of phonon scattering by crystalline defects on the lattice thermal conductivity. Studies in this temperature range have the advantage that the effects of dispersion are negligible and also that the conductivity is, to a good approximation, determined entirely by the phonon interaction with the boundaries of the crystal and the defects it contains.

In designing the cryostat an attempt was made, of course, to design for a limiting temperature as low as possible. This was accomplished by designing for the maximum practical pumping speed on the ^3He.

Design

The cryostat is shown schematically in Fig. 9.5. Basically, it is of metal construction surrounded by an ^4He bath. The bath is contained in a glass Dewar with an integral liquid-nitrogen jacket.

The cryostat itself is enclosed in an evacuated copper cylinder with a demountable Wood's-metal joint. It consists of another small container into which ^4He liquid can enter through the valve shown. The valve can then be closed and the liquid pumped until a temperature of about 1°K is reached, which is sufficient to condense the ^3He. The valve is a piece of brass with a $\frac{1}{16}$-in. hole leading to the ^4He pumping line; the valve can be closed by a pointed stainless steel rod driven into the hole. With this arrangement a seal, tight to a helium leak detector, is readily obtained. The container has a volume of about 80 cm^3, which is sufficient liquid for many hours of operation.

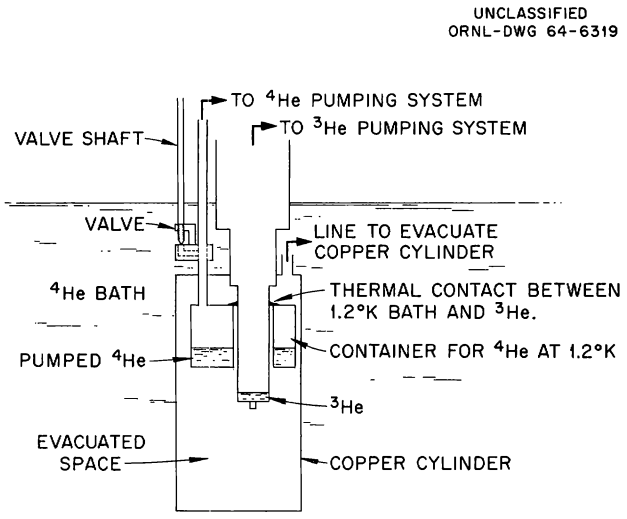

Fig. 9.5. Schematic Drawing of Cryostat.

In designing the ^3He part of the system, the factor which controls the available pumping speed is the tubulation at the room-temperature end of the system. Therefore, tubing of the largest practical diameter was used at this point, and $2\frac{1}{2}$ in. was felt to be a reasonable maximum. The mass of gas flowing through a tube of radius r is[14]

$$Q_m = \frac{4}{3}\sqrt{\frac{2\pi}{R}}\, r^3 \frac{d}{dx}\left(\frac{P}{\sqrt{T}}\right),$$

where P = pressure, T = temperature, x = distance along the tube, and R = gas constant. At the other end of the ^3He pumping line, where the liquid ^3He will collect, it is desirable to keep the diameter of the tubulation small to minimize the heat leak to the liquid; but if it is too small, it will also impede the gas flow in spite of the low temperature. Thus, probably the best way to optimize the design is to require that dP/dx be the same at both ends. Since the ratio of the

[14] E. H. Kennard, *Kinetic Theory of Gases*, p. 331, McGraw-Hill, New York, 1938.

temperatures at the ends is 1000, the ratio of the radii should be $(r_{hot}/r_{cold})^3 = (1000)^{1/2}$ so that $(r_{hot}/r_{cold}) \sim 4$. Therefore, $\frac{3}{4}$-in.-diam tubing with a 0.006-in.-thick wall was chosen for the lower end; for easiest assembly a short length of $1\frac{1}{4}$-in.-diam tubing connected it to the $2\frac{1}{2}$-in. main pumping line.

In determining the lengths of the tubes in the three sections of the pumping line, it was, first of all, obviously desirable to make the $2\frac{1}{2}$-in.-diam tube as long as possible. Second, in considering the $\frac{3}{4}$-in. tube, it was apparent that the pumping speed varied inversely as the length; but the heat conducted down the tube also varied inversely as the length. Thus, the length of this tube to a first approximation would not affect the ultimate temperature attained, because the major heat leak would be due to conduction down the walls of the tube and through the ^{3}He gas contained therein. However, the heat leak controls the time available for an experiment, and this tube was made 4 in. long, which yielded a combined heat flow down the walls and through the gas of about 50 μw. With reasonable care it is possible to reduce other sources of heat to a figure well below this one.

The gas-handling system for the ^{3}He is of standard design: the pumping system for the ^{3}He consists of an oil diffusion pump, with a speed in excess of 100 liters/sec, backed by a mechanical forepump with a specially sealed shaft to prevent leakage. In addition, a reservoir must be provided for the ^{3}He, and in this case it is just the small storage vessel in which the gas was shipped. With this system the pumping speed at the top of the $2\frac{1}{2}$-in. tube is of the order of 100 liters/sec. With a heat input of 50 μw to the ^{3}He, then, the pressure should be of the order of 10^{-4} mm, which should correspond to a temperature in the neighborhood of 0.25°K.

Performance

From the rate of pressure rise in the ^{3}He reservoir while the ^{3}He liquid is being pumped, it is possible to measure the heat leak to this liquid. During preliminary runs, this was found to be 1.3 mw; and this high loss rate was found to be caused by insufficient radiation shielding in the ^{3}He pumping line. However, with this leak rate, the pressure at the top of the $2\frac{1}{2}$-in. tube was 5×10^{-3} mm, which corresponds to a pressure over the ^{3}He of about 3×10^{-3} mm after correcting for the thermomolecular pressure difference. This vapor pressure corresponds to a bath temperature of 0.32°K. By introducing an improved radiation baffle in the $2\frac{1}{2}$-in. tube, the heat leak was cut to 110 μw. The pressure was then too small to measure, but since we know the loss rate is down by an order of magnitude, the temperature of the ^{3}He liquid can be estimated at about 0.25°K.

10. Neutron Scattering

TRIPLE-AXIS NEUTRON SPECTROMETER FACILITY

H. G. Smith M. K. Wilkinson

The construction of the Triple-Axis Neutron Spectrometer Facility for the HN-4 beam hole at the ORR has been completed and is currently being assembled for operation.

In addition to conventional neutron scattering experiments of interest to solid-state physics, the HN-4 facility was designed for inelastic neutron scattering studies at various temperatures and applied magnetic fields. For most of the experiments anticipated, a high degree of automatic control is required, and, with this in mind, a quite flexible control system has been designed and built by the Instrumentation and Controls Division.

The instrument consists of a basic neutron spectrometer designed at Brookhaven and built by the Potdevin Machine Company, Teterboro, New Jersey. A Picker diffractometer is mounted on the detector arm of the spectrometer, and the neutron detector shield (consisting of 50 lb of boron carbide cast in 32 lb of epoxy resin) is mounted on the Picker detector arm. A crystal such as one of beryllium or germanium is mounted on the crystal table of the Picker instrument and is used for energy analysis on the third axis in inelastic scattering studies.

A modified Harvey-Wells magnet (magnetic fields up to 20 kilogauss between pole pieces with 1-in. gap) is mounted on the crystal table of the main spectrometer and can rotate about the second axis, which generally contains the crystal to be studied. The magnet is often necessary in experiments involving both elastic and inelastic neutron scattering from magnetic crystals.

Most of the planned studies will require maintaining the samples at low temperatures. Therefore, a liquid-helium cryostat for powder and single-crystal studies has been designed and constructed and is now operating very efficiently. The cryostat is attached directly to the magnet, with the sample region tapered to fit between the pole pieces.

The various spectrometer axes are controlled automatically by a punched paper tape prepared on a computer. The control unit reads the necessary instrumental setting angles from the paper tape and drives the specimen crystal, magnet, main spectrometer arm, analyzing crystal, and Picker detector arm to their specified positions by use of Slo-Syn stepping motors and preset indexers. Because of the flexibility of the control system, several modes of operation are possible, and the mode desired for a given experiment (such as the "constant-Q" method in inelastic scattering) is determined by the computer program used to prepare the control tape.

The experimental data are registered on a printing scalar connected to a BF_3 counter through the usual amplifying stages and are recorded by several means. A punched paper tape output is used for data processing in the computer with the relevant computer programs. The same data are also printed in decimal form for immediate inspection of the data, which is desirable for preliminary measurements in setting up a problem. A miniature Brown recorder records a histogram plot of the peak profiles of the elastically scattered neutrons (Bragg peaks) or of the inelastically scattered neutrons (phonon peaks).

The first axis of the triple-axis unit is, of course, the conventional large single-crystal neutron monochromator, which may be of Be, Zn, Cu, Ge, or some other suitable crystals, depending on the particular experiments in mind. The crystal is mounted on a large goniometer head at the lower end of a rotating plug in the top of the main shielding blocks, and it can be aligned and centered remotely by the use of long telescoping shafts and universal joints to control the arcs and sledges of

the goniometer head. The advantage of this control system is that it allows an entire zone of crystal planes to be brought into position to reflect neutrons into any one of the four desired beam ports in the central shielding block. This results in a wide selection of various neutron energies in the thermal range. The instrument is mounted on a machined track for accurate positioning in front of any beam port. Each beam port can be opened or closed by individual nickel-steel and borated-paraffin shutters. The main reactor beam is stopped by a similar shutter with tungsten inserts added. The 2- by 2-in. channel in the wheel can be used to extract either a very small beam of thermal neutrons for Laue photography or a "cold" neutron beam by filtering through polycrystalline beryllium or other cold neutron filters.

A second monochromator may be mounted 9 in. after the first monochromator on another rotating plug, and a monoenergetic beam can be extracted through a single fixed beam port on the opposite side of the main beam from the first monochromator. Although this second neutron beam will not be as versatile as the first, it should prove valuable for preliminary studies, crystal alignment, photographic studies, etc.

The main radiation shielding consists of three large concrete blocks with a total weight of about 18 tons. Most of the central shield contains the nickel-steel and borated-paraffin shutter wheels (3 ft in diameter) spaced at the desired angles by wedges of the same materials. The spaces between the main shields and the surrounding walls are filled with large slabs of high-density Masonite laminated with steel and boron carbide. When the monochromatic beam port is open, a combination fast- and thermal-neutron beam catcher is also required. The radiation levels in the experimental area have been found to be very satisfactory.

Cobalt-wire flux measurements at the first monochromator position indicate that the thermal-neutron flux (1.5×10^9 neutrons cm^{-2} sec^{-1}) is down by a factor of 2, compared with similar measurements taken a few years ago at the HB-4 beam hole. The fast flux is higher by a factor of 2. Although this increased ratio of fast to thermal flux is not desirable from an experimental point of view, it will probably not be serious except for a very few problems, and such problems may have to wait until the HFIR facilities are available.

Part III. Metals

F. W. Young, Jr.

11. Investigations of Metal Surfaces

F. W. Young, Jr. L. H. Jenkins
L. D. Hulett U. Bertocci
J. R. Savage

SURFACES OF COPPER IN SOLUTIONS CONTAINING COPPER SULFATE

(electrochemical potentials vs crystal orientation; E)

Systems at Chemical Equilibrium

Investigations of the equilibrium shape and electrochemical potential of copper surfaces exposed to 0.2 *M* $CuSO_4$ solutions (pH adjusted to ~1 with H_2SO_4) which contained only hydrogen as a dissolved gas have been completed. Figure 11.1 shows a cell in which it was possible to isolate the surface of interest by mounting the single crystal as indicated, after appropriate electropolishing and washing had produced a flat, clean surface. After the cell had been alternately evacuated and flushed with hydrogen, the test solution – free of dissolved oxygen – was introduced. The entire apparatus was maintained at 23°C in an air bath for varying periods up to four months. One system was allowed to stand at ambient temperature for one year. Periodically, potential differences between (100), (110), (111), (321), and polycrystalline surfaces were measured, as well as the potentials vs a glass electrode.

The presence of an unavoidable oxide film produced by polishing and washing the crystals resulted in a measured potential difference of <2 mv for the first few hours after admission of solution to the system. However, after 2 to 4 hr no significant potential differences were observed except in the case of the (100), which often exhibited a difference in rest potential of ~0.5 mv for several days before adopting that value of the remainder of the samples.

Since the glass reference electrode had been well dried when the system was evacuated, it generally needed to soak in the solution for about one day before reproducible readings were obtained. After this time, no change in the potential difference between any of the copper crystals and the glass electrode was observed, nor could any differences be detected in the rest potential of any crystals with respect to the glass reference. It was concluded that if there is any equilibrium electrochemical potential difference between differently oriented single-crystal surfaces, it was

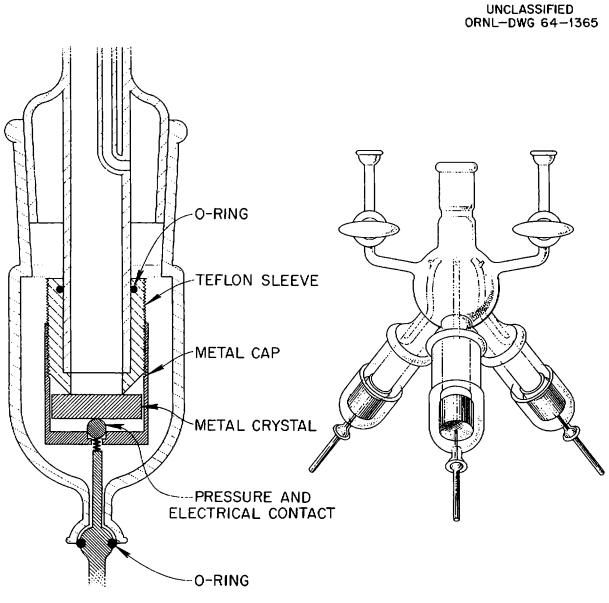

Fig. 11.1. Cell for Study of Surfaces of Single Orientation.

less than ~0.2 mv, the experimental error in the systems measured.

After varying exposure times, crystals were removed from the system, were washed, dried, and the surfaces were examined. In no case was any evidence of faceting, pitting, formation of preferred orientations, or any change from the original surface structure detected. These observations coupled with the failure to find orientation-dependent differences in rest or equilibrium potentials suggest that, in the system studied, no surface orientation is thermodynamically more stable than any other.

Oxidation of Copper by Cupric Ions

If oxygen is admitted to an acidic solution containing copper ions at equilibrium with copper metal,

$$Cu^{2+} + Cu^{0} \rightleftharpoons 2Cu^{+}, \qquad (1)$$

the equilibrium is destroyed, since cuprous ions are oxidized to cupric:

$$2Cu^{+} + 2H^{+} + \tfrac{1}{2}O_2 \longrightarrow H_2O + 2Cu^{2+}. \qquad (2)$$

Equilibrium conditions are restored when the cuprous ion concentration is reestablished by the oxidation of metal by cupric ions, as in (1).

The changes in surface structure resulting from oxidation by cupric ions were studied under the same experimental conditions used for equilibrium electrochemical potential measurements. After the equilibrium system was prepared as previously described, oxygen was admitted by allowing an extremely slow leak of atmospheric air into the system. The resulting dissolution occurred at rates varying in different cells from ~0.5 to 100 $\mu a/cm^2$. After a period of time the copper crystals were removed from the cell and were examined by optical microscopy.

It was determined that the changes in surface topography were affected by dissolution rates, in the range of rates studied, only in degree, not in kind. Figure 11.2 illustrates typical structures observed on the close-packed surfaces. These and similar observations led to the following suppositions:

1. On the (110), nucleation of steps for dissolution is relatively easy. Movement of atom steps over the surface, the process by which dissolution is accomplished, is also an easy process.
2. While step nucleation is not as easy on the (111) as on the (110), the movement of steps is not significantly more difficult.
3. Nucleation of steps on the (100) is a difficult process, and movement of the steps is apparently even more difficult.

The orientations of the ledges and facets developed on the low-index faces were determined

UNCLASSIFIED
PHOTO 66023

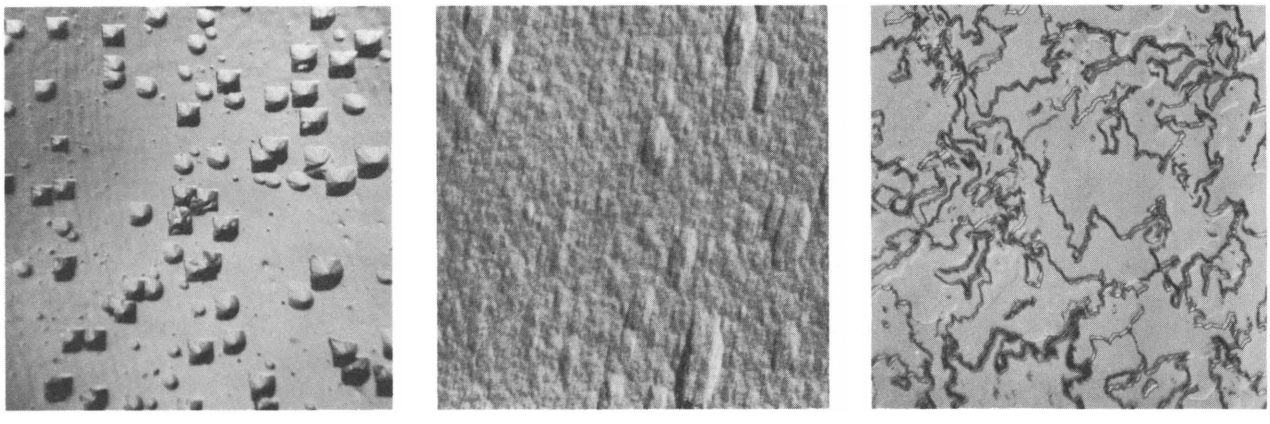

(100) (110) (111)

Fig. 11.2. Facets Developed After 48 hr at an Oxidation Rate by Cupric Ion of 10 $\mu a/cm^2$.

with a two-circle reflection goniometer with the following results:

1. Major facets developed on the (110) are {111} and other {110}'s, 60° from the original surface. No {100} facets are developed, but, rather, facets ~5° from the {100} toward the {110}. Strong reflections were also observed from other high-index orientations on the [100] zone. Very few reflections were observed along the [110] zone.

2. Facets developed on the (111) also had strong {110} reflections, as well as reflections from other {111}'s at 70° from the original surface. As in the case of the (110), no {100} facets developed, but, rather, ones slightly removed (~5°) from the {100}; also, similar major reflections were obtained along the [100] zone.

3. Strong reflections ~5° from (100) were obtained from the bottoms of the pits developed on this orientation. Faint {110} reflections were obtained, but no {111} reflections were observed. The sides of the pits were almost vertical, and since no {100} facets ever developed on any surface, they were thought to be about 5° from the (100) at 90° to the surface.

The exact significance of these observations is not clear, but it seems reasonable that the following considerations are important, since they offer clues as to the stability and motion of steps on various orientations: (1) the {100} facets never are developed, (2) most developed facets lie on the [100] zone, and (3) some orientations along this zone are produced in all systems. The work is being continued.

Galvanostatic Potentials in Reacting Systems

While the crystals in the preceding systems are being oxidized by cupric ions, it is possible also, by means of an external emf, to dissolve and/or deposit additional material. Galvanostatic pulses of current were passed through the systems, and the potential developed by a crystal was measured vs that of a crystal not receiving the galvanostatic treatment. Figure 11.3 shows a typical variation of this measured potential difference (overpotential) with current density applied. Ideally, if a companion dissolution process were not occurring, the change of potential with current density for deposition and dissolution would be symmetrical about the point of zero current and zero potential. The degree of displacement of the point of symmetry for such a curve of potential vs current is determined by the extent of the secondary process – the rate of dissolution due to oxidation by cupric ions. In the data shown, cupric-ion oxidation was occurring at a rate of 0.4 $\mu a/cm^2$ at a potential of 2.2 mv.

The initial slope of the potential-current curve in Fig. 11.3 is so great (~5000 ohms/cm^2) that a cupric-ion oxidation rate of ~1 $\mu a/cm^2$ in the system produces a corresponding potential of ~5 mv on the crystal undergoing oxidation. Since most of the systems studied contained about 100 ml of solution and a total metal surface of ~5 cm^2 exposed to solution, a rate of oxidation such as the one described above would go undetected by routine analytical methods, for the copper concentration in solution is increased only ~0.1% in ten days. For these reasons it is felt that the previous reports of rest potential differences of 3 to 4 mv between (100) and the (111) and/or other orientations in $CuSO_4$ solutions are erroneous. In all probability, either all oxygen had not been

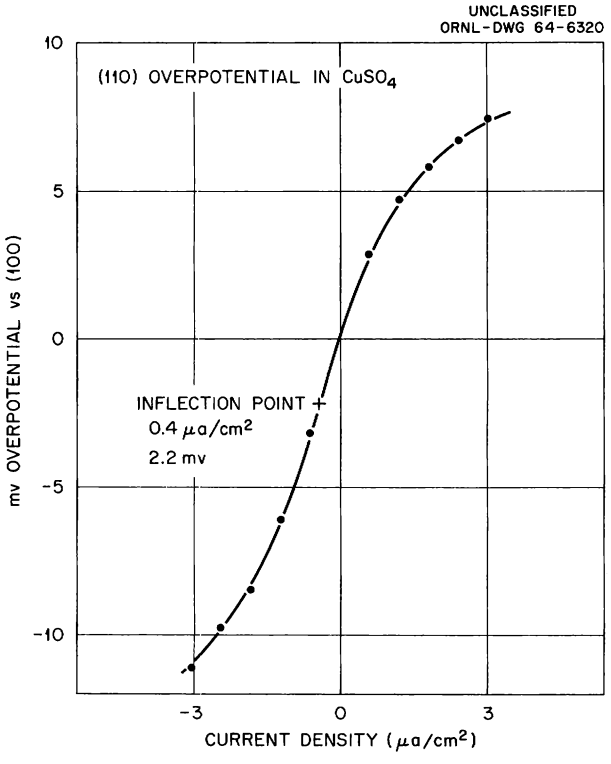

Fig. 11.3. Overpotential–Current-Density Relationships for (110) Surface in 0.2 *M* $CuSO_4$ with an Oxidation Rate by Cupric Ion of 0.4 $\mu a/cm^2$.

completely removed by evacuation or there was a very small leak in the apparatus. The potential differences observed and their change with time were most likely corrosion potentials corresponding to extremely slow oxidation rates.

KINETICS OF PIT FORMATION AND LEDGE MOTION DURING THE DISSOLUTION OF (111) SURFACES OF COPPER

(interferometric microscopy; E)

The study of the development of pits and ledges during the anodic dissolution of (111) surfaces of copper crystals has been continued. The arrangement of a pit and of the ledges about the (111) pole shown in Fig. 11.4 was described previously;[1] and in Fig. 11.4, the angle α is a function of dissolution conditions.

The kinetics of growth of the lateral dimensions of the pits was described previously. During the past year the pit profiles were measured by time-lapse interferometry, as dissolution proceeded, using a Nomarski polarized-light interferometer attached to a Reichert microscope. A series of interference micrographs of a pit being formed under the indicated conditions is shown in Fig. 11.5. From these photomicrographs the dissolution profiles can be constructed for the pit at successive stages of its growth. These profiles were analyzed according to the kinematic theory of crystal dissolution.[2] This theory, which is based on the assumption that dissolution rate is a function only of crystallographic orientation, predicts the dissolution shape of the pit as a function of time. It predicts that points of constant slope follow straight-line trajectories in space. Another expression of this prediction is that on the family of curves representing the sequential dissolution profiles of the crystal, points on successive profiles with the same crystallographic orientation have abscissas that are proportional to time. This condition has been tested and found to be true for a wide variety of conditions of pit formation. Since the kinematic condition is obeyed, it is possible to derive the dependence of step flux J on step density ρ from such data, and this has been done for a number of conditions of dissolution. The J vs ρ curves for dissolution conditions of 5 ma/cm^2 and bromide ion concentrations of 0.03, 0.25, and 1.0 M are shown in Fig. 11.6. It is clear that as bromide ion is increased, the curve changes from one which has no inflection point, type I, to one which includes an inflection point, type II. As suggested by Cabrera,[2] it was observed that the better conditions for the formation of well-defined pits correspond to those for which the type II curve applied.

Additional information has also been obtained on the ledges on the surface between the pits. Electron micrographs of replicas of ledges, from a surface of given orientation, which were formed under a variety of experimental conditions are shown in Fig. 11.7. The ledge profiles can be estimated from the shadows of the polystyrene balls. It is readily seen that ledge fronts decrease in slope with increasing time and current density

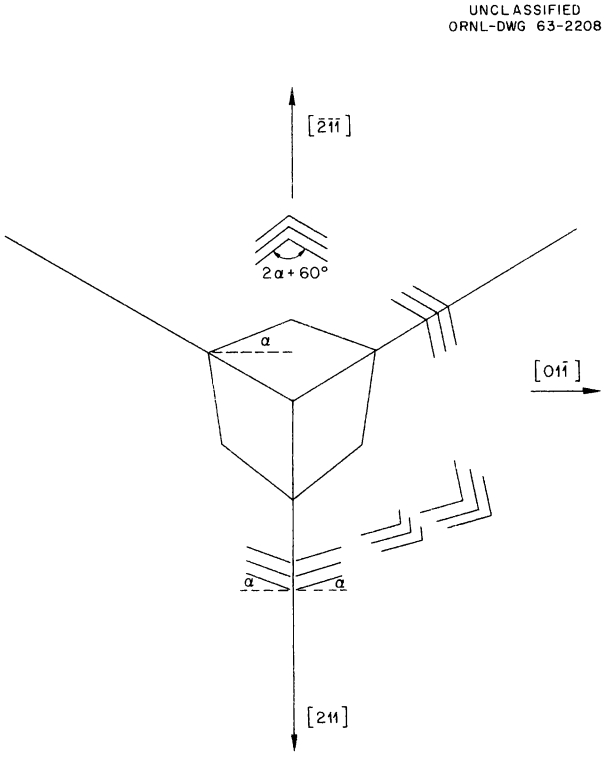

Fig. 11.4. Ledge Configuration About a Dislocation Etch Pit at the (1$\bar{1}\bar{1}$) Pole.

[1] F. W. Young, Jr. and L. D. Hulett, *Metal Surfaces*, ed. by W. D. Robertson and N. A. Gjostein, p. 375, American Society for Metals, Novelty, Ohio, 1963.

[2] N. Cabrera, *Reactivity of Solids*, ed. by J. H. DeBoer, p. 345, Elsevier, Amsterdam, 1961.

UNCLASSIFIED
PHOTO 66024

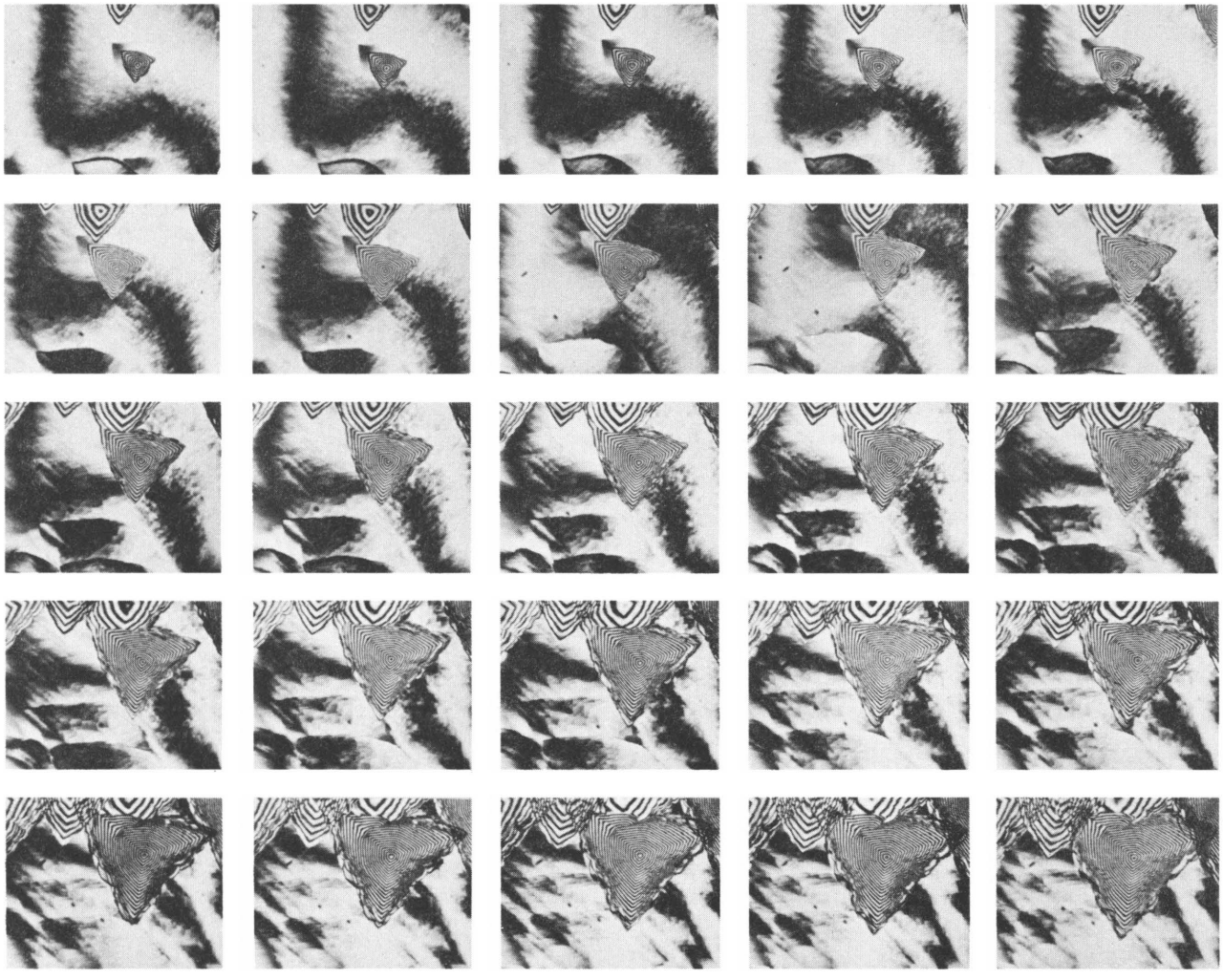

Fig. 11.5. Time-Lapse Interference Photomicrographs of an Etch Pit Being Formed at a Dislocation. Dissolution conditions: 10 ma/cm^2, 6 *M* HCl, 1.0 *M* HBr. Time interval between frames: 10 sec.

and with decreasing bromide ion concentration. The profile of these ledge fronts and the qualitative nature of their decay are compatible with the J vs ρ curves derived from the pit profiles for similar conditions.

The kinematic theory, which deals only with average step density and cannot properly include fluctuations in step spacing, has no basis for accounting for the bunching of atomic steps to form ledges, a process which must occur at the beginning of the dissolution of a polished surface. More recently, Mullins and Hirth[3] have reformulated the theory in a way which allows the consideration of fluctuations in step spacing and the consequences thereof. According to their assumptions, the formation of ledges is more probable for conditions that apply for the J vs ρ curve of type II. It has been found that for the conditions for which J vs ρ curves of type I apply, ledges are ill-defined, while as the curves become more pronouncedly type II, the ledges become sharper (see Figs. 11.6 and 11.7).

[3]W. W. Mullins and J. P. Hirth, *J. Phys. Chem. Solids* **24**, 1391 (1963).

In a solution of suitable bromide ion concentration, it was possible to make ledges appear and disappear reversibly by changing the current density. The sequence of photomicrographs in Fig. 11.8 demonstrates this effect. At the beginning of this sequence (current density of 10 ma/cm^2) the ledges were visible and would remain so indefinitely. When the current was increased to 30 ma/cm^2 the ledges disappeared but then reappeared when the current was returned to 10 ma/cm^2. This cycle was repeated a number of times, and it was determined that the photomicrographs represent steady-state conditions. Note that the slope in the bottom of the light pit also changes drastically with the changes in current density, and surfaces of small slope are generated or erased at the pit periphery. This behavior is consistent with that expected if changing the current density from 10 to 30 ma/cm^2 results in changing the J vs ρ curve from type II to type I.

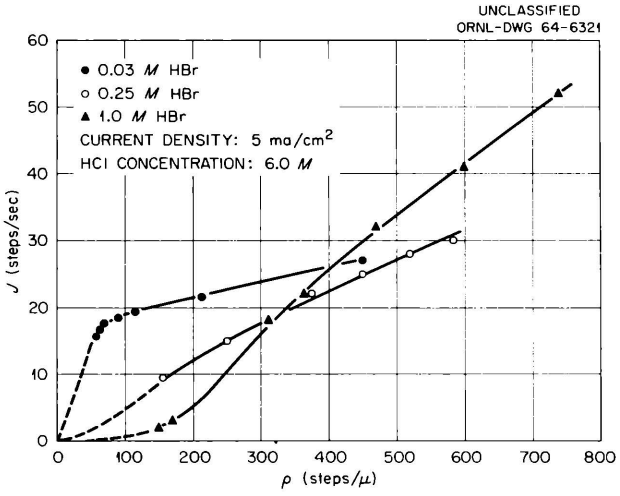

Fig. 11.6. Step Flux vs Step Density Curves for Dissolution in Solutions of Varying Bromide Ion Concentration.

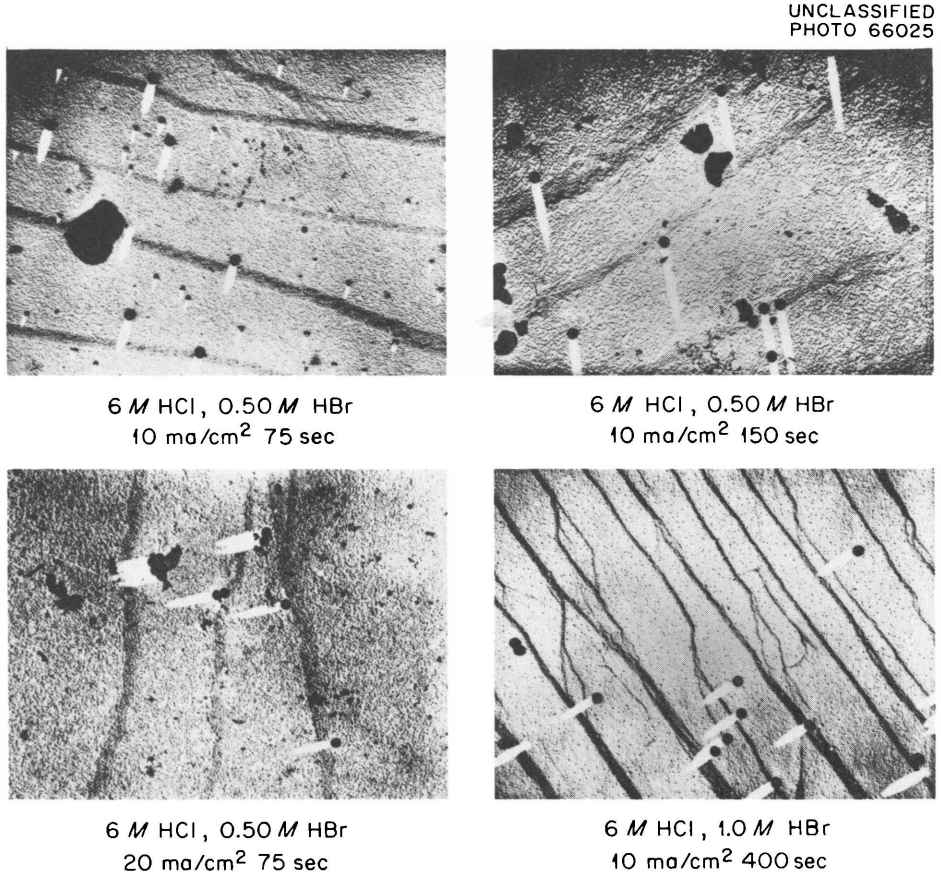

Fig. 11.7. Electron Photomicrographs of Ledges Formed Under Varying Dissolution Conditions. Diameter of polystyrene balls, 0.25 μ.

UNCLASSIFIED
PHOTO 66026

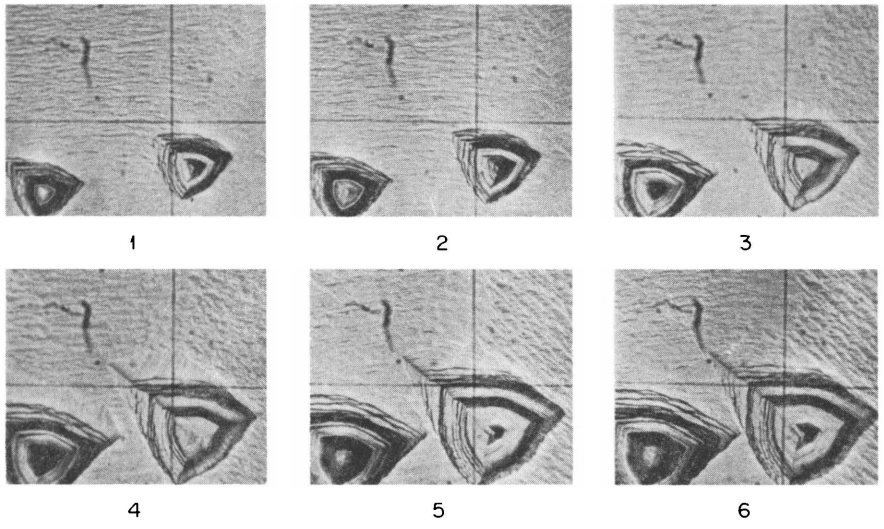

Fig. 11.8. Effect of Current Density on Ledges. Frames 1 and 2: 10 ma/cm^2; frames 3 and 4: 30 ma/cm^2; frames 5 and 6: 10 ma/cm^2.

ELECTROCHEMICAL STUDIES OF COPPER SINGLE CRYSTALS IN HALIDE SOLUTIONS

(optical microscopy; E)

Copper single crystals have been used for studying the electrochemical behavior of copper in halide solutions at low current densities. During such experiments, cathodic and anodic overvoltages have been recorded, and the faceting pattern formed by electrolysis has been examined at the optical microscope and by means of a two-circle reflection goniometer. Most experiments so far have been carried out in $CuCl_2$-HCl solutions, but some experiments have been done in bromide solutions as well.

Chloride Solutions

The complete elimination of oxygen from the system proved to be extremely difficult; as a result, a number of experiments have been carried out where a steady leakage of oxygen caused the copper surface to corrode at a rate ranging from 20 to 50 μa/cm^2. After further improvements of the experimental setup shown in Fig. 11.1, the spontaneous corrosion rate dropped below any unambiguously detectable value.

The potential differences between different surface orientations under slow corrosion conditions showed that after a very short period of time a steady state was reached in which the (100) orientation was nobler than (110) and (111) by about 15 to 20 mv. This potential difference could be maintained within 3 to 5 mv for several days.

Overvoltage curves recorded on such specimens are shown in Fig. 11.9. It can be seen that when the superimposed cathodic current balanced the anodic corrosion current, the overvoltage curves obtained on the different orientations intersected, which shows that the potential differences recorded at zero current density were mainly due to differences in kinetic parameters.

Inspection of the surfaces after the tests showed extensive faceting on all orientations. Examination with the reflection goniometer revealed that the original (100) orientation had disappeared completely, and the facets formed lay in a region between 2 and 4° from (100), producing a square reflection pattern with corners toward $\langle 100 \rangle$. The reflection patterns for (110), (111), and (321) orientations were remarkably similar to each other; sharp reflections were found at {111} and {110}, and also there was a diffuse reflection around {100}, approximately square-shaped with corners about 15° from {100} toward $\langle 100 \rangle$.

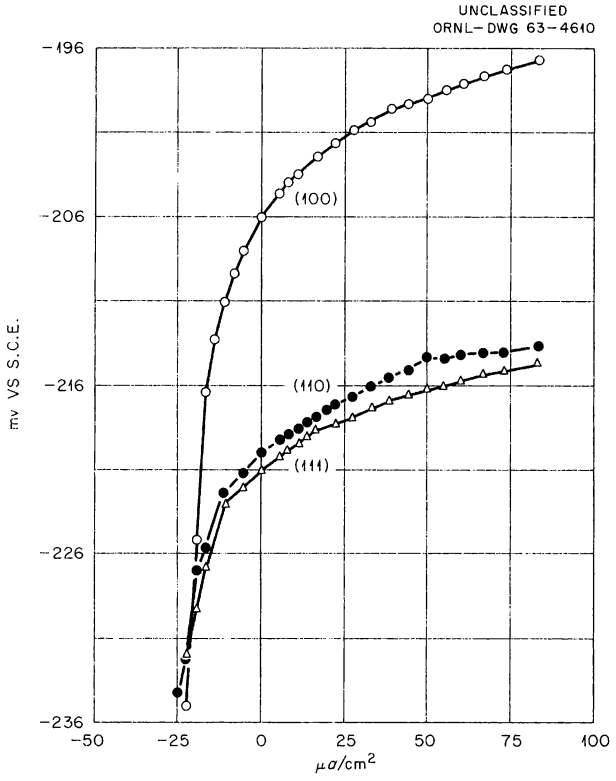

Fig. 11.9. Overvoltages of Copper Single Crystals Corroding in 0.03 *M* Cu, 2.7 *M* HCl.

Curves of overvoltage vs current density obtained when little or no corrosion was present are given in Fig. 11.10 for (100), (111), and (110).

In order to determine the point of maximum slope on the curves of overvoltage vs current density, the data in some experiments were taken at extremely low cathodic and anodic current densities. Examples of such data are shown in Fig. 11.11. A very interesting feature of the overvoltage curves is their symmetry with respect to the inflection point. However, the inflection point does not coincide with the point of zero current density. If the assumption is made that a steady corrosion is occurring on the electrode, the potential at the inflection point could be interpreted as the equilibrium value for that particular orientation, and the (cathodic) current density relative to it could be interpreted as a measure of the (anodic) corrosion rate.

Also, by passing an anodic current through the system for a sufficient time, a faceting pattern could be obtained. The surface structure and the reflection pattern were very similar to those observed under corrosion conditions.

The experimental results so far obtained reduce considerably the choice of what is the kinetically decisive phenomenon for the dissolution of copper in, and deposition of copper from, halide solutions; they rule out the contribution of slow reactions in solution and indicate that the charge-transfer process is also comparatively fast at low current densities. Also, the explanation for the high resistances encountered during reaction at extremely low current densities and for the remarkable difference in overvoltages and etching patterns between (100) and all other orientations has to be found in the characteristics of the different crystal surfaces.

Preliminary measurements of the differential capacitance of (100), (111), and (321) electrodes seem to show that surface diffusion of adsorbed atoms could be the rate-determining step on the

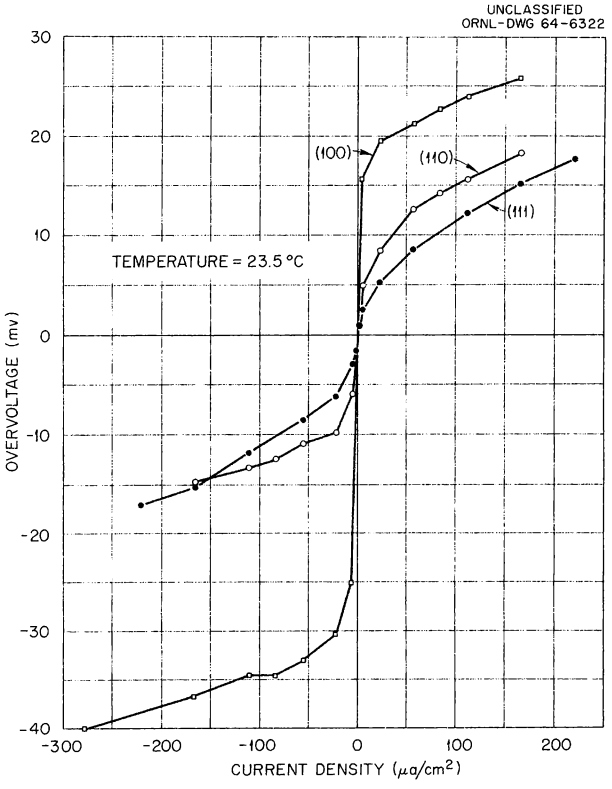

Fig. 11.10. Overvoltages of Copper Single Crystals in 0.03 *M* Cu, 2.7 *M* HCl.

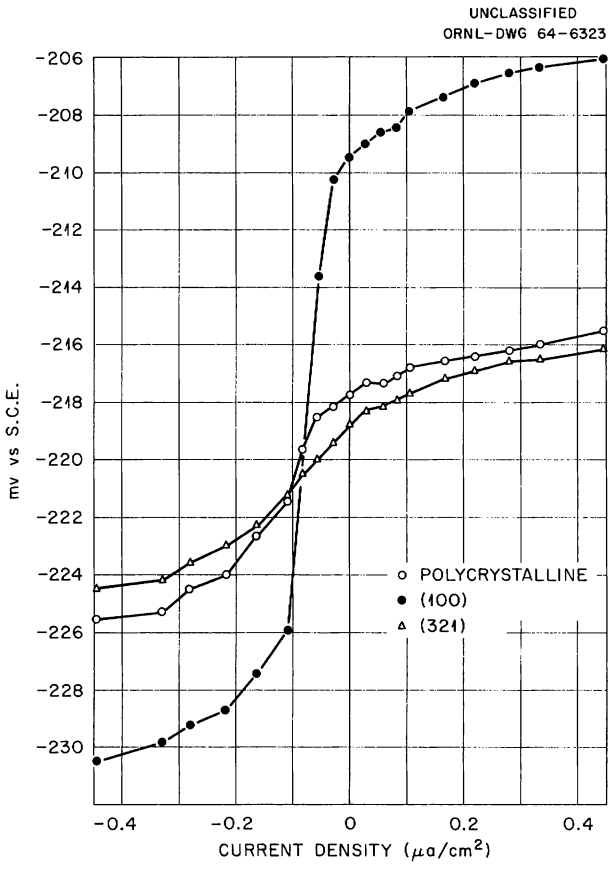

Fig. 11.11. Overvoltages of Copper Single Crystals in 0.04 *M* Cu, 2.7 *M* HCl.

last two, but no satisfactory explanation can be found for the extremely low capacitance of (100) surfaces.

Finally, concerning the question of a difference in equilibrium potential for different orientations, the only useful criterion for establishing the position of the equilibrium values for the different orientations of copper seems to be based on the evaluation of the derivative of the emf vs current density; the method is necessarily rather inaccurate, and it is not presumed that it can provide information whose approximation is better than ~2 mv. Within this limit, however, no difference can be found between the equilibrium potentials for different orientations of copper single crystals and also for polycrystalline electrodes. All the differences recorded so far between rest potentials can be easily accounted for in terms of differences in their kinetic behavior. This conclusion is supported by the findings on single-crystal spheres or on any electrode where more than one orientation is present; in spite of the relatively high exchange current reported for copper, rearrangement of the surface structure does not seem to take place.

Bromide Solutions

Experiments in bromide solutions are in progress. Figure 11.12 shows overvoltage curves for (100) oriented copper in bromide solutions of two different concentrations of copper. It can be seen that the high voltage shift in the range from −1 to 1 $\mu a/cm^2$, which had been observed for (100) oriented surfaces in chloride solutions, and which is also found here, is not affected when the copper concentration is varied from 0.1 to 0.2 *M*. The faceting pattern, however is different in bromide solutions. After anodic attack at 25 $\mu a/cm^2$, reflections show the formation of {110}, {111}, and an orientation near to, but significantly different from, the {311}, as well as the presence of the original (100) orientation.

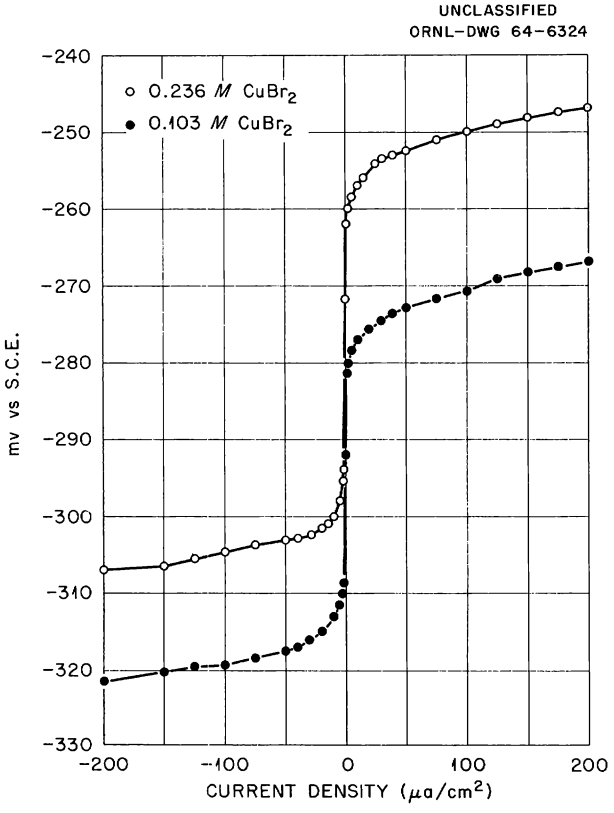

Fig. 11.12. Overvoltages of (100) Copper Single Crystals in 4 *M* KBr + 0.5 *M* HBr + $CuBr_2$.

OBSERVATIONS OF DISLOCATIONS IN COPPER, USING BORRMANN X-RAY TRANSMISSION TOPOGRAPHS[4]

(E)

F. W. Young, Jr. M. C. Wittels
F. A. Sherrill

By use of the Borrmann diffracted beams for Ag $K\alpha$ radiation, x-ray topographs have been made of copper-crystal plates $1 \times 1 \times Z$ cm ($Z \leq 0.1$) with (111) faces. Dislocation lines were generally recorded as lines of less intensity on the x-ray plate. Both annealed and neutron-irradiated crystals were investigated. In the latter the dislocations were pinned and were not moved by the small stresses accidentally imposed while making the topographs, and dislocation arrangements in the bulk crystal were determined. The Burgers vectors were deduced from {111} topographs, employing the condition that for no contrast, $\boldsymbol{g} \cdot \boldsymbol{b} = 0$. For edge dislocations the additional condition, $\boldsymbol{g} \times \boldsymbol{n} = 0$, was necessary for no contrast, and it was demonstrated that this type of contrast was more pronounced for dislocations grouped in a slip trace. It was found that dislocations could be seen all the way through crystals for $Z \leq 0.06$ cm. A semiquantitative correlation has been established between etch pits formed at dislocation sites on the (111) surfaces and the dislocations revealed by the x-ray topography. It has been possible to obtain complete sets of topographs on only a few annealed crystals; for these, an analysis of the dislocations produced by accidental microstrains has been possible.

GROWTH OF COPPER CRYSTALS OF LOW DISLOCATION DENSITY[5]

(Bridgman; etch pits; E)

F. W. Young, Jr. J. R. Savage

A study was made of the perfection and of the factors controlling perfection of copper crystals grown by a Bridgman technique. Crystals grown from both 99.999+% and OFHC copper were acid-sawed and polished, and dislocation densities were determined by etch-pit techniques. The orientation of the growth direction of unseeded crystals of both purities was random. There was a correlation between perfection and growth direction for the 99.999+% copper crystals in that the more perfect crystals had growth direction far from the [111] zone. Dislocation densities as low as $10^3/cm^2$, with no subboundaries, were obtained in some of the purer as-grown crystals. The OFHC crystals were much less perfect and contained many subboundaries. After annealing slices of the purer crystals at 1075°C, dislocation densities as low as $10^2/cm^2$ were obtained. The vacancy-condensation mechanism for dislocation generation apparently was not significant in accounting for the residual dislocation density in these crystals.

---

[4]Abstract of paper by F. W. Young, Jr., F. A. Sherrill, and M. C. Wittels to be submitted for publication in the *Journal of Applied Physics*.

[5]Abstract of paper by F. W. Young, Jr., and J. R. Savage submitted for publication in the *Journal of Applied Physics*.

12. Low-Temperature Irradiation Studies

R. R. Coltman
J. K. Redman
C. E. Klabunde
G. F. Fielder

LOW-TEMPERATURE THERMAL-NEUTRON IRRADIATION FACILITY

Construction and testing of the new low-temperature irradiation facility[1] located at the Bulk Shielding Reactor is completed for thermal-neutron damage studies. Several uninterrupted runs of 300 to 400 hr were made, and a total operating time of 3000 hr has been accumulated. During this period, some tests of low-temperature expansion engines with pure and glass-impregnated Teflon piston rings have been made. (The most common method at present uses the Kapitza principle of a ringless, gas-guided piston.) Satisfactory short-term (1000 hr) results have been obtained.

Results from recent experiments point to the need for lower irradiation temperatures than those presently attainable (3.6°K at full reactor power and 3.1°K at one-tenth full power). The irradiation temperature depends only on the pumping speed of the low-pressure return side of the liquefier circuit. Increasing the pumping speed at room temperature reaches a practical limit due to pressure drop in the circuit. For this reason the design and construction of a small pump (2 scfm displacement) to be operated at 10°K at the cold end of the circuit is under way.

During the early part of this reporting period, various flux determinations measured by low-temperature damage rates indicated the need for greater thermal-flux purity. A new cryostat housing incorporating additional D_2O was installed, and the total thickness of D_2O between the cryostat and the reactor face is now 24 in. The present facility provides a better thermal-flux purity than was obtainable in the ORNL Graphite Reactor. A thermal-neutron damage purity of about 85% is obtained in copper, which has a fairly small capture cross section of about 3 barns. The absolute value of the thermal-neutron flux is 8×10^{11} neutrons cm^{-2} sec^{-1} (about 25% higher than in the ORNL Graphite Reactor facility).

THERMAL-NEUTRON DAMAGE IN CADMIUM

(isochronal recovery; electrical resistance; E)

The study of thermal-neutron damage in cadmium can provide valuable basic radiation damage information for several reasons.

1. High-purity cadmium is readily available (nominal purity of the material used in the experiments described here is 99.9999%) and is easily fabricated into suitable specimens.
2. There have been relatively few studies, either theoretical or experimental, of irradiation damage of the hexagonal metals.
3. The mean recoil energy of a ^{113}Cd atom from a neutron-capture event is 130 ev.[2] This should produce very simple damage in the form of one or two Frenkel pairs per event.
4. In natural cadmium virtually all the neutron captures originate from the ^{113}Cd isotope, which yields stable ^{114}Cd. In this material, then, there is no problem with transmutations.

[1] R. R. Coltman *et al.*, *Solid State Div. Ann. Progr. Rept. May 31, 1963*, ORNL-3480, p. 57.

[2] R. R. Coltman *et al.*, *J. Appl. Phys.* **33**, 3509–22 (1962).

UNCLASSIFIED
ORNL-DWG 64-4519

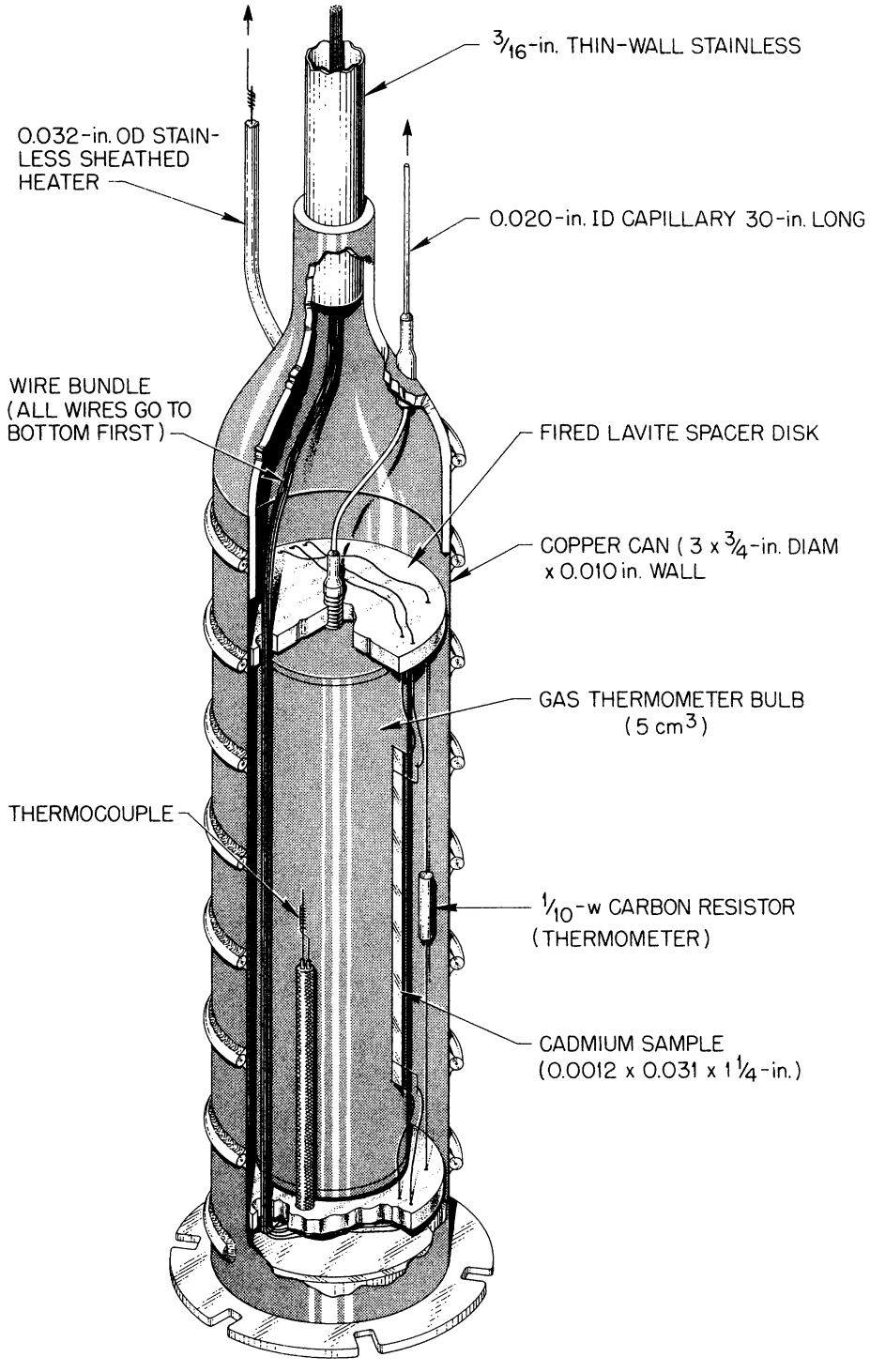

Fig. 12.1. Schematic Sketch of the Specimen Can, Showing the Sensing Bulb of the Gas Thermometer.

5. The capture cross section of cadmium is quite high (2450 barns), thus permitting the study of damage concentration effects over a wide range with a modest thermal-neutron flux. The capture cross section is not so high, however, that self-shielding is a serious problem. The specimen used in the studies reported here is in the shape of a ribbon ($0.0012 \times 0.037 \times 1.27$ in.), which gives a damage concentration at the center only 20% less than that at the surface of the specimen.

By the use of electrical resistance to detect damage, complete detailed isochronal annealing studies of (n,γ) damage in cadmium have been made for four initial damage concentrations which varied by a factor of 107. A constant damage rate was observed for all irradiations. For the accurate measurement of low temperatures in these experiments, a constant two-volume helium gas thermometer (charged to 839 mm at room temperature) was employed. The specimen can and sensing bulb of the thermometer are shown in Fig. 12.1. The pressure response rate would be exceedingly poor through a 30-ft capillary fine enough to keep the parasitic volume small. This situation was avoided by purposely making the total parasitic volume 20 times the bulb volume, and using $\frac{1}{8}$-in. tubing to replace all but 2 ft of the capillary. Most of this volume is in the temperature-controlled laboratory. With this arrangement the nonlinear pressure-temperature relationship provided maximum sensitivity in the range of 3 to 30°K with an average reproducibility of 0.1% of the absolute temperature. Above 30°K, a copper-constantan thermocouple was used. The rapid response of a carbon resistor thermometer was utilized for control purposes.

Figure 12.2 shows the isochronal recovery of thermal-neutron damage in cadmium. The atomic concentration of capture events for each of the relative dose numbers is (1) 3.5×10^{-6}; (4) 14×10^{-6}; (34) 119×10^{-6}; and (107) 381×10^{-6}. It may be seen in this figure that there is a pronounced suppression of the low-temperature recovery (up to 26°K) as the initial damage concentration is increased. At higher temperatures the recovery rate increases with increasing dose so that at 160°K recovery is almost complete for all doses. A plot of the percent recovery at 26°K vs the logarithm of the dose indicates that 72% recovery would be reached for an infinitesimal dose. It can be seen in Fig. 12.2 that dose (1) closely approaches this limiting case. It may also be noticed in this figure that straggling of the high-temperature recovery decreases as the

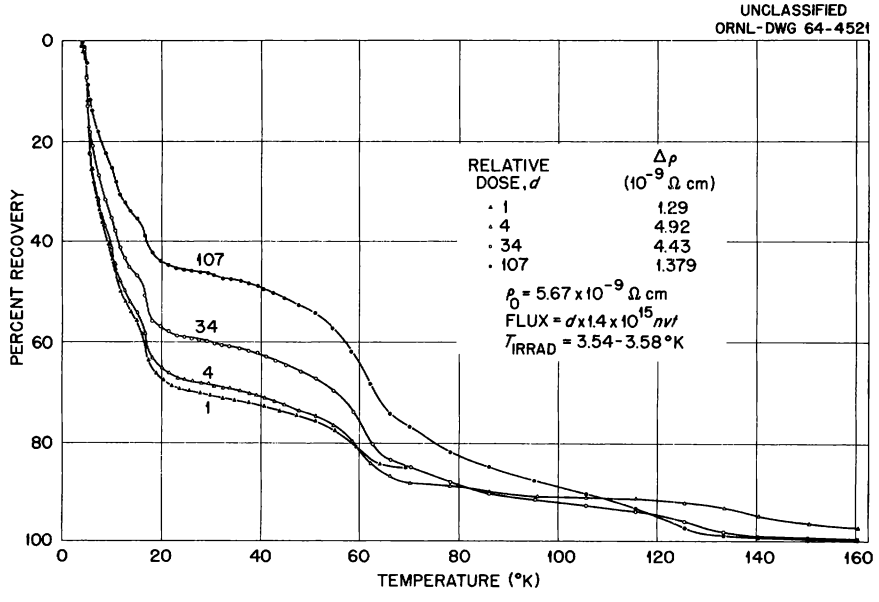

Fig. 12.2. Isochronal Recovery of Thermal-Neutron Damage in High-Purity Cadmium.

dose is increased. The crossings of the recovery curves in this range show at least a qualitative self-consistency. Figures 12.3 and 12.4 show the numerical derivatives of the raw data presented in Fig. 12.2. Note that the scales in Figs. 12.3 and 12.4 are not the same.

Certain features of the data shown in Figs. 12.3 and 12.4 should be mentioned. For isochronal recovery it can be shown that the recovery peak of a first-order process is located at the same temperature regardless of initial damage concentration. Peaks associated with second- and higher-order processes, however, are shifted downward in temperature with increasing dose. The magnitude of the shift depends upon the absolute temperature range involved with the recovery. The first recovery peak centered at 5.3°K appears to show no temperature shift with dose and is believed to describe a first-order process. The magnitude of the peak decreases with increasing dose. On the high-temperature side of the 5.3°K peak, a second peak is seen, which shifts downward in temperature with increasing dose until it is obscured by the 5.3°K peak. Two peaks centered at 11.3 and 17.1°K are superimposed upon a rather large and peculiar background process. If this is a single process, then it may extend from about 5 to 25°K. Also, subtraction of this apparent background from the 11.3 and 17.1°K peaks indicates that each of these may correspond to a first-order process which is suppressed with increasing dose. The small peak at 31°K does not appear to be first order, yet the small temperature shifts are not consistent with dose. The recovery associated with this peak is less than 2% of the total damage.

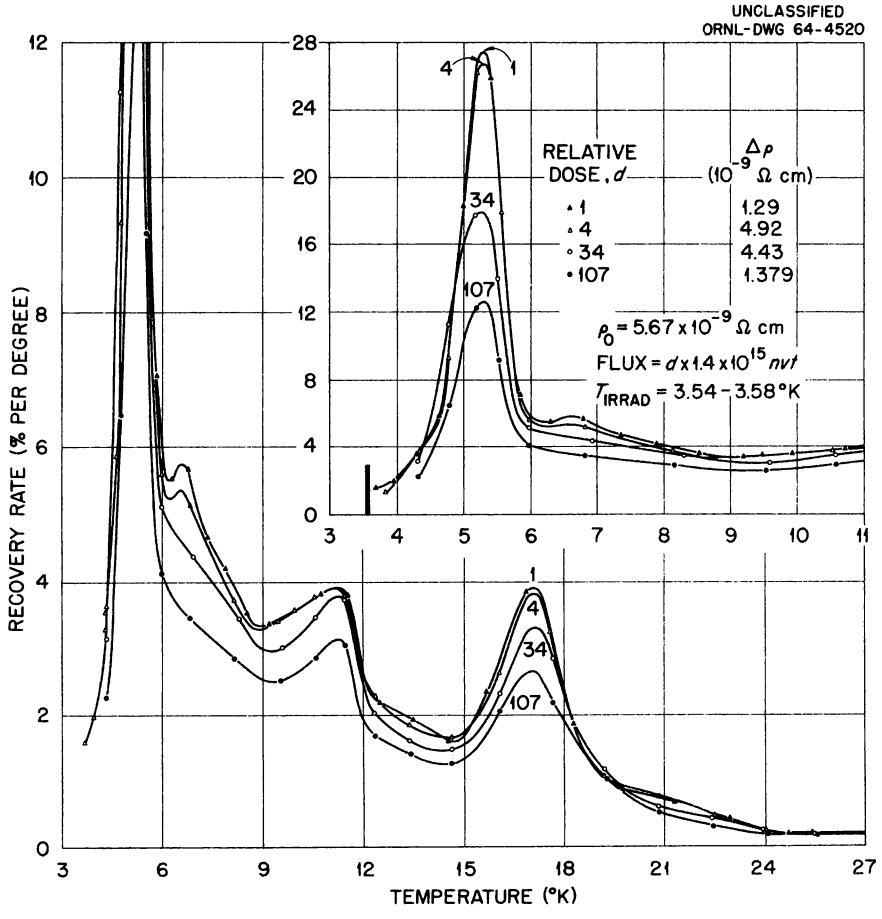

Fig. 12.3. Derivative of the Isochronal Recovery of Thermal-Neutron Damage in High-Purity Cadmium.

Similarly, the recovery between 35 and 50°K does not seem well defined when a comparison between doses is made. This may indicate that more than one process is involved in this temperature range. The prominent peak at 60.5°K behaves like a first-order process insofar as no dose-dependent temperature shift is seen. The strong temperature dependence of the last two peaks suggests processes higher than first order. Note that the magnitude of the latter three peaks increases with increasing dose, indicating that they all share in the recovery which is suppressed at the lower temperatures because of higher initial concentration.

A general model of impurity trapping at lower temperatures and subsequent release of defects from the traps at higher temperatures would give maximum suppression of the low-temperature recovery at lower doses. The opposite effect is observed. It is recognized that impurity effects may be present, but they cannot account for the principal behavior. A qualitative correlation between the recovery spectrum reported here and that obtained by Corbett, Smith, and Walker[3] for electron damage in copper is not apparent to us. It is believed that the suppression of the recovery at low temperatures may be explained by self-trapping or clustering of mobile interstitial atoms, which is accompanied by interstitial-vacancy annihilation. At the higher temperatures the increase in recovery rate may be associated with the dissolution of clusters. At the present time we cannot propose a firm model which meets all the demands imposed by the complex recovery behavior of (n,γ) damage in cadmium.

[3] J. W. Corbett, R. B. Smith, and R. M. Walker, *Phys. Rev.* **114**, 1460 (1959).

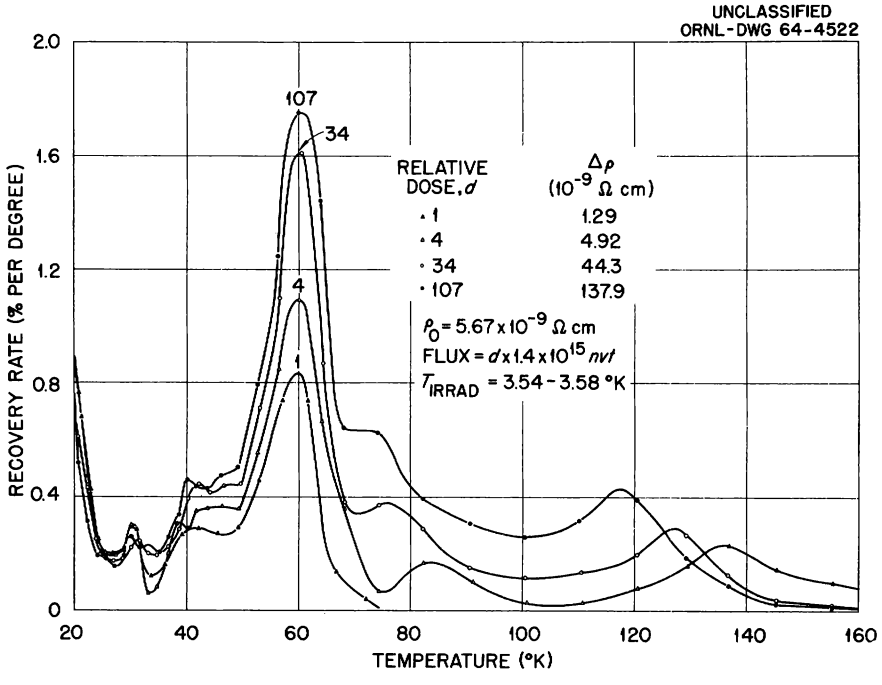

Fig. 12.4. Derivative of the Isochronal Recovery of Thermal-Neutron Damage in High-Purity Cadmium.

13. Elasticity and Anelasticity Studies

EFFECT OF FAST-NEUTRON IRRADIATION ON THE BORDONI INTERNAL FRICTION PEAK IN DEFORMED SINGLE-CRYSTAL COPPER

(E)

D. O. Thompson[1] P. B. DeNee
V. K. Paré

The Bordoni peak is prominent in the spectrum of thermally activated mechanical relaxation processes which occur in various metals after deformation. In copper vibrated in the kilocycle frequency range the relaxations are found from 20 to 150°K. Their association with deformation, coupled with the fact that doping with various impurities affects very little the temperatures at which they occur, leads to the conclusion that they involve thermally activated motion of dislocations over barriers which are intrinsic to the metal concerned. The relaxation character of this internal friction distinguishes it from the "vibrating-string" type of dislocation process which has been discussed theoretically by Koehler[2] and by Granato and Lücke.[3] The vibrating-string internal friction can be observed at room temperature in undeformed crystals and has been used extensively in studies of dislocation pinning by radiation defects.

Theories of the Bordoni peak have been proposed by Seeger[4] and Donth,[5] Bruner,[6] and Brailsford.[7] In Seeger's model the barrier is taken to be the Peierls energy and is thus important only for dislocations which lie near enough to close-packed directions so that they can be bound by it. The relaxation process is the jumping of these dislocations over the barrier by thermal generation of pairs of kinks of opposite sign. Donth[5] has studied theoretically the rate at which this generation will occur. The effects associated with subsequent diffusion of the kinks along the dislocation have been discussed by Seeger and Schiller.[8]

According to Bruner, the relaxation involves both dislocations and point defects which act as pinning points. For a dislocation split into two partials, the thermally activated jump could be a transition from pinning of one partial to pinning of the other. Bruner and Mecs[9] have also suggested that jumping of the pinning defect itself might be the relaxation process.

The picture proposed by Brailsford is that the Peierls energy is involved but is so high that thermal generation of kink pairs does not occur in the temperature range of the Bordoni peak. The relaxation is supposed to be associated with the diffusion of kinks in dislocations which lie across close-packed directions. No discussion is offered as to why the Peierls energy should be so high or as to what other consequences would follow from its large magnitude.

Of these models, Bruner's is the only one in which point defects participate directly in the relaxation and thus are essential to it. In the other two models, point defects are not involved directly in the thermally activated jump process; however, they could limit the resulting dislocation

[1] Present address: North American Aviation Science Center, Thousand Oaks, Calif.

[2] J. S. Koehler, *Imperfections in Nearly Perfect Crystals*, p. 197, Wiley, New York, 1952.

[3] A. Granato and K. Lücke, *J. Appl. Phys.* **27**, 583 (1956).

[4] A. Seeger, *Phil. Mag.* **1**, 651 (1956).

[5] H. Donth, *Z. Physik* **149**, 111 (1957).

[6] L. J. Bruner, *Phys. Rev.* **118**, 399 (1960).

[7] A. D. Brailsford, *Phys. Rev.* **122**, 778 (1961).

[8] A. Seeger and P. Schiller, *Acta Met.* **10**, 348 (1962).

[9] L. J. Bruner and B. M. Mecs, *Phys. Rev.* **129**, 1525 (1963).

motion and thus influence the internal friction peak.

To provide information for distinguishing among these models, a series of experiments was done in which point defects were introduced by irradiation and removed by annealing. A pure copper crystal was deformed 6% in tension at room temperature, and the internal friction was measured as a function of temperature from 10 to 270°K. Runs were made with the sample in the as-deformed condition; after holding at 100°C for 24 hr; after total fast-neutron doses of 5×10^{13}, 4×10^{14}, 9×10^{15}, and 5×10^{16} neutrons/cm^2; and after various anneals. The results of the two preirradiation runs and of runs after the first two irradiations are shown in Fig. 13.1. It can be seen that the preirradiation "anneal" at 100°C gave effects entirely similar to those of a small radiation dose. Although this behavior seems anomalous, it is in fact quite plausible. It has been shown in previous neutron-irradiation experiments[10] that a large majority of the pinning defects are vacancies which complete their diffusion to the dislocations only after ~24 hr at 100°C. Thus, in order to obtain consistent results, each of the irradiations in this work was followed by such a holding period. So that the effects of the first irradiation could be attributed only to the irradiation itself and not to the subsequent 100°C holding period, it was also preceded by a 100°C treatment, which caused the internal friction behavior to change from the first to the second curve in Fig. 13.1. It is reasonable to assume that the first 100°C treatment allowed

[10] V. K. Paré and D. O. Thompson, *Acta Met.* **10**, 382 (1962).

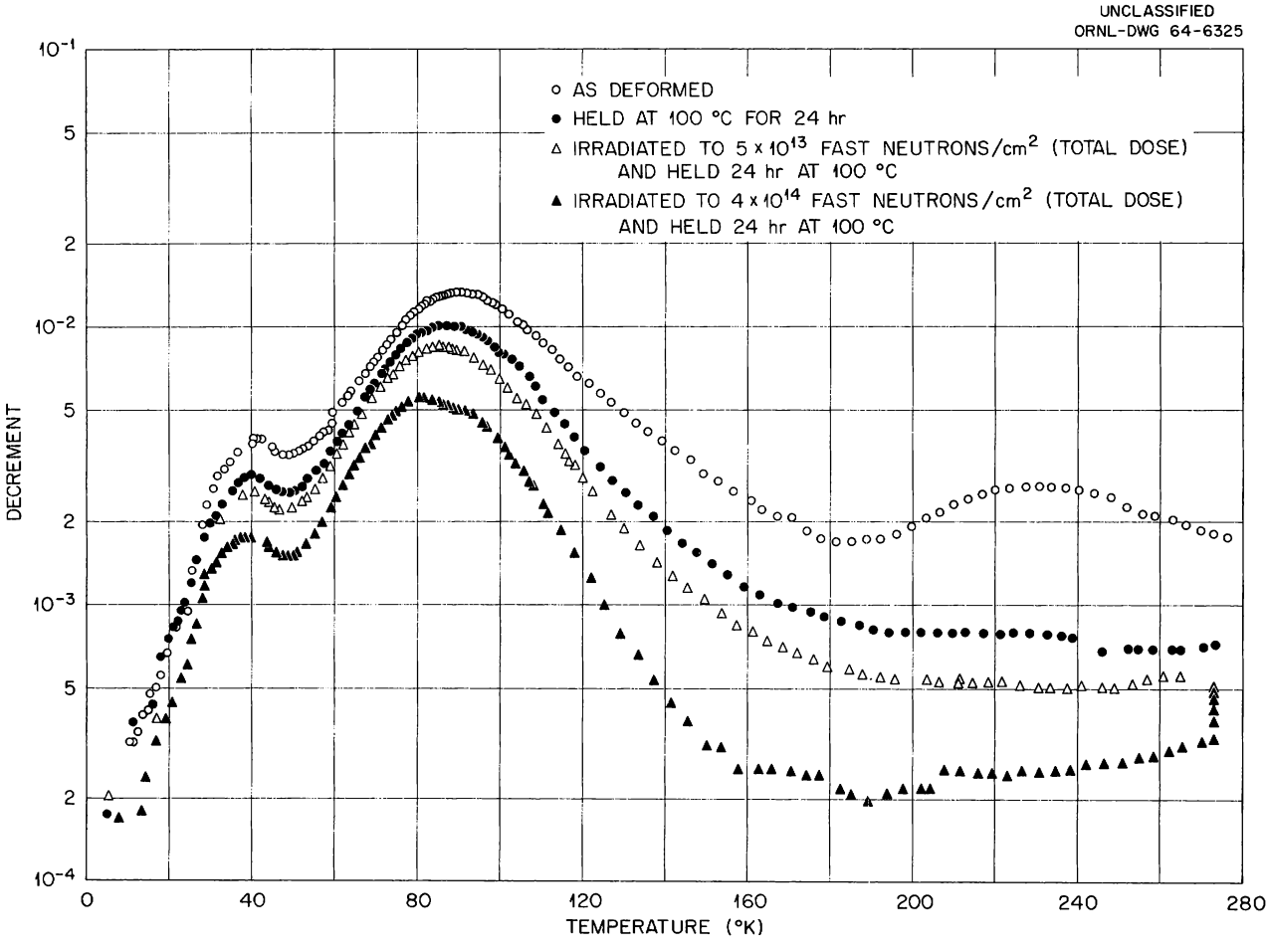

Fig. 13.1. Temperature Dependence of Internal Friction (Logarithmic Decrement) of a Copper Crystal Deformed 6% in Tension.

diffusion to the dislocations of vacancies which had been created by the plastic deformation. Thus the treatment could well have been equivalent to an irradiation.

The curves in Fig. 13.1 are similar to other Bordoni peaks studied in copper. It is possible to see evidence of the main components found by Thompson and Holmes[11] at ~30, ~40, ~80, and ~93°K. The theory of Brailsford is the only one which offers reasonably unambiguous predictions as to the response of the Bordoni peak to radiation-defect pinning points. By reducing the available diffusion path length for kinks, pinning points will decrease both the magnitude of the process and its relaxation time. Thus irradiation should not only reduce the height of the peak structure but move it toward lower temperature. Both effects are clearly visible in Fig. 13.1. Because of the multicomponent structure, it is difficult to define the temperature at which a given peak occurs. A rough estimate shows, however, that the relationship between the shift toward lower temperature and the decrease in magnitude of the main peak is approximately that which is predicted in Brailsford's theory. This comparison requires a knowledge of the average activation energy associated with the peak; the value used was 0.12 ev.[12]

The data from the remaining runs have not yet been processed, but the results can be summarized in terms of the height of the main (80°K) peak. The two further irradiations reduced the peak decrement to $\sim 3 \times 10^{-3}$. The first anneal, at 400°C for 22 hr, apparently eliminated the effects of all the previous postdeformation treatments, restoring the peak to its original height, 1.3×10^{-2}. An anneal at 525°C then reduced the height to $\sim 1.0 \times 10^{-2}$, and a further one at 650°C reduced it to $\sim 7 \times 10^{-3}$.

The persistence of the Bordoni peak through these anneals is significant since it has been shown that any of them is sufficient to remove all radiation-defect pinning points from the dislocations. It thus appears that point defects cannot be directly involved in the Bordoni relaxation process, though they may serve to limit the associated dislocation motion and thus affect the internal friction.

[11] D. O. Thompson and D. K. Holmes, *J. Appl. Phys.* **30**, 525 (1959).

[12] S. Okuda, *Sci. Papers Inst. Phys. Chem. Res. (Tokyo)* **57**, 116 (1963).

DOSE DEPENDENCE OF THE DISLOCATION BREAKAWAY STRESS IN FAST-NEUTRON-IRRADIATED COPPER AS MEASURED BY AMPLITUDE-DEPENDENT INTERNAL FRICTION[13]

(E/T)

D. O. Thompson[1] V. K. Paré

Measurements of the strain amplitude dependence of the internal friction in copper have been made at 100°C as a function of fast-neutron dose. Although it is found that the Granato-Lücke theory of amplitude-dependent internal friction does not describe the results obtained, the dose dependence of the dislocation breakaway stress can be deduced by other means. After taking into account the variation with neutron dose of the mean free dislocation length, it is found that the breakaway stress is proportional to the cube root of the integrated flux in the dose range from 10^{11} to 10^{14} neutrons/cm^2 ($E > 0.6$ Mev). Extrapolation of the breakaway stress results to doses greater than 10^{19} neutrons/cm^2 shows essential agreement with earlier neutron-hardening results. The results are discussed in terms of a source-hardening mechanism.

APPARATUS FOR ANELASTICITY MEASUREMENTS USING FLEXURAL VIBRATION

(internal friction; E)

P. B. DeNee V. K. Paré

The etch-pit techniques developed by Young[14] offer the possibility of correlating the anelasticity of copper crystals with their dislocation structure. Since the dislocations can be revealed as etch pits only on surfaces parallel to close-packed crystal faces, the randomly oriented cylindrical samples heretofore used are not suitable for making the desired correlations. Further, their length makes them difficult to handle without introducing bending moments which might generate additional dislocations. A different type of sample has thus

[13] Abstract of a paper by D. O. Thompson and V. K. Pare submitted for publication in the *Journal of Applied Physics*.

[14] F. W. Young, Jr., *J. Appl. Phys.* **32**, 192 (1961); **32**, 1815 (1961).

been selected. It is a rectangular bar approximately $0.72 \times 0.25 \times 0.07$ in., with its largest faces of (111) orientation. This size is compatible with existing crystal-growing, acid-cutting, and polishing equipment.[15] Thus it can, in principle, be made with very low dislocation density if desired.

In order to keep the frequency of operation in a desirable range (15 to 20 kc) and facilitate studies over a wide range of strain amplitude, a holder has been built and tested in which the sample is driven electrostatically in the fundamental flexural mode. (In the existing apparatus[16] a cylindrical sample is driven longitudinally by an eddy-current system.) The sample is mounted on four screw pins at the displacement nodes of the fundamental mode of oscillation. The driving force is obtained by applying an alternating voltage, superimposed on a constant direct voltage, between an electrode and the sample. In the presence of the direct voltage, there is a component of force on the sample which is proportional to the alternating voltage and has the same frequency. Both these characteristics are required for adaptation to the semiautomatic closed-loop anelasticity equipment. The capacitance/frequency-modulation detection unit[16] is retained in the revised system.

To facilitate testing the flexural sample holder assembly, the necessary electronic equipment has been set up for internal friction and modulus measurements. Tests have shown that with this equipment the internal friction can be measured over a range of strain amplitude of 5×10^{-9} to 3×10^{-5}, when the logarithmic decrement of the sample is 2×10^{-3}.

This apparatus serves also for research measurements which do not require the capabilities of the semiautomatic closed-loop equipment. An experiment is being performed in which the internal friction and its amplitude dependence are measured before and after an irradiation dose of 8×10^{15} neutrons/cm^2, in copper crystals having a wide range of dislocation densities. The principal objective of this work is to see whether there is a correlation between the dislocation density and the residual internal friction after irradiation. Such a correlation would exist if, as has been inferred from other work,[17] the density of radiation-defect pinning points on a dislocation approaches, with increasing dose, a saturation value, as a result of clustering by diffusion along the dislocation.

Further tests have been concerned with the effect of driving the mounting pins into the flexural samples. One of the first mounting attempts produced a dislocation density of about 10^8 cm^{-2} near the pins; however, by the use of sharper pins and a more careful technique, the density of fresh dislocations generated in a later sample was about 2×10^5 cm^{-2}, primarily within a radius of 1 mm from the pins. It thus appears that with further refinements it should be possible to make anelastic measurements on copper crystals of very low dislocation density.

EFFECT OF ANELASTICITY ON ULTRASONIC SECOND-HARMONIC GENERATION IN COPPER

(elastic constants; dislocations; T)

M. A. Breazeale[18]

Many solid-state phenomena, such as damping of dislocation motion, thermal resistivity, and the attainment of thermal equilibrium among phonons, depend on the interaction of phonons or other stress fields with one another. This interaction takes place through the nonlinear elastic properties of the solid.

These properties can best be described by a generalization of the theory of elasticity in which one accounts for finite displacements. For infinitesimally small displacements, Hooke's law is valid, and the elastic behavior of the material can be described by the ordinary elastic constants. For finite displacements the nonlinear properties become significant. In this case one must include higher-order elastic constants to describe the behavior of the material under stress. These constants arise as coefficients in the strain-energy expansion in terms of strain components. In this expansion it is no longer accurate enough to include only the customary second-order coefficients

[15] F. W. Young, Jr., and T. R. Wilson, *Rev. Sci. Instr.* **32**, 559 (1961).

[16] D. O. Thompson and F. M. Glass, *Rev. Sci. Instr.* **29**, 1034 (1958).

[17] D. O. Thompson and V. K. Paré, *Solid State Div. Ann. Progr. Rept. May 31, 1963*, ORNL-3480, p. 65.

[18] Summer employee, 1963, and consultant from the University of Tennessee, Knoxville.

(which are the ordinary elastic constants). One must include at least the third-order coefficients (i.e., the third-order elastic constants). These coefficients, which allow a more accurate description of the nonlinear behavior of the material, and hence a better description of phonon-phonon interactions, enter into the ultrasonic experiments described here.

In general, there are two phenomena which can give rise to discrepancies between the infinitesimal theory of elasticity and experiment and thus necessitate a more complete theory. First, the solid may be anelastic or plastic. Second, the deformation may be so large that the strain is no longer proportional to the applied stress. In the experiments described here, these phenomena are both evident. These results, and the results of previous radiation damage studies, indicate that one may be able to use irradiation to control the effect of anelasticity in metal single crystals in order to study the nonlinearity and the associated anharmonicity.

In an effort to develop further a method for ultrasonic measurement of the third-order elastic constants of metals, experiments were performed using copper single crystals.[19] The experimental method used is based on the fact that in a nonlinear medium an initially sinusoidal wave becomes distorted as it progresses, with the result that harmonics of the fundamental frequency are generated. This phenomenon has been observed in gases,[20] liquids,[21] and solids.[22] The experimental arrangement is shown schematically in Fig. 13.2. Electrical pulses of 1 to 2 μsec duration having a peak amplitude of approximately 1000 v are applied to a 30 Mc/sec quartz transducer bonded to the metal sample under study. Detection of the fundamental and second harmonic is accomplished by use of i.f. amplifiers tuned to the frequency of interest.

A simplified analysis of the propagation of a finite amplitude wave in a solid has been made in order to define the "discontinuity distance" in copper crystals. One assumes that the wave is generated as a sinusoid, but that as it progresses it becomes distorted into a sawtooth form. The distance of propagation required for the leading edge of the sawtooth wave to have a vertical tangent is defined as the discontinuity distance. The analysis shows that the discontinuity distance is given by

$$L = \frac{U_0 \lambda}{2\pi U_a} ,$$

where U_0 is the velocity of a wave, of wavelength λ, having infinitesimal amplitude, and U_a is the excess velocity resulting from finite amplitudes. This means that the phase velocity in the part of the wave where the maximum stress occurs is

$$U = U_0 + U_a .$$

The quantity U_a is dependent on the direction of propagation in the crystal. For example, for a longitudinal wave propagating in the $\langle 100 \rangle$ direction in a cubic crystal, U_a is given by

$$\frac{U_a}{U_0} = \frac{\sigma(C_{11} + C_{12} + 3C_{111} + C_{112})}{2(C_{12}^2 C_{11})/(C_{11} + C_{12}) - C_{11}^2} ,$$

where σ is the applied stress amplitude. This expression for the discontinuity distance can be

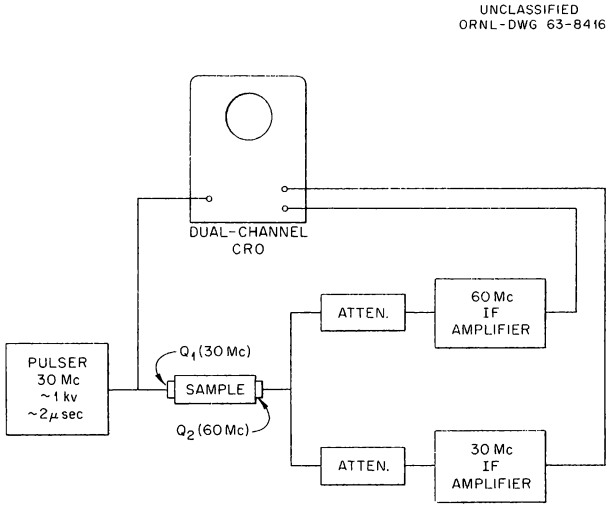

Fig. 13.2. Experimental Arrangement for Observing Harmonic Generation. Q_1 and Q_2 are quartz transducers.

[19] Provided by F. W. Young, Jr.

[20] A. L. Thuras, R. T. Jenkins, and H. T. O'Niell, *J. Acoust. Soc. Am.* **6**, 173 (1935).

[21] M. A. Breazeale and E. A. Hiedemann, *Naturwissenschaften* **45**, 157 (1958); *J. Acoust. Soc. Am.* **30**, 751 (1958); *J. Acoust. Soc. Am.* **33**, 700 (1961).

[22] M. A. Breazeale and D. O. Thompson, *Appl. Phys. Letters* **3**, 77 (1963).

used to determine whether one is meeting the conditions under which an approximate solution of the nonlinear wave equation is valid.

Such an approximate solution gives, under the assumption of a sinusoidal driver at $x = 0$, the results that for small path length x the second harmonic should be a quadratic function of the source amplitude and a linear function of x. This solution is valid for $x < 1/\alpha$, where α is the ultrasonic attenuation coefficient.

Measurements have been made on a series of copper single crystals, all oriented along the $\langle 111 \rangle$ direction. The behavior of the fundamental and the second harmonic in a 9.1-cm copper crystal is shown in Fig. 13.3, in which is demonstrated the effect of annealing at 625°C for 20 hr. The ordinate is plotted in terms of reduced variables as indicated. It is seen that the fundamental is linear in source voltage and the second harmonic is quadratic, as predicted by theory. This is shown more clearly in Fig. 13.4, which is a log-log plot of the data taken after annealing. In this plot a straight line of slope 2 represents a second-order curve. The deviation of the curves from linearity is associated with large amplitude attenuation. A plot of the attenuation coefficient for the 30-Mc fundamental component is given in Fig. 13.5. The influence of annealing is presumably an indication that dislocations play a role in the attenuation.

Further tests of theoretical predictions were made by use of copper crystal samples of various lengths. It is predicted that for sufficiently small attenuation and propagation distance, the second harmonic will increase linearly with distance. It is found experimentally in liquids that, if the attenuation is too great, the second harmonic goes through a maximum at a certain distance. The presently available theory requires that one remain in the linear region in order to determine the third-order elastic coefficients. It is thus of interest to determine whether the linear region in solids behaves in the same way as in liquids, and further to test whether the linear region may be controlled

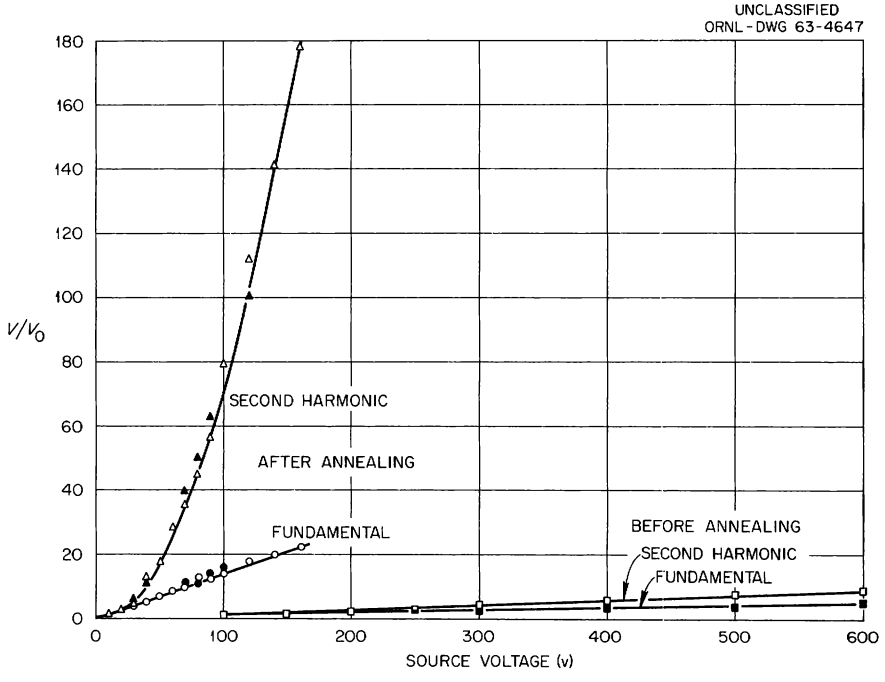

Fig. 13.3. Amplitude of Second Harmonic and Fundamental in $\langle 111 \rangle$ Direction in Copper, Showing Effect of Annealing. For either the fundamental or the second harmonic, V/V_0 is the ratio of the amplitude at the given source voltage to that at 10 v.

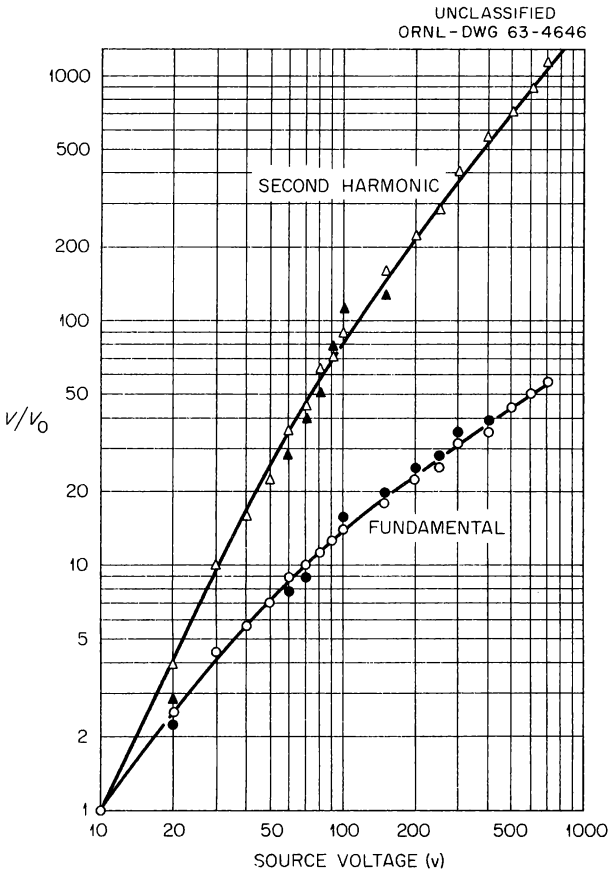

Fig. 13.4. Behavior of Second Harmonic After Anneal.

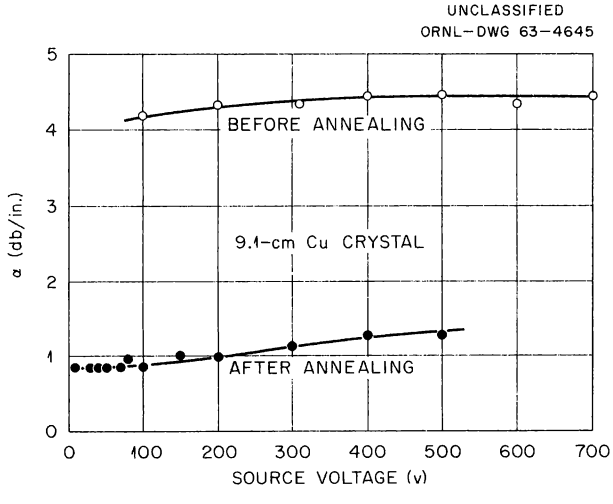

Fig. 13.5. Attenuation of 30-Mc/sec Fundamental Before and After Anneal.

by neutron bombardment of the copper crystals. The behavior of the second harmonic measured in samples of different lengths before and after a neutron bombardment of 3.6×10^{15} neutrons/cm^2 is given in Fig. 13.6. Again, the ordinate is a relative scale. One sees that the amplitude of the second harmonic increases with distance, as it should. Further, the expected linear increase with distance is improved after bombardment. As the distance increases, the second harmonic evidently is approaching a maximum value; however, it appears that at shorter distances the approach to linearity is in reasonable agreement with theoretical predictions. Thus it appears that neutron bombardment can be used to separate anelastic effects from nonlinear effects.

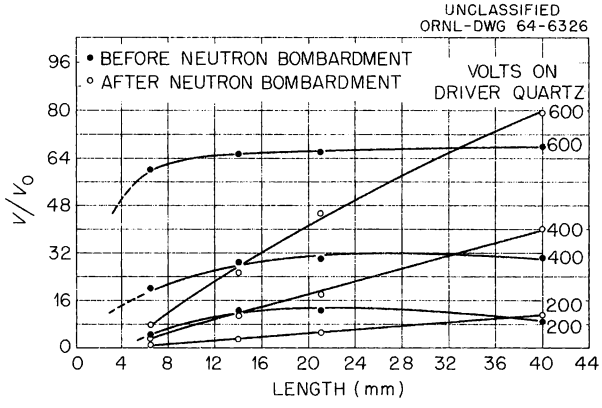

Fig. 13.6. Behavior of Second Harmonic in Copper as a Function of Distance, Showing Effect of Neutron Bombardment.

CAPACITANCE MICROPHONE DETECTOR FOR ULTRASONIC WAVES

(absolute displacement amplitude; E)

D. O. Thompson[1] M. A. Breazeale[18]

The preceding article describes experiments directed toward the measurement of third-order elastic constants of crystals by observation of second harmonic distortion generated in large-amplitude ultrasonic sound wave pulses. To obtain quantitative results by this means, it is necessary to measure on an absolute basis the

amplitude of both the fundamental and the second harmonic components of the wave. The piezoelectric (quartz) transducers normally used in ultrasonic work are not very suitable for this purpose since the relationship of output voltage to sound wave amplitude is highly sensitive to the transmission characteristics of the bond between the sample and the transducer and also is affected by the damping coefficient of transducer oscillation.

For this reason a detector has been built which senses displacement of the surface of the sample through the resulting change of the capacitance between the sample and a plate mounted approximately 0.001 in. away. A dc potential is applied between the sample and the plate. When the end of the sample is vibrated by ultrasonic waves passing through the sample and impinging on the end, an alternating potential appears at the plate. This alternating voltage is amplified and displayed on an oscilloscope. The built-in transistor amplifier circuit is a wide-band type, whose gain is constant within 1% from 5 Mc to 100 Mc. Since, if the sample-plate gap has been measured, the input voltage to the amplifier can be directly related to the displacement of the sample surface, the entire unit functions as a frequency-independent detector of absolute displacement amplitude.

Figure 13.7 is a photograph of the sample holder and detector along with a stainless steel coaxial line to be used in studies in which the sample is to be at very low temperatures. By the use of this device, displacements as small as 1 A are detectable at 30 Mc.

Design and engineering work on the transistor circuit were done by F. M. Glass and H. Adams of the Instrumentation and Controls Division. The mechanical components were fabricated by J. L. Breedlove of the Plant and Equipment Division.

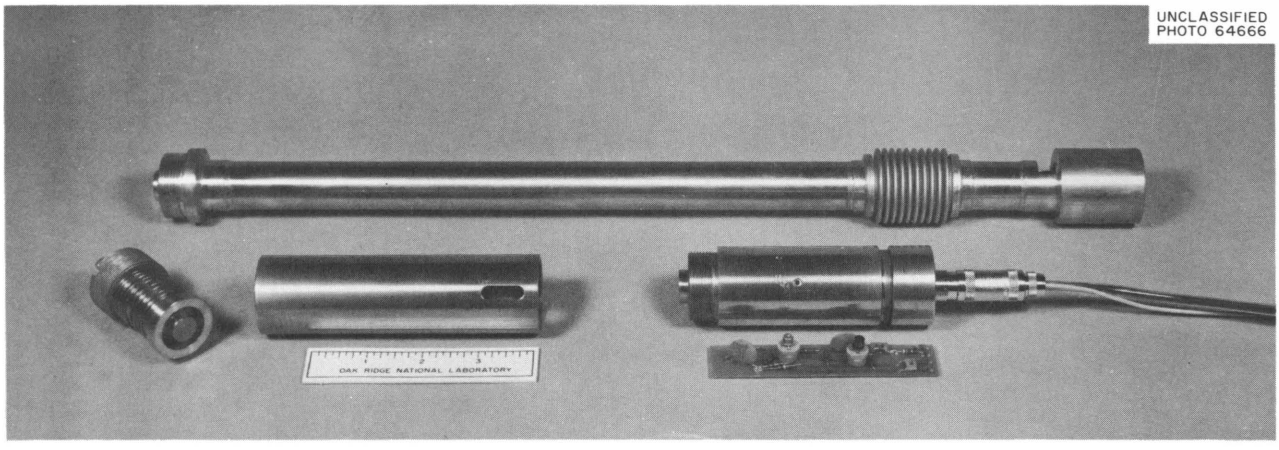

Fig. 13.7. Capacitance Detector and Sample Holder Assembly. The cylinder at the right holds the electrode plate and the transistor amplifier circuit, shown in the foreground. The slotted cylinder and spring-loaded assembly constitute the sample holder. The long tube is a coaxial line for use when low-temperature measurements are desired.

14. Ar^+ Ion Bombardment of Metal Surfaces

A. L. Southern

MASS SPECTROMETRIC STUDIES OF SPUTTERED PARTICLES FROM COPPER MONOCRYSTALS[1]

($3\text{-kev } Ar^+$; E)

Copper single crystals were bombarded with Ar^+ ions of 3 kev energy, and the positive ions ejected at 90° from the bombarding beam were mass analyzed. The mass spectrometer was a 6-in.-radius 60°-sector system capable of operating at a vacuum of $\sim 10^{-9}$ torr. Analyses were made of the positive ejected ions as a function of baking out the system. A clean surface as prepared for sputtering experiments was used as the basic surface; then several high-vacuum techniques were employed, and the degree of surface cleanliness was evaluated by comparing the spectra of the extraneous ejected positive ions. The peak heights and half-widths and areas under the peaks for masses 63 and 65 as a function of angle of incidence were investigated. There is no simple correlation between peak heights and areas, and apparently there is no simple comparison with any of these properties and the angle of incidence. It was found that the ratio of sputtered peak heights for $^{63}Cu^+$ to $^{65}Cu^+$ compared favorably with the isotopic ratio only for an angle of incidence between 72 and 80°.

SPUTTERING YIELDS AND EJECTION PATTERNS

(Ar^+ on Au, Zn, Cu, Al; E/T)

In connection with the studies of atom-ejection patterns,[2] two additional types of collectors have been used. Previous ejection patterns were collected only on plates, which tend to distort the pattern away from the center. Normally, atoms ejected from a polycrystalline surface have a cosine distribution, for which the ideal collector would be a sphere. While intensity could most easily be measured with the spherical collector also for single-crystal patterns, a hemispherical collector should have a better sticking coefficient since the surface is perpendicular to the ejection direction in all cases. Therefore, ejection directions are now measured using hemispherical collectors. In order to measure the intensity as a function of ejection angle, the collector was changed to a half-cylinder film which could be flattened for analysis.

Face-centered cubic structures such as copper have had three focusing collision sequences identified: [110], [001], and [111]. The [110] is predominant and in agreement with Silsbee's postulation. The ejection in [001] and [111] appears to result from "assisted focusing" chains, as discussed by Nelson and Thompson.[3] Experiments have been performed on gold in order to compare its "efficiency of focusing" with aluminum and copper. As the atomic core size becomes smaller in comparison with the lattice spacing, the intensity of ejection in the [001] might be expected to increase relative to the [110]. Figure 14.1 shows the ejection patterns of the (001) and (110) planes of aluminum, copper, and gold collected on a plate, with the appropriate stereographic plot.

---

[1]Abstract of paper to be presented and published in the Twelfth Annual Conference on Mass Spectrometry and Allied Topics, Montreal, Canada, June 7–12, 1964.

[2]A. L. Southern, M. T. Robinson, and D. R. Burrowbridge, *Solid State Div. Ann. Progr. Rept. Aug. 31, 1962*, ORNL-3364, p. 79.

[3]R. S. Nelson and M. W. Thompson, *Proc. Roy. Soc. (London)* **259**, 458 (1961).

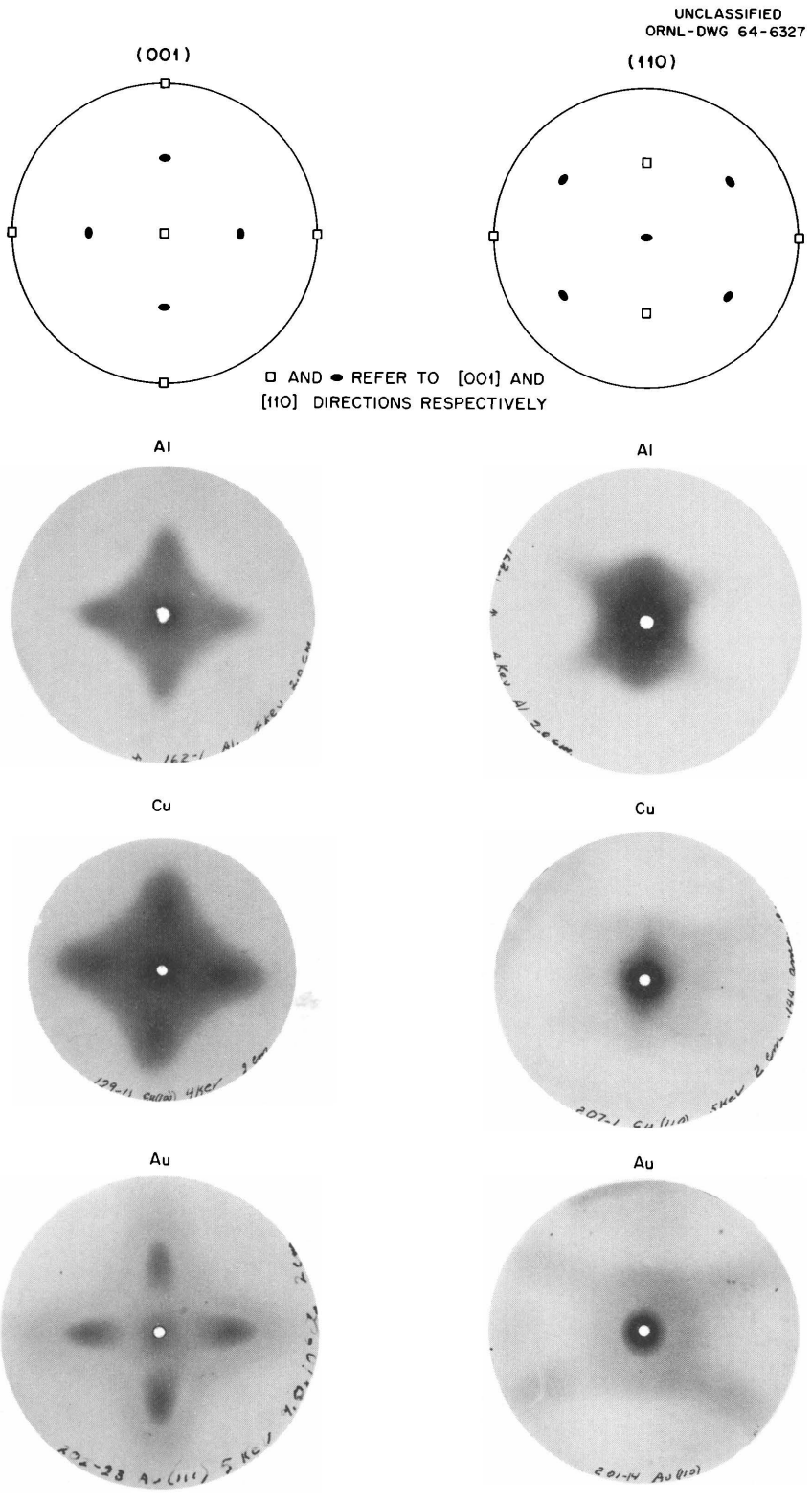

Fig. 14.1. Atom-Ejection Pattern for Aluminum, Copper, and Gold (001) and (110) Planes Under Normally Incident Ar^+ Ion Bombardment.

For the (001), notice the absence of the [001] spot for gold and the presence of this spot for aluminum. Also, the [110] spots are dark and more defined in gold than in copper or aluminum. A similar comparison can be made for the (110). Figure 14.2 shows a comparison of the ejection patterns from the (001), (110), and (111) planes of gold for the three types of collectors used. The atom-ejection patterns for the (110) particularly show the advantage of using a hemispherical collector over a plane collector.

The sputtering yield vs ion energy for a polycrystalline and three planes of monocrystalline gold are shown in Fig. 14.3. These results are compatible with the transparency model proposed for copper.[4] The more open orientation has the lowest yield. The yields for aluminum, copper, and gold for the (111) plane bombarded with 5-kev Ar^+

[4]A. L. Southern, W. R. Willis, and M. T. Robinson, *J. Appl. Phys.* **34**, 153 (1963).

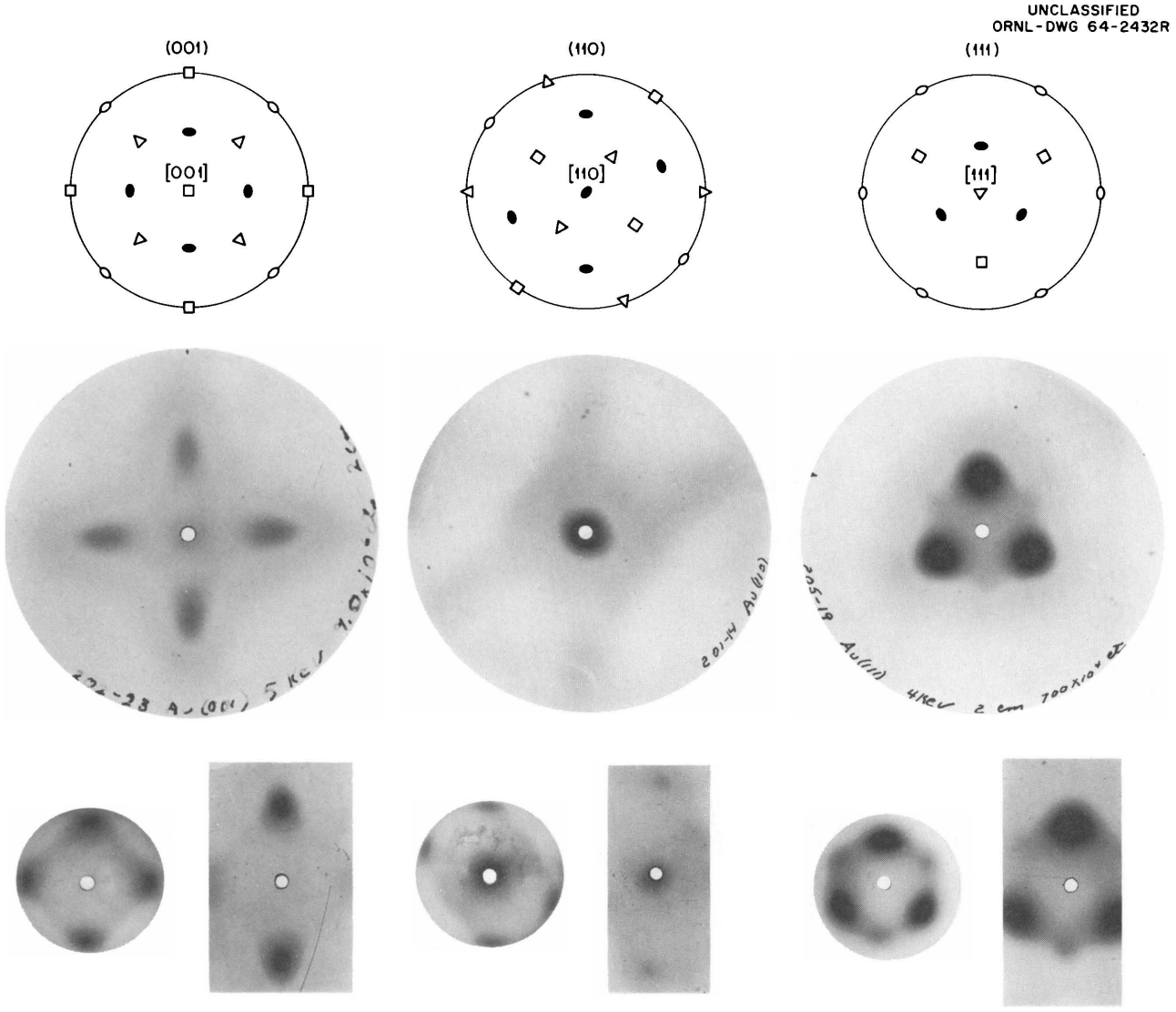

Fig. 14.2. Atom-Ejection Pattern of the (001), (110), and (111) Planes of Gold Under Normally Incident Ar^+ Ion Bombardment. The second row is patterns collected on plates, and the third row alternates from hemispherical to cylindrical collectors.

ions normal to the surface are 2.54, 9.3, and 10.6 atoms/ion respectively.

It has been previously observed[2] that a focusing process other than the Silsbee focusing collision may exist in the hcp metal zinc. Recent studies have demonstrated the existence of these focusing processes in cadmium and magnesium. In the hcp metals one would expect strong focusing in the $[11\bar{2}0]$, and this direction extends from the $(10\bar{1}0)$ and $(11\bar{2}0)$ planes. In addition, there are staggered chains of atoms extending from (0001) as well as $(10\bar{1}0)$ and $(11\bar{2}0)$.

The two most likely focusing mechanisms for the (0001) are two-atom focusing or focusing along a staggered chain of atoms. Experimental ejection patterns seem to favor the two-atom focusing. The $[20\bar{2}3]$ direction is composed of a surface atom, an atom in the second layer, and the next two atoms are in the seventh and eighth layers; this direction is 32° from the normal for zinc. When the (0001) of zinc is bombarded with Ar^+ ions normal to the surface, an atom-ejection pattern is formed which has six spots located 32° from the surface normal in $[20\bar{2}3]$. Figure 14.4 shows the atom-ejection pattern of the (0001), $(10\bar{1}0)$, and $(11\bar{2}0)$ planes

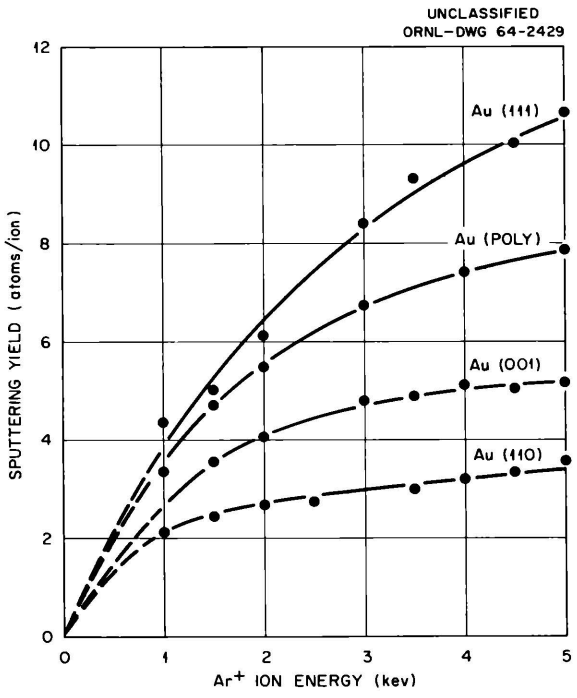

Fig. 14.3. Sputtering Yield of the (001), (110), (111), and Polycrystalline Gold as a Function of Normally Incident Ar^+ Ion Energy.

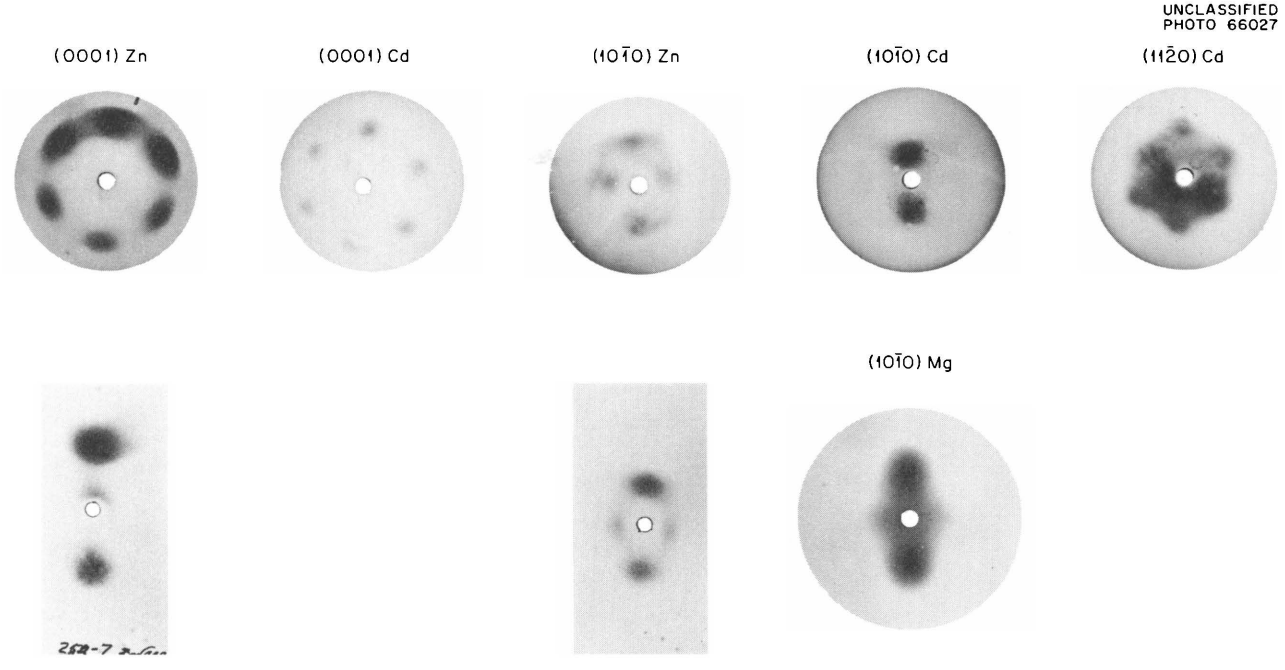

Fig. 14.4. Atom-Ejection Pattern for Zinc and Cadmium (0001), $(10\bar{1}0)$, and $(11\bar{2}0)$ Planes and $(10\bar{1}0)$ Plane of Magnesium Under Normally Incident Ar^+ Ion Bombardment at 4 kev Energy. The top row is patterns collected on a hemispherical collector, and the bottom row is of half cylinders and a plate collector.

of cadmium and zinc and the $(10\bar{1}0)$ plane of magnesium. Atoms ejected in $[11\bar{2}0]$ should be ejected normal to the surface from the $(11\bar{2}0)$ and 30° to the normal for the $(10\bar{1}0)$. The spots of the $(10\bar{1}0)$ pattern of Fig. 14.4 measure 18 and 26° from the surface normal and are approximately in $[40\bar{4}1]$ and $[11\bar{2}0]$ directions. The ejection in $[11\bar{2}0]$ may be due to Silsbee-type focusing, but that in the $[40\bar{4}1]$ may be similar to "assisted focusing" in the [111] direction for the fcc metals. Figure 14.4 also shows the ejection pattern from the $(10\bar{1}0)$ of magnesium as collected on a glass plate. The two spots are approximately 24° from the surface normal, and again these are approximately in the $[11\bar{2}0]$ direction. The pattern for the $(11\bar{2}0)$ plane of cadmium is similar to that for the basal plane. The spots, about 20° from the normal, may be due to staggered chain focusing, and apparently there is no evidence for ejection along the close-packed focusing chain from this face.

The sputtering yield of the (0001) and $(10\bar{1}0)$ planes of zinc are shown in Fig. 14.5. The yield of $(11\bar{2}0)$, which is under investigation, is lower than those of (0001) and $(10\bar{1}0)$. It is of interest to note that the fraction of sputtered material included in the spots is significantly smaller for the hcp crystals than for the fcc crystals.

Ejection patterns for the (0001) plane of zinc collected on glass plates were reported previously,[2] and it was suggested that the background indicated irradiation damage of the crystal. Recent studies of the bombarded area on the crystal showed a roughening of the surface with bombardment which may also affect the ejection patterns. Electron microscopy and electron diffraction studies suggested that the surface roughness consisted of oriented zinc crystallites.

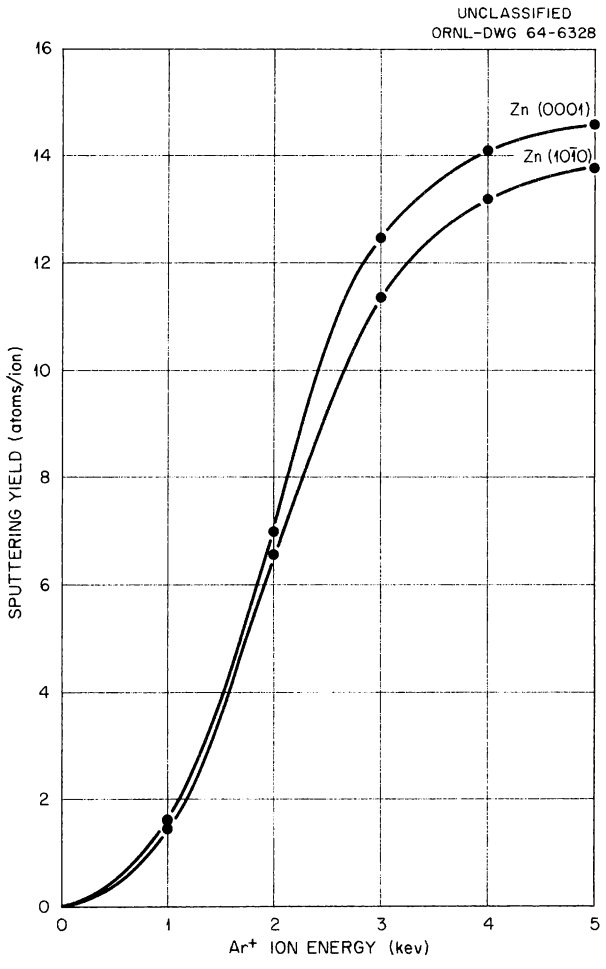

Fig. 14.5. Sputtering Yield of the (0001) and $(10\bar{1}0)$ Planes of Zinc as a Function of Normally Incident Ar^+ Ion Energy.

Part IV. Nonmetals

J. H. Crawford, Jr.

15. Insulating Crystals

COLOR-CENTER PRODUCTION AT LIQUID-NITROGEN TEMPERATURE

(electron irradiation; doped KCl; E)

W. C. Mallard[1] W. A. Sibley E. Sonder

The influence of trace impurities[2] and the equilibrium behavior of F- and M-centers[3] studied previously suggest that the steady-state electron or hole concentration during irradiation may be of pivotal importance in the room-temperature coloration processes. In order to analyze the kinetics of the current carriers and defects produced during irradiation, it was desirable to determine, experimentally, the energy necessary to produce an electron-hole pair. Work on this problem was started during the summer of 1963. The initial work was based on the proposition that at liquid-nitrogen temperature the maximum rate of introduction of the V_k-band (self-trapped hole) would be equal to that of electron-hole pairs if the electrons were not permitted to recombine. It was hoped that this could be accomplished by using KCl samples doped with strong electron traps.

Results of the original summer study, "Self-Trapped Hole Production in KCl:Pb and KCl:Tl,"[4] including some of the complications discovered, are summarized in the following abstract:

"Preliminary investigation at liquid nitrogen temperature of the increase in optical absorption of KCl near 350 mμ, due to 40 kvp x-ray irradiation, has shown the following: (1) Doping with Pb or Tl enhances the x-ray produced absorption near 350 mμ (V_1, V_k region). Heating a heavily Pb-doped sample to 625°C[5] in air created a further enhancement. (2) A greater temperature stability of the absorption was noted in the doped and heated samples. Heating to 145°K caused relatively small decreases in the absorption. Since the V_1-band is unstable at that temperature, this would suggest that it is the V_k-band whose production is being enhanced.[6] (3) The initial rate of increase in the height of the V_k band in a heavily doped (1 mole % $PbCl_2$ in the melt) and heated sample was more than a factor of five faster than the F-band. There were indications that the rate later decreased. (4) A sharp absorption band at 253 mμ was observed in the heavily Pb-doped and heated KCl sample. This band was not observed in other specimens."

This work indicated that it is by no means assured that all electrons are prevented from recombining with holes if lead or thallium is present. Moreover, the behavior of samples heated to 625°C, and the turning over of the V_k-center introduction curves raised a number of new questions. As a result, it was decided to broaden the original experiment somewhat, to continue the study of the initial rate of V_k-center introduction by x rays in variously doped samples at Emory University, and to study the effect of impurity on the saturation of V_k-centers and on the introduction efficiency of F-centers by using the Van de Graaff accelerator at this laboratory.

Figures 15.1 and 15.2 show the two main results of the electron-irradiation studies to date. In Fig. 15.1 the height of the V_k-band is shown plotted vs the energy absorbed from the electron

[1]Emory University, Atlanta, Ga.

[2]"Effect of Lead on the Room-Temperature Colorability of KCl," this chapter.

[3]E. Sonder and W. A. Sibley, *Phys. Rev.* **129**, 1578 (1963).

[4]W. C. Mallard, E. Sonder, and J. H. Crawford Jr., *Bull. Am. Phys. Soc.* **9**, 354 (1964).

[5]T. J. Neubert and J. A. Reffner, *J. Chem. Phys.* **36**, 2780 (1962).

[6]C. J. Delbecq, B. Smaller, and P. H. Yuster, *Phys. Rev.* **111**, 1235 (1958).

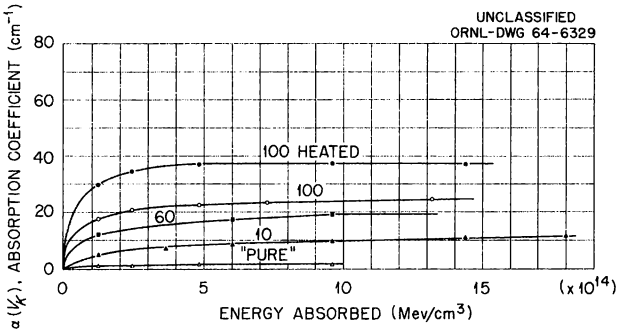

Fig. 15.1. Growth of the V_k-Band in KCl Due to Electron Irradiation at Liquid-Nitrogen Temperature. The numbers on the curves indicate lead content in ppm Pb/K. The samples, the data for which are labeled "heated," were heated to 450°C for 10 min, and then rapidly cooled before mounting in the cryostat.

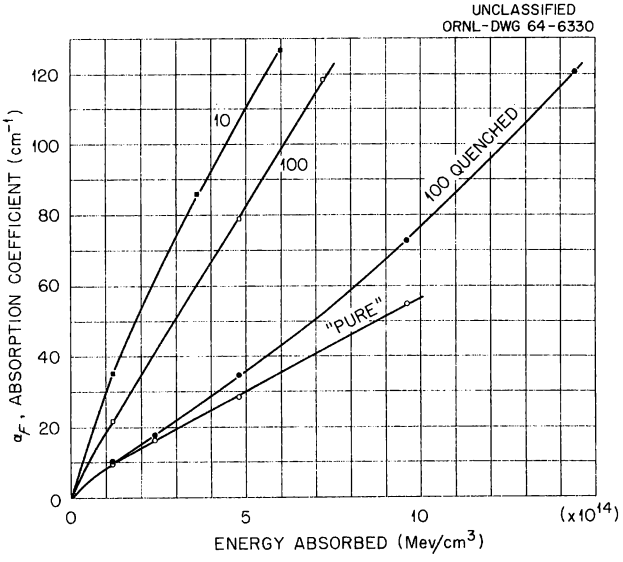

Fig. 15.2. Growth of the F-Band in KCl Due to Electron Irradiation at Liquid-Nitrogen Temperature. The numbers on the curves indicate the lead content in ppm Pb/K.

beam for a number of samples. It is clear that the self-trapped hole concentration quickly saturates and that the concentration is highly dependent upon the lead concentration and the heat treatment of the sample prior to irradiation. It should, however, be pointed out that in the case of the samples containing 100 ppm of lead, even though the saturation height of the V_k-band is increased from 25 to near 40 cm^{-1} by heating, no change in height of the lead A-band (272 mμ) due to heating was observed prior to irradiation. Thus, the correlation between the maximum number of V_k-centers formed and the lead concentration (as indicated by the lead A-band) is only partial.

Figure 15.2 shows another, and somewhat surprising, result of the low-temperature electron irradiations. Rabin and Klick[7] had indicated that F-band coloration rates at liquid-nitrogen temperature were only slightly, if at all, dependent upon (calcium) impurity content. Our results show that the effects of impurity are large, at least for the case of lead. Moreover, the effect is opposite to what we found at room temperature,[2,3] where the presence of lead caused a decrease in the late-stage coloration efficiency. The results shown are of a preliminary nature, and it is not clear yet what other factors are affecting them.

K-BAND IN KCl AT LOW TEMPERATURES

(color centers; optical spectroscopy; E/T)

R. B. Murray

The K-band is a weak optical absorption band occurring just on the high-energy side of the F-band in alkali halide crystals which have been colored either by irradiation or by additive coloration. The defect responsible for absorption in the K-band has not been identified unambiguously, although it appears that the K-band results from optical absorption by the F-center. In an experimental investigation of the K- and L-bands in various alkali halides, Lüty[8] observed that the ratio of the heights of the F- and K-bands was independent of F-center concentration over a wide range of F-center densities (for KCl, 2×10^{16} to 2×10^{18} cm^{-3}). He interpreted his results as indicating that the K-, L_1-, L_2-, and L_3-bands arise from transitions of the F electron to higher excited states. In a recent theoretical study of the excited states of the F-center, Wood[9] suggested that the K-band may be due to a transition of the F electron which is forbidden in the rigid lattice and which arises only through distortions occurring

[7]H. Rabin and C. C. Klick, *Phys. Rev.* **117**, 1005 (1960).

[8]F. Lüty, *Z. Physik* **160**, 1 (1960).

[9]R. F. Wood, *Bull. Am. Phys. Soc.* **9**, 240 (1964); also, R. F. Wood and H. W. Joy, *Phys. Rev.* (in press).

in a vibrating lattice. The possibility was raised in that work[9] that the *K*-band might be associated with transitions to two excited states of nearly the same energy and hence might exhibit a doublet structure. In order to examine this possibility, a series of experiments was performed on the shape of the *K*-band in KCl at low temperatures.

Both additively colored and irradiated crystals have been examined at liquid-nitrogen and -helium temperatures. All irradiations were performed at room temperature to avoid absorption bands due to those hole centers (*V*-bands) which are formed in low-temperature irradiations. Crystals with a nominal thickness of 1 mm were irradiated with 1.5-Mev electrons from a Van de Graaff accelerator. The crystals were contained in a cryostat, described in an accompanying report.[10]

The absorption spectrum, at liquid-nitrogen temperature, in the *F*- and *K*-band region of a heavily irradiated crystal is shown in Fig. 15.3. The absorption spectrum of another crystal (which had been irradiated much less) at liquid-nitrogen temperature is shown in Fig. 15.4. Comparison of Figs. 15.3 and 15.4 shows that the peak energy and width of the *K*-band are quite insensitive to temperature in this interval. The peak energy and width of the *K*-band (Figs. 15.3 and 15.4) are consistent with the measurements of Lüty on additively colored KCl. Also, the ratios of the *K*- and *F*-band intensities of Fig. 15.4 are in agreement with Lüty's work.

It is clear from Figs. 15.3 and 15.4 that only the high-energy side of the *K*-band is resolved from the *F*-band. In order to determine the shape of the *K*-band on the low-energy side, it is necessary to subtract the contribution from the *F*-band. This is very difficult, however, because the *F*-band is much more strongly absorbing than the *K*-band, and the detailed shape of the high-energy side of the *F*-band is not well known. The procedure followed here has been to adopt a theoretical expression for the shape of the *F*-band as given by Klick and co-workers.[11] They treat the *F*-band absorption in a configuration coordinate model in which one of the approximations usually employed has been eliminated. This results in a predicted band shape (absorption coefficient vs photon energy) which is a modified Gaussian function, asymmetrical about the peak, and which is found to be in good agreement with the experimental *F*-band on the low-energy side.

The results of fitting such a modified Gaussian function, using the parameters of Klick *et al.*, to a measured *F*-band are shown in Figs. 15.5 and 15.6. The abscissa is the square of the energy difference between the photon energy, *E*, and the

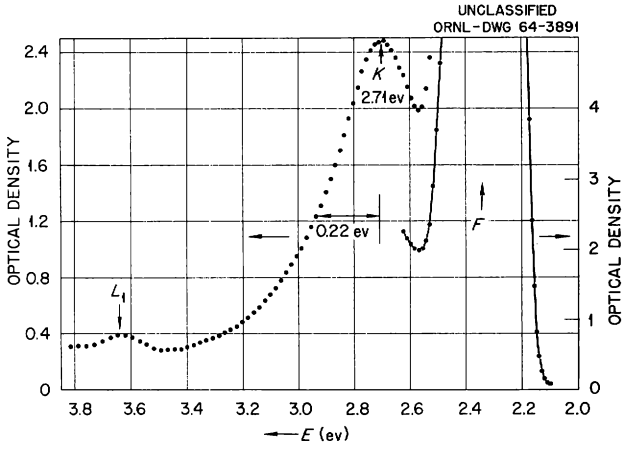

Fig. 15.3. Absorption Spectrum of KCl Irradiated at Room Temperature, Measured at Liquid-Helium Temperature.

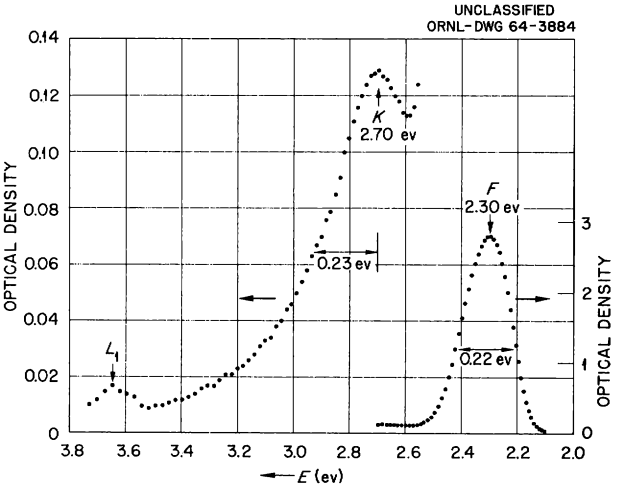

Fig. 15.4. Absorption Spectrum of KCl Irradiated at Room Temperature, Measured at Liquid-Nitrogen Temperature.

[10] "Near-Ultraviolet Luminescence in Potassium Iodide," this chapter.

[11] C. C. Klick, D. A. Patterson, and R. S. Knox, *Phys. Rev.* 133, A1717 (1964).

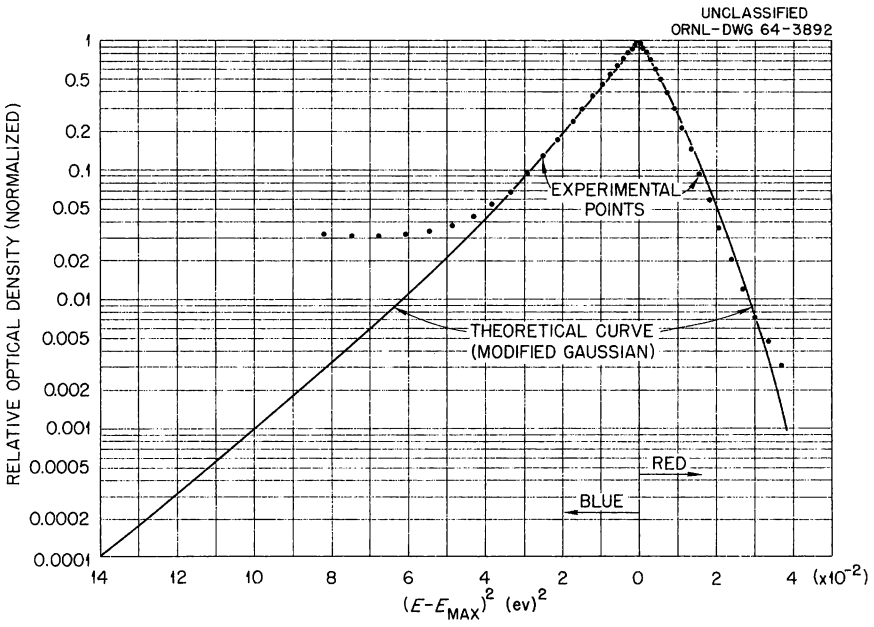

Fig. 15.5. Fit of Modified Gaussian Function to an Experimental F-Band Measured at Liquid-Helium Temperature. The ordinate of the theoretical function was adjusted to fit the experimental points; otherwise, the theoretical function is completely specified by the parameters of Klick *et al.*[11]

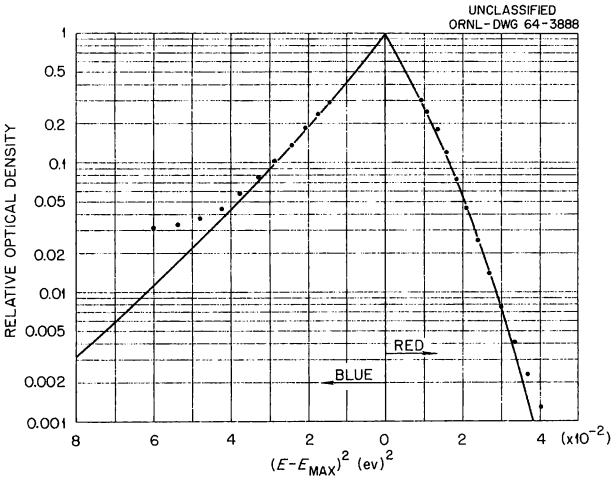

Fig. 15.6. Fit of Modified Gaussian Function as in Fig. 15.5, but with an F-Band with Higher Optical Density.

energy at the band peak, E_{max}. A strict Gaussian function on such a plot would appear as two straight lines symmetrically disposed about E_{max}. The departure of the experimental points from the calculated function on the high-energy side is, of course, due to the onset of the K-band.

Having fitted a theoretical function to the F-band data as described, it is then possible to subtract the calculated F-band contribution from the total optical density, as measured, in order to determine the contribution from the K-band. In so doing, it must be understood that the result is quite sensitive to the assumed shape of the F-band, since one is taking a small difference between large numbers. The result of this subtraction procedure is shown in Fig. 15.7. It is seen that the K-band thus determined is distinctly asymmetrical, with a long tail extending to the high-energy side. This asymmetry is in the same direction as that characterizing the F- and F'-bands of KCl. In the subtraction as described above, no account has been taken of the contribution of those M absorption bands which are known, from the work of Okamoto,[12] to lie in the 480- to 546-mμ region. It is possible to estimate the contribution of those bands from the data of Okamoto, and such an estimate shows that their contribution amounts to $\sim$10% of the measured optical density at 480 mμ (2.58 ev) and decreases rapidly with increasing photon energy.

[12] F. Okamoto, *Phys. Rev.* **124**, 1090 (1961).

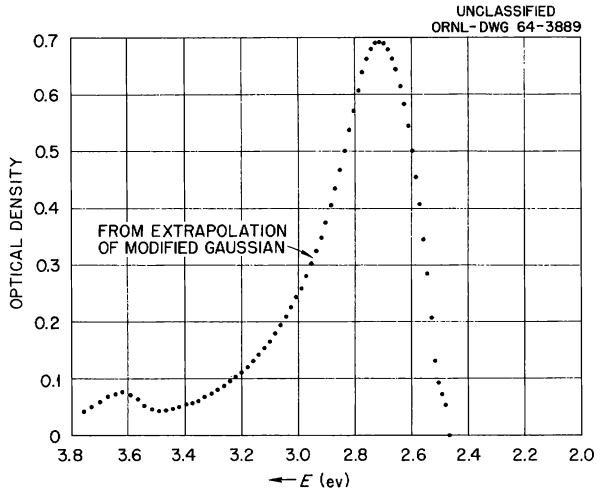

Fig. 15.7. K-Band at Liquid-Helium Temperature as Determined by Subtracting F-Band Contribution Described by Modified Gaussian Function.

Although it is not possible to estimate this contribution accurately, it is clear that a correction for the M-bands would result in a further steepening of the low-energy side of the K-band, with little effect on the high-energy side. The K-band asymmetry of Fig. 15.7 would then be even more pronounced.

It is to be emphasized that the asymmetry in the K-band shown in Fig. 15.7 depends sensitively on the assumed contribution from the F-band. To illustrate this, one can take an opposite approach and ask for the shape of the F-band which would be required to give a symmetrical K-band. This is easily determined graphically and is shown in Fig. 15.8. Figure 15.8 shows experimental data on the high-energy side of the F-band, the modified Gaussian function of Klick fitted to the data (as in Figs. 15.5 and 15.6), and a calculated curve which, when subtracted from the experimental points, gives a K-band that is symmetrical about its peak energy. It is clear that the latter curve does not differ greatly from the theoretical modified Gaussian, and there is no obvious reason to exclude it as providing a description of the high-energy side of the F-band. The point is simply that one can change the shape of the K-band on the low-energy side profoundly by relatively small variations in the assumed shape of the F-band. The continuous curve of Fig. 15.8 does not take into account the contribution of the M-bands; as indicated previously, this effect is small and does not change the conclusion.

The problem of overlap of the F- and K-bands discussed above does not extend to the high-energy side of the K-band, since the F-band contribution at the K-band peak is negligible. The experimental data as obtained should then represent the high-energy side of the K-band except for the small contribution from the L_1-band which occurs far from the K-band center. One can, therefore, ask whether the high-energy side of the K-band follows a Gaussian function. A plot of the high-energy side of the K-band is shown in Fig. 15.9, and for comparison there is shown a Gaussian function having the same half width at half maximum (0.22 ev) as the experimental data. It is seen that the data points do not even resemble a Gaussian function, but fall off much more slowly. The F-band is, of course, characterized by a similar behavior.

One experiment was performed with additively colored KCl. The results, which were obtained at liquid-nitrogen temperature, were not different from those given above.

Finally, it is seen in Figs. 15.3, 15.4, 15.7, and 15.9 that there is no evidence of a doublet structure in the K-band which is revealed in these measurements. The data points fall off smoothly, with no apparent change in slope.

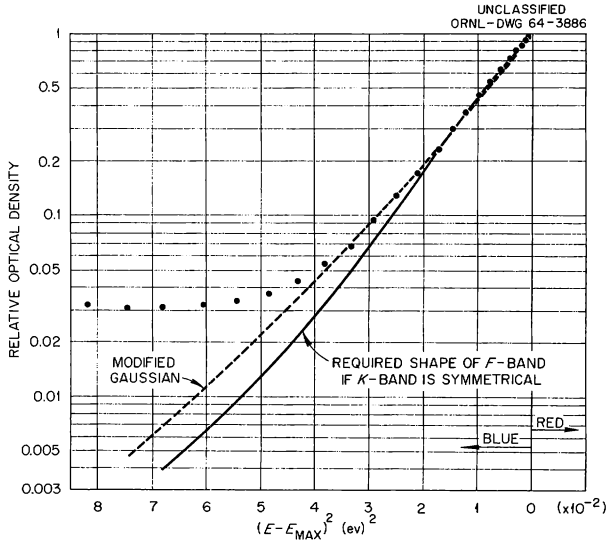

Fig. 15.8. Shape of the High-Energy Side of the F-Band Necessary to Make the K-Band Symmetrical About Its Peak Energy.

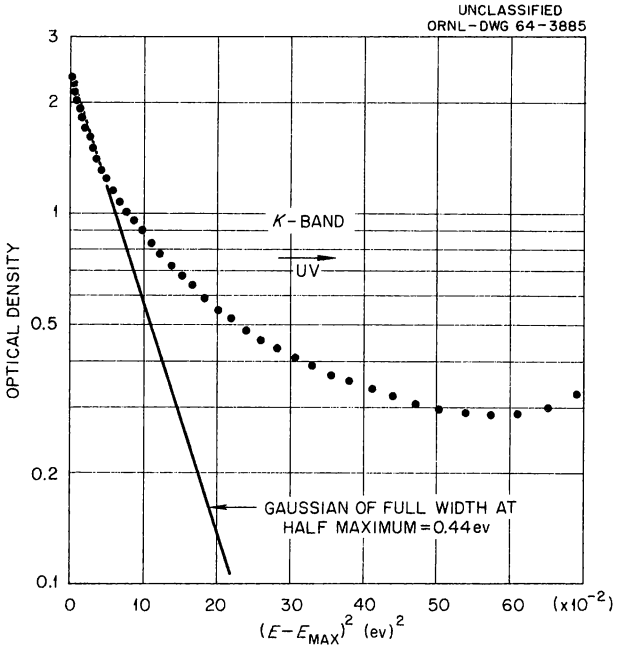

Fig. 15.9. High-Energy Side of the *K*-Band. The abscissa is the square of the difference between the photon energy and the energy of the band maximum.

Summary

The conclusions drawn from these experiments are as follows: (1) By fitting the *F*-band with a theoretical modified-Gaussian function, the resulting *K*-band is distinctly asymmetrical, with a long tail to the high-energy side. This result must be tempered with the understanding that small changes in the assumed shape of the *F*-band alter the *K*-band significantly. (2) The high-energy side of the *K*-band is clearly non-Gaussian, falling off much more slowly than a Gaussian function. (3) There is no evidence for a doublet structure in the *K*-band.

EFFECT OF LEAD ON THE ROOM-TEMPERATURE COLORABILITY OF KCl[13]

(color centers; gamma and electron irradiation; E)

W. A. Sibley E. Sonder C. T. Butler

The introduction of *F*-centers in lead-doped KCl by ionizing radiation has been measured as a function of lead content for different radiation intensities. For the lowest intensity (gamma irradiation), as little as 0.5 ppm impurity caused a marked decrease in the late-stage coloration, and less than 100 ppm completely suppressed the late stage. Lead impurities are less effective in decreasing late-stage colorability when higher irradiation intensities (electron irradiation) are used. These results suggest that previously observed variations in the late-stage coloration characteristics could have been due to trace amounts of impurities of the order of 1 ppm. Furthermore, it is suggested that these trace impurities are not depleted during irradiation, but affect the late-stage colorability by acting as electron or hole traps or as recombination centers.

F-CENTER PRODUCTION AT ROOM TEMPERATURE

(color centers; KCl; gamma irradiation; E)

E. Sonder L. C. Templeton

Late-stage coloring at room temperature should be a reflection of the intrinsic coloration chemistry in alkali halides. It is for this reason that a study of the saturation of radiation-produced *F*-centers was begun last year.[14] The initial measurements showed that the rate of approach to a limiting *F*-center value was orders of magnitude slower than the rate of establishing the *F*-*M* equilibrium. They also showed that the limiting value was greater when higher radiation intensities were used. Moreover, there was an indication that, once the limiting value characteristic of a given radiation intensity has been approached, lowering of the intensity causes a decay of the *F*-center concentration toward a value characteristic of the new intensity. Since that time a number of additional samples have been irradiated to explore the variation of this limiting *F*-center value and its rate of approach, as a function of temperature, radiation intensity, and sample. The results for three samples are reproduced in Fig. 15.10. For comparison, the initial portion of the curve, reported previously,[14] is also shown. The following conclusions can be drawn from the data.

---

[13] W. A. Sibley, E. Sonder, and C. T. Butler, abstract of paper submitted to the *Physical Review*.

[14] E. Sonder and W. A. Sibley, *Solid State Div. Ann. Progr. Rept. May 31, 1963*, ORNL-3480, p. 95.

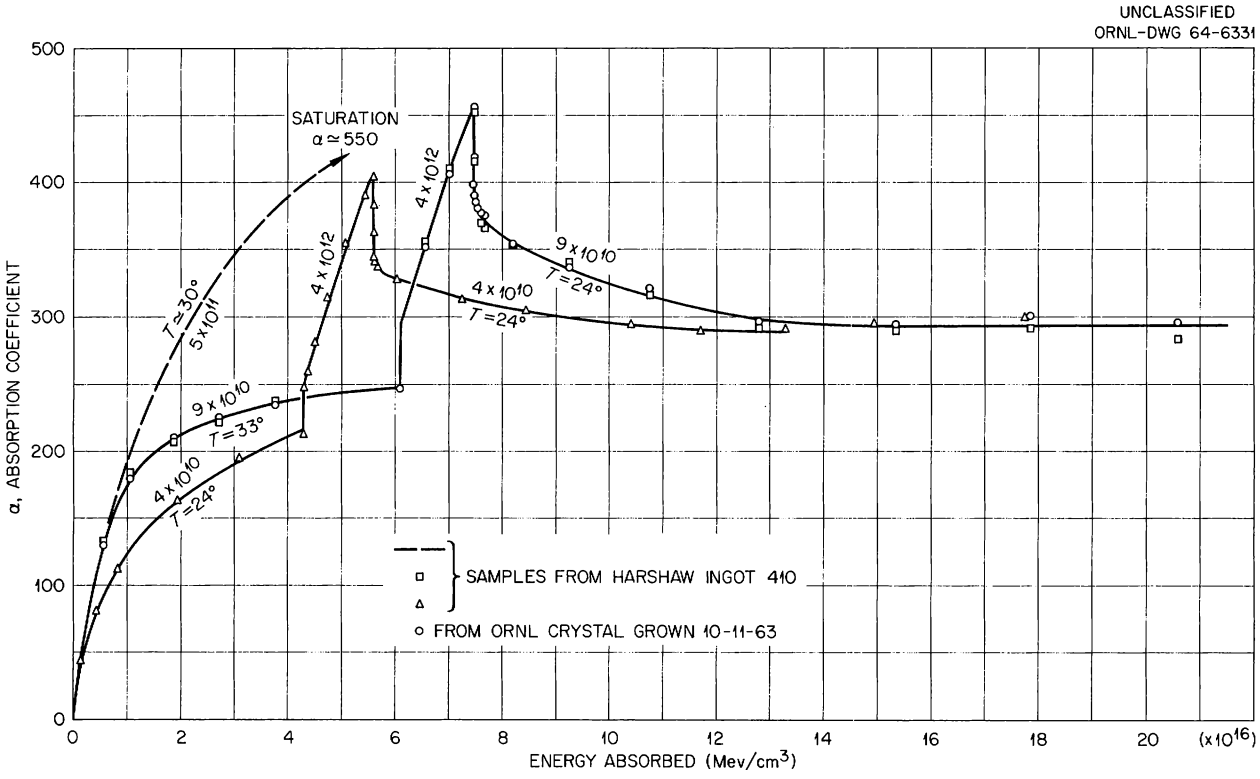

Fig. 15.10. Growth and Decay of the *F*-Band in KCl Due to Ionizing Radiation at Different Intensities and Different Temperatures. The labels for the curves give the radiation energy absorbed in Mev/sec per cubic centimeter of sample, as well as the temperature in degrees C. The vertical jumps of the curves, which occur when the intensity is changed, are due to a readjustment of the *F*-center–*M*-center equilibrium.

1. The limiting value is dependent upon intensity. This is not surprising since it is by use of high-intensity irradiation that we achieve the high *F*-center concentration used in these experiments. Comparison of the dashed curve with that for the circles and squares shows that, for an intensity ratio of approximately a a factor of 2, a similar ratio in limiting value occurs.
2. The initial rate of approach to the limiting value does not seem to be greatly affected by intensity, although at lower intensity *and* lower temperature a slower rate of rise seems to result, as shown by the curve drawn through the triangles.
3. Lowering the temperature by ~10°C seems to have an effect on the limiting value comparable to that caused by doubling the radiation intensity. This is evident by the fact that the curves through the squares and triangles both saturate near $\alpha = 300\ cm^{-1}$.
4. For two nominally pure samples so far used, one obtained from Harshaw and the other grown at this laboratory, there was very little difference in the radiation behavior when temperature and radiation rate were the same.
5. Even though a difference was discernible in the rate of initial approach to saturation for different conditions of both temperature and radiation intensity (compare curve through triangle with that through squares), the scatter of data made it impossible to discern any difference in the rate of decay of *F*-centers to approach the limiting value from above.

It is clear that both temperature and radiation intensity affect the steady-state *F*-center concentration. There is no evidence yet that trace impurities in amounts present in "pure" samples are important. We are developing temperature-control equipment for the gamma sources to permit better temperature control; this should decrease the scatter of data evident in Fig. 15.10.

A MODEL FOR RADIATION EQUILIBRIUM BETWEEN *F*- AND *M*-CENTERS IN KCl

(color centers; T)

J. H. Crawford, Jr.

The mechanism for *F*-center aggregation into *M*-centers and higher aggregate bands during *F*-band excitation has been a problem of great interest ever since the investigations of Molnar[15] and Petroff.[16] Recently, studies by Faraday *et al.*[17] and Sibley and Sonder[18,19] of the relation between *F*- and *M*-center concentrations in KCl exposed to ionizing radiation at room temperature have shown that (1) the *M*-center concentration (N_M) is approximately proportional to N_F^2 over a wide range of *F*-center concentration (N_F) for all specimens investigated; (2) the slope of the N_M vs N_F^2 curves varies widely for crystals of different origin, indictating that the relation is strongly structure sensitive; and (3) for specimens from the same ingot, the slope decreases with increasing intensity (I) of ionizing radiation. The quadratic relationship is expected according to the presently accepted van Doorn–Haven model[20] of the *M*-center, namely a coupled pair of *F*-centers, according to the reaction $2F \rightarrow M$. The decrease in slope with increasing intensity suggests that *M*-centers are destroyed by an electronic process, possibly by hole capture. This is further borne out by the fact that, by simply changing radiation intensity, the N_M vs N_F^2 relation shifts from the curve characteristic of one intensity to that for the other at a rate rapid compared with the rate of introduction of new *F*-centers.[19] Also, destruction of *M*-centers in additively colored crystals by x-ray exposure has been observed.[21]

The dependence of slope ($N_M/N_F^2 = S$) on intensity is shown in Fig. 15.11, in which $1/S$, obtained from the results of Sonder and Sibley,[19] is plotted against I (energy absorbed per unit volume per unit time). The absorption coefficient ratios (α_M/α_F^2) were converted into center concentrations by use of the Gaussian form of Smakula's equation, oscillator strengths of 0.58 and 0.25 for the *F*-[22] and *M*-centers,[23] respectively, and respective half widths[24] at room temperature of 0.35 and 0.11 ev:

$$S = N_M/N_F^2 = 1.7 \times 10^{-16}\, \alpha_M/\alpha_F^2 . \qquad (1)$$

The curve of Fig. 15.11 exhibits an intercept of 5.0×10^{18} cm^{-3} at $I = 0$, an initial linear portion with a slope of 6.5 sec/ev, and a bending over at high intensities.

This behavior can be accounted for on the basis of the following kinetic model: (1) Electron capture by *F*-centers produces mobile *F*′-centers, which migrate to neighboring *F*-centers and α-centers (anion vacancies) to form *M*-centers. (2) Hole capture by *M*-centers releases sufficient energy to cause dissociation into α-centers which

[15]Described by F. Seitz, *Rev. Mod. Phys.* **18**, 384 (1946); **26**, 7 (1954).

[16]S. Petroff, *Z. Physik* **127**, 443 (1950).

[17]B. J. Faraday, H. Rabin, and W. D. Compton, *Phys. Rev. Letters* **7**, 57 (1961).

[18]W. A. Sibley and E. Sonder, *Phys. Rev.* **128**, 540 (1962).

[19]E. Sonder and W. A. Sibley, *Phys. Rev.* **129**, 1578 (1963).

[20]C. Z. van Doorn and Y. Haven, *Philips Res. Rept.* **11**, 479 (1956); C. Z. van Doorn, *Philips Res. Rept.* **12**, 309 (1957).

[21]See, for example, G. Baldini, L. Dalla Croce, and R. Fieschi, *Nuovo Cimento* **20**, 806 (1961).

[22]E. Sonder, *Phys. Rev.* **125**, 1203 (1962).

[23]C. J. Delbecq, *Z. Physik* **171**, 560 (1963).

[24]H. Rabin, *Phys. Rev.* **129**, 129 (1963).

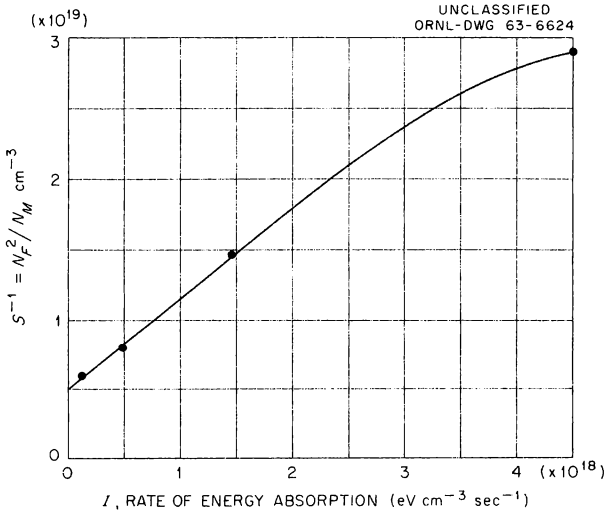

Fig. 15.11. Reciprocal of the Slopes of N_M vs N_F^2 Curves as a Function of the Ionizing Intensity (Based on Data from ref. 19).

upon electron capture become F-centers. The approximate differential equations governing the M- and F'-centers are

$$\dot{N}_M = \alpha N_F N_{F'} - \beta p N_M , \quad (2)$$

$$\dot{N}_{F'} = \gamma n N_F - (\delta + \epsilon p) N_{F'} , \quad (3)$$

where n and p are the electron and hole concentrations, and the Greek letter coefficients are described in Table 15.1. Since the α-center concentration is small compared to N_F, its contribution to $\dot{N}_M$ is assumed to be negligible, and it is omitted in Eq. (2). In Eq. (3) the lifetime of the F'-center in the room-temperature range is controlled by both thermal decomposition (ionization) and hole capture. Since the rate of establishment of N_M/N_F^2 characteristic of a new value of I is large compared to the rate of creation of new defects by the radiation field, Eqs. (2) and (3) may be solved for steady-state conditions, leading to

$$\frac{1}{S} = \frac{N_F^2}{N_M} = \frac{\beta p(\delta + \epsilon p)}{\beta \gamma n} . \quad (4)$$

Except for high ionization rates, the capture of electrons by holes may be neglected; hence, for a given rate of electron-hole excitation L,

$$n = L\tau_n = \frac{L}{4\pi D_n W_n}; \quad p = L\tau_p = \frac{L}{4\pi D_p W_p} , \quad (5)$$

where the D's are the diffusion coefficients of electrons and holes, $W_n = \Sigma_i r_{i,n} N_i$, and $W_p = \Sigma_j r_{j,p} N_j$, the sum being taken over all electron- or hole-capturing sites, and $r_{i,n}$ and $r_{j,p}$ are the capture radii of the centers for electrons and holes

Table 15.1. Definition and Approximate Values of the Kinetic Parameters in Eqs. (2) Through (6) (Evaluated at 300°K)

Parameter = Conventional Symbol	Magnitude	Units
$\alpha = 4\pi D_{F'} r_{F,F'}$	$\sim 10^{-17}$	$cm^3\ sec^{-1}$
$D_{F'} = a^2 \nu_{F'}^0 \exp(-E_M/kT)$	$\sim 0.1\ e^{-E_M/kT}$	$cm^2\ sec^{-1}$
$r_{F,F'}$	$\sim 10^{-7}$	cm
$\beta = 4\pi D_p r_{M,p}$		$cm^3\ sec^{-1}$
$r_{M,p}$	$\sim 10^{-7}$	cm
$\gamma = 4\pi D_n r_{F,n}$		$cm^3\ sec^{-1}$
$r_{F,n}$	$\sim 10^{-7}$	cm
$\delta = k_{F'}$	$\sim 5 \times 10^2$	sec^{-1}
$k_{F'} = \omega_{F'} \exp(-E_{F'}/kT)$	$\sim 10^{11}\ e^{-E_{F'}/kT}$	sec^{-1}
$\epsilon = 4\pi D_p r_{F',p}$		$cm^3\ sec^{-1}$
$r_{F',p}$	$\sim 10^{-6}$	cm
$W_n = \Sigma_i r_{i,n} N_i$	$\sim 10^{10}$	cm^{-2}
$W_p = \Sigma_j r_{j,p} N_j$	$\sim 10^{10}$	cm^{-2}
E_M (motion energy of F')	~ 0.6	ev
$E_{F'}$ (binding energy of F')	~ 0.5	ev
a (Cl^- nearest-neighbor separation)	4.4×10^{-8}	cm

respectively. The sum includes not only F, F', α, M, etc., but impurity atoms as well. For most nominally pure specimens, the concentration of the latter is comparable to, or greater than, that of the defect centers, at least up to $N_F \sim 2 \times 10^{17}$ cm^{-3} (10 ppm impurity). Therefore, if the r's are comparable, the W's are relatively insensitive to N_F, even in undoped crystals. Using the values of n and p from Eq. (5) and the equivalents of the kinetic parameters from Table 15.1, Eq. (4) can be written:

$$\frac{N_F^2}{N_M} = \frac{r_{M,p}\,(k_{F'} W_p + r_{F',p} L)}{4\pi D_{F'} r_{F,F'} r_{F,n}} \frac{W_n}{W_p^2}, \qquad (6)$$

which yields a constant value for constant L. Equation (6) has the proper form to explain the observed dependence of N_F^2/N_M upon I. If E_p is the average energy consumed in creating an electron-hole pair, $I = LE_p$ and the slope of Eq. (6) is

$$\frac{d(N_F^2/N_M)}{dI} = \frac{r_{M,p}\, r_{F',p}}{4\pi D_{F'} r_{F,F'} r_{F,n} E_p} \frac{W_n}{W_p^2}, \qquad (7)$$

and the intercept is

$$\left(\frac{N_F^2}{N_M}\right)_{I=0} = \frac{r_{M,p}\, k_{F'}}{4\pi D_{F'} r_{F,F'} r_{F,n}} \frac{W_n}{W_p}. \qquad (8)$$

Using the approximate values of the parameters of Table 15.1 and assuming that $E_p \tilde{=} 25$ ev[25] and F'-centers have an activation energy of motion[26] of 0.6 ev, one obtains values of 0.4 sec/ev and 5×10^{19} cm^{-3} for the slope and intercept respectively. When the order-of-magnitude nature of this calculation is considered, the agreement of these values with experiment is quite good. Therefore, it is concluded that this mechanism is a reasonable one, as long as N_F and I are not too large.

From Eq. (6), it is evident that the temperature dependence of the intercept enters through $k_{F'}/D_{F'} \propto \exp(E_M - E_{F'})/kT$ and that of the slope through $1/D_{F'} \propto \exp E_M/kT$. A check of this model could be based upon this temperature dependence,[27] since the thermal ionization energy of F'-centers is known[28] to be ~ 0.5 ev. Also, since Eq. (7) predicts a slope proportional to W_n/W_p^2, selective doping with an impurity that is dominantly an electron- or hole-capture center might afford another check on the model. Indeed, the value of N_F^2/N_M is markedly enhanced in Ca^{2+}-doped specimens;[18] this is in the expected direction, since an isolated Ca^{2+} ion would have a large electron-capture probability for electrons and a negligible one for holes.

A previously suggested mechanism[23,29] based upon the anion vacancy (α-center) as the moving entity interacting with F'-centers was also examined. Although the steady-state solution has the proper form, the predicted value of N_F^2/N_M is too large by at least 10^7 because of the much larger energy of motion[30] of the α-center. A detailed treatment of both mechanisms in which the assumptions and magnitudes are discussed is being prepared for publication.

RADIATION-INDUCED OPTICAL ABSORPTION NEAR THE ABSORPTION EDGE OF KCl

(E)

E. Sonder L. C. Templeton

Considerable uncertainty still exists concerning optical absorption bands introduced near the absorption edge of KCl by ionizing radiation. In particular, Christy and Phelps[31] and Lüty[32] have published diametrically opposed views to explain a band located between 210 and 220 mμ. Christy and Phelps report a square-root relationship between the V_3-band (located by them at 217 mμ at room temperature) and the F-band; they

[25]This value was taken from the average energy required to re-create F-centers in KCl irradiated and optically bleached at low temperature [H. Rabin and C. C. Klick, *Phys. Rev.* **117**, 1005 (1960)].

[26]This is the activation energy associated with F-center aggregation induced by F-band excitation [C. Z. van Doorn, *Philips Res. Rept.*, suppl. No. 4 (1962)].

[27]Preliminary studies of this type have been reported by H. Tommen, *Phys. Letters* **2**, 189 (1962).

[28]H. Pick, *Ann. Physik* **31**, 365 (1938).

[29]C. Z. van Doorn, *Philips Res. Rept.*, suppl. No. 4 (1962).

[30]For the α-center it is assumed that $E_M \geq 1$ ev. See the survey by A. R. Allnatt and P. W. M. Jacobs, *Trans. Faraday Soc.* **58**, 116 (1962).

[31]R. W. Christy and D. H. Phelps, *Phys. Rev.* **124**, 1053 (1961).

[32]F. Lüty, *J. Phys. Chem. Solids* **23**, 677 (1962).

suggest that the V_3-center is a Cl_3^- molecule ion. Lüty claims that radiation-induced absorption in this wavelength range is composed of the U-band (hydride ion) located at 214 mμ and the V_2-band near 230 mμ (ref. 33), depending upon whether or not hydrogen in the form of OH^- is present in the crystal as an impurity. In connection with our recent study of F-center introduction by radiation,[34,35] extensive data were also obtained of the ultraviolet coloration of various irradiated KCl samples. The spectra did not clearly support either of the authors mentioned above. It was clear, however, that at least in some of the samples no simple square-root dependence between ultraviolet absorption and the F-band existed. In fact, quite complicated coloring behavior was found. For example, in the case of a crystal grown at this laboratory from reagent-grade KCl (Fig. 15.12), the main ultraviolet band, appearing at 215 mμ, grew at first, but then decreased in height, while the F-band kept on growing. Later, as the curve for the 19×10^7 r irradiation shows, the absorption grew again and moved to a shorter wavelength. However, the optical density on the short-wavelength side of the band seemed to grow as rapidly as it did at the peak of the band. Unfortunately, the Cary 14 spectrophotometer, used for these measurements, is limited to wavelengths longer than ~190 mμ. A more careful study of the optical absorption near and below 200 mμ was carried out using a Cary 15 spectrophotometer whose short-wavelength limit, when purged with high-purity nitrogen gas, is 168.5 mμ. Studies of

[33] "Effect of Plastic Deformation on the Production of F-, M-, and V-Centers in KCl," this chapter.

[34] W. A. Sibley and E. Sonder, *Phys. Rev.* **128**, 540 (1962).

[35] E. Sonder and W. A. Sibley, *Phys. Rev.* **129**, 1578 (1963).

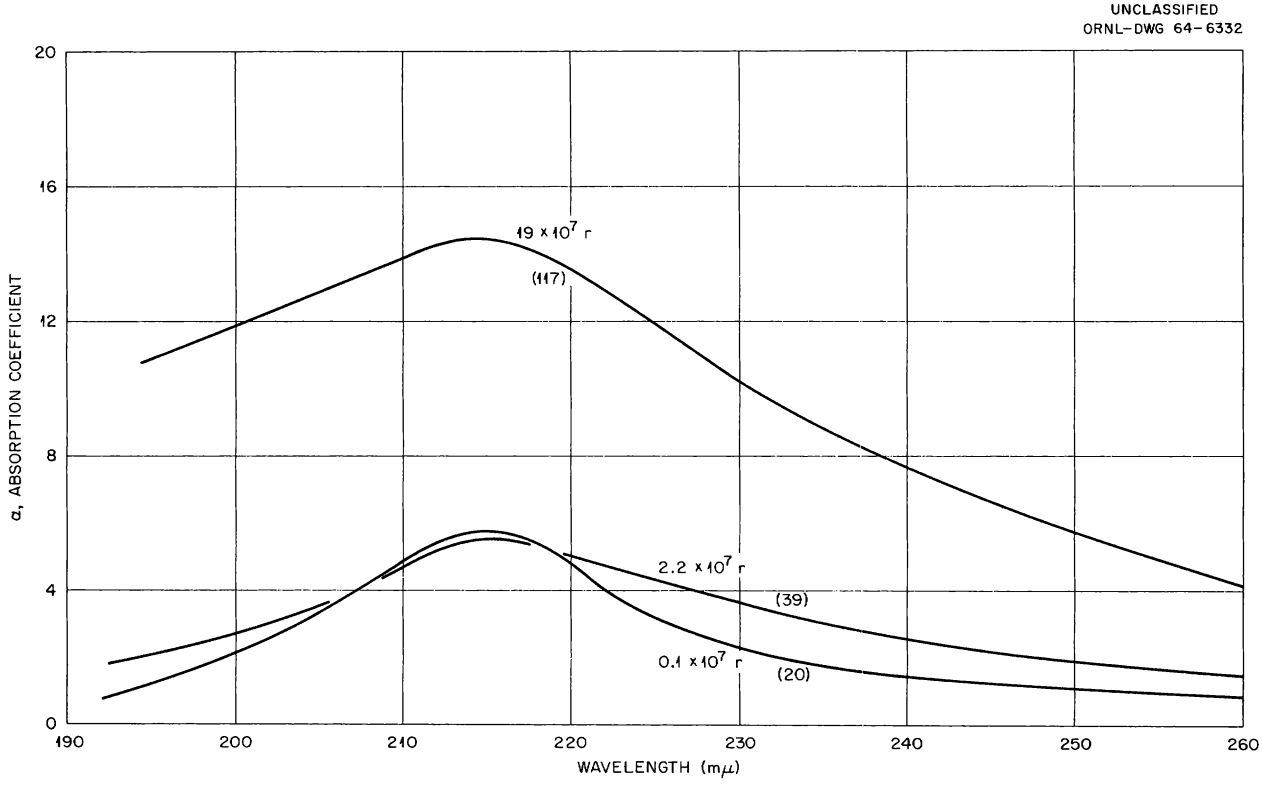

Fig. 15.12. Ultraviolet Absorption Spectra of Gamma-Irradiated Reagent-Grade KCl. The labels on the curves give the approximate gamma-ray dose and resulting F-band height (in parentheses). The change in shape of the absorption at 215 mμ is clearly evident when one compares the curves for the 0.1- and 2.2×10^{17}-r irradiations. Part of the absorption at 230 mμ is probably due to the V_2-band.

radiation-induced optical absorption near and below the 215-mμ absorption band are now in progress. Some early results obtained at room temperature are shown in Fig. 15.13. The spectra shown are for a Harshaw KCl sample irradiated in the ^{137}Cs source. The optical absorption of the sample prior to irradiation has been subtracted to produce the curves shown; the sharp rise below 180 mμ is due to *increased* absorption near the absorption edge (i.e., it indicates a radiation-induced band or radiation-induced movement of the edge). The numbers in parentheses are estimates of the *F*-band absorption coefficient. Comparison of these with the corresponding *F*-band absorption coefficients given in Fig. 15.12 shows that the first stage of the Harshaw sample (Fig. 15.13) was appreciably smaller than that of the reagent-grade KCl sample (Fig. 15.13). This suggests that the sample of Fig. 15.13 was purer than that which gave the data of Fig. 15.12. That is probably the reason why the growth of optical absorption in the vicinity of 215 mμ was much less erratic. The increase in optical density was monotonic with dose; however, the peak absorption shifted toward shorter wavelengths as irradiation progressed. Upon bleaching the sample for a day with room light, the optical density increased near 220 and 182 mμ, but decreased near 190 and below 180 mμ. These changes are shown by the circles in Fig. 15.13. The data suggest that there are more than two bands present.

Since, after heavy irradiation, the increase near 212 mμ is still greater than that near 185 mμ, it would seem that a band in the vicinity of 212 mμ is still growing. This would seem to disagree with Lüty's suggestion that the absorption in that vicinity is due solely to the *U*-band, which should saturate very rapidly. On the other hand, the broadness of the absorption and the changes in peak position and shape with irradiation and bleaching are not consistent with the square-root relation between a simple Cl_3^- ion absorbing at 217 mμ and the *F*-band that Christy has reported.

It is probably the broadness of the bands in this region that has contributed to the disagreement[31] in the literature. Lüty[32] did his measurements at -180°C and obtained narrower bands. However, his irradiations were light so that he would not have observed slowly appearing bands. He was also limited to wavelengths longer than 190 mμ. Therefore, it appears that examination of the spectrum between 190 mμ and the absorption edge at liquid-nitrogen temperature after heavier irradiations than Lüty used would be a fruitful next step in this investigation.

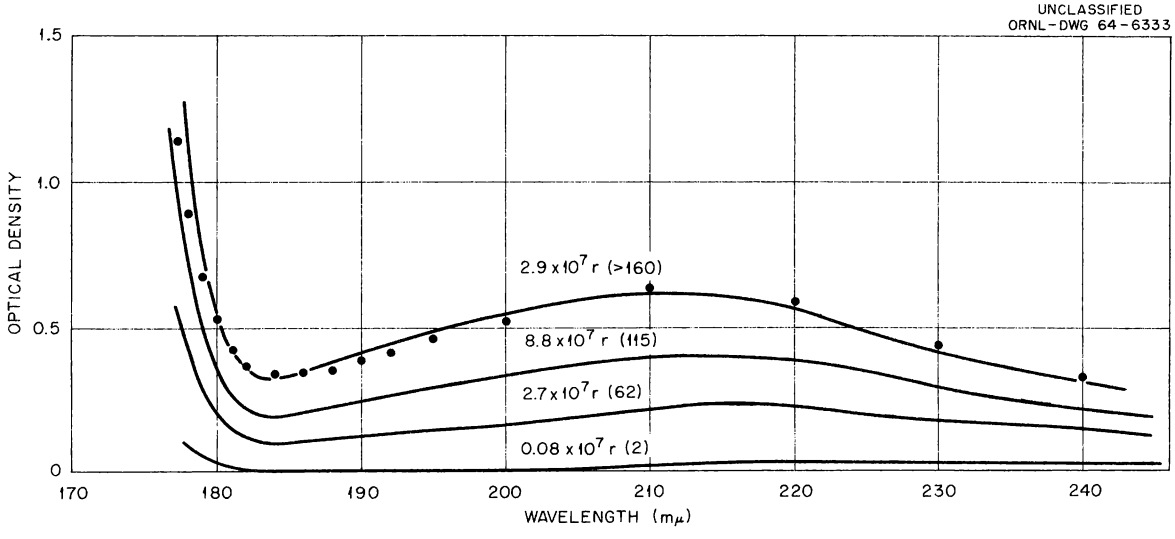

Fig. 15.13. Extended Ultraviolet Spectra of Harshaw KCl Obtained with Purged Spectrophotometer. The optical density of the sample prior to irradiation has been subtracted from the curves. The numbers give the radiation dose and an estimate of the *F*-band absorption coefficient (in parentheses).

EFFECT OF PLASTIC DEFORMATION ON THE PRODUCTION OF *F*-, *M*-, AND *V*-CENTERS IN KCl[36]

(gamma irradiation; annealing; E)

W. A. Sibley

The effect of plastic deformation and heat treatment on the room-temperature production of *F*-, *M*-, and *V*-centers by ^{60}Co gamma rays was investigated. Deformation of an irradiation sample caused a reappearance of the "first-stage" type of coloration for *F*-centers when the sample was irradiated further. This deformation-induced enhancement of the colorability could be annealed out by heat treating the samples in air at 450°C for 10 min. The V_2-band was shown to behave very similarly to the *F*-band for the same treatments.

EFFECT OF IMPURITIES ON THE HARDENING AND COLORATION OF KCl IRRADIATED AT ROOM TEMPERATURE

(color centers; gamma and electron irradiation; E)

W. A. Sibley J. R. Russell

Introduction

The question of how *F*-centers are formed in the early and late stages[37] of coloration is as yet unanswered in spite of the progress which has been made in the color-center field during the last few years.[38] It is known that the late-stage coloration depends sensitively on trace impurities[39,40] and intensity of irradiation.[41] Furthermore, the production of late-stage *F*-centers is probably accompanied by the production of interstitials.[42,43] However, it has not been possible to determine which of the proposed models[38] for *F*-center formation in the late stage is the more realistic. Early-stage coloration is particularly interesting since it can be influenced markedly by some impurities and not at all by others.[44] It is also sensitive to the intensity of irradiation,[38] deformation, and heat treatments,[41] and it may or may not contribute to the change of density or dimension in NaCl and KCl crystals upon irradiation.[45,46]

At least two explanations for the rapid *F*-center formation in the early stage have been offered. Etzel[44] has proposed that when large numbers of positive-ion vacancies are present in the crystal (these vacancies are introduced with divalent impurities to maintain charge neutrality), then the probability for the capture of holes by these vacancies to form *V*-centers is greater than it would be in a "pure" crystal. As a result, the probability for the recombination of holes and electrons is reduced, and the probability for the formation of *F*-centers is increased. Crawford and Nelson[47] have suggested that the cation vacancies introduced by the impurities can be converted to anion vacancies by irradiation. They propose that a halide ion adjacent to an isolated cation vacancy captures a hole and that the resulting halogen atom relaxes into the cation vacancy, forming an oriented molecule ion. This leaves a negative-ion vacancy which may trap an electron to form an *F*-center.

A test of the two mechanisms presented above can be made by measuring either the density change or the fractional change in the linear dimension of a specimen with irradiation. If the second model is correct, very little change in density or linear dimension would be observed for early-stage coloration. On the other hand, the first proposal should give a change even in the early stage, since vacancies must be produced during

---

[36]Abstract of published paper: *Phys. Rev.* **133**, A1176 (1964).

[37]These general coloration stages have been defined by R. B. Gordon and A. S. Nowick, *Phys. Rev.* **101**, 977 (1956).

[38]J. H. Schulman and W. D. Compton, *Color Centers in Solids*, Macmillian, New York, 1962.

[39]W. A. Sibley and E. Sonder, *Phys. Rev.* **128**, 540 (1962).

[40]W. A. Sibley, E. Sonder, and C. T. Butler, to be published.

[41]P. V. Mitchell, D. A. Wiegand, and R. Smoluchowski, *Phys. Rev.* **121**, 484 (1961).

[42]J. S. Nadeau, *J. Appl. Phys.* **34**, 2248 (1963); **35**, 1248 (1964).

[43]W. A. Sibley and E. Sonder, *J. Appl. Phys.* **34**, 2366 (1963).

[44]H. W. Etzel, *Phys. Rev.* **87**, 906 (1952).

[45]H. Rabin, *Phys. Rev.* **116**, 1381 (1959).

[46]H. Paus and K. Thommen, *Phys. Letters* **5**, 315 (1963).

[47]J. H. Crawford and C. M. Nelson, *Phys. Rev. Letters* **5**, 314 (1960).

this time. Rabin[45] has made a study of the fractional change in the linear dimensions of several doped and undoped NaCl crystals as a function of *F*-center concentration, and he found that the expansion occurs in roughly two stages. The initial expansion per *F*-center is small, whereas at later stages of coloration the expansion per *F*-center is large. Moreover, the doped samples which have a large early-stage *F*-center coloration have a relatively small expansion. These results tend to favor the Crawford and Nelson idea, but the results of Paus and Thommen[46] on density change with *F*-center concentration in KCl apparently indicate a contribution to the volume expansion by early-stage *F*-centers. Therefore, until more work is done in this area, it is not possible to say conclusively which concept is more appropriate.

A study of the radiation hardening of doped and undoped KCl is another possible method of determining which type of model is more correct. Previously,[42,43] it was shown that radiation hardening in KCl for rather heavy irradiation doses is most likely due to interstitials or interstitial clusters introduced into the crystals concurrently with *F*-centers. However, there was some suggestion[43] that small irradiation doses produce very little hardening compared with the amount of coloration. This would mean that two different mechanisms of *F*-center production, one giving a hardening center and one not, are active during irradiation. If this experimental observation could be confirmed, the simplest form of Etzel's model would be excluded since it should depend on only one type of *F*-center production, which presumably would include interstitial formation.

The purpose of this work is to determine whether early-stage coloration contributes to radiation hardening and to provide a larger base of experimental data on the coloration of calcium- and strontium-doped KCl by investigating early- and late-stage coloration as a function of radiation intensity and impurity concentration.

Experimental Procedure

Deformation samples from 0.7 to 1.0 cm long and about 0.05 to 0.1 cm^2 in cross section were cleaved from large ingots of KCl, KCl:Ca, and KCl:Sr single crystals grown by the Kyropoulos method. The starting material for these crystals was recrystallized reagent-grade KCl powder supplied by the Allied Chemical Corporation. The doping agents were $CaCl_2$ (purified, anhydrous) from Allied Chemical and reagent-grade $SrCl_2 \cdot 6H_2O$ from J. T. Baker and Company. It was found that drying at 200°C for 16 hr and cooling in a desiccator were necessary to eliminate the water contained in both the doping agents. In all cases the KCl starting material and the doping agent were thoroughly mixed before being packed into a platinum crucible. The powder in the crucible was then heated in vacuum to about 650°C and left overnight. The crystals were then pulled under an N_2 atmosphere. A series of eight crystals were grown, in the order: "pure," three calcium doped, "pure," and three strontium doped. Table 15.2 gives the crystal designation and the concentrations of some of the impurities they contain. Figure 15.14 is a plot of the concentration of calcium and strontium in the melt to that in the crystal; it is in good agreement with the results of Kelting and Witt[48] whieh are shown by dashed lines. The concentration of calcium and strontium

[48]H. Kelting and H. Witt, *Z. Physik* **126**, 697 (1949).

Table 15.2. List of Samples and Some of Their Impurities

Ingot and Section	Impurity[a] (ppm)								
	Ca	Sr	Rb	Na	Br_2	I_2	N_2	P_2	S_2
0611-IV	<3	<3	37	6	32	8	85	<2	<2
0613-I	48	<3	2	<6	32	6	117	<2	<2
0613-IV	123	≪3	3	10	37	6	80	<2	14
0619-I	167	<3	3	13	44	3	42	<2	10
0619-IV	441	<3	3	13	60	4	53	<2	19
0621-I	305	<3	<3	6	74	9	69	<2	<2
0621-IV	538	<3	<3	6	62	11	53	<2	4
0625-IV	<3	<3	<3	<6	61	11	37		<2
0702-I	<3	35	<2	13	35	2	57	15	3
0702-IV	<3	119							
0704-I	<3	133	3	16	60	6	80	<2	<2
0704-IV	<3	270	3	6	39	6	80	<2	7
0701-I	<3	229	3	10	68	5	20	<2	<2
0710-IV	<3	468	2	10	68	5	20	<2	5

[a]The maximum lead concentration in any of the crystals was 10 ppb.

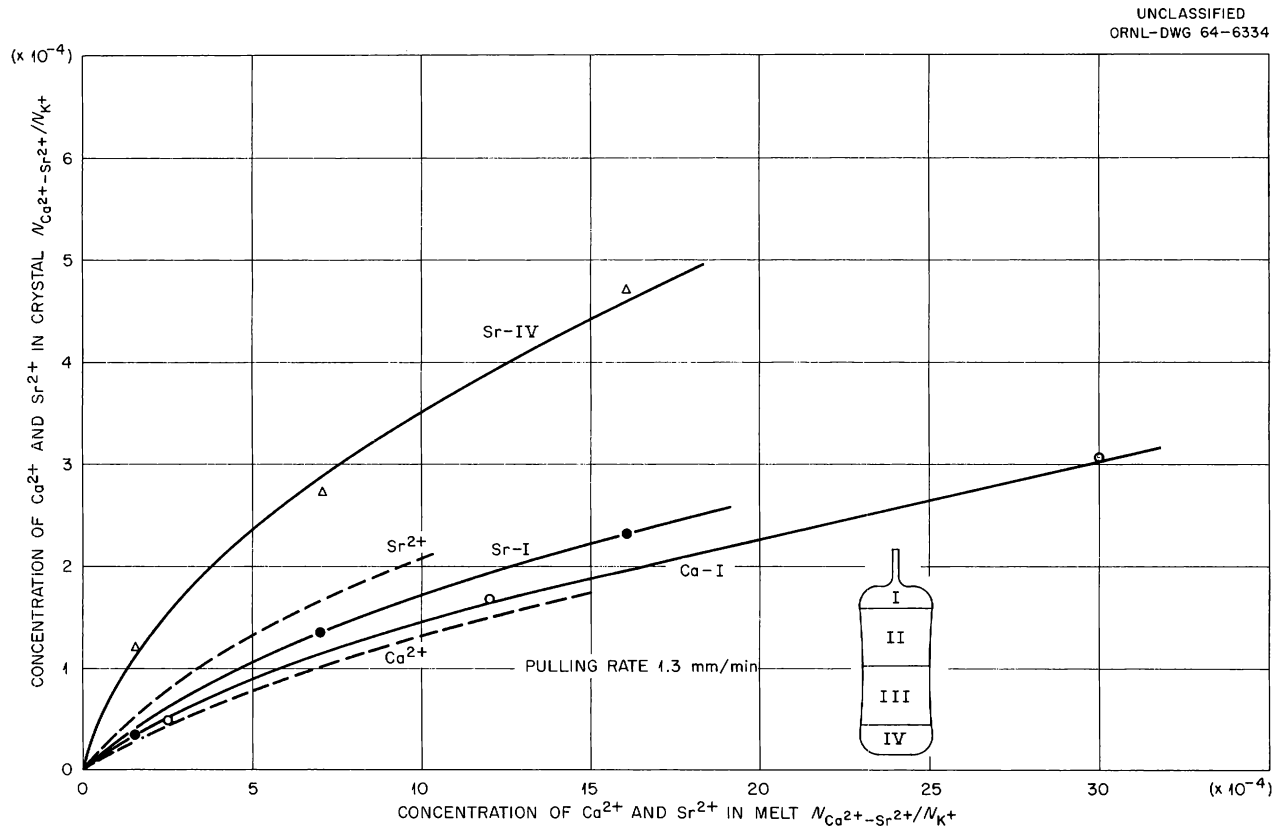

Fig. 15.14. Calcium and Strontium Concentration in KCl Single Crystals Pulled from the Melt at the Rate of 1.3 mm/min Plotted Against the Impurity Concentration of the Melt. The Roman numerals indicate the section of the ingot, as shown in the inset, from which the analyzed specimens were cleaved. The data shown by the dashed curves are taken from the work of Kelting and Witt.[48]

was analyzed by flame-photometry techniques and is accurate to ±5%. Only those specimens which had no observable cleavage steps or grain boundaries were utilized for deformation study. After cleavage, the samples were wrapped individually in 1-mil aluminum foil for the irradiations. Optical plates were cleaved from sections of the ingot adjacent to the deformation samples; the experimental details for their preparation have been described previously.[39]

The irradiations were performed using a Van de Graaff electron accelerator producing 1.5-Mev electrons and a ^{60}Co gamma source of 3.5×10^6 r/hr. The electron current density at the samples was 0.18 $\mu a/cm^2$. The temperature of the samples during electron irradiation never exceeded 34°C, and the temperature of the gamma facility was controlled such that the optical samples were at 34 ± 1°C during the irradiations. The irradiation temperature of the deformation specimens was about 5°C lower. Optical measurements were made with a Cary 14R spectrophotometer; an Instron testing machine, operating with a crosshead speed of 0.05 cm/min, was used to obtain the flow stress. Further details of the experimental procedure have been given earlier.[43]

In view of the fact that small variations in impurity concentration and temperature of irradiation can cause rather large changes in both the coloration curves and the flow stress, care was taken to repeat several of the optical experiments and to use four to ten samples for each deformation data point.

Experimental Results

Radiation Hardening. – The gamma coloration curves for "pure," calcium-doped, and strontium-doped samples are shown in Fig. 15.15. This is

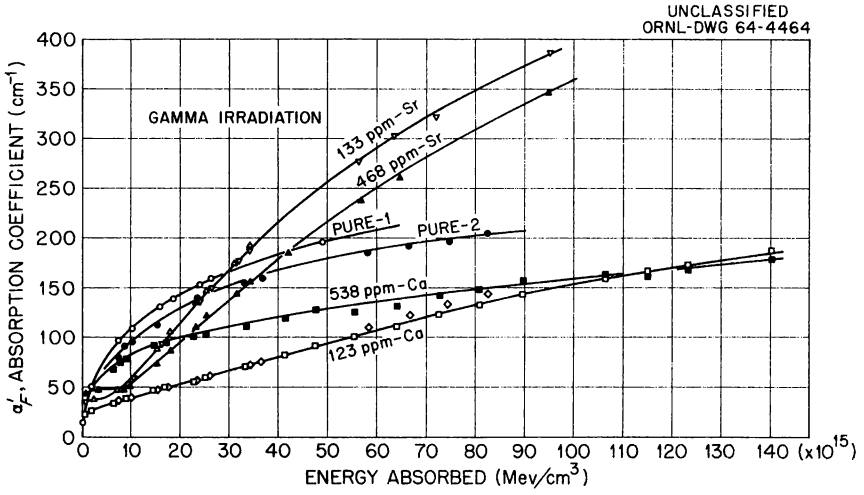

Fig. 15.15. *F*-Center Coloring Curves for Crystals Containing Different Amounts of Impurity. The amount and type of impurity are shown on the curves.

a plot of the corrected *F*-center absorption coefficient[49] vs the energy absorbed in the crystal. Notice that the calcium- and strontium-doped specimens have quite different coloration characteristics and that there is some variation between the two "pure" samples even though their known impurity concentrations are about the same.

Theoretically, one would expect the flow stress of a crystal to increase as the square root of the concentration of barriers or effective hardening defects in the lattice.[50] This quadratic relation is quantitatively illustrated for our data by Figs. 15.16 and 15.17, where the incremental increase in flow stress $[\Delta\tau = \tau(\text{irradiated}) - \tau_0]$ is plotted linearly against the square root of the *F*-center concentration (C_F) in parts per million for the samples of Fig. 15.15. The concentration can be written in terms of mole fraction of *F*-centers as

$$C_F = \frac{(1.1 \times 10^{16})}{N_0} \alpha'_F \epsilon = 0.24 \times 10^{-6} \alpha'_F , \quad (1)$$

where ϵ, the half width of the *F*-band, is 0.35 ev, and N_0 is 1.6×10^{22} cm^{-3}. The deviation from the quadratic relation for small irradiation doses is apparent in the figures and becomes larger with increasing impurity concentration; however, for heavy doses the relation is apparently quite good. The dashed lines on the figures are drawn to intercept the abscissa such that, when a value corresponding to the intercept is subtracted from

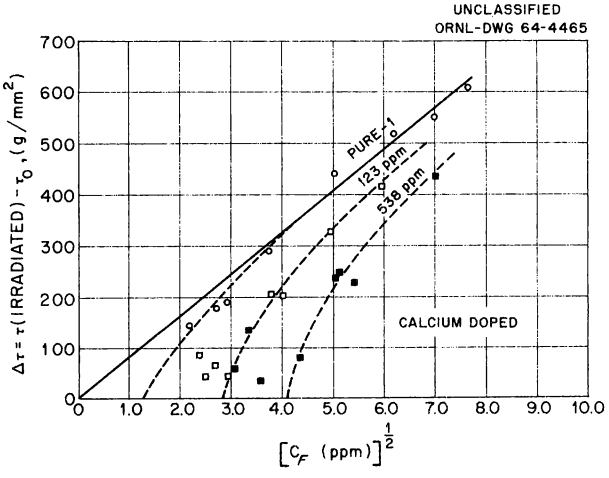

Fig. 15.16. Increase in Flow Stress, $\Delta\tau$, vs $C_F^{1/2}$ Plotted in ppm for One "Pure" and Two Calcium-Doped Crystals. The straight line is obtained by subtracting a constant amount from C_F.

[49] Because of the absorption of cluster centers occurring at the same wavelength as the *F*-band, the measured absorption coefficient at the peak of the *F*-band, α_F, has been corrected by subtracting an amount equal to the maximum *M*-band absorption coefficient, α_M. No correction was made for the Z_1 band, which grows in rapidly with early-stage coloration and then saturates. See R. Cappelletti, L. Dalla Croce, and R. Fieschi, *Phys. Status Solidi* **3**, 1347 (1963).

[50] R. L. Fleischer, *Acta Met.* **10**, 835 (1962).

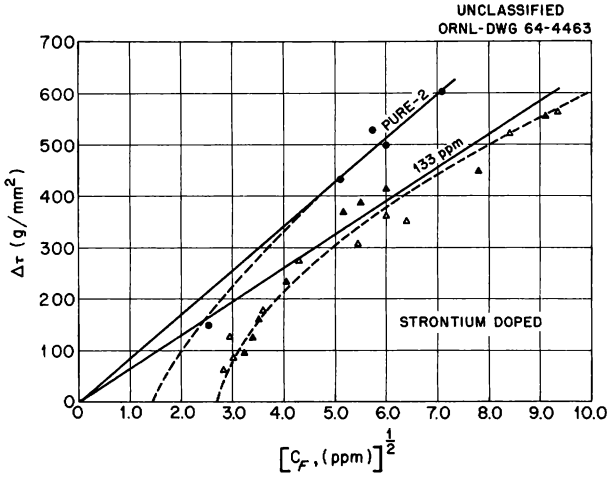

Fig. 15.17. Increase in Flow Stress, $\Delta\tau$, vs $C_F^{1/2}$ Plotted in ppm for One "Pure" and Two Strontium-Doped Crystals.

the F-center concentration, the resultant plot is a straight line through the origin of the graph, as is shown by the solid lines in the figures. This procedure implies, of course, that the hardening depends on the square root of the defect concentration.

Colorability. – Figure 15.18 depicts the F-center growth curves for gamma-irradiated KCl, KCl:Ca, and KCl:Sr crystals. The impurity concentrations of the individual optical samples are noted on the graphs. The specimens absorbed energy at the rate of about 0.8×10^{11} Mev cm^{-3} sec^{-1} during the irradiation. It is interesting that both classes of impure crystals behave very much like lead-doped crystals in that there appears to be increasing suppression of late-stage colorability with increasing impurity concentration.[40] However, there are several important differences in the growth curves of the calcium- and strontium-doped crystals. Apparently, there is an enhancement of late-stage colorability for lightly doped KCl:Sr crystals since the figure shows that the total F-center concentrations for this class are greater than for either of the undoped KCl crystals.

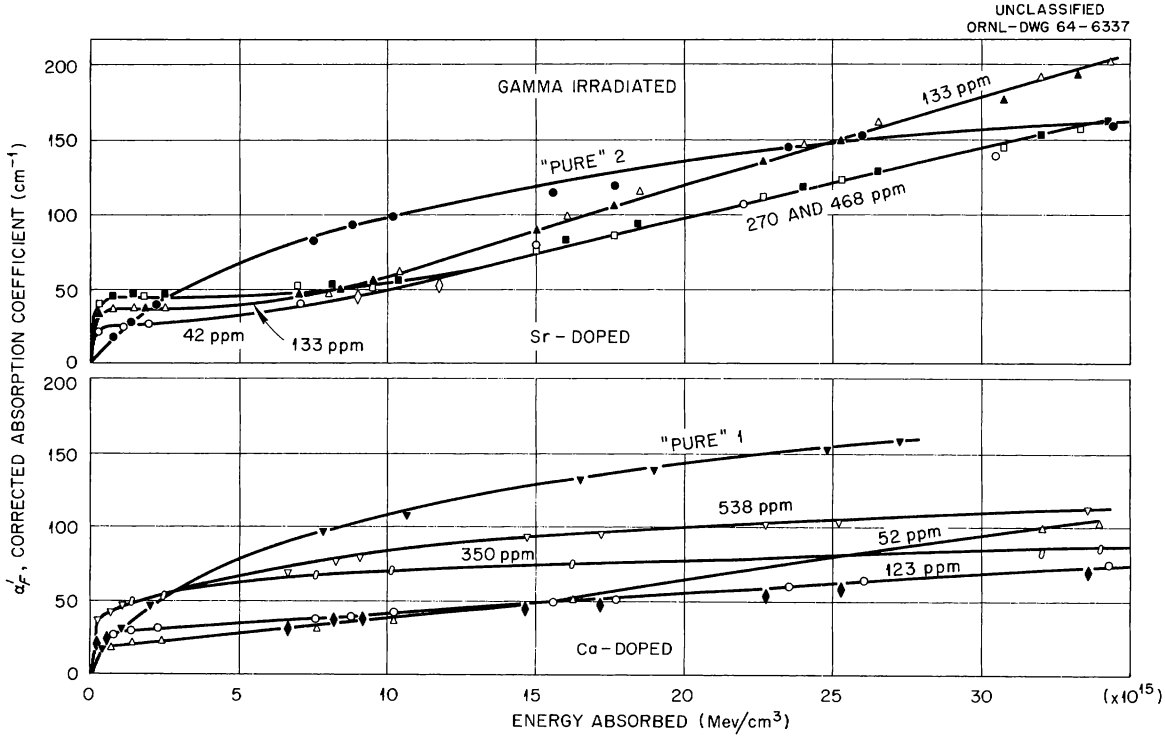

Fig. 15.18. F-Center Growth Curves for Gamma-Irradiated KCl, CKI : Ca, and KCl : Sr Samples. The amount and type of impurity for the various samples are shown in the figure.

There are also some differences in the shape and height of early-stage coloration per impurity concentration in the two classes of crystals.

The growth curves for electron-irradiated samples cleaved from the same section of the ingot as those used for the data of Fig. 15.18 are shown in Fig. 15.19. These samples absorbed energy at a rate which was about a factor of 60 greater than that for the gamma irradiations (4.5×10^{12} Mev cm^{-3} sec^{-1}). It is not to be implied from the two curves labeled 48 and 50 ppm KCl:Ca that the difference in colorability is simply due to the difference in impurity concentration. It is just as likely that the change is due to variations in electron current density and sample temperature as to impurity difference. Both the KCl:Ca and KCl:Sr classes of crystals show that increasing impurity concentration suppresses the late-stage colorability, but we would like to point out that the KCl:Sr crystals again have a somewhat different behavior than either the KCl:Ca or KCl:Pb crystals. From a comparison of Figs. 15.18 and 15.19, it is evident that the KCl:Sr samples show the least suppression of late-stage colorability per unit impurity concentration at the lowest radiation intensity. This is just the opposite of KCl:Ca and KCl:Pb.[40] The early-stage coloration is also different for calcium- and strontium-doped crystals, just as it was in the gamma-irradiation case. The differences in early-stage coloration can be shown more clearly by plotting the incremental increase in the maximum early-stage height vs the square root of the impurity concentration for both classes of impure crystals and both intensities of irradiation, as is done in Fig. 15.20. Notice that for both classes high-intensity irradiation increases the early-stage F-center production relative to low-intensity irradiation. The

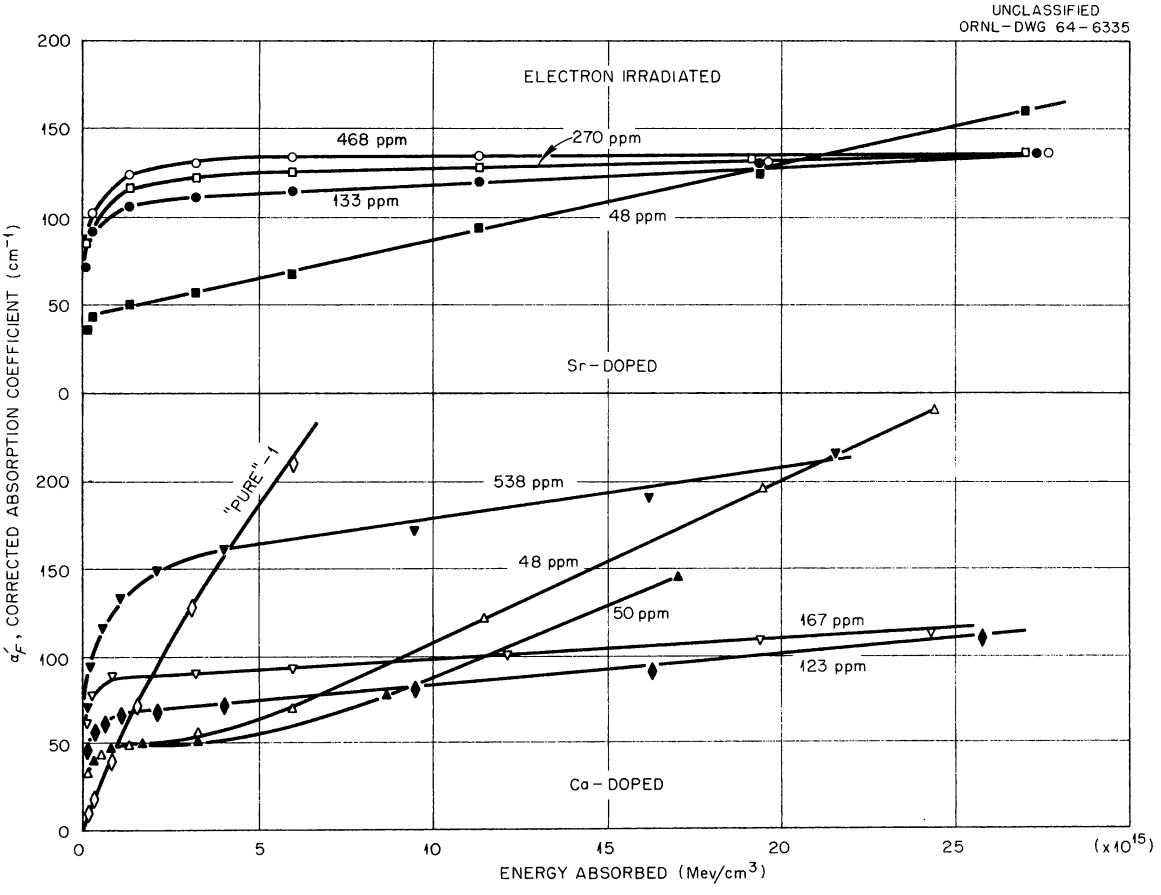

Fig. 15.19. F-Center Growth Curves for Electron-Irradiated, KCl, KCl:Ca, and KCl:Sr Crystals. The top part of the figure is for strontium-doped samples, and the bottom portion is for calcium-doped specimens.

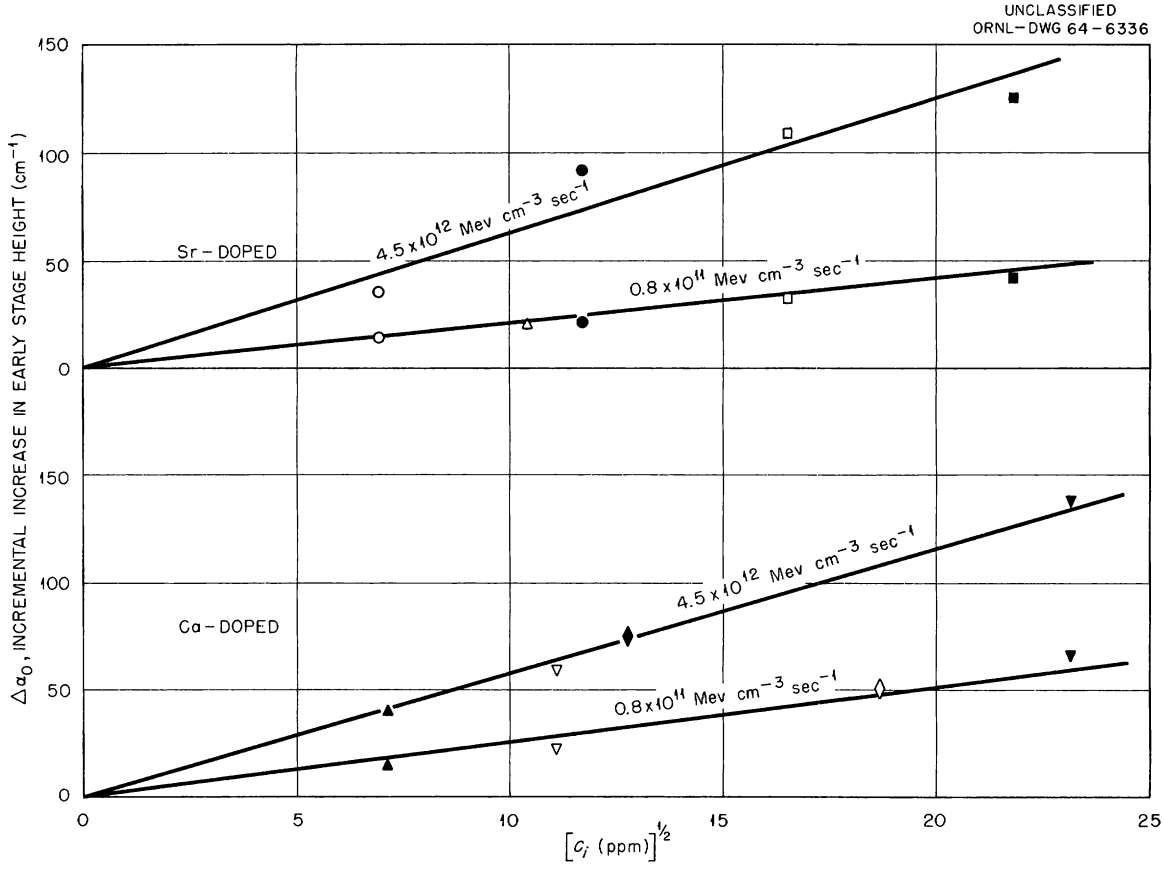

Fig. 15.20. Incremental Increase in Early-Stage Height vs the Square Root of the Total Calcium or Strontium Impurity Concentration. The irradiation intensities used are shown in the figure.

reason for plotting the incremental increase in early-stage height as a function of the square root of the impurity concentration rather than linearly will be discussed later.

Other Observations. – Another point of interest concerns V-band formation in these samples. It has been reported previously[44] that crystals having a high initial F-center coloration rate also show large V-bands. In our case, the V_2 absorption occurred at about 222 and 226 mμ for KCl:Ca and KCl:Sr samples respectively. In both classes of crystals the V_2-band grew in with the early-stage F-centers. It appeared that another band was growing in about 198 mμ after the V_2-band had saturated. However, it was found[51] that the ultraviolet absorption edge moved rapidly to longer wavelengths with irradiation; thus, it is difficult to say whether the apparent band at 198 mμ is real or just the shift of the V_2-band.

Discussion

In order to compare the two coloration models for early-stage coloration, we will review the experimental observations. The early-stage coloration mechanism does not contribute to the hardening process. This can be seen most clearly when log $[\Delta\tau/d(\Delta\tau)/d(C_F^{1/2})]$ is plotted vs log $(\alpha_F' - \alpha_0)$. This is done in Fig. 15.21 for five different samples. The values of α_0, which are chosen from the intercepts of Figs. 15.16 and 15.17, are given in Table 15.3, as is the normalization factor

[51] E. Sonder and L. Templeton (private communication) find that the absorption edge moves to longer wavelengths with gamma irradiation and that the background extinction increases in the ultraviolet region with irradiation. This combination could give the apparent new peak at 198 mμ.

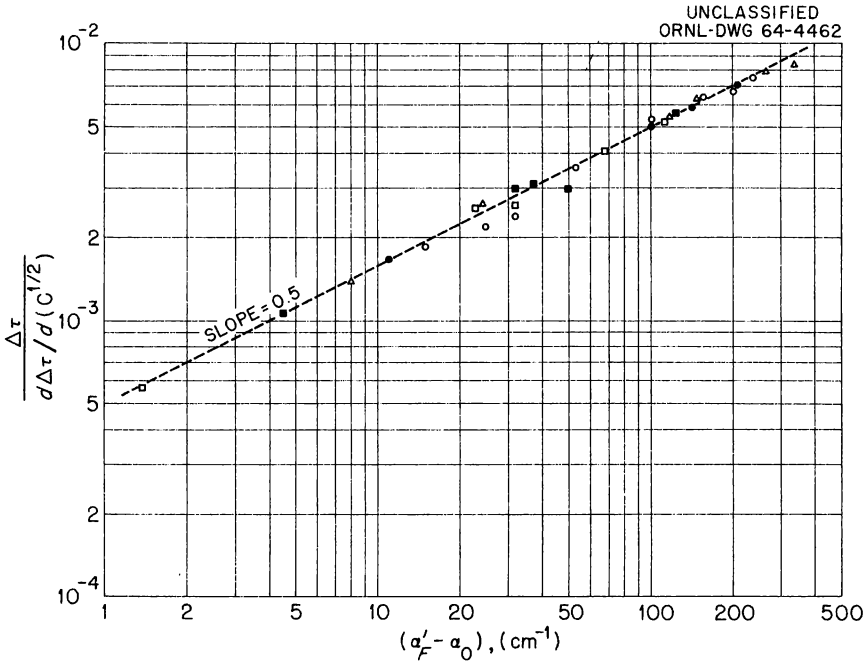

Fig. 15.21. Composite Plot of Log Flow Stress vs Log $(\alpha_F' - \alpha_0)$. The curves for all sets of samples have been normalized.

Table 15.3. Parameters Obtained from Analysis of Data

Sample	$\Delta\alpha_0$, Incremental Increase in Early-Stage Height[a]		α_0, Taken from Intercept Values[b] (gamma)	$d(\Delta\tau)/d(C_F^{1/2})^b$ (g/mm^2)
	Gamma	Electron		
				$\times 10^3$
Pure (1)	5	9	5	81.6
123 ppm (Ca)	31	66	36	80.0
538 ppm (Ca)	75	150	74	78.0
Pure (2)	5	9	9	85.3
133 ppm (Sr)	35	108	31	65.2
468 ppm (Sr)	43	136	31	~64.0

[a]Since the height of the early-stage coloration, $\Delta\alpha_0$, is dependent on dose and impurity concentration, the value of $\Delta\alpha_0$ shown above for the doped samples is determined from an extrapolation of the late-stage coloration line (taken from Figs. 15.18 and 15.19).

[b]Taken from Figs. 15.16 and 15.17.

$[d(\Delta\tau)/d(C_F^{1/2})]$ for these specimens. The incremental increase in early-stage coloration, $\Delta\alpha_0$, taken from Figs. 15.18 and 15.19, is also shown so that a comparison with the predicted values, α_0, can be made. The dashed line in Fig. 15.21 is taken from Fig. 6 of ref. 43, and it indicates good agreement between the two separate investigations.

Figure 15.20 indicates that the fraction of F-centers produced in early-stage coloration per impurity ion is small and that there may be a square-root relation between the two. The Crawford and Nelson concept of early-stage coloration predicts that only isolated cation vacancies, a small fraction of the total impurity concentration since most are associated with divalent impurities at room temperature, can participate in the process. A check of this model can be made by comparing the experimental results with a quantitative expression for the mole fraction of cation vacancies not associated with divalent impurities. This expression may be written as[52]

$$\frac{n_d}{N^0} = \frac{K}{2z} e^{-\epsilon_D/kT} \left[-1 + \left(1 + \frac{4C_i z}{K} e^{\epsilon_D/kT} \right)^{1/2} \right], \tag{2}$$

where K is the entropy factor, z is the coordination number, ϵ_D is the association energy of the defects, C_i is the mole fraction of positive divalent ion impurities, and k and T have their usual meaning. When $K = 2.5$, $z = 12$, C_i's are greater than 10^{-5}, and ϵ_D is 0.32 ev or greater, then at room temperature $4C_i z/K \exp(\epsilon_D/kT) > 1$; in this case,

$$\frac{n_d}{N_0} = -\frac{K}{2z} \exp(-\epsilon_D/2kT) + \frac{K^{1/2}}{z^{1/2}} C_i^{1/2} \exp(-\epsilon_D/2kT). \tag{3}$$

If this expression is differentiated with respect to $C_i^{1/2}$, we find a value which can be compared with the experimental slopes in Fig. 15.20:

$$\frac{d(n_d/N_0)}{d(C_i^{1/2})} = \frac{K^{1/2}}{z^{1/2}} \exp(-\epsilon_D/2kT) = 0.78 \times 10^{-3}. \tag{4}$$

The corresponding slopes in Fig. 15.20 range from 0.52 to 1.5×10^{-3}. Therefore, the data not only agree with the square-root dependence predicted by the second model, but the experimental slopes are of the proper order of magnitude. In view of the fact that many processes are active in the crystals during early-stage coloration, it cannot be expected that a real value for ϵ_D could be obtained from a determination of $d(n_d/N_0)/d(C_i^{1/2})$. For example, it is possible that precipitates are changed by the irradiation and that molecules such as OH^- can be broken up by the irradiation. An indication of these complications is seen in the erratic behavior of the incremental increase in flow stress for the doped crystals caused by very short irradiations, as shown in Figs. 15.16 and 15.17. Moreover, Cook and Dryden[53] found that most of the impurity-vacancy pairs are in higher complexes. Therefore, Eq. (2) should also include trimers and higher complexes.

The observation that the V_2-centers grow in concurrent with the early-stage F-centers is consistent with either model for early-stage coloration. However, it is not yet known what the V_2-center is, and for this reason, it is not possible to say with certainty that it has anything to do with hole trapping as has been proposed.

The late-stage coloration for KCl:Ca and KCl:Sr crystals is suppressed by impurities. The calcium-doped specimens, in particular, show a marked suppression with impurity; the late stage is not completely suppressed, however, even for 533 ppm, although it is in KCl:Pb for ~250 ppm lead. Even though KCl:Sr also shows suppression with impurity, it is important to note that for high-intensity radiation (electrons), the impurities are apparently more effective than for low intensities (gammas). This behavior is just the opposite of KCl:Pb crystals, where it took ~250 ppm to completely suppress the late-stage coloration for electron irradiation and only 60 ppm for gamma irradiation. The fact that different impurities affect the late-stage colorability in such opposite ways could explain some previous observations,[54,55] where

[52] A. B. Lidiard, *Handbuch der Physik*, vol. 20, p. 246, Springer, Berlin, 1957.

[53] J. S. Cook and J. S. Dryden, *Proc. Phys. Soc.* **80**, 479 (1962); *Australian J. Phys.* **13**, 260 (1960).

[54] K. Akimoto and W. A. Sibley, *J. Appl. Phys.* **34**, 1767 (1963).

[55] E. Sonder and W. A. Sibley, *Phys. Rev.* **129**, 1578 (1963).

changing the radiation intensity resulted in a relative reversal of the colorability of two samples.

Fleischer[50] has derived a quantitative relation between the incremental increase in flow stress ($\Delta\tau$) and the square root of the defect concentration. This relation can be written as

$$\Delta\tau = \frac{G}{n} C^{1/2} , \qquad (5)$$

where G is the shear modulus and n is a number which is determined from effectiveness of a particular type of hardening center. From our data, $n \cong 12$, which is what would be expected for interstitial or interstitial-cluster hardening in KCl. Thus, we see that late-stage colorability contributes to the hardening by producing interstitials, whereas there is no contribution from early-stage coloration.

Summary

1. There is very little contribution by the early-stage coloration process to the hardening.
2. The number of F-centers formed in early-stage coloration per impurity ion is very small ($\sim$10%).
3. Both of the above observations support the Crawford and Nelson concept of early-stage coloration.
4. The late-stage coloration process contributes to the hardening. This is most likely due to the production of interstitials during irradiation.
5. Late-stage coloration is suppressed by impurities such as calcium, strontium, and lead. However, there are marked differences in how each type of impurity affects the growth curves.

LUMINESCENCE OF GAMMA-IRRADIATED KCl UNDER PLASTIC DEFORMATION

(gamma irradiation; uv excitation; spectroscopy; color centers; temperature dependence; E)

C. T. Butler

Studies are being made on the luminescence of gamma-irradiated KCl single crystals during plastic deformation. This phenomenon was named radiotriboluminescence and abbreviated TL by earlier workers.[56–59] Here, however, triboluminescence will be abbreviated DL (deformation luminescence) to reserve the abbreviation TL for thermoluminescence. Deformation luminescence was chosen for study because the spectrum of the emission resembles somewhat that obtained by Timusk and Martienssen[60] when they irradiated uncolored material with 10.3-ev untraviolet light. Therefore, it represents a possible means of investigating the same phenomenon utilizing "bulk" excitation, in which, for instance, no correction is necessary for a finite depth of penetration of exciting energy. "Bulk" is used here in the sense that the energy deposited in the crystal per unit macroscopic volume is essentially constant throughout the entire crystal at a given instant.

Experimental Procedures

Samples for an experiment were cleaved from a single ingot of KCl to dimensions of $2 \times 4 \times 10$ mm. Ingots of nominally pure KCl from Harshaw, Optovac, and ORNL were used, and most of the deformations were carried out on a table-model Instron. The samples could be positioned reproducibly at the same spot on the load cell by a guide and push-rod device, so that the same corresponding face was presented to the detecting apparatus for each sample used. An EMI 9558Q multiplier phototube, cooled to dry-ice temperature, in conjunction with a 430-mμ interference filter was used to detect the emission. The output of the phototube was amplified, fed through a low-pass filter, and recorded as a function of time. The luminescence intensity rose to a more or less steady value after about 5% deformation; this steady value, therefore, was chosen to be called the "intensity" (see Fig. 15.22). Before the phototube was set up on the Instron, pilot experiments were run to determine the spectrum of the DL. In these experiments a motor-driven jeweler's vise was used to deform the specimens. In this

---

[56] F. G. Wick, *Sitzber. Akad. Wiss. Wien, IIa*, **145**, 689 (1936).

[57] J. Trinks, *Sitzber. Akad. Wiss. Wien, IIa*, **147**, 217 (1938).

[58] F. T. Metz *et al.*, *J. Phys. Chem.* **61**, 86 (1957).

[59] H. R. Leider, *Phys. Rev.* **110**, 990 (1958).

[60] T. Timusk and W. Martienssen, *Phys. Rev.* **128**, 1656 (1962).

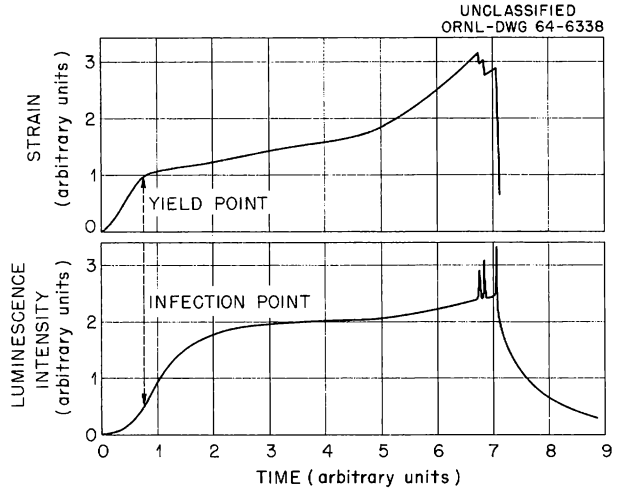

Fig. 15.22. Typical Stress-Time and DL-Time Curves for Gamma-Colored KCl.

case the luminescence was analyzed from 200 to 750 mμ with a $\frac{1}{2}$-m Bausch and Lomb monochromator and a cooled EMI 9558Q. For the irradiations, each sample was wrapped in aluminum foil and placed at a reproducible position in a temperature-controlled 3.5×10^6 r/hr ^{60}Co source. The temperature of the samples during irradiation was near 33°C. A special optical holder was employed for most of the experiments which allowed both the absorption spectrum and the DL intensity to be measured on the same sample. By this means any sample-dependent variations were omitted from optical absorption and luminescence measurements on a given specimen, although such variations still existed from sample to sample.

In all the experiments, it was necessary to correct for self-absorption of the emitted luminescence by Libby's relation:

$$I_a = \frac{\alpha_L d}{1 - e^{-\alpha_L d}} I_r ,$$

where α_L is the absorption coefficient in cm^{-1} of the crystal at 430 mμ, d is the thickness of the crystal in cm, I_a is the intensity observed if there were no self-absorption, and I_r is the intensity actually recorded. This correction formula assumes point-source geometry, and the experiment was arranged to approximate such a case. Once the dependence of the emitted light upon the Instron's crosshead speed had been determined, a value of 0.05 cm/min was used for all subsequent experiments.

A considerable sample dependence was observed for the absolute value of the emitted intensity. Within a given ingot, however, samples receiving identical treatment usually showed DL intensities having a variance of about 7%. No attempt was made to correct the data for variation of surface area, cross-sectional area, thickness, or volume, since these all interacted in a way to make any such correction extremely difficult – if not meaningless.

Characteristics of the DL

The ultraviolet-excited luminescence from a typical uncolored commercial crystal contains only impurity bands which arise from various amounts of silver, thallium, lead, copper, oxygen, or other impurities. The same crystal under deformation, after a light gamma irradiation, would show only a single, broad band, peaking near 430 mμ and having a full width at half maximum (ΔE) of about 0.7 ev. In some cases a very small thallium or other impurity emission would also be present, but usually the 430-mμ emission would be the only distinguishable feature of the spectrum. Table 15.4 lists some of the conditions under which a 430-mμ emission is observed.

For all crosshead speeds from 0.005 to 5 cm/min, the luminescence intensity behaves with deformation as shown in Fig. 15.22. The intensity begins rising immediately upon initiation of deformation, goes through an inflection point near the yield point of the sample, and eventually attains a steady value. As mentioned previously, the variation of intensity throughout the "easy-glide" portion of the stress-strain curve is usually small. The light output usually increases again with the onset of the "work-hardening" stage, but may remain constant or even decrease. Large light bursts are observed if the sample cracks or fails, and a large burst can be produced by suddenly releasing pressure on the crystal. An absolute time scale is not shown on the figure, since recording time varies from several seconds to an hour or more, depending upon the crosshead speed. At the lowest deformation rate, a series of small light bursts (about 1.5 bursts/sec) are often observed to occur. They begin a few seconds after the

Table 15.4. Conditions for Obtaining a 430-mμ Emission

Treatment Condition	Peak (ev)	ΔE (ev)	Reference
During uv excitation (>8 ev) of uncolored KCl	2.88	~0.6	*a*
During gamma irradiation	2.85	0.74	*b*
During bombardment with 40- to 80-kev electrons	2.76	0.71	c
During plastic deformation of gamma-colored material	2.99	0.71	
Afterglow of gamma-irradiated material	2.86	0.7	*d*

[a]T. Timusk and W. Martienssen, *Phys. Rev.* **128**, 1656 (1962).

[b]C. T. Butler, *Solid State Div. Ann. Progr. Rept. Aug. 31, 1962*, ORNL-3364, p. 110.

[c]E. T. Arakawa, Health Physics Division, unpublished results.

[d]C. T. Butler, unpublished results.

yield point is reached and continue until the light output is about half its steady value.

The intensity of the DL increases with increasing rate of deformation. As Fig. 15.23 shows, this increase goes as a fixed power of the crosshead speed for the three lowest speeds studied but shows marked saturation at the highest speed. This is true for all irradiation doses studied. The absolute light output at a given deformation rate is sample dependent, but no quantitative studies of this effect have been made.

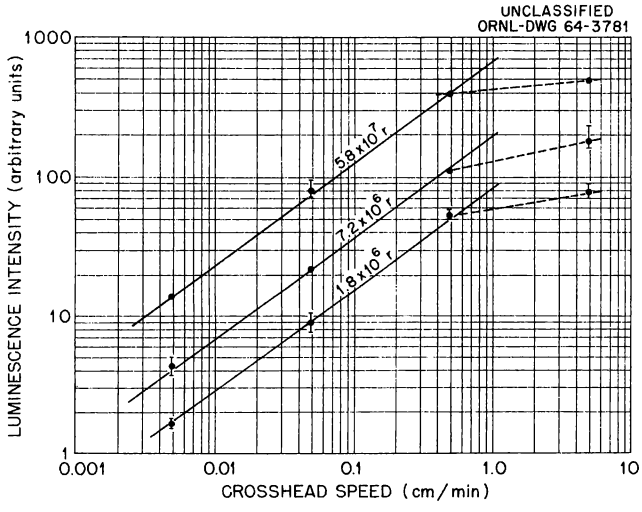

Fig. 15.23. Relative DL Intensities vs Crosshead Speed at Various Irradiation Doses.

Relationship of DL to Color Centers

Several preliminary experiments have been performed to determine the relationship of the DL to known color centers. In Fig. 15.24, the *F*-center introduction curves for one sample each from Harshaw and Optovac ingots are shown, along with DL introduction curves for material from the same ingots. Each DL curve has been normalized to match its corresponding color-center curve at one point, marked *N*. For each crystal the DL- and *F*-center curves are seen to have qualitatively the same shape. Figure 15.25 shows a cross plot of DL intensity vs absorption coefficient, α_F, at the peak of the *F*-band for the Harshaw ingot. It is seen to be a straight line.[61] The inset shows the same cross plot for the DL intensity vs α_M.

To check further the relation of the DL intensity to known color centers, several additional experiments were performed, two of which will be described. After a given radiation dose, material from the Harshaw ingot used earlier was subjected to a modified ioschronal annealing sequence. Actual isochronal anneals are impossible since the sample is destroyed each time the DL is observed; thus, a given sample cannot be subjected to successive anneals at different temperatures for equal

[61]The presence of *F*-centers alone may not suffice to cause DL, since there are indications that additively colored KCl shows very little, if any, DL.

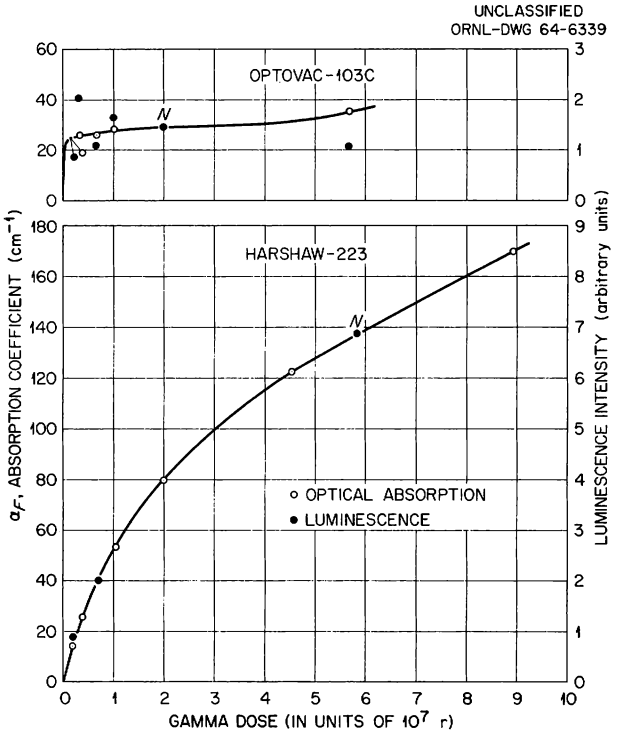

Fig. 15.24. *F*-Center Introduction Curves with Normalized DL Introduction Curves. Normalization points are marked *N*.

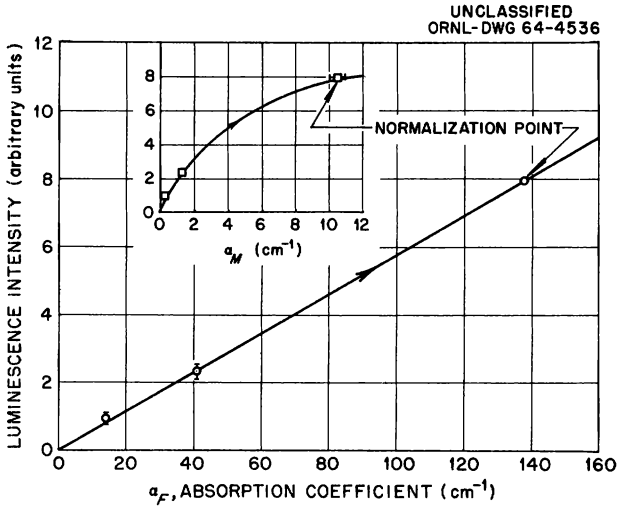

Fig. 15.25. DL Intensity vs the Absorption Coefficient at the Peak of the *F*-Band. The arrow indicates that the data were taken during the initial coloration process. The inset shows the corresponding data for the *M*-center.

times. Our modification involved heating *different* samples, all with identical preparation, for equal times at successively higher temperatures. This corresponds to a vertical cut at a particular time through a series of isothermal plots. Figure 15.26 shows the annealing behavior of the luminescence and the *F*-, *M*-, and *U*-centers. The fraction remaining is plotted against the temperature of anneal. Each is seen to increase at first and then to decrease in some manner. Only the DL and *M*-center seem to anneal in a single step, and both have a stability temperature[62] of about 385°K. Moreover, each apparently disappears with second-order kinetics, showing an activation energy of about 0.75 ev. The dependence of DL upon the *M*- and *F*-center concentrations during annealing is shown in Fig. 15.27.

If a piece of KCl is colored to some *F*-center concentration and is subsequently bleached with visible light, the *F*-center is observed to decay monotonically from its initial value while the *M*-center at first grows, reaches a maximum, and then decays. The *R*-center and other higher-order centers, after a delay period, grow slowly and eventually saturate. Figure 15.28 shows the results of an experiment in which DL and optical absorption data were collected on a set of samples bleached for different times with 470-mμ radiation. The luminescence is seen to behave more like the

[62]Defined as that temperature at which the rate of disappearance of the quantity is a maximum.

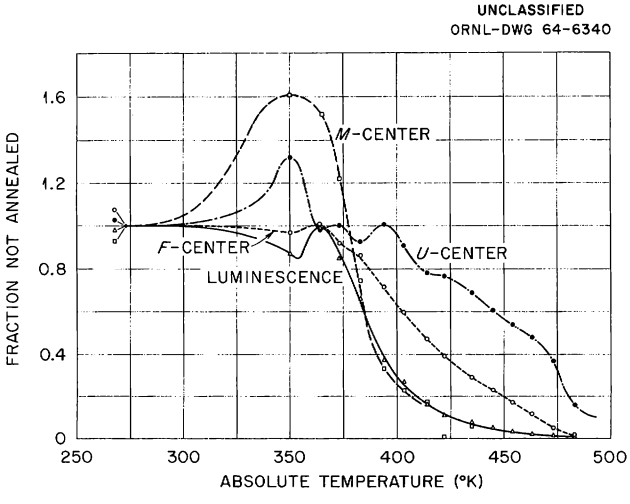

Fig. 15.26. Fraction Not Annealed of the DL, and the *F*-, *M*-, and *U*-Centers vs Absolute Temperature.

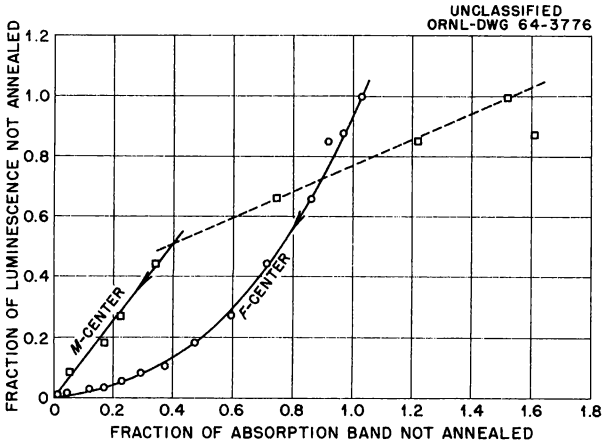

Fig. 15.27. Fraction Not Annealed of the DL vs the Fraction Not Annealed of the *F*- and *M*-Centers.

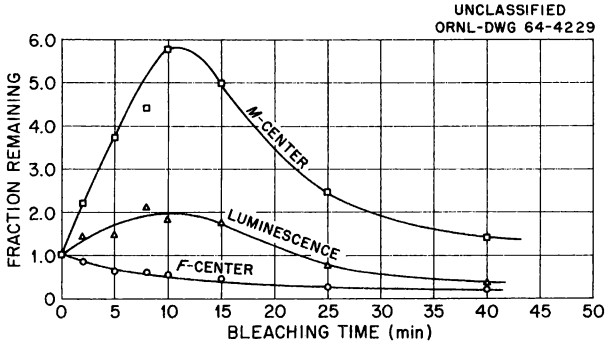

Fig. 15.28. Fraction Not Bleached of the DL and the *F*- and *M*-Centers vs Bleaching Time.

M-center than either the *F*-center or higher-order centers. The actual concentration of *F*-centers has been found by subtracting $(0.8\alpha_M + 4\alpha_R)$ from the measured α_F.[63]

Discussion

Since these are only preliminary investigations and since some of the data scatter rather badly, no conclusions concerning the origin of the triboluminescence or the details of the energy transfer may be drawn at this time. Timusk and Martienssen[60] obtained a 430-mμ emission when they irradiated uncolored KCl with light having an energy above the absorption edge. As a result of this and other experiments, they proposed that the emission was a result of a hole annihilating an *F*-center electron leaving a negative-ion vacancy. From the data presented here, however, it is apparent that their mechanism cannot be the only one operative during plastic deformation of gamma-irradiated KCl.

NEAR-ULTRAVIOLET LUMINESCENCE IN POTASSIUM IODIDE

(color centers; spectroscopy; electron irradiation; recombination mechanism; optical excitation; E)

R. B. Murray F. J. Keller[64]

All nonactivated alkali iodides exhibit a luminescence emission in the near-ultraviolet region of the spectrum upon excitation by photons or charged particles. This emission is quite weak at room temperature and increases rapidly as the crystal is cooled to liquid-nitrogen temperature or below. This characteristic near-ultraviolet emission is the basis for operation of nonactivated alkali iodide scintillators (e.g., NaI or CsI) at low temperatures. The origin of this luminescence emission in NaI has previously been attributed to the radiative decay of trapped exciton.[65] In a recent study of the scintillation process in CsI,[66] it was suggested that the ultraviolet emission following charge-particle excitation might arise from the radiative decay of an exciton state resulting from the recombination of an electron with a self-trapped hole. It was further suggested by virtue of the qualitatively similar nature of the ultraviolet emission that this emission band may arise from the same process in all alkali iodides.

In order to examine the proposed recombination mechanism, experiments have been initiated on the production of color centers and the luminescence

[63]S. Schnatterly and W. D. Compton, *Phys. Rev.* 135, A227 (1964).

[64]ORINS Predoctoral Fellow from the University of Tennessee.

[65]W. J. Van Sciver, *IRE Trans. Nucl. Sci.* 3, 39 (1956); also Stanford University Report HEPL-38, 1955 (unpublished).

[66]R. Gwin and R. B. Murray, *Phys. Rev.* 131, 508 (1963).

processes in KI and KI(Tl). The principal objective has been to focus attention on the self-trapped hole (V_k-center) in order to determine whether there exists a correlation between the self-trapped hole and the characteristic ultraviolet emission, which is known[67-69] to occur at 370 mμ. Most of the experiments to date have been performed with KI crystals containing Tl, since it is only in doped crystals that V_k-centers have been produced in sufficient quantity.

Experimental Methods

Low-temperature irradiations and measurements of absorption spectra, emission spectra, excitation spectra, and thermoluminescence glow curves were carried out with a rotatable-base cryostat obtained commercially. This cryostat is of stainless steel construction except for the radiation shields and a sample-mounting block, which are of copper. Crystal samples were rectangular and were typically 2 mm thick. The cryostat base can be rotated while under vacuum, so that a radiation beam can be admitted through a thin aluminum window; the base is then rotated through 90° to align quartz windows for spectral measurements. The crystal temperature is indicated by a copper-constantan thermocouple attached to the sample-mounting block. In most of the experiments reported here, the crystal was irradiated with a beam of 1.5-Mev electrons from a Van de Graaff accelerator; the electron current density during irradiation was typically of order 10^{-2} μa/cm^2.

Absorption Spectra and Thermal Stability of Self-Trapped Holes

The absorption spectrum of KI(Tl) at liquid-nitrogen temperature exhibits sharp Tl absorption bands in the near-ultraviolet region and is otherwise transparent throughout the visible and near infrared. The principal Tl absorption bands at 77°K occur at 282, 233, and 224 mμ. Upon irradiation by gamma rays, x rays, or electrons at liquid-nitrogen temperature, several broad absorption bands are introduced in the visible and near infrared which are known from previous work[70,71] to arise from optical absorption of V_k-centers. In addition, sharper bands are produced in the ultraviolet region, and these have been previously interpreted[71] as due to transitions in Tl^+ ions perturbed by the presence of nearby color centers. Radiation-induced absorption bands in KI(Tl) ($\sim 10^{-3}$ mole fraction Tl) are shown at several temperatures in Fig. 15.29. In this particular experiment the crystal sample was a cube 1 cm on an edge and was irradiated at liquid-nitrogen temperature with ^{137}Cs gammas. The principal V_k absorption bands are located at 404 and 800 mμ. As the crystal is slowly warmed above liquid-nitrogen temperature, it is observed that the V_k-bands disappear abruptly near 110°K and are replaced by new absorption bands which are presumed to be associated with other trapped hole centers. The absorption coefficient at the peak of the 404-mμ V_k-band is shown as a function of temperature during a warmup in Fig. 15.30. A thermoluminescence glow peak occurs in the same temperature region as that in which the V_k-centers disappear, as shown in Fig. 15.31. Glow peaks at higher temperatures (Fig. 15.31) are associated with the disappearance of other color centers, as revealed by the absorption bands in Fig. 15.29. Details of these processes have been discussed previously.[71]

Luminescence

In order to examine the proposed recombination mechanism, it is necessary to prepare a crystal which contains both V_k-centers and a source of electrons. This may be achieved simply through irradiation with 1.5-Mev electrons by either of two methods: (1) irradiation of KI(Tl) at liquid-nitrogen temperature, which yields strong V_k absorption and a weak F-band, and (2) irradiation of the KI(Tl) at room temperature, which introduces a strong F-band, and subsequent irradiation at liquid-nitrogen temperature, which introduces strong V_k absorption. The radiation-induced absorption spectrum of a crystal of KI(Tl) (10^{-3} mole

[67] R. Fieschi and G. Spinolo, *Nuovo Cimento* **23**, 738 (1962).

[68] N. N. Vasil'eva and Z. L. Morgenshtern, *Opt. Spectry. (USSR) (English Transl.)* **12**, 41 (1962).

[69] K. Teegarden and R. Weeks, *J. Phys. Chem. Solids* **10**, 211 (1959).

[70] C. J. Delbecq, W. Hayes, and P. H. Yuster, *Phys. Rev.* **121**, 1043 (1961).

[71] H. N. Hersh, *J. Chem. Phys.* **31**, 909 (1959).

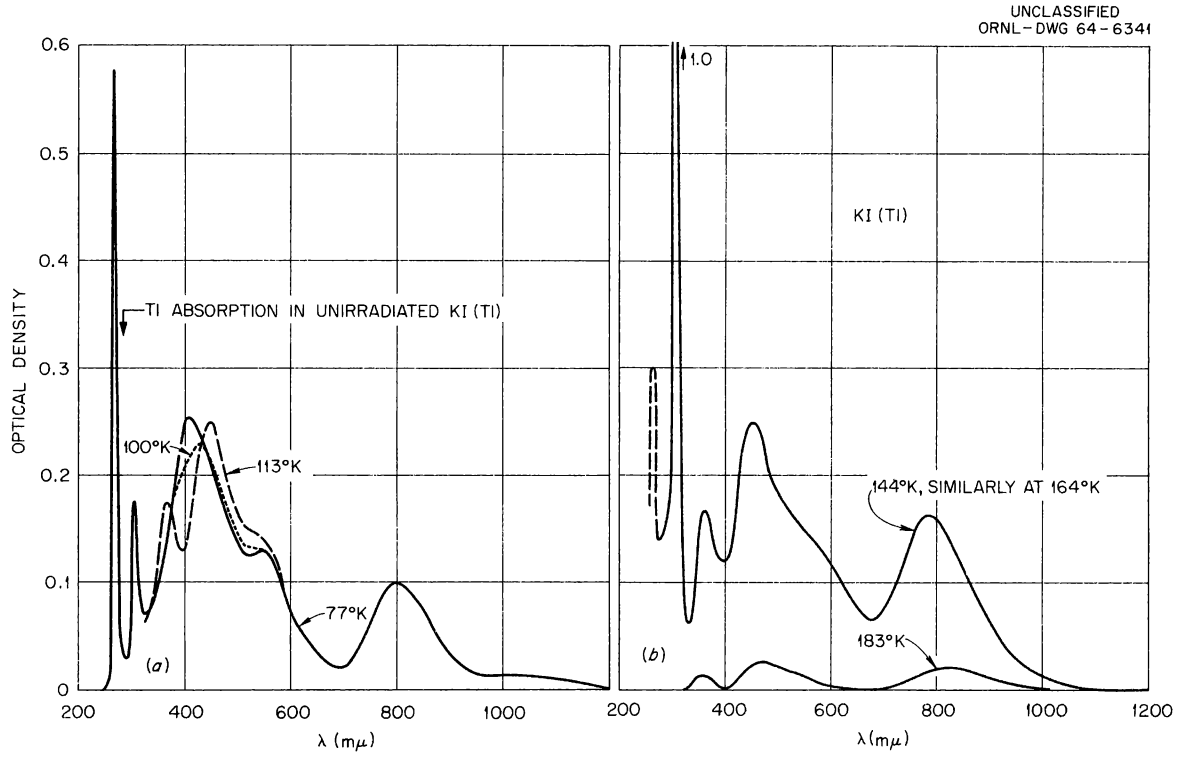

Fig. 15.29. Radiation-Induced Absorption Spectrum in KI(TI).

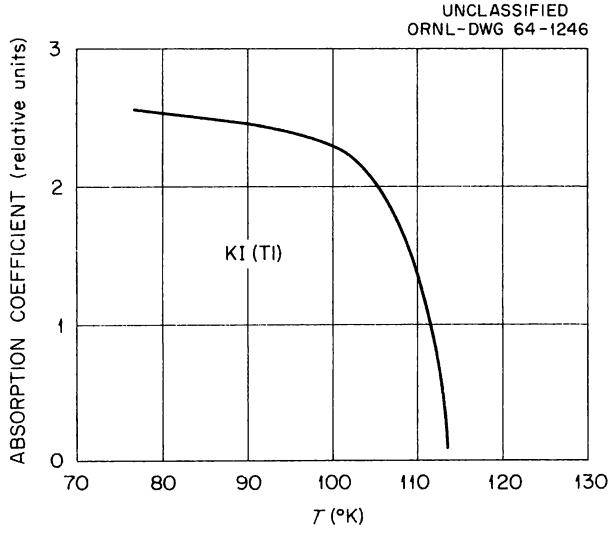

Fig. 15.30. Absorption Coefficient at Peak of 404-mμ V_k-Band as a Function of Temperature as Crystal is Continuously Warmed.

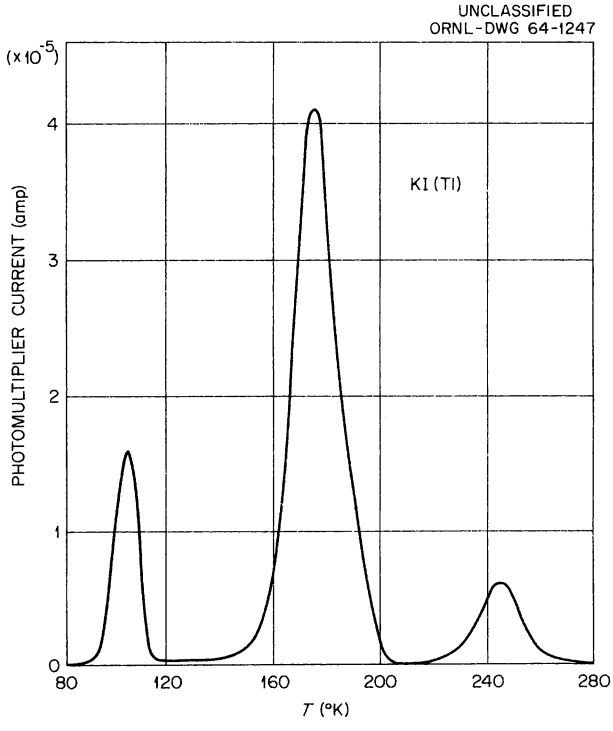

Fig. 15.31. Thermoluminescence Glow Curve for KI(TI). Heating rate, 1.4°C/min.

fraction Tl) irradiated as in (2) above is shown in Fig. 15.32. This spectrum was measured at liquid-nitrogen temperature and represents those bands introduced by the irradiation.

Referring to the crystal whose spectrum is given in Fig. 15.32, illumination with nearly monochromatic light in the F-band region at liquid-nitrogen temperature was found to result in a luminescence at shorter wavelengths. The emission spectrum of the luminescence radiation is shown in Fig. 15.33, curve (*a*). The crystal was then warmed slowly to ~120°K, during which time the absorption spectrum was continuously monitored. The V_k-bands were found to disappear abruptly near 110°K. The crystal was then cooled from 120°K back to liquid-nitrogen temperature, and the emission spectrum was remeasured upon excitation by F-light. The results, which are shown as curve (*b*) of Fig. 15.33, show the complete disappearance of the 370-mμ band, which is the emission band of interest in the present work. The 425-mμ band is a well-known emission from the Tl^+ ion in KI; this emission is presumed to be excited by the recombination of electrons with Tl^+ ions which have previously captured a hole (i.e., Tl^{2+}) to produce Tl^+ in an excited state which subsequently undergoes radiative deexcitation. The decrease in intensity in the 425-mμ band is due simply to a decrease in the number of F-centers, thus reducing the number of electrons available to participate in the luminescence processes. This effect occurs upon continuous illumination at a fixed temperature.

The number of V_k-centers in a particular crystal can be reduced not only by thermal annihilation but by optical bleaching as well. A reduction in the inventory of V_k-centers by optical bleaching at 404 mμ results in an attenuation of the 370-mμ emission relative to the 425-mμ Tl^+ band. This effect is shown in Fig. 15.34, where curve (*a*) is

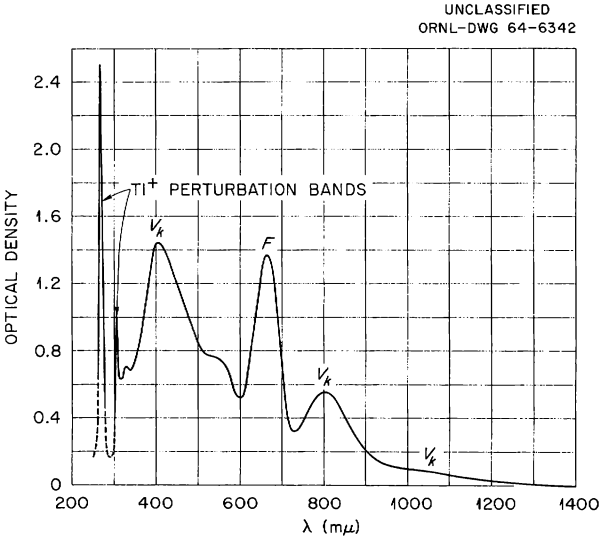

Fig. 15.32. Radiation-Induced Absorption Spectrum of KI(Tl) Irradiated with 1.5-Mev Electrons at Room Temperature and Then at Liquid-Nitrogen Temperature. Spectrum measured at liquid-nitrogen temperature.

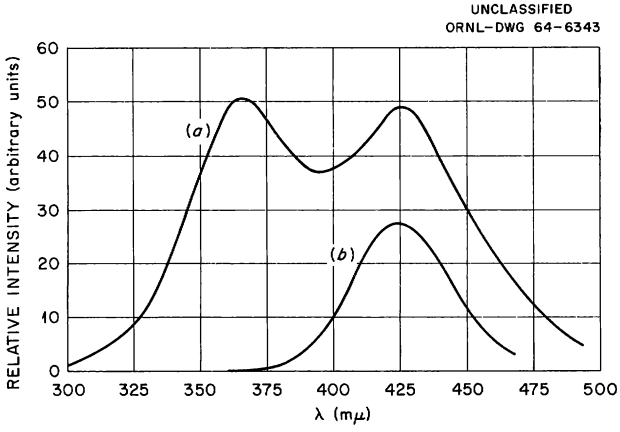

Fig. 15.33. Luminescence from KI(Tl) During Stimulation with F-Band Light. Curve (*a*): following electron irradiation as in Fig. 15.32. Curve (*b*): after thermal destruction of V_k-centers at 120°K. Both curves were measured at liquid-nitrogen temperature.

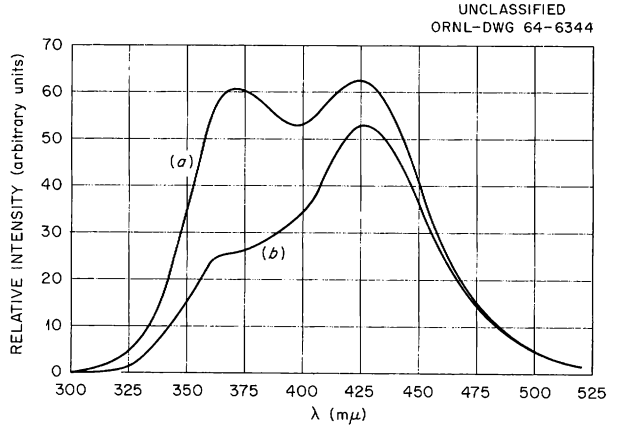

Fig. 15.34. Emission Spectra from KI(Tl) During Optical Excitation. Curve (*a*): following electron irradiation as in Fig. 15.32. Curve (*b*): after optical bleach of approximately three-fourths of the V_k-centers. Both curves measured at liquid-nitrogen temperature.

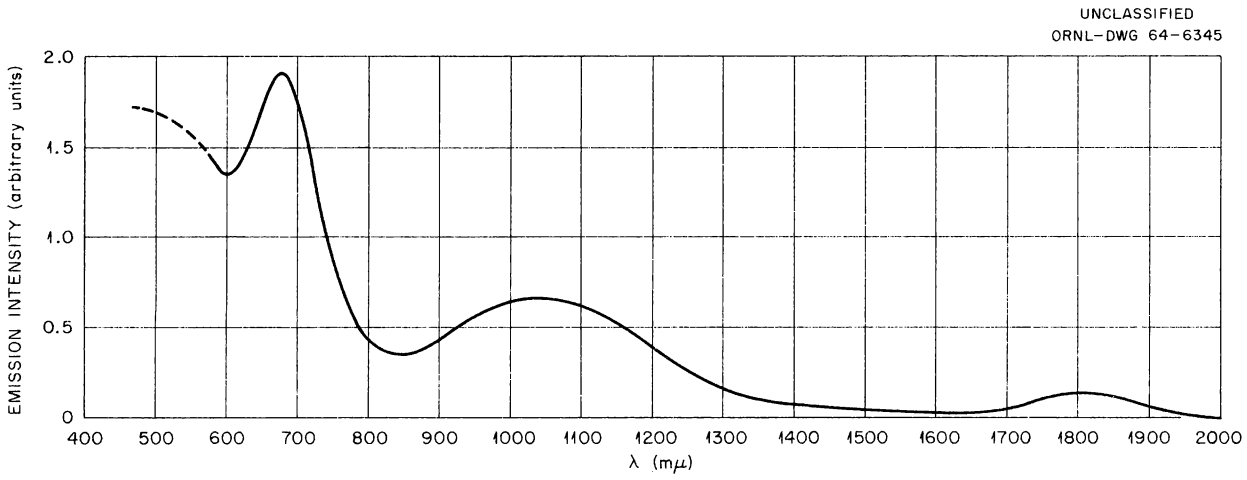

Fig. 15.35. Excitation Spectrum of Radiation Emitted at 360 mμ. The excitation spectrum is the same for light emitted by Tl^+ at 425 mμ. The curve corresponds approximately to equal numbers of photons per unit wavelength interval. The crystal was at liquid-nitrogen temperature.

the initial emission spectrum observed upon optical excitation and curve (*b*) is the spectrum observed following an optical bleach in which about three-fourths of the V_k-centers were destroyed. Both spectra were obtained at liquid-helium temperature. The data of Fig. 15.34 indicate an approximately quantitative dependence of the 370-mμ emission intensity on the number of V_k-centers.

Excitation Spectra

The luminescence emission as shown in Figs. 15.33 and 15.34 can be excited not only by *F*-light but by shorter- and longer-wavelength radiation as well. Studies of the excitation spectrum at liquid-nitrogen temperature of irradiated KI(Tl) reveal that both the 370- and 425-mμ bands have the same excitation spectrum. An example of the excitation spectrum is shown in Fig. 15.35. This spectrum has been corrected so that the curve of Fig. 15.35 corresponds approximately to equal numbers of photons per wavelength interval. The peak in the excitation spectrum at 665 mμ corresponds to excitation in the *F*-band. This correlation is further supported by the experimental observation that the 665-mμ peak in the excitation spectrum is attenuated by optical bleaching of the *F*-band. It is concluded from these measurements that the observed luminescence emission is stimulated by the optical excitation of electrons. The identity of the electron source that can be stimulated by long-wavelength light is not known. It has been previously suggested[71] that electrons may be optically excited from Tl^0 centers (Tl^+ + electrons), although there are no corresponding optical absorption bands in the long-wavelength region. An alternative mechanism, which cannot be ruled out at this time, is excitation of electrons from *F'*-centers.

Discussion

The results presented above are taken as evidence in favor of the proposed mechanism for the emission of the 370-mμ band, namely, the recombination of electrons with self-trapped holes. It is possible to orient V_k-centers along a chosen [110] direction by a well-known bleaching technique; it, therefore, is of interest to look for polarization effects in the luminescence of oriented self-trapped holes. Experiments of this type are in progress.

LIGHT SCATTERING IN ALKALI HALIDE SINGLE CRYSTALS[72]

(KCl; E/T)

W. A. Sibley

Light scattering by crystals of potassium chloride obtained from several commercial suppliers was measured. The experimental observations can be explained by postulating that the scattering comes from dislocations which are surrounded by scattering centers having an anisotropic polarizability ellipsoid. The scattering units are calculated to have a length of about 3×10^{-4} cm and a width of less than 2.5×10^{-6} cm.

---

[72]Abstract of published paper: *Phys. Rev.* **132**, 2065 (1963).

16. Semiconductor Studies

NATURE AND YIELD OF PHOTON- AND NEUTRON-INDUCED DEFECTS IN SEMICONDUCTORS

(0.667- to 2.76-Mev photons; 0.2- to 14.1-Mev neutrons; temperature dependence, 77 to 320°K; *n*-type Ge, Si, and GaAs; E)

J. W. Cleland J. H. Crawford, Jr.
R. F. Bass[1]

In our continuing study of radiation-induced changes in the electrical properties of elemental and compound semiconducting materials, we have extended our work on the apparent rate of introduction of lattice defects by photons,[2] thermal-energy neutrons,[3] and monoenergetic and fission-spectrum neutrons.[2] A paper describing this work has been submitted for publication,[4] and the abstract follows:

"The apparent rate of introduction of lattice defects has been determined in a variety of elemental and compound semiconducting materials by electrical property measurements subsequent to ambient and certain low temperature irradiations with photons (0.667 to 2.76 Mev), thermal energy neutrons, monoenergetic neutrons (0.2 to 14.1 Mev), fission spectrum neutrons, pulsed reactor neutrons, and ^{241}Am-Be neutrons. The apparent removal rate of conduction electrons in *n*-type samples of Ge, Si, and GaAs is a sensitive function of the incident photon energy, and the agreement between theory and experiment improves relative to the energy of the incident photon. The nature and yield of thermal neutron induced (n,γ) lattice defects is apparently quite temperature dependent, and the final defect concentration depends markedly upon the type of defect structure created and upon any subsequent migration or annealing. The apparent removal rate of conduction electrons in *n*-type Ge is a sensitive function of the incident neutron energy up to that energy ($\sim$0.7 Mev) required to produce a defect structure or disordered region; however, the apparent removal rate is not a sensitive function of the energy, initial carrier concentration, or irradiation temperature (77° to 320°K) for neutrons of yet higher energy (1.0 to 14.1 Mev). The apparent carrier removal rate in *n*-type Si is a sensitive function of the average incident neutron energy from 0.2 to about 4.0 Mev. The average rate of removal of conduction electrons per incident fission spectrum neutron has been determined in a pure fission spectrum neutron locale as –(5–7) (*n*-type Ge), –(3–5) (*n*-type Si), and –(4) (*n*-type GaAs), and reasonable agreement was obtained for similar experiments that utilized a pulsed neutron facility. These data suggest the importance of an understanding of the average energy of the neutron spectrum for any measurement of lattice defect introduction rates in a normal reactor locale, and that one must clearly differentiate between the formation of Frenkel or disordered region type defects in any analysis of radiation induced defects in semiconducting materials."

In the above and in previous work,[5] it has been shown that fast-neutron bombardment of *n*-type

[1]Present address: Northrup Ventura, Newbury Park, Calif.

[2]J. W. Cleland and R. F. Bass, *Solid State Div. Ann. Progr. Rept. May 31, 1963,* ORNL-3480, pp. 80–81.

[3]J. W. Cleland, R. F. Bass, and J. H. Crawford, Jr., *Solid State Div. Ann. Progr. Rept. Aug. 31, 1961,* ORNL-3213, pp. 66–71.

[4]To be published in a supplement to the *Proceedings of the International Conference on the Physics of Semiconductors, Paris, France, 1964.*

[5]J. H. Crawford, Jr., and J. W. Cleland, *J. Appl. Phys.* **30**, 1204 (1959); B. R. Gossick, *J. Appl. Phys.* **30**, 1214 (1959); J. W. Cleland and J. H. Crawford, Jr., *Proc. Intern. Conf. Semicon. Phys., Prague, 1960,* p. 299, Czechoslovakia Academy of Science, Prague, 1961.

germanium produces disordered regions or regions of high defect density whose spatial extent is of the order of 100 A. The heavily damaged region is a *p*-type island embedded in an *n*-type matrix and is, therefore, surrounded by a space-charge zone (*p-n* junction) whose radial extent is much greater than that of the disordered region. The space-charge zone is denuded of conduction electrons and acts as an insulating void by restricting current flow. Although such disordered regions might also be expected in silicon, the smaller dielectric constant and the fact that neutron bombardment produces intrinsic rather than converted material would lead to a much smaller space-charge zone.

If there is a marked shift in the position of the Fermi level from the matrix to the center of the disordered region, the primary effect of neutron irradiation on the electrical behavior of semiconductors enters through the space-charge zone surrounding the disordered region. Therefore, some caution must be exercised in interpreting the observed changes in carrier concentration. Nevertheless, for comparison, it is convenient to use a consistent unit; hence, the changes in the Hall coefficient resulting from neutron bombardment have been converted to an *apparent* removal rate of conduction electrons.

Figure 16.1, which is a composite graph of the average apparent removal rate of conduction electrons in *n*-type germanium and silicon as a function of neutron energy, exhibits the general trend that has been observed as a consequence of many separate experiments. It should be stated that these data represent averages for different samples of varying initial carrier concentration as exposed to different neutron sources and to different total neutron doses.

A wide range of neutron energies from a variety of sources was used in these studies. The range from 0.2 to 1.5 Mev was covered using the $^{7}Li(p,n)^{7}Be$ reaction.[6,7] Also shown are the

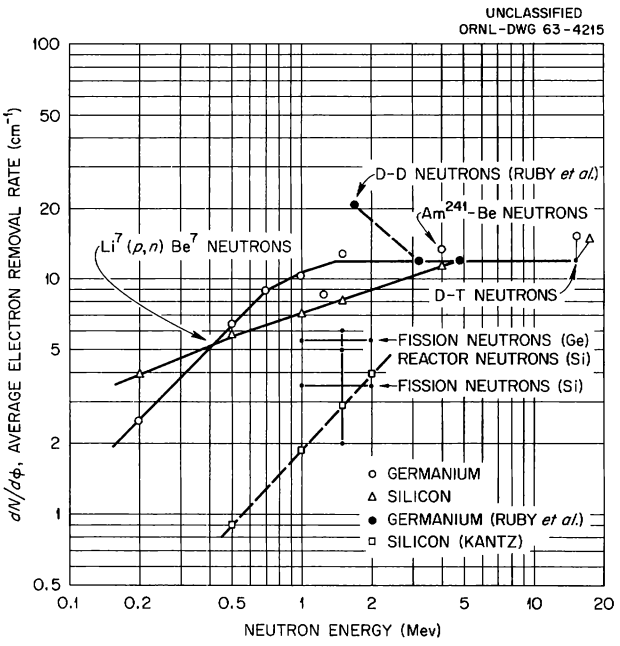

Fig. 16.1. Average Apparent Removal Rate of Conduction Electrons in *n*-Type Ge and Si vs Neutron Energy.

earlier results of Ruby *et al.*,[8] who used the $^{2}H(d,n)^{3}He$ reaction for 1.7-, 3.2-, and 4.8-Mev neutrons. Their results may not be directly comparable because both irradiation and measurement were conducted at 77°K instead of near room temperature. Curtis and Cleland[9] obtained an apparent removal rate of about eight conduction electrons per incident 14.1-Mev neutron in nearly intrinsic samples of germanium. Recently, the apparent damage rate of 14.1-Mev neutrons has been measured[10] for a number of samples of germanium and silicon for a total dose of 8.5×10^{11} cm^{-2}.

The most significant aspect of the monoenergetic-neutron results of Fig. 16.1 is the trend of damage rate with neutron energy. For *n*-type germanium the apparent electron removal rate averaged for a large number of specimens increases up to ~1.0 Mev and saturates for higher energies, whereas

[6]We are indebted to Dr. Alan B. Smith, Reactor Engineering Division, Argonne National Laboratory, for these irradiations.

[7]The initial publication of some preliminary data in this energy range (ref. 2) was in error in that the fission foil was weighed as ^{235}U mass per total area, but recorded as ^{235}U mass per unit area. Every total dose between 0.2 and 1.5 Mev in Table 12.3 (ref. 2) should be multiplied by 2.89, and every removal rate between 0.2 and 1.5 Mev in Table 12.3 (ref. 2) should be divided by 2.89.

[8]S. L. Ruby *et al.*, *Phys. Rev.* **111**, 1493 (1958).

[9]J. W. Cleland, O. L. Curtis, Jr., and J. H. Crawford, Jr., *Solid State Div. Ann. Progr. Rept. Aug. 31, 1958*, ORNL-2614, pp. 4–5; O. L. Curtis, Jr., and J. W. Cleland, *J. Appl. Phys.* **31**, 423 (1960).

[10]We are indebted to J. E. Strain of this laboratory for these irradiations.

that for silicon increases monotonically at least up to about 4.0 Mev. The germanium behavior is not inconsistent with the space-charge model and the simple damage theory. The total volume affected by the space-charge zone is relatively insensitive to the size of the disordered region, and previous studies have suggested[11] that 0.7 to 1.0 Mev is the threshold for disordered-region production. In silicon, for which the electrical effects of disordered regions are not nearly so pronounced, the monotonic increase in damage rate probably reflects the increase in the number of defects per scattered neutron over this energy range.

Also shown in Fig. 16.1 are the results of a variety of reactor, fission-spectrum, and ^{241}Am-Be source neutron irradiations of germanium and silicon. Fission-spectrum neutrons were obtained both from the conversion of thermal-energy neutrons by fission plates[2] and from the bare critical assembly[12] of the Sandia Pulsed Reactor. Kantz[13] has estimated the apparent removal rate of conduction electrons per unit flux for vacuum float-zone *n*-type samples of silicon from resistivity measurements and has indicated that the apparent removal rate was a sensitive function of the average energy of the neutron spectrum for seven different reactor locales, where the average neutron energy varied from 0.4 to 2.3 Mev. Strain[14] has fabricated[15] an ^{241}Am-Be neutron source,[16] and a lithium-diffused silicon detector indicated that the average neutron energy was about 4.0 Mev.

It is difficult to make a direct comparison of the present data with those of Kantz since he (1) did not specify the initial carrier concentration of his material; (2) made resistivity measurements only (for the most part); (3) made such measurements only during irradiation; (4) used a 1, 5, and 10% resistivity change for samples of 1, 10, and 100 ohm-cm respectively; and (5) related the resistivity change to carrier removal rates under the assumption of a negligible change in carrier mobility. An attempt has been made to indicate the approximate rate of removal of conduction electrons from silicon of about 55 ohm-cm resistivity, as estimated from Kantz's data in Fig. 16.1.

It is evident that the fission-neutron values are lower than the corresponding monoenergetic-neutron values in Fig. 16.1 by about a factor of 2 for both germanium and silicon and that the data of Kantz (reactor) agree more closely with the fission-neutron data than they do with the monoenergetic-neutron data. The corresponding data points for the pulsed reactor (bare critical assembly) experiments are not shown; however, they agreed very closely with the fission-neutron data as opposed to the monoenergetic-neutron data.

Smits and Stein[17] have recently calculated the neutron energy dependence of the defect production rate in silicon and have included the energy dependence of the total elastic cross section, nonisotropic scattering, inelastic scattering, charged-particle emission, and energy losses due to ionization by energetic knocked-on atoms. The predicted and observed neutron energy dependence of damage in silicon are shown[18] in Fig. 16.2. Also shown are the monoenergetic-neutron results

---

[11] D. K. Holmes and G. Leibfried, *J. Appl. Phys.* **31**, 1946 (1960).

[12] We are indebted to Dr. H. J. Stein of the Sandia Corporation for these irradiations. The apparent total dose was 8×10^{12} (3.0 Mev threshold) and 6×10^{13} (10 kev threshold) cm^{-2} as determined by activation of sulfur pellets.

[13] A. D. Kantz, *J. Appl. Phys.* **34**, 1944 (1963).

[14] We are indebted to J. E. Strain and E. H. Acree of this laboratory for these irradiations.

[15] By-product ^{241}Am has recently been made available by the Atomic Energy Commission for commercial use. This material has a 458-year half-life, 3.24 curies/g specific activity, 5.44- and 5.48-Mev alpha radiation (100%), and an extremely weak (60-kev) gamma radiation (34%) that can be readily shielded out by any high-*Z* container material. Pelletized intimate mixtures of AmO_2 and Be in a weight ratio of 1 to 10, doubly encapsulated in type 304L stainless steel, provide $\sim 2.1 \times 10^6$ neutrons/sec per curie of ^{241}Am.

[16] Eight ^{241}Am-Be cylinders (1 1/16 in. in diameter × 1 1/4 in. high), each containing 0.6 g of ^{241}Am in 6.0 g of beryllium were fabricated, and four of these sources were placed in a holder that consisted of four 1 1/4-in.-diam source tubes that surrounded a central 3/4-in.-diam sample tube. Phosphorus (2-Mev threshold; 300-mb cross section) and silica (4-Mev threshold; 200-mb cross section at 6.0 Mev neutron energy) detectors were placed at the center line of the sample tube and yielded a dose rate from the four sources of 7.6×10^4 neutrons cm^{-2} sec^{-1} above 2.0 Mev and 1.9×10^4 neutrons cm^{-2} sec^{-1} above 6.0 Mev. The actual neutron flux (eight sources) was 1.2×10^5 neutrons cm^{-2} sec^{-1}, and irradiation of two *n*-type samples of germanium results in a total electron removal of about 1×10^{12} cm^{-3} after 170 hr exposure.

[17] F. M. Smits and H. J. Stein, *Bull. Am. Phys. Soc.* **9**, 289 (1964).

[18] We are indebted to Dr. H. J. Stein of the Sandia Laboratory for this unpublished figure.

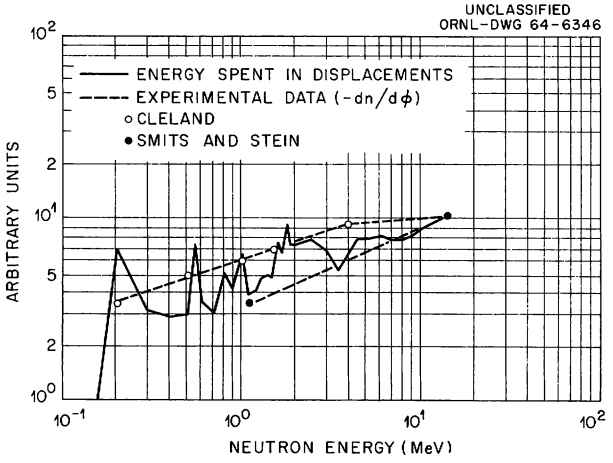

Fig. 16.2. Predicted and Observed Neutron Energy Dependence of Damage in Silicon.

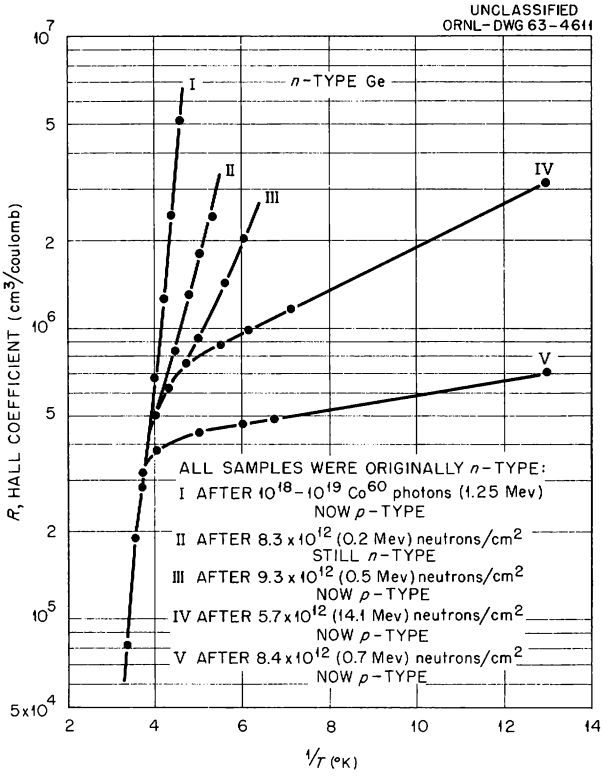

Fig. 16.3. Hall Coefficient vs Inverse Temperature of Originally *n*-Type Ge Samples After Irradiation.

of the present work and the reactor and 14-Mev neutron results of Smits and Stein.

The predicted variation of defect-production rate with energy was significantly less than linear, and the predicted neutron energy dependence of damage showed several oscillations in magnitude between 0.2 and 2.0 Mev neutron energies. The experimental data points to date agree with the less than linear energy dependence; however, the arbitrary choice of monoenergetic-neutron energies (0.2, 0.5, 1.0, and 1.5 Mev) that were employed does not permit an experimental check on the predicted oscillations in magnitude of the energy spent in displacements.

It is evident from these experiments that one must clearly differentiate between the formation of Frenkel or disordered-region defects in any analysis of the radiation behavior of semiconducting materials. It has been demonstrated[19] previously that no low-lying acceptor states are introduced in germanium of low dislocation density by ^{60}Co photons. Figure 16.3, which is a graph of log Hall coefficient vs inverse temperature, shows that little, if any, evidence for low-lying *p*-type acceptor states was obtained after a total irradiation of 10^{19} ^{60}Co photons/cm^2, or after $\sim 10^{13}$ (0.2- or 0.5-Mev) neutrons/cm^2; however, the apparent hole concentration of converted material is increased, and the apparent activation energy is decreased for irradiations of 8.4×10^{12} (0.7-Mev) and 5.7×10^{12} (14.1-Mev) neutrons/cm^2. Since it has been established from work on *n*-type germanium that the threshold for disordered region production is $\sim$0.7 ev, these data suggest that disordered regions are also responsible for low-lying acceptor states which can cause conversion to low-resistivity *p*-type material.

ANNEALING OF ^{60}Co GAMMA-IRRADIATED GERMANIUM

(isochronal annealing at 77 to 450°K; As or Sb doped; carrier concentration; E)

J. C. Pigg H. Saito[20]

The studies of the annealing properties of ^{60}Co gamma-irradiated germanium have been con-

[19] J. W. Cleland, R. F. Bass, and J. H. Crawford, Jr., *Appl. Phys. Letters* **2**, 113 (1963).

[20] Visiting scientist from Kyoto University, Kyoto, Japan.

tinued[21,22] using a broader range of impurity concentrations and two different impurity types in an attempt to study the annealing dependence on impurity concentration reported by Curtis and Crawford[23] and on impurity type reported by Brown *et al.*[24] A summary of the isochronal annealing of the carrier concentration change measured at liquid-nitrogen temperature is shown in Fig. 16.4.

The fractional change in carrier concentration shown in Fig. 16.4 has been considered to be correlated with the total concentration of states arising from the induced defects.[22] There are two major annealing stages in all the samples studied. The low-temperature stage (stage A) occurs in the range of annealing temperature between 280 and 380°K. The high-temperature stage (stage B) occurs between 390 and 450°K.

Stage A is much more pronounced in the arsenic-doped samples and in the highly doped samples with concentrations above 2×10^{14} cm^{-3}. There is also an indication that stage A may be a two-step process for the arsenic-doped samples and the highly antimony-doped sample. The data in Fig. 16.4 reflect the combined changes in both the deep- and shallow-state concentrations. Crawford and Cleland[25] have shown that the deep state can be increased by annealing in the temperature range of 370°K such that the total concentration of states remains essentially unchanged. This effect in the isochronal anneal is illustrated in the concentrations measured at 273°K (Fig. 16.5). An extreme example is shown by the 1.3×10^{15} arsenic-doped sample in which the deep state grows from 90 to 97% in the range from 330 to 380°K.

Stage B begins at a higher temperature in the arsenic-doped samples than in the antimony-doped samples. This can be interpreted in terms of a higher binding energy for the As(V) complex than for the Sb(V) complex.

The behavior of the total induced state concentration of sample EP 9-1 has been observed in many samples which were antimony-doped with concentrations of the order of 10^{13}. This behavior is not understood at present.

The annealing of the scattering concentration as measured by reciprocal mobility is shown in

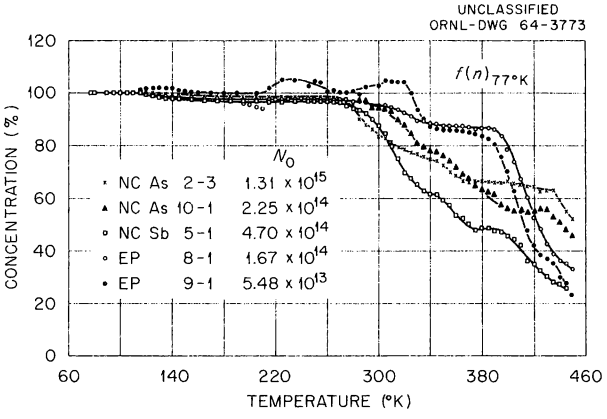

Fig. 16.4. Isochronal Anneal of Total Induced-State Concentration.

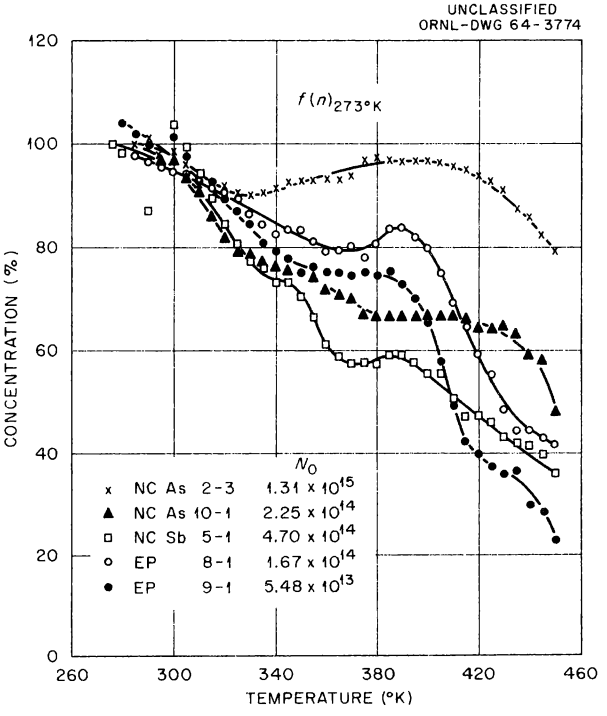

Fig. 16.5. Isochronal Anneal of Deep-State Concentration.

[21] J. C. Pigg, *Solid State Div. Ann. Progr. Rept. May 31, 1963*, ORNL-3480, p. 84.

[22] J. C. Pigg, *Annealing of Gamma-Ray-Induced Changes in Antimony-Doped Germanium*, ORNL-3443 (May 14, 1963).

[23] O. L. Curtis, Jr., and J. H. Crawford, Jr., *Phys. Rev.* **126**, 1342 (1962).

[24] W. L. Brown, W. M. Augustyniak, and T. R. Waite, *J. Appl. Phys.* **30**, 1258 (1959).

[25] J. H. Crawford, Jr., and J. W. Cleland, *J. Appl. Phys.* **30**, 1204 (1959).

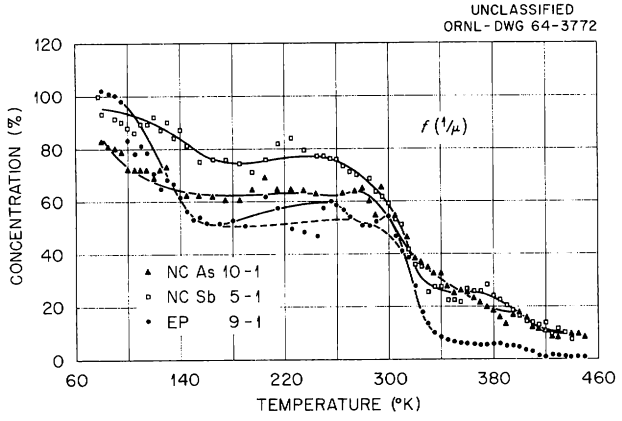

Fig. 16.6. Isochronal Anneal of Reciprocal Mobility.

Fig. 16.6. The qualitative behavior is the same for all samples. There is a pronounced anneal at low temperature which is completed long before the onset of stage A. There is another pronounced anneal corresponding to stage A which removes most of the remaining change in $F(1/\mu)$, and a final anneal which is associated with stage B.

The final anneal of the mobility can be attributed to the final removal of the induced defect concentration. The anneal correlated with stage A can be understood from the model in terms of a shift from monopole to dipole scattering as the isolated vacancies and impurity atoms form complexes. It does not seem likely that the low-temperature (100°K) recovery can also be explained as being associated with vacancy motion; this is a rather low temperature for an 0.8-ev process, which is the activation energy presently attributed to vacancy motion.[22] Therefore, the low-temperature annealing of $1/\mu$ is probably due to some type of defect rearrangement not understood at the present time.

RADIATION EFFECTS AND THEIR ANNEALING IN ^{60}Co GAMMA-IRRADIATED ANTIMONY-DOPED GERMANIUM[26]

(77°K; isochronal or isothermal annealing; carrier removal to 450°K; E)

J. C. Pigg J. H. Crawford, Jr.

The annealing of changes in the electrical properties of antimony-doped germanium caused by ^{60}Co gamma irradiation at 77°K has been investigated by both isochronal and isothermal techniques. The previously observed levels at 0.2 ev below the conduction band and near or below the middle of the forbidden band were studied individually. It was found that both the rate of carrier removal and the subsequent course of recovery upon annealing above 273°K were markedly dependent upon the antimony concentration (N_{Sb}). The rate of electron removal (dn/dt) is smaller for lower antimony concentrations. Upon annealing in the range between 273 and 450°K, two distinct stages are observed. Stage A accounts for the major recovery of the change in carrier concentration for samples with high antimony concentration ($N_{Sb} = 10^{15}$ cm^{-3}) and for the major recovery of reciprocal mobility for both high- and low-purity material. By contrast, the major recovery of carrier concentration for the low antimony concentrations ($N_{Sb} \approx 10^{14}$ cm^{-3}) occurs in the high-temperature stage, stage B. Stage B proceeds with an apparent activation energy of $\sim$1.2 ev. The annealing data are considered in terms of a model in which the formation of antimony-vacancy and antimony-divacancy complexes occur as parallel processes to vacancy capture by sinks. A new energy level at 0.09 ev below the conduction band was observed after annealing at 370°K. This level has been tentatively attributed to oxygen-vacancy complexes.

RADIATION EFFECTS IN CdS AND CdTe

(gamma and thermal-neutron irradiation; Hall coefficient; electrical resistivity; 52 and 350°K; E)

R. O. Chester

The effects of ^{60}Co, ^{137}Cs, and thermal-neutron irradiations on single crystals of high-purity *n*-type CdS were investigated. The specimens were obtained from the Eagle-Picher Company, Cincinnati, Ohio. Spectroscopic analysis showed the major impurities present to be 10 ppm silicon and 0.5 ppm manganese. Ohmic contacts were obtained by etching the samples in pyrophosphoric acid, as suggested by Aven,[27] and immediately applying indium with an ultrasonic soldering iron.

[26] Abstract of paper to be published in the August issue of the *Physical Review*.

[27] M. Aven, personal communication.

Hall and resistivity measurements were obtained in the temperature region 52 to 350°K with rectangular Hall bars.

Typical initial donor concentrations are 10^{15} to 10^{16} per cm^3. Two donor states are indicated by the carrier concentration as a function of temperature at ~0.04 and 0.1 ev below the conduction band. There is also some evidence of a much shallower level, although the temperature range examined did not extend to temperatures low enough to locate it definitely. This level may possibly be the ~0.002-ev level indicated by Itakura and Toyoda.[28] Irradiation with gamma rays and thermal neutrons did not introduce any donor levels in the 0.03- to 0.2-ev range which could be distinguished from the initially present 0.04- and 0.1-ev levels as illustrated by the typical ^{60}Co irradiated specimen shown in Fig. 16.7. The density of these donors or other donors with very similar ionization energies changed, however, during irradiation. The variation of the 0.04-ev donor ionization energy with total center density is given in Fig. 16.8. Various samples are represented, both before and after irradiation. These data agree fairly well with those obtained from low-temperature mobility measurement of doped CdS by Spear and Mort.[29] Data for the 0.1-ev level are not detailed enough to give a statistically significant energy variation vs concentration or to determine unambiguously whether the 0.1-ev level is a donor or is associated with the double-acceptor center postulated by Halsted and Segall.[30] The rate of donor introduction is not constant, as indicated for ^{60}Co-irradiated CdS in Fig. 16.9.

Room-temperature Hall mobility of CdS is 330 $cm^2\ v^{-1}\ sec^{-1}$ and is unaltered by the types of radiation employed. The observed mobility down to 150°K is well described in terms of carrier scattering by longitudinal optical phonons and piezoelectric scattering as calculated by Zook and Dexter[31] and Hutson[32] (Fig. 16.10). At low temperatures the observed mobility falls below the calculated mobility owing to scattering from

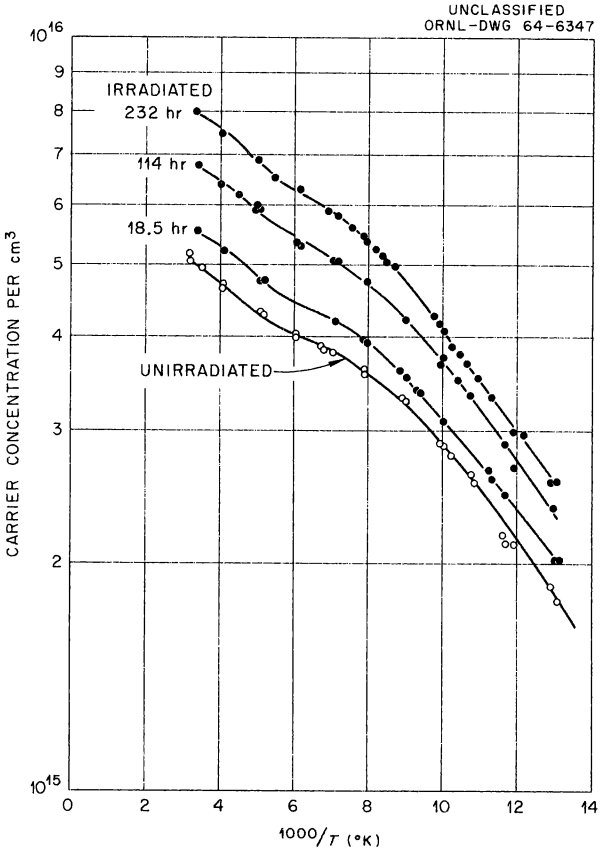

Fig. 16.7. CdS Sample No. 1 – *n*-Type, Irradiated in ^{60}Co Source.

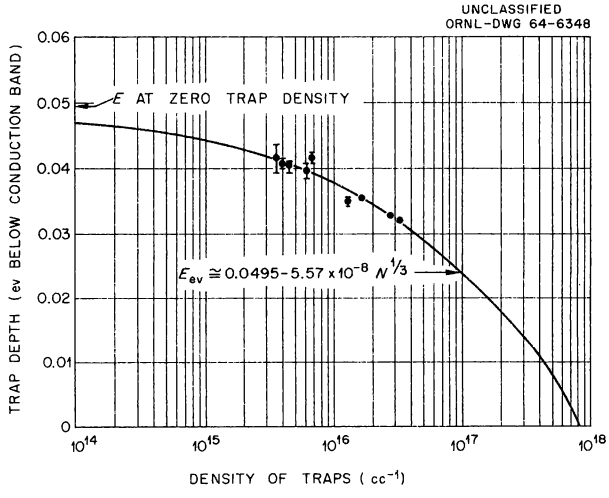

Fig. 16.8. Dependence of Trap Depth on Total Trap Density for CdS.

[28] M. Itakura and H. Toyoda, *J. Phys. Soc. Japan* **18**, 150 (1963).

[29] W. E. Spear and J. Mort, *Proc. Phys. Soc.* **81**, 130 (1963).

[30] R. E. Halsted and B. Segall, *Phys. Rev. Letters* **10**, 392 (1963).

[31] J. D. Zook and R. N. Dexter, *Phys. Rev.* **129**, 1980 (1963).

[32] A. R. Hutson, *J. Appl. Phys.* **32**, 2287 (1961).

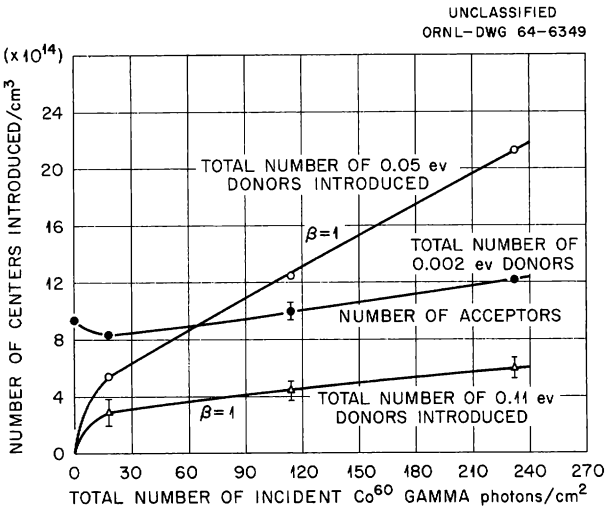

Fig. 16.9. Number of Electrically Active Centers Introduced vs Total Incident ^{60}Co Gamma Flux. CdS sample No. 1.

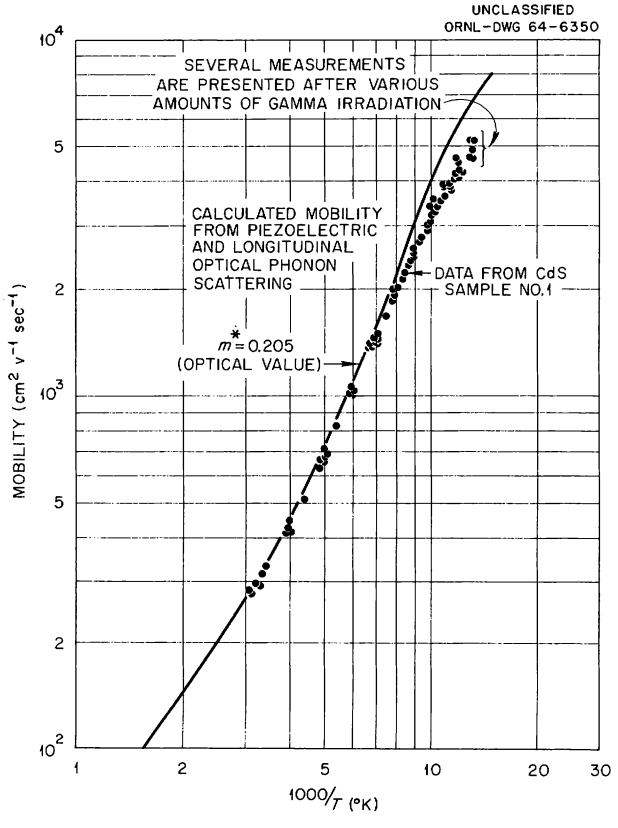

Fig. 16.10. Comparison of Theoretical and Observed Electron Hall Mobility in CdS.

charged centers. After irradiation the low-temperature difference is increased because the number of scattering centers has been increased.

An *n*-type zone-refined single crystal of CdTe was obtained from R. E. Halsted, Research Laboratory, General Electric Company, Schenectady, New York. Contacts were made to the material by first etching in HF, boiling in an NaOH solution, and then applying Hg-In alloy with an ultrasonic soldering iron. Hall measurements were made in the temperature range 300 to 52°K. Initial donor concentrations were $(4–5) \times 10^{14}$ per cm^3. Three donor energy levels were indicated at ~0.02, 0.06, and 0.1 ev. Preliminary analysis indicates that no new levels in this range were introduced; however, the relative amounts of these levels and the density of acceptor levels did change. A typical sample is indicated in Fig. 16.11. Room-temperature mobility of *n*-type CdS is usually ~820 $cm^2\ v^{-1}\ sec^{-1}$, as would be predicted from longitudinal optical phonon scattering of conduction electrons. After prolonged ^{60}Co or thermal-neutron irradiation, it was necessary to consider CdTe as a two-carrier system. Thermal-neutron irradiation has been used to convert samples to *p* type, with an acceptor level at 0.3 to 0.4 ev above the valence band.

No annealing effects were observed in the temperature ranges under investigation either before or after irradiation. Irradiation in all cases was done at ambient temperatures. Cobalt-60 irradiation

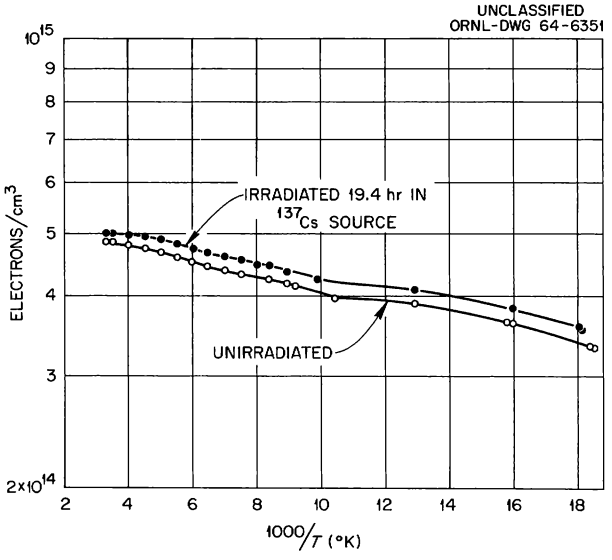

Fig. 16.11. Cadmium Telluride – Sample No. 5.

of CdS at liquid-nitrogen temperature did not produce a significantly different damage rate from ambient-temperature irradiations.

Theoretical cross sections for atomic displacements in solids have been calculated by Oen and Holmes.[33] The threshold energies used for cadmium and sulfur atom displacements in CdS were 8.6 ev for sulfur and 7.3 ev for cadmium. These are the values deduced by Kulp and Kelley[34] in their fluorescence studies on CdS as a function of bombarding electron energy. Cadmium-113 has a thermal-neutron capture cross section of 27,000 barns, at least two orders of magnitude larger than any other isotope of cadmium, sulfur, or tellurium. Cadmium-113 decays into stable ^{114}Cd with a recoil energy of 54 ev, enough to knock the cadmium from its lattice site. Hence, thermal-neutron irradiation might produce effects due primarily to displacement of the cadmium atom.

The calculated and typical observed damage rates are indicated in Tables 16.1 and 16.2. The observed damage rates are lower than the calculated rates, often by as much as an order of magnitude. A similar disparity is observed in the case of germanium and silicon. Also, the damage rate is greater, the greater the initial donor density. Therefore, it seems reasonable to assume that vacancies and interstitials are mobile at the temperatures investigated, and the donor centers observed are the result of more stable complexes, such as vacancy-impurity complexes as have been detected in silicon.

[33]O. S. Oen and D. K. Holmes, *J. Appl. Phys.* **30**, 1289 (1959).

[34]B. A. Kulp, *Phys. Rev.* **125**, 1865 (1962); B. A. Kulp and R. H. Kelley, *J. Appl. Phys.* **31**, 1057 (1960).

Table 16.1 Observed Radiation Damage Rates

Compound	Type of Irradiation	Total Dose (photons/cm^2)	Damage Rate: Donors Introduced per Incident Particle		
			0.04-ev Level	0.1-ev Level	Acceptors
		$\times 10^{15}$			
CdS	^{60}Co gamma	130	0.003	0.0016	0.0005
CdS	^{137}Cs gamma	955	0.0003	0.0015	0.0013
CdS	^{137}Cs gamma	2550	0.0001	0.00004	0.00013

Compound	Type of Irradiation	Total Dose (photons/cm^2)	Change in Carrier Concentration: Room Temperature	Change in Carrier Concentration: Liquid-Nitrogen Temperature
		$\times 10^{15}$		
CdS	Thermal neutron	2.9	−0.35	~ 0
CdTe	^{60}Co gamma	1.4	−0.0015	+0.0072
CdTe	^{137}Cs gamma	85	+0.0019	+0.00023
CdTe	Thermal neutron	14	Large negative	Large negative
			Converted to *p*-type	

Table 16.2 Theoretical Radiation Damage Rates

Threshold Energy for Displacing an Atom

of:	in:	is:
Cd	CdS	7.3 ev
S	CdS	8.7 ev
Cd	CdTe	Unknown (assumed 7.3 ev)
Te	CdTe	Unknown (assumed 7.3 ev)

Cross Section for Displacing an Atom

of:	in:	with:	is:	Removal Rate (atoms displaced/cm^3/ incident $h\nu/cm^2$)
S	CdS	^{60}Co gamma	1.4 barns	0.027
Cd	CdS,CdTe	^{60}Co gamma	3.0 barns	0.057
S	CdS	^{137}Cs gamma	0.40 barn	0.0076
Cd	CdS,CdTe	^{137}Cs gamma	0.20 barn	0.0038
Te	CdTe	^{137}Cs gamma	0.14 barn	0.0027
Te	CdTe	^{60}Co gamma	3.5 barns	0.066

Ratio of Removal Rates

of:	in:	with:	is:
Cd/S	CdS	^{60}Co gamma	2.1
Cd/S	CdS	^{137}Cs gamma	1/2.0
Cd/Te	CdTe	^{60}Co gamma	1/1.2
Cd/Te	CdTe	^{137}Cs gamma	1.4

Part V. Radiation Metallurgy

M. S. Wechsler

17. Radiation Metallurgy

The research of the Radiation Metallurgy Section is directed toward the problem of the radiation embrittlement of metals and alloys. The mechanical properties of structural alloys depend in large measure on the relative atomic arrangement of the various alloying constituents. One aspect of the change in properties upon irradiation involves a rearrangement of the positions of the alloying atoms, thus forming structures not found at the same temperatures in unirradiated alloys. A practical case where such atomic rearrangements may be particularly important is that of austenitic stainless steels. Here the alloy is in a metastable state before irradiation. Upon irradiation, this metastability may be eliminated with an accompanying deterioration of mechanical properties.

The effect of irradiation on diffusion-controlled processes is being studied theoretically and experimentally. A discussion is given below of recent developments in the theory of the kinetics of radiation-enhanced diffusion. The theory is applied to radiation-enhanced ordering in Cu-Al alloys. In addition, the results of recent irradiation experiments on Cu–15 at. % Al are described. It has been found that the rate of radiation-enhanced ordering in this alloy is decreased by prior cold working. This is interpreted to indicate that the cold working introduces sinks for radiation-produced defects, thus decreasing the effectiveness of each defect in facilitating the ordering reaction.

Another type of diffusion-controlled process is the segregation or clustering of solute atoms in alloys. Segregation in alloys is exemplified by the Cu-Ni system, and the effect of irradiation in accelerating segregation has been investigated. In this case, the experiments were performed by the isochronal annealing of samples that were given prior irradiation, deformation, or quenching treatments.

It is of interest to extend the experiments on the face-centered cubic copper-base alloys to alloy systems that exhibit the body-centered cubic structure. This will serve to test the generality of the earlier observations. Furthermore, the results on body-centered cubic alloys will have a greater bearing on the important problem of radiation embrittlement in low-carbon pressure-vessel steels. For these reasons, an investigation of Fe-Si alloys has been initiated, and some preliminary resistivity measurements are described below.

Still another type of diffusion-controlled process of considerable significance in connection with mechanical properties is the precipitation reaction. For steels, the precipitation of nitrogen is particularly important. This is being studied by means of low-frequency internal friction, and a special device has been developed that enables measurements to be made during reactor irradiation. It is found that the loss of nitrogen from solid solution in alpha iron is accelerated by irradiation.

In addition to the work on radiation-induced atomic rearrangements, research is in progress on the direct effect of radiation on flow and fracture properties. From the more basic point of view, the techniques of etch pitting and electron microscopy are being used to study dislocation arrangements and mobility in iron and iron alloys. This is a relatively new effort, and no observations have been made as yet on irradiated samples.

The effect of neutron irradiation on the tensile properties of iron and steel is also being investigated. The long-range objective of this phase of the work is a determination of the specific influence of the dose rate. This has a bearing on the use of structural materials in reactor environments because of the fact that the materials-testing irradiations are conducted at high fluxes for relatively short periods of time, whereas structural materials in service are expected to receive comparable doses at low fluxes over much longer periods of time. A careful study of this aspect of radiation effects is laborious and lengthy, but

the first in a series of irradiations in the ORR directed toward this problem is under way.

Finally, there are the investigations of the impact properties of commercial steels. This work is closely coordinated with that dealing with tensile properties because of the close connection between plastic deformation and fracture in metals. The present series of irradiations is devoted largely to synthetic heat-affected-zone samples. Earlier experiments have indicated that, despite the higher initial ductile-brittle transition temperature in the heat-affected-zone material, the increase in transition temperature upon irradiation at about 50°C (120°F) is roughly the same as for the base-plate material. These experiments are now being extended to elevated-temperature irradiations.

It should be mentioned in conclusion that new facilities are being designed for conducting irradiations in the BSR. These include a neutron converter for fission-spectrum irradiations and a cryostat for performing irradiations at liquid nitrogen temperature.

KINETICS OF RADIATION-ENHANCED DIFFUSION IN Cu–15 at. % Al

(electrical resistivity; T)

J. H. Barrett

Because interstitials and vacancies are produced in equal numbers during irradiation, either one might produce radiation enhancement of diffusion. Experimental results for the temperature dependence of radiation-enhanced diffusion effects in the Cu–15 at. % Al alloy have been analyzed[1,2] on the basis of diffusion enhancement due to vacancy motion and on the basis of diffusion enhancement due to interstitial motion. This analysis did not yield a clear-cut decision as to which defect is active in enhancing diffusion though it did suggest that the active defect is the interstitial. In order to develop other means for distinguishing which defect is the active one, the kinetics of some of the experiments have been analyzed. To perform this analysis, it was assumed that the electrical resistivity is some function of the short-range order of the alloy and that the short-range order is some function of J, the number of defect jumps per lattice site in the alloy. These two assumptions lead to the form $\rho = \rho(J)$ for the resistivity. The time dependence of J can be computed for various assumed experimental conditions. Using these expressions for $J(t)$, the *relative* kinetics of different experimental runs can be compared.

By using methods reported previously,[1] it is possible to deduce the form of $J(t)$ in certain cases. If vacancies are the diffusion-enhancing defects, $J \propto t^{3/2}$ for first runs and $J \propto t$ for second runs. First runs are experiments on previously unirradiated samples; second runs are experiments on samples irradiated for a week or more with a subsequent anneal at 210°C. If interstitials are the diffusion-enhancing defects, $J \propto t$ for both first and second runs. Figure 17.1 shows experimental first- and second-run curves[3] for a sample. The second-run curve is also shown translated to the left along the log t scale until it coincides with the first-run curve at $f = 0.5$; this corresponds to the assumption that J is proportional to the same power of t for both runs. In addition, the

[1]M. S. Wechsler *et al.*, *Solid State Div. Ann. Progr. Rept. Aug. 31, 1962*, ORNL-3364, pp. 127–34; J. M. Williams *et al.*, *Solid State Div. Ann. Progr. Rept. May 31, 1963*, ORNL-3480, pp. 135–42.

[2]J. H. Barrett and E. J. Lee, chap. 5, this report.

[3]Curves 1 and 2 of Fig. 17.1 are the same as runs 4-I and 4-II of Fig. 18.5, p. 134, of *Solid State Div. Ann. Progr. Rept. Aug. 31, 1962*, ORNL-3364.

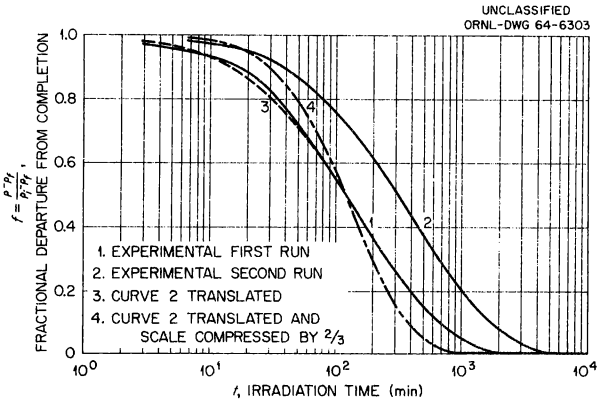

Fig. 17.1. Fractional Departure from Completion of the Decrease in Electrical Resistivity of Cu–15 at. % Al vs Time of Irradiation at 100°C for First and Second Runs at Position 4, Hole C, of the ORNL Graphite Reactor. Experimental points have been left off the curves.

second-run curve is shown translated on the log t scale to coincide with the first-run curve at $f = 0.5$ followed by a compression of the log t scale by a factor of $\frac{2}{3}$; this corresponds to the assumption that $J \propto t^{3/2}$ for the first run and $J \propto t$ for the second run. The curves in Fig. 17.1 strongly indicate that the first and second runs have the same dependence of J on t. This result points to the conclusion that the interstitial is the diffusion-enhancing defect during irradiation of Cu-Al.

Another experiment for which an analysis of the kinetics was found to be informative was an interrupted irradiation.[4] Figure 17.2 shows the results of this experiment. The curve, up to the time of withdrawal from the reactor and after reinsertion in the reactor, was drawn through the experimental points. The method used to estimate the behavior of the resistivity during the interruption of the irradiation required knowledge of the behavior that would have occurred if the irradiation had not been interrupted. The experimental curve suggested that the decrease of resistivity after the specimen was reinserted in the reactor was a resumption of the decrease that was occurring when the irradiation was interrupted. It was estimated from the experimental curve that the decrease which occurred during the period of interruption was equal to the decrease that would have occurred during an uninterrupted 180-min irradiation. An "uninterrupted" time scale was constructed by treating the total time of the interruption as the equivalent of 180 min. In Fig. 17.2 the experimental values obtained after resumption of irradiation are replotted on this "uninterrupted" time scale. By ignoring the transient behavior, curve 1 was drawn through the experimental points on the "uninterrupted" time scale.

The variation with time of the defect concentration after withdrawal of the sample to the edge of the reactor can be predicted by methods reported previously.[1] The accumulated number of jumps J for each type of defect was computed from

[4] M. S. Wechsler *et al.*, *Solid State Div. Ann. Progr. Rept. Aug. 31, 1959*, ORNL-2829, pp. 110–18, Fig. 72.

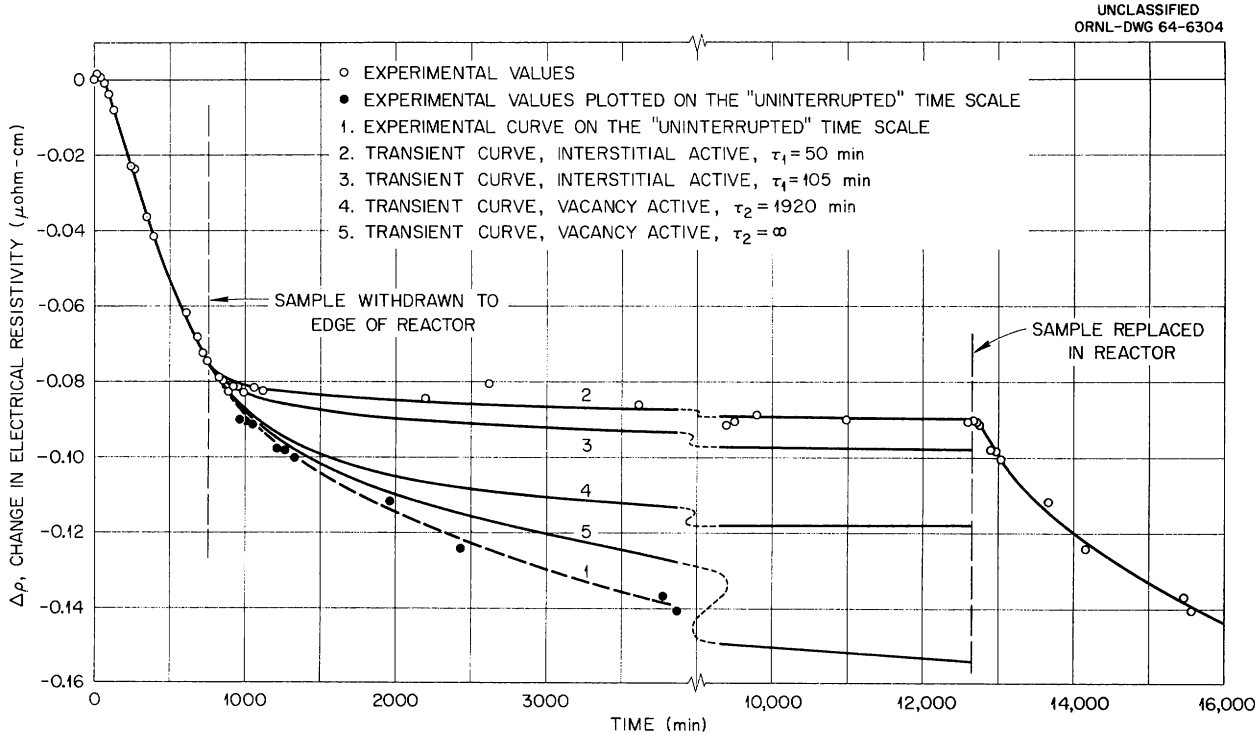

Fig. 17.2. Change of Electrical Resistivity of Cu–15 at. % Al vs Time for Interrupted Irradiation at 45°C in Hole 52 of the ORNL Graphite Reactor.

the concentration of that defect. From such a computed value of $J(t)$, the equivalent time that would have produced the same $J(t)$ during an uninterrupted irradiation was calculated. From this equivalent time value and the "uninterrupted" irradiation curve, the value of the resistivity was obtained. In this way curves were constructed to describe the behavior of $\rho(t)$ following withdrawal of the sample to the edge of the reactor. Four curves are drawn; two assume the diffusion-enhancing defect to be the interstitial, and two assume it to be the vacancy.

If the interstitial is the active defect, the kinetics may be described by simple interstitial-vacancy recombination, for which the concentration of interstitials is $(K/\gamma\nu_i)^{1/2}$ before interruption of the irradiation. After interruption, the interstitial concentration decays with second-order kinetics, so that the concentration is given by

$$i = \frac{(K/\gamma\,\nu_i)^{1/2}}{1 + (t - t_I)/\tau_1} ,$$

where t_I is the time of interruption, $\tau_1 = (K\gamma\nu_i)^{-1/2}$, K is the displacement production rate per atomic site, γ is a dimensionless constant that is a measure of the capture radius for the annihilation of an interstitial at a vacancy, and $\nu_i = \nu_{oi} \exp(-M_i/kT)$ is the interstitial jump rate. Curve 2 of Fig. 17.2 was constructed for $\tau_1 = 50$ min; it gives a good fit to the experimental points. However, from the parameters already determined by analysis[2] of the temperature dependence of the enhanced-diffusion effects ($K = 10^{-10}$ sec^{-1}, $\gamma = 25$, $\nu_{oi} = 10^{14}$ sec^{-1}, and $M_i = 0.82$ ev), the value calculated for τ_1 is 105 min. Curve 3 was constructed using this value. The various parameters which are inserted into the theory[2] can be adjusted so as to give a value of 50 min for τ_1 and still retain good agreement with the experiments on the temperature dependence. For instance, this could be done by changing ν_{oi} from 10^{14} to 4.4×10^{14} sec^{-1} with appropriate changes in other parameters involved in the theory of the temperature dependence. The fit of the theory to the experimental temperature dependence would be affected only slightly. Since the parameters put into the theory were somewhat arbitrarily chosen in the first place, such alterations are not out of the question.

If the vacancy is the active defect, its concentration is $(2K\beta t)^{1/2}$ before interruption of the irradiation and is $(2K\beta t_I)^{1/2} \exp(-t/\tau_2)$ after the interruption, where $\tau_2 = (\beta\nu_v)^{-1}$, β is approximately the concentration of fixed sinks, and $\nu_v = \nu_{ov} \exp(-M_v/kT)$. From the parameters determined by analysis[2] of the temperature dependence of enhanced diffusion ($K = 10^{-10}$ sec^{-1}, $\beta = 2 \times 10^{-7}$, $\nu_{ov} = 10^{14}$ sec^{-1}, and $M_v = 0.78$ ev), a value of 1920 min was calculated for τ_2. Curve 4 was constructed using this value. Curve 5 was constructed using $\tau_2 = \infty$. Up to times reaching a considerable fraction of τ_2, the behavior of the curves is independent of τ_2. In order to obtain agreement with the experimental points, τ_2 should have a value of approximately 100 min. This value could be achieved by changing ν_{ov} from 10^{14} to 2×10^{15} sec^{-1} and readjusting some of the other parameters. However, the resulting agreement between theory and experiment for the temperature dependence probably would not be so good as that previously obtained,[2] particularly for the second runs.

It is to be concluded that the transient behavior shown in Fig. 17.2 following interruption of the irradiation can be described by theory better if the interstitial, rather than the vacancy, is assumed to be the active defect. This conclusion is in accord with that reached by comparison of the relative kinetics of the curves in Fig. 17.1. This is also in accord with the better agreement[2] of experiment and theory for the temperature dependence when the interstitial is assumed as the active defect.

EFFECT OF DEFORMATION UPON NEUTRON RADIATION-ENHANCED DIFFUSION IN Cu–15 at. % Al

(0 to 210°C; electrical resistivity; single crystals; short-range order; E)

J. M. Williams M. S. Wechsler B. C. Kelley

Neutron irradiation of alpha Cu-Al alloys at temperatures of 0 to 210°C produces a decrease in the electrical resistivity which is attributable

to an increase in short-range order.[5-8] The radiation-produced point defects enhance diffusion, with the result that the alloy can achieve its equilibrium degree of order at lower temperatures than would otherwise be possible. The resistivity decrease saturates as the equilibrium ordered state is approached. The magnitude of the resistivity decrease depends on the initial preparation of the samples and the irradiation temperature. For slow-cooled single crystals irradiated at 100°C, the magnitude of the change is 0.16 microhm-cm.

The rate of the ordering reaction is a measure of the radiation-enhanced diffusivity, which in general depends upon the temperature and the neutron flux. The analysis of the temperature and flux dependence of the radiation-enhanced ordering rate in terms of the theory of radiation-enhanced diffusion gives information as to the mechanism of annihilation of the point defects.[9,10] In well-annealed single crystals the vacancies and interstitials disappear predominantly by mutual annihilation. However, the introduction of large numbers of point-defect sinks, such as dislocations, would be expected to change the removal mechanism to fixed-sink annihilation, concomitantly reducing the number of jumps necessary for removal of each radiation-produced defect. Thus, the rate of radiation-enhanced ordering should be reduced in samples subjected to deformation prior to irradiation.

The experimental plan for this investigation was based on the following prospective behavior of the deformed samples. The cold work was expected to produce dislocations and point defects and to disturb the state of short-range order. It has been stated in previous reports[10,11] that a heat treatment of 2 hr at 750°C followed by cooling at 15°C/hr to room temperature results in a state of short-range order characteristic of 210°C. Therefore, aging of the cold-worked samples at 210°C should restore them to about the same state of order as that for annealed, slow-cooled samples. This temperature is high enough to allow annealing of point defects also, but too low to permit removal of dislocations.

Single-crystal rods about 6 in. long and 0.049, 0.057, 0.060, 0.064, and 0.074 in. in diameter were grown from the melt. The specimens were annealed 2 hr at 750°C and cooled at 15°C/hr to room temperature. Their resistivities were measured at liquid nitrogen temperature (−196°C) with the samples in a knife-edge sample holder. Then the four samples of diameters 0.057, 0.060, 0.064, and 0.074 in. were cold worked to a common diameter of 0.050 in. by drawing them through a succession of dies, each die 0.003 in. smaller than the previous one. The samples were drawn at room temperature at a speed of 2 in./min. The 0.049-in.-diam sample was not cold worked at all. This procedure resulted in the preparation of five samples of about 0.050 in. diameter, each with a different amount of cold work. The degree of cold work ranged from 0 to 54% reduction in area (RA) for the five samples. Following the cold working, the resistivities were again measured at −196°C by use of the knife-edge sample holder. A $2\frac{1}{2}$-in. length of each of the specimens was then mounted in a reactor irradiation capsule and was suitably wired for measurement of the resistivity. The capsule was immersed in liquid nitrogen, and the resistivities of the specimens were again determined. The results, shown in Fig. 17.3, agreed within 1% with the measurements made in the knife-edge sample holder. This is within the accuracy of the gage-length determination for the samples mounted in the capsule. Figure 17.3 shows that the highest degree of cold working caused an increase in the resistivity from 8 to 10 microhm-cm, or about 25%.

In order to restore the degree of order characteristic of 210°C, as is discussed above, the capsule was then placed in a furnace, and the samples were aged 25 hr at 210°C. The results of the measurements following this aging treatment are

[5]M. S. Wechsler and R. H. Kernohan, "The Effect of Radiation on Diffusion-Controlled Reactions in Copper-Base Alloys," p. 81 in *Radiation Damage in Solids*, vol. II, International Atomic Energy Agency, Vienna, 1962.

[6]M. S. Wechsler, "Fundamental Aspects of Radiation Effects on Diffusion-Controlled Reactions in Alloys," p. 86 in *Radiation Effects on Metals and Neutron Dosimetry*, American Society for Testing and Materials, Philadelphia, 1962.

[7]C. R. Houska and B. L. Averbach, *J. Appl. Phys.* **30**, 1525 (1959).

[8]B. S. Borie and C. J. Sparks, *Metals and Ceramics Div. Ann. Progr. Rept. May 31, 1962*, ORNL-3313, pp. 204–6; to be published in *Acta Crystallographica*.

[9]J. H. Barrett, Jr., *Bull. Am. Phys. Soc.* **9**, 284 (1964).

[10]J. M. Williams *et al.*, *Solid State Div. Ann. Progr. Rept. May 31, 1963*, ORNL-3480, pp. 135–42.

[11]J. M. Williams *et al.*, *Solid State Div. Ann. Progr. Rept. Aug. 31, 1962*, ORNL-3364, pp. 129–34.

also shown in Fig. 17.3. It is seen that the resistivity remaining after aging at 210°C was only 10% greater than the annealed value for the most heavily deformed sample.

For the irradiation, a heater was placed in the capsule, and the entire assembly was placed in Hole C of the ORNL Graphite Reactor. The resistivities were measured as a function of irradiation time at 100°C. Figure 17.4 shows the change in resistivity plotted vs the logarithm of the irradiation time for the five specimens. The undeformed single crystal exhibits the rather rapid approach to equilibrium that we previously observed at this temperature and flux level.[5] The rate of the decrease for the deformed specimens, however, is markedly reduced. The time for a given amount of resistivity change for the sample of 23% RA is greater than that for the undeformed specimen by a factor of about 400; for the sample of 31% RA as compared to the undeformed sample, this factor is about 2000. The two specimens that were most severely deformed (40, 54% RA) showed essentially no changes in resistivity.

The large reduction in the rate of the resistivity decrease for the cold-worked specimens results from the annihilation of defects at the dislocations produced by the cold working. The dislocation density for the 23% RA specimen may be calculated under the assumption that the fixed-sink mechanism predominates. For this mechanism at steady state the concentration of either vacancies or interstitials is[10]

$$c = \frac{K}{\alpha \lambda^2 \nu},$$

where K is the defect production rate, α is the dislocation density, λ is the defect jump distance, and ν is the defect jump rate. The cumulative

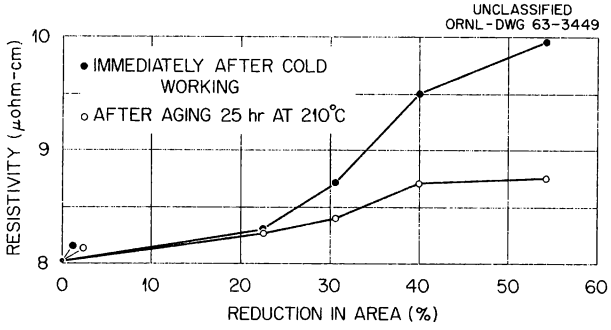

Fig. 17.3. Resistivity vs Percent Reduction in Area at Room Temperature for Cu–15 at. % Al, Before and After Aging at 210°C.

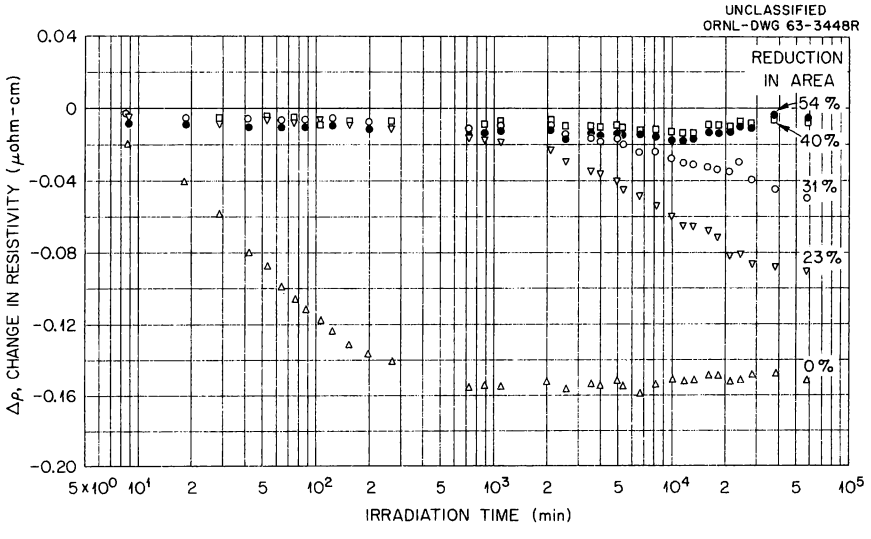

Fig. 17.4. Change in Resistivity vs Irradiation Time at 100°C for Cu–15 at. % Al Cold Worked to Various Reductions in Area and Aged at 210°C. Irradiated in Hole C of the ORNL Graphite Reactor.

number of defect jumps after irradiation time t is then given by

$$J(t) = c\nu t = \frac{K}{\alpha\lambda^2}\, t\,. \qquad (1)$$

For the reactor location used, the value of K has been determined as 10^{-10} sec^{-1} in previous reports,[6,11] and the value of λ^2 is about 10^{-15} cm^2. Unfortunately, due to the permanent shutdown of the ORNL Graphite Reactor, it was not possible to obtain the saturation values of the resistivity decreases for the cold-worked samples. However, let us assume that the saturation resistivity decrease would have been the same as that for the undeformed sample. Then from Fig. 17.4, the time for half completion for the 23% RA sample is $t = 2 \times 10^4$ min $= 1 \times 10^6$ sec. Then, letting $J = 1$ for the number of defect jumps per atom for half completion,[10] we deduce from Eq. (1) a dislocation density of 10^{11} cm^{-2}. This would appear to be a reasonable value for a fairly heavily cold-worked sample.

ANNEALING OF Cu-Ni ALLOYS FOLLOWING NEUTRON IRRADIATION, QUENCHING, AND DEFORMATION

(25 to 65 wt % Cu; electrical resistivity; isochronal annealing at 77 to 853°K; quenching from 875 to 1325°K; E)

W. Schüle[12] M. S. Wechsler
B. C. Kelley J. M. Williams

It has been shown by means of magnetic susceptibility measurements that neutron irradiation of Cu-Ni alloys stimulates segregation of the components.[13] Furthermore, the segregation is accompanied by a decrease in the electrical resistivity.[14] In order to better understand the mechanism for this effect, it was decided to investigate the annealing behavior of some Cu-Ni alloys after irradiation, quenching, and deformation treatments. The changes in resistivity upon isochronal annealing were measured for several samples, each of which had been subjected to one of the following treatments: (1) neutron irradiation at −180°C; (2) quenching from 600, 850, and 1050°C; (3) quenching from 600°C and irradiation at −180°C; and (4) deformation at below −100°C.

A number of foil resistivity specimens were prepared from Cu-Ni alloys ranging in composition from 25 to 65 wt % Cu. They were annealed 3 hr at 850°C *in vacuo* and slow cooled at 22°C/hr to room temperature. One of the specimens was selected as a standard specimen, and its resistance was determined at liquid nitrogen temperature (−196°C) with a Rubicon six-dial microvolt potentiometer. Thereafter, the resistances of the other specimens were measured at liquid nitrogen temperature by comparison with this standard sample by use of a Kelvin bridge.

Part of the samples were placed in the Hole 50 cryostat of the ORNL Graphite Reactor and irradiated three weeks at −180°C. The samples were then removed and held at −196°C until the radioactivity had decayed to such a low level that the isochronal annealing could be carried out in the laboratory.

Figure 17.5 shows the isochronal annealing curves for increasing temperatures for the four alloy compositions studied. The change in resistivity is taken with respect to the slow-cooled or preirradiation value. The points for −196°C in Fig. 17.5 indicate that little change in resistivity was produced as a result of the irradiation at −180°C. However, we see that upon isochronal annealing a decrease in resistivity occurs which starts gradually at −50°C and reaches a minimum

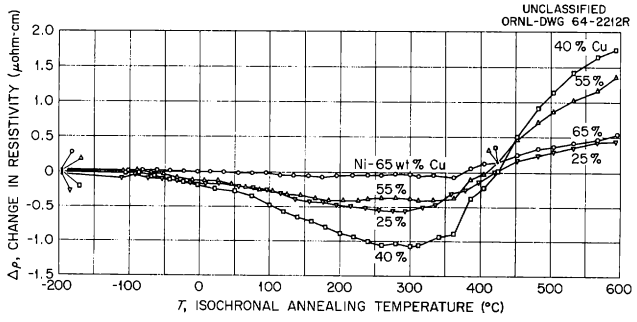

Fig. 17.5. Change in Resistivity of Cu-Ni Alloys upon Isochronal Annealing After Irradiating Three Weeks at −180°C. Measurements at −196°C.

[12]Present Address: CCR — Euratom, Ispra (Varese), Italy.

[13]F. M. Ryan, E. W. Pugh, and R. Smoluchowski, *Phys. Rev.* 116, 1106 (1959).

[14]A. Ascoli, "Neutron-Bombardment-Enhanced Segregation in Cu-Ni Alloys," p. 105 in *Radiation Damage in Solids*, vol. II, International Atomic Energy Agency, Vienna, 1962.

at 250–300°C. Thereupon, the resistivity increases again and eventually exceeds the pre-irradiation value. For unirradiated samples given the same annealing treatment, no decrease in resistivity was observed for the Ni–55 wt % Cu and Ni–65 wt % Cu samples, and only a slight decrease was observed for the Ni–40 wt % Cu sample (Fig. 17.6). The decrease in resistivity upon isochronal annealing following irradiation at −180°C (Fig. 17.5) is believed to be due to enhanced segregation of the nickel and copper which takes place when the radiation-produced defects become mobile.

Since the largest decrease in resistivity was observed for the Ni–40 wt % Cu alloy (Fig. 17.5), this composition was selected for further study. Figure 17.7 shows the isochronal annealing curve for Ni–40 wt % Cu upon increasing the temperature to 580°C and then decreasing the temperature to 250°C. We note that, upon decreasing the temperature, the original resistivity is recovered at about 350°C. This indicates that the freezing-in temperature, below which no change in the state of segregation takes place upon cooling in the unirradiated alloy, is about 350°C. At temperatures above 350°C the vacancies in thermal equilibrium are in sufficient concentration to produce the equilibrium state of segregation in reasonable times.

For the quenching experiments, a sample was suspended in a vertical vacuum furnace at the desired quenching temperature and then dropped into a vessel of diffusion pump oil contained at room temperature within the vacuum system. Figure 17.8 shows the isochronal annealing curves for Ni–40 wt % Cu samples quenched from 600, 850, and 1050°C. The curves for a slow-cooled sample and a sample irradiated at −180°C are also shown for comparison. The excess resistivity (about 2 microhm-cm) retained upon quenching is attributed to the quenching-in of the more random state characteristic of the higher temperatures. As can be seen in Fig. 17.8, an increase in the quenching temperature in the range 600 to 1050°C produces a decrease in the quenched-in resistivity. This behavior has been noted previously for Cu-Al alloys[15] and is presumably due to greater defect mobility during the quench for the higher quenching temperatures. In the isochronal annealing curves the decrease in resistivity for the quenched samples (Fig. 17.8) starts at a higher temperature

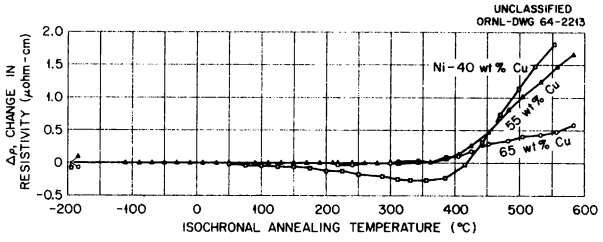

Fig. 17.6. Change in Resistivity upon Isochronal Annealing of Slowly Cooled Cu-Ni Alloys. Measurements at −196°C.

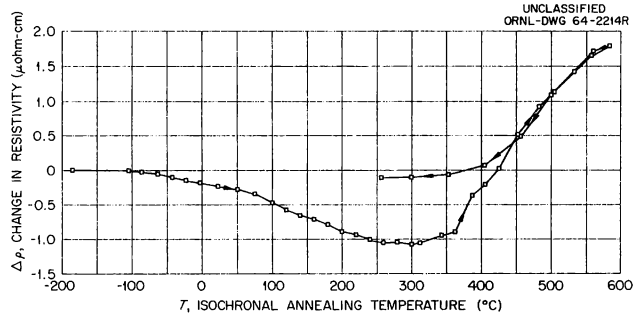

Fig. 17.7. Change in Resistivity upon Isochronal Annealing of Ni–40 wt % Cu Previously Irradiated Three Weeks at −180°C. Measurements at −196°C.

[15] M. S. Wechsler and R. H. Kernohan, *Acta Met.* 7, 599 (1959).

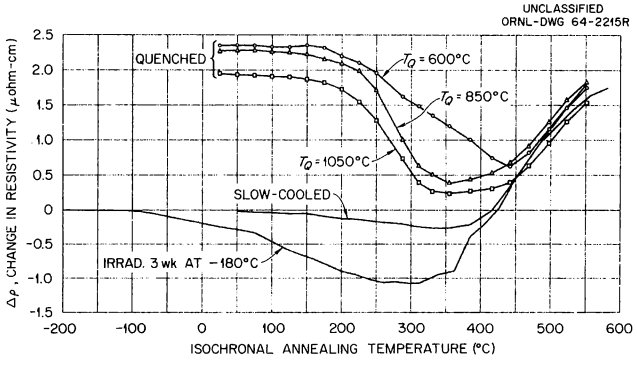

Fig. 17.8. Change in Resistivity upon Isochronal Annealing of Ni–40 wt % Cu Following Quenching from 600, 850, and 1050°C. Curves for a sample irradiated at −180°C and a slow-cooled sample are also shown for comparison. Measurements at −196°C.

(about 150°C) than for the irradiated sample (about −100°C). This is an indication that the defect whose motion produces the segregation after quenching is not the same one responsible for the segregation after low-temperature irradiation.

In another experiment on Ni–40 wt % Cu, the combined effects of quenching and irradiation were studied. A sample was quenched from 600°C and then irradiated for three weeks at −180°C. The resulting isochronal annealing curve is shown in Fig. 17.9, where the curves from previous figures are also shown for comparison. The annealing behavior in the lower range of temperatures (−100 to 200°C) is very similar to that for the sample that was only irradiated. This suggests that segregation occurs in the quenched-plus-irradiated sample in this temperature range by the same mechanism as in the sample that was only irradiated. If this mechanism were interstitialcy diffusion due to radiation-produced interstitials, it is difficult to understand why the interstitials in the quenched-plus-irradiated sample did not recombine with the vacancies quenched from 600°C and thereby cause a different annealing behavior than for the irradiated-only sample. It may be that the segregation in irradiated samples is due to enhanced nucleation of the segregation process at damage clusters produced by the irradiation. In this case, quenched vacancies would have little effect. This idea will be tested by doing low-temperature electron irradiations, where no damage clusters are created.

Finally, in Fig. 17.10 the isochronal annealing curve for a sample cold worked below −100°C is compared with the previous curves. For the deformation, a 0.016-in. foil of Ni–40 wt % Cu was cooled in liquid nitrogen, passed through a rolling mill whose rolls had been cooled with dry ice, and immediately immersed again in liquid nitrogen. Several such passes were made until the final thickness was 0.008 in. Then a resistivity sample was cut from the foil while it was immersed in liquid nitrogen. The resulting isochronal annealing curve (Fig. 17.10) is quite broad and complicated, and no analysis of it is attempted at this time.

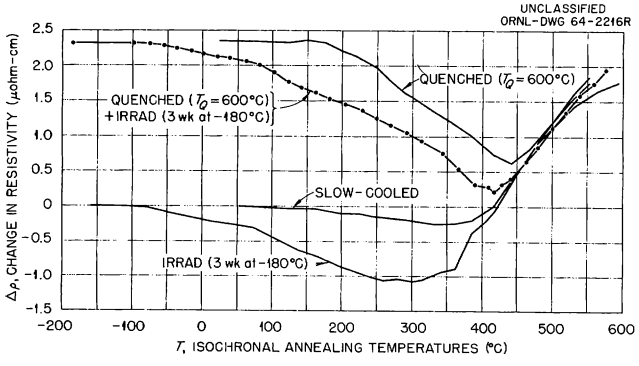

Fig. 17.9. Change in Resistivity upon Isochronal Annealing of Ni–40 wt % Cu Following Quenching from 600°C and Irradiation at −180°C. Curves following other treatments are shown for comparison. Measurements at −196°C.

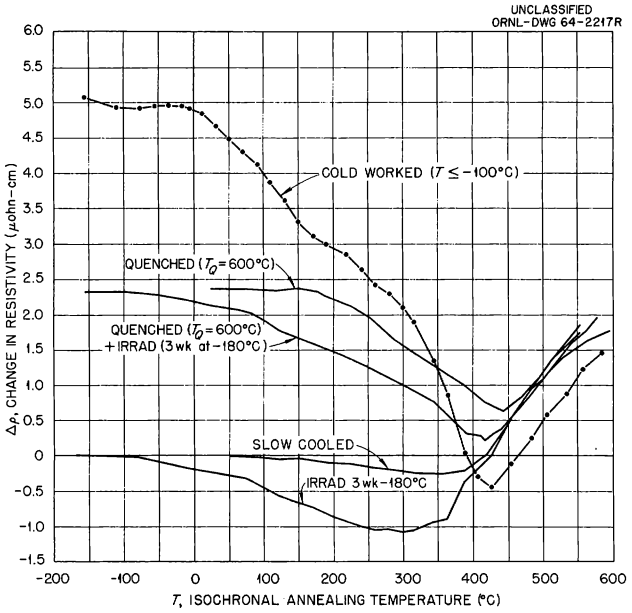

Fig. 17.10. Change in Resistivity upon Isochronal Annealing Following Various Cold-Working, Quenching, and Irradiation Treatments for Ni–40 wt % Cu. Measurements at −196°C.

RESISTIVITY MEASUREMENTS IN Fe–3.7 wt % Si

(77 to 1325°K; quenching; E)

J. M. Williams M. S. Wechsler

The common feature of the Cu-Al and Cu-Ni work described above is that the irradiation accelerates the rate at which the alloys can be equilibrated at lower temperatures. It is a matter of both fundamental and practical interest to determine whether or not such effects take place in

body-centered cubic metals, particularly iron and its alloys. Accordingly, a study of dilute Fe-Si alloys has been undertaken. The studies made thus far consist of laboratory resistivity measurements in preparation for irradiation experiments. Measurements of the resistivity as a function of temperature from −196 to 1050°C have been made for an Fe–3.7 wt % Si alloy. Also, the change in resistivity upon quenching from temperatures up to 850°C has been investigated.

A number of resistivity samples with 1-in. gage lengths were cut from a 0.008-in.-thick foil of Fe–3.7 wt % Si. The samples were annealed 2 hr at 1000°C and cooled at 50°C/hr to 400°C followed by a 25°C/hr cool to room temperature.

For the at-temperature measurements, a sample was mounted in a Lavite holder with thermocouples spot-welded to the ends of the sample just outside the potential probes. The resistance was first measured at liquid nitrogen temperature. Then the sample was placed in a vacuum furnace, and the resistivity was measured as a function of temperature up to 850°C (run A, Fig. 17.11). At this point, the temperature controller failed, and the sample was cooled to room temperature. After the controller was repaired, a new curve was obtained, which extended to 1050°C (run B, Fig. 17.11). The two curves showed roughly the same behavior, but they did not superimpose. Some earlier results for iron[16,17] are also shown in Fig. 17.11.

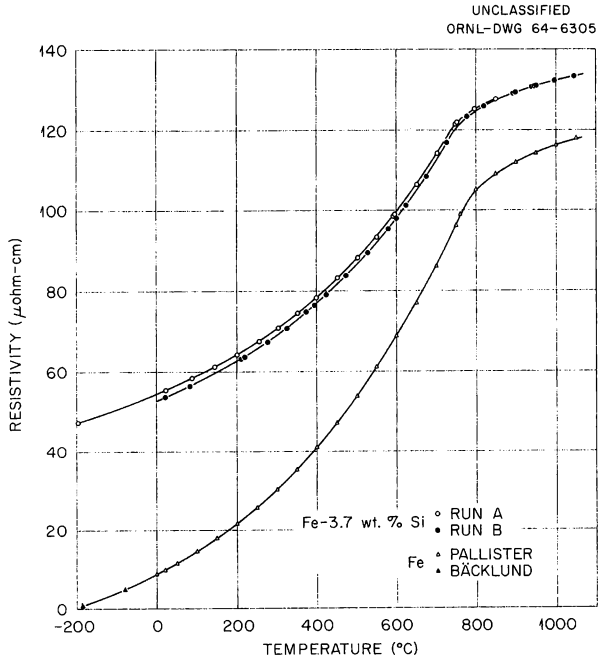

Fig. 17.11. Resistivity as a Function of Temperature for Fe and Fe–3.7 wt % Si.

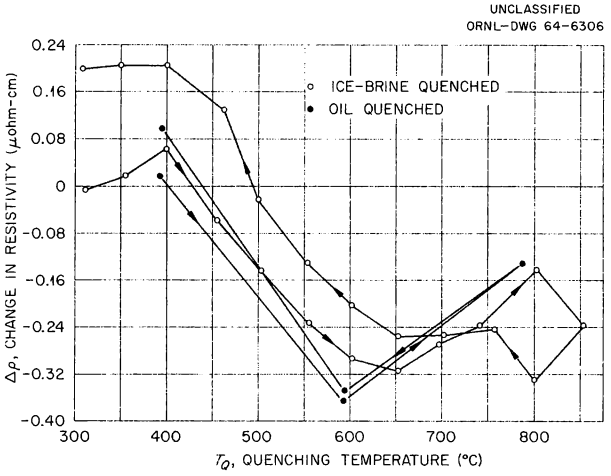

Fig. 17.12. Change in Resistivity vs Quenching Temperature for Fe–3.7 wt % Si. Measurements at −196°C.

For the quenching experiments, the samples were suspended in a vertical vacuum furnace for 1 hr at the quenching temperature. Two quenching media were used, iced brine and diffusion pump oil. For the quenches into iced brine, the vacuum chamber was filled with helium, the bottom of the vacuum tube was opened, and the sample was dropped into a container filled with iced brine. For the quenches into diffusion pump oil, the oil was contained within the vacuum chamber, and the sample was quenched without interrupting the vacuum.

The results of the quenching experiments are shown in Fig. 17.12. The results of the iced-brine quenches were less reproducible than those for the oil quenches, as can be seen by the erratic behavior near 800°C and the lack of reversibility upon reducing the quenching temperature. The higher resistivity values upon decreasing the temperature are attributed to a coating of oxide, which was more severe for the iced-brine quenches than for the oil quenches. However, for both types of

[16] P. R. Pallister, *J. Iron Steel Inst. (London)* **161**, 87 (1949).

[17] N. G. Bäcklund, *J. Phys. Chem. Solids* **20**, 1 (1961).

quenches there is a decided decrease in the resistivity upon quenching from above 400°C, which suggests a rearrangement of the iron and silicon atoms. Experiments will be performed to see if this rearrangement is enhanced by irradiation.

IN-REACTOR INTERNAL FRICTION MEASUREMENTS OF INTERSTITIAL REARRANGEMENTS IN BCC METALS

(Fe–0.015 wt % N; V; neutrons > 1 Mev; E)

J. T. Stanley W. E. Brundage

Recent research has stressed the critical importance of interstitial impurities in the body-centered cubic metals. In particular, the concentration and distribution of nitrogen in pressure-vessel steels are thought to have a significant effect on the mechanical properties of these alloys. For example, it has been pointed out[18,19] that the creep resistance of steels is markedly affected by the concentration of nitrogen in solid solution; the higher the nitrogen concentration in solid solution, the better the creep resistance. Furthermore, the poorer creep resistance of aluminum-killed steels as compared to silicon-killed steels may be associated with the reduction in the nitrogen in solid solution due to the formation of aluminum nitride. In certain reactor applications this factor may be important in connection with reactor pressure vessels, since the better notch ductility of the aluminum-killed steels is offset by the poorer creep resistance. The nitrogen in steel may also be responsible for the different effects of irradiation on the aluminum- and silicon-killed steels. For example, Nichols and Harries[20] have found that the increase in yield stress upon irradiation reaches a peak as a function of irradiation temperature for the aluminum-killed but not for the silicon-killed steels. It has been suggested[21] that the dependence on irradiation temperature is possibly due to free vacancies produced by the irradiation. More free vacancies are perhaps present in the aluminum-killed steels because the nitrogen is tied to aluminum as aluminum nitride and therefore is not available for trapping vacancies.

The study of the effect of neutron irradiation on the precipitation of carbon in alpha iron[22] has indicated that the loss of carbon from solid solution after solution annealing and quenching is accelerated by the irradiation. Two mechanisms are suggested for the enhanced loss of carbon from solid solution. Upon warm-up after low-temperature irradiation during which the radiation-produced defects do not anneal out, the carbon atoms are thought to be trapped by the vacancies produced by the radiation. However, when the irradiation is carried out at ambient temperature (about 60°C), the accelerated loss of carbon is believed to occur as a result of nucleation sites for precipitation provided by the radiation-produced damage clusters.

The above discussion emphasizes the importance of studying the effect of radiation on the arrangement of nitrogen in iron and steel. Perhaps one of the most effective ways to study the rearrangement of interstitial impurities in body-centered metals is by internal friction measurements of the Snoek anelastic relaxation peak, which yield information concerning the amount of the interstitial impurity in solid solution and its mobility. For this reason, a flexure pendulum apparatus was developed (described in a previous report[23]) that enables such measurements to be made during reactor irradiation. The present report presents some results of irradiation of iron-nitrogen alloys that were obtained with the use of the in-reactor flexure pendulum. In addition, torsion pendulum measurements on vanadium-nitrogen-oxygen alloys made in the laboratory following irradiation are reported.

---

[18] J. M. Robertson and R. W. Nichols, "High-Temperature Mechanical Properties of Steels Used in Gas-Cooled Reactor Pressure Vessels," p. 14 in *Steels for Reactor Pressure Circuits*, Special Report No. 69, The Iron and Steel Institute, London, 1961.

[19] J. Glen and J. D. Murray, "Metallurgical Aspects of Creep in Carbon- and Low-Alloy Steels," p. 40 in *Steels for Reactor Pressure Circuits*, Special Report No. 69, The Iron and Steel Institute, London, 1961.

[20] R. W. Nichols and D. R. Harries, "Brittle Fracture in Irradiation Effects in Ferritic Pressure Vessel Steels," p. 162 in *Radiation Effects on Metals and Neutron Dosimetry*, ASTM-STP-341, American Society for Testing and Materials, Philadelphia, 1962.

[21] S. F. Pugh, "Radiation Damage in Alloys," *Proceedings of the International Summer School on Solid State Physics, Mol, Belgium, August 1963*, to be published.

[22] H. Wagenblast and A. C. Damask, *J. Phys. Chem. Solids* **23**, 221 (1962).

[23] J. T. Stanley, *Quarterly Progress Report: Irradiation Effects on Reactor Structural Materials*, HW-76635, p. 10.1 (Feb. 15, 1963).

Aging of the Nitrogen Peak in Iron-Nitrogen Alloy

Specimens were cut from 0.005-in.-thick Ferrovac E foil which had been cold rolled from $1\frac{1}{2}$-in.-diam bar. The specimens were decarburized by heating in moist hydrogen at 720°C for 72 hr. The decarburized specimens were then heated to 950°C for 1 hr in a dry hydrogen atmosphere and slow cooled (100°C/hr) to 590°C to obtain a large grain size. The specimens were nitrided at 590°C with a mixture in an atmosphere of ammonia and hydrogen gas. The gas mixture was adjusted to produce a nitrogen content of about 0.015 wt % nitrogen. The nitrided specimens were quenched in water from 590°C to retain the nitrogen in solid solution.

The apparatus used for these experiments was designed to fit into the low-temperature irradiation facility in Hole 50 of the ORNL Graphite Reactor. The method of measuring internal friction was the same as the one previously described,[23] but the apparatus was more compact, allowing rapid heating and cooling. The size of the apparatus can be judged from Fig. 17.13, which is approximately to scale. The diameter of the tube which carries the heater and solenoid winding is $\frac{5}{16}$ in. The drawing shows only half of the apparatus which holds two specimens, back to back. The capsule was about 8 in. long.

With this apparatus the specimen could be cooled rapidly enough to retain nitrogen in solution after annealing at 400°C. This treatment will be referred to as a re-solution anneal, as it restores the original nitrogen internal friction peak after an aging treatment at some lower temperature. The re-solution anneal is carried out by heating the specimen to 400°C *in vacuo* and then cooling rapidly by simultaneously turning off the heater current and admitting helium gas into the chamber.

Out-of-reactor experiments in a mockup of the reactor facility showed that essentially all of the nitrogen could be retained in solution if the specimen cooled from 400 to 50°C in about 6 min. To achieve this cooling rate in the mockup, it was necessary to cool the chamber walls with dry ice. In the low-temperature irradiation facility the chamber walls were kept cool by the flow of cold helium gas through the heat exchanger.

Even though the specimen is cooled fast enough to retain all of the nitrogen in solution as detected by the internal friction peak, it is still possible for there to be differences in the number of nucleation sites for precipitation for different rates of

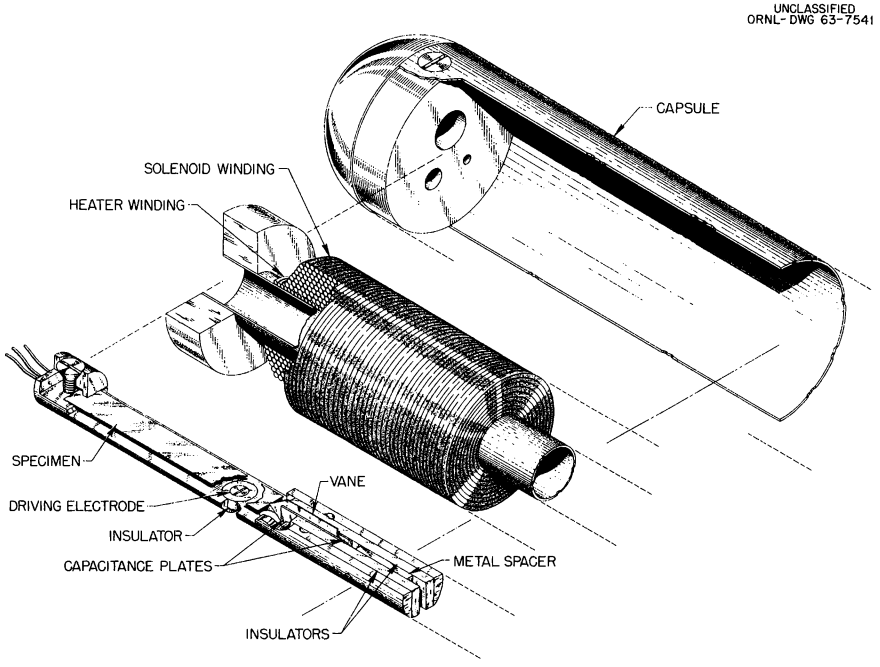

Fig. 17.13. In-Reactor Flexure Pendulum Apparatus.

cooling. However, studies of the aging of the nitrogen peak at 65°C showed little difference between the specimen water-quenched from 590°C and gas-quenched from 400°C as described above. These two sets of data are shown in Fig. 17.14, along with data for the specimen after various amounts of irradiation at low temperature.

The results presented in Fig. 17.14 represent measurements made on two specimens of about the same nitrogen content. The aging run after the 23-day irradiation was made on one specimen (specimen A), and the rest of the aging runs were for another specimen (specimen B).

The measurements for specimen B were made in the order listed in the caption, and, except for the initial water quench, each aging run was preceded by a 400°C re-solution anneal as described above. The results in Fig. 17.14 show that irradiation does increase the rate of nitrogen precipitation and that the 400°C re-solution anneal removes most of the effect of the irradiation.

A comparison of the aging runs made after the 23-day irradiation and the 3-day irradiation shows that the time for half completion of the reaction is about the same in both cases, but that aging is somewhat faster in the early stages of precipitation for the 23-day irradiation and slower in the later stages. A possible explanation of this effect might be based on trapping of nitrogen atoms at irradiation-produced defects as proposed by Wagenblast and Damask[22] for iron-carbon alloys. Thus, after the 23-day irradiation there would be enough defects produced to remove about one-third of the nitrogen atoms by trapping. This process occurs very rapidly and accounts for the more rapid loss of nitrogen from solid solution in the early stages. The slower precipitation in the later stages would be explained by assuming that, since the nitrogen content is lowered rapidly by trapping, the number of precipitates which grow to the critical size is reduced. However, at the present time such reasoning must be regarded as speculative since in such a complicated system there are many other possible explanations.

Breakup of Precipitates by Irradiation

The present concepts of neutron damage in metals indicate that each primary collision of a

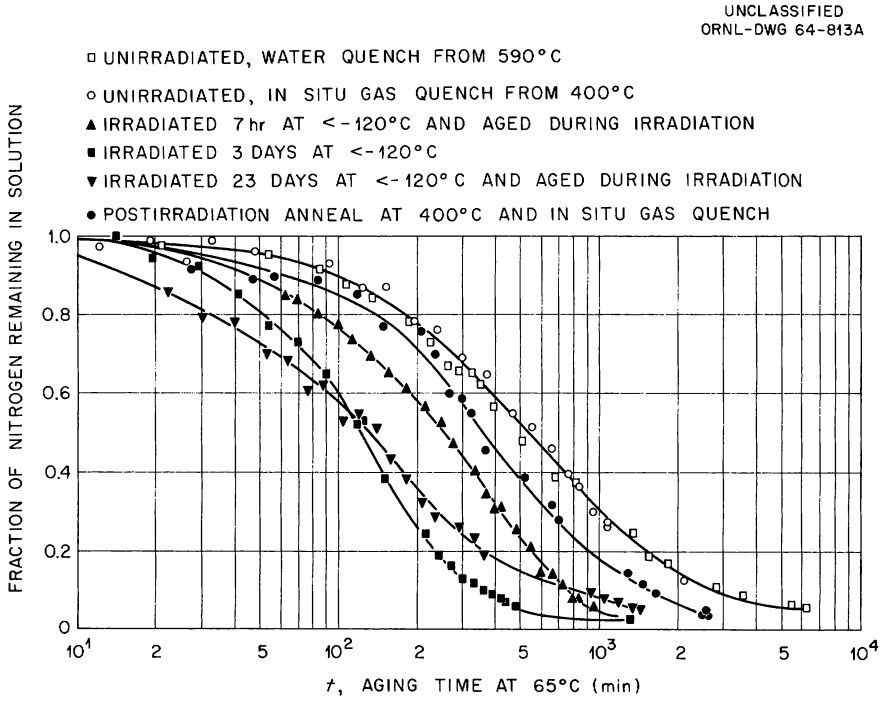

Fig. 17.14. Fractional Change in the Nitrogen Peak Height vs Aging Time at 65°C for Fe–0.015 wt % N.

fast neutron with a metal atom produces a region of intense damage approximately 100 A in diameter. If this damaged region encompasses a precipitate particle, it is likely that the particle will be redissolved in the lattice and may then reprecipitate as a number of smaller particles. Such a redistribution of precipitate would have a marked effect on the mechanical properties of the material. Experimentally, it is difficult to separate such effects from others that occur during irradiation. However, Piercy[24] has shown that precipitate particles in Cu-Co alloys are broken up by neutron irradiation and then are reprecipitated as smaller particles. In the Cu-Co alloys a measure of the size of the precipitate particles can be obtained from magnetic susceptibility measurements. Such techniques are applicable to only a few alloys. It would be possible to obtain some information about the breakup of nitride precipitates in iron if an increase in the nitrogen in solution were detected during irradiation. The in-reactor internal friction apparatus is particularly well suited for such an experiment. However, rough calculations, based on our present ideas about the size of the damage region produced by a primary displacement event and a guess about the rate of precipitation of the nitrogen in the damaged region, show that the level of nitrogen solubility produced by this mechanism will probably be too small to be observed. Nevertheless, breakup of precipitate was put forth as a possible explanation for some effects observed in an earlier experiment.[23]

An experiment has been carried out on an iron-nitrogen specimen to see if breakup of precipitates can be observed as a change in the amount of nitrogen in solution during irradiation. The specimen contained about 0.03 wt % N and was aged out of the reactor at 65°C for about 120 hr. Figure 17.15 shows that the nitrogen internal friction peak decreased to about 0.0015 after 20 hr and remained constant thereafter. Irradiation did not change the height of the internal friction peak, and therefore it is concluded that the amount of nitrogen in solution remained constant. This experiment shows that breakup of precipitate particles by irradiation did not occur at a rate great enough to explain the results of an earlier experiment, and therefore those results are probably due to a particle-size effect.

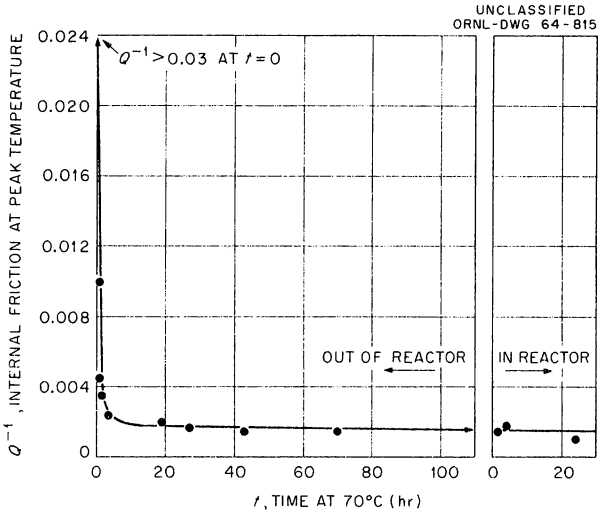

Fig. 17.15. Effect of Irradiation on a Fully Aged Sample. Out-of-reactor aging followed by in-reactor aging at 70°C of a sample of Fe–0.03 wt % N. Vibration frequency, 48 cps.

Irradiation of Vanadium

The trapping of interstitial impurity atoms in bcc metals by vacancies may be an important factor in the response of these metals to irradiation. Some examples have been mentioned above. As we have seen, the study of this process in iron is complicated by the low solubility of the interstitials at low temperatures. In contrast, the solubility of the interstitial impurities, nitrogen and oxygen, in vanadium is high; and large Snoek-type internal friction peaks occur in vanadium. An investigation has been made of the effect of irradiation on the oxygen and nitrogen peaks in vanadium in an effort to observe the trapping of these interstitials by vacancies.

The internal friction of a vanadium specimen (obtained from A. D. Mackay, Inc.) was measured in a torsion pendulum from room temperature to 320°C. The results are shown in Fig. 17.16. The two internal friction peaks were identified as due to oxygen and nitrogen, according to the work of Powers and Doyle.[25] Since the oxygen and nitrogen contents are below their respective solubility limits, there is no precipitation of

[24]G. R. Piercy, *J. Phys. Chem. Solids* **23**, 463 (1962).

[25]R. W. Powers and Margaret V. Doyle, *J. Appl. Phys.* **30**, 514 (1959).

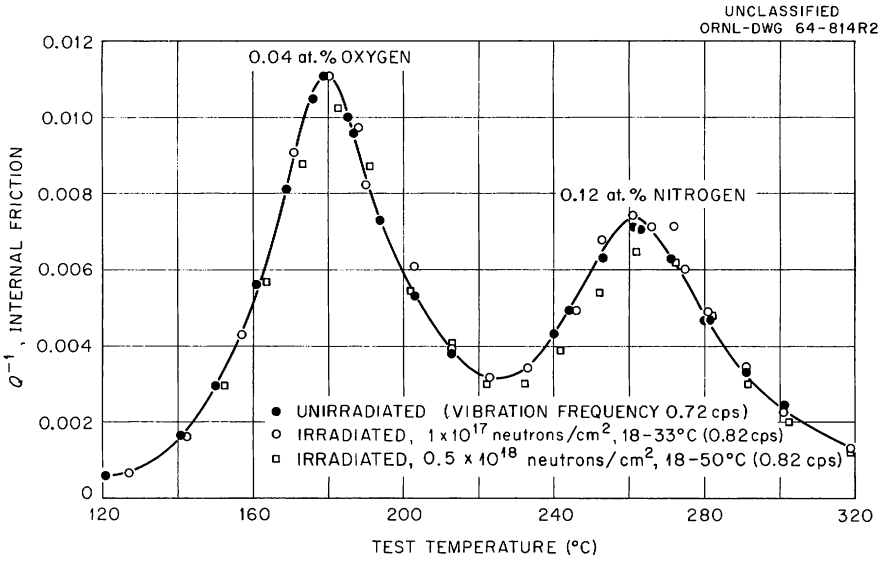

Fig. 17.16. Internal Friction of Vanadium Tested in a Torsion Pendulum After Irradiation in the Bulk Shielding Reactor. Neutron doses for neutrons with energy above 1 Mev.

oxides or nitrides. The specimen was removed from the torsion pendulum and irradiated at the face of the BSR for $12\frac{1}{2}$ hr. The fast-neutron flux in this position is 3×10^{12} neutrons cm^{-2} sec^{-1} (>1 Mev), and the dose in this irradiation was 1×10^{17} neutrons/cm^2. During the irradiation, the pool water temperature rose from 18 to 33°C. The specimen was held at room temperature for ten days and was then placed in the torsion pendulum for measurement. The results of the internal friction measurements after the irradiation are shown in Fig. 17.16. No change in either the oxygen or nitrogen peak was observed. The same specimen was again irradiated in the BSR for 51 hr, receiving an additional dose of 0.5×10^{18} neutrons/cm^2. The internal friction measurements were repeated and are shown in Fig. 17.16. After this irradiation, the oxygen peak had decreased by about 5%, and the nitrogen peak had decreased about 10%.

A rough calculation of the vacancy concentration produced by a 51-hr irradiation at the face of the BSR gives 0.2 at. %, assuming no annihilation of vacancies during irradiation. If the 10% decrease in the height of the nitrogen peak were due to trapping of nitrogen by radiation-produced vacancies, it would be possible to estimate the binding energy between the nitrogen atom and the vacancy. On the basis of the law of mass action, the atomic concentration of the nitrogen vacancy pairs is given by

$$N_{NV} = N_N N_V \exp(E_b/kT),$$

where N_{NV}, N_N, and N_V are the concentrations of the nitrogen-vacancy pairs, free nitrogen atoms, and free vacancies, respectively, and E_b is the nitrogen-vacancy binding energy. Then substituting $N_{NV}/N_N = 0.1$, $N_V = 0.002$, and $T = 535$°K (262°C), we find that $E_b = 4000$ cal/mole. This value of the binding energy is less than half of the binding energy of carbon atoms to vacancies in iron, 9200 cal/mole, as determined by Arndt and Damask.[26] In the above, no account has been taken of vacancy binding to oxygen atoms. Also, the calculation of the vacancy concentration is quite approximate. However, we may conclude that the binding energy between vacancies and interstitial impurities may not be insignificantly small in vanadium.

[26]R. A. Arndt and A. C. Damask, *Acta Met.* 12, 341 (1964).

FISSION-SPECTRUM IRRADIATION FACILITY FOR THE BSR

(E)

W. E. Brundage

Accurate evaluations of the results of radiation experiments often require that the intensity and the energy distribution of the incident neutrons be well known. Experiments needing relatively high flux of high-energy neutrons generally must be performed in a reactor where the flux level and spectrum are subject to variations due to such factors as reactor control-rod motion and changes in core loading or adjacent experiments. Unless these factors can be adequately controlled, a continual flux-monitoring program must be carried out.

One method of overcoming these difficulties is to irradiate in a region surrounded by a source of fission neutrons since the fission spectrum is well known. A design study demonstrating the feasibility of such a facility for use in the BSR has been completed. Once preliminary flux calibration is performed, it is expected that the neutron spectrum will not change with time. Also, over long periods of time, the intensity will be proportional to the flux of thermal neutrons at the outer surface of the fission source, which may be measured with relative ease and accuracy.

The facility, shown schematically in Fig. 17.17, is similar in geometry to a lower-power (500 w) converter also proposed[27] for the BSR. Neutrons from one face of the reactor will thermalize by passing through D_2O and will be absorbed in a tubular "neutron-converter" element containing ^{235}U. Samples, placed inside the tube, will be irradiated with the high-energy neutrons from the fissioning ^{235}U.

The proportion of partially moderated neutrons reflected back into the sample chamber will be reduced by having a minimum amount of moderating material in the vicinity of the converter.

The converter tube, 3 in. in inside diameter and 12 in. long, will contain about 300 g of 93%-enriched ^{235}U in the form of an aluminum-uranium alloy. This alloy will be clad with aluminum, and the inside of the tube will be lined with cadmium.

[27] R. R. Coltman *et al.*, *Solid State Div. Ann. Progr. Rept. May 31, 1963*, ORNL-3480, p. 57.

In order to achieve sufficiently high fission flux, 15 kw of heat will be generated in the converter tube. No satisfactory system for removing this power could be found without introducing some moderator into the "unmoderated region." By optimizing flow conditions,[28] it was found that the heat could be removed with water flowing through small square channels outside the converter tube. Figure 17.18 represents a horizontal

[28] The heat flow calculations were performed by G. H. Llewellyn of the Design Engineering Dept.

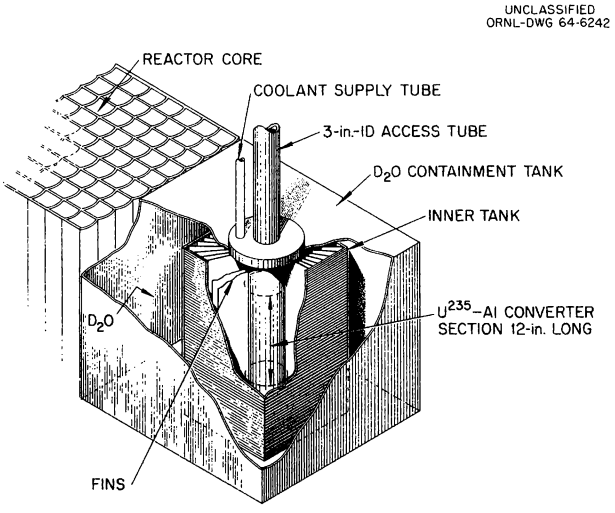

Fig. 17.17. Fission-Spectrum Irradiation Facility.

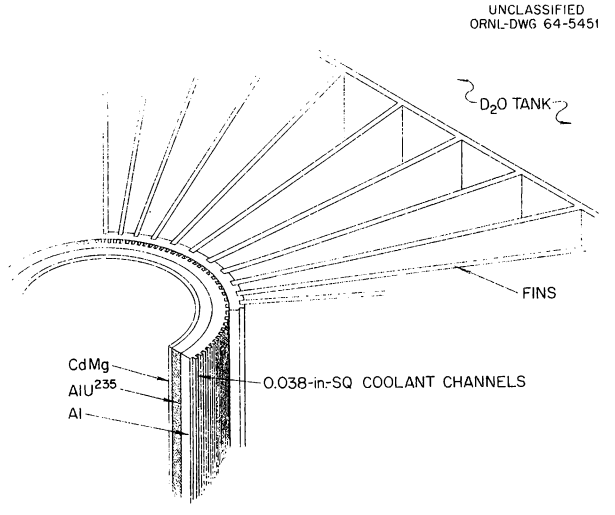

Fig. 17.18. Section Through Converter Tube.

section through the facility. It can be seen that only half of the circumference of the tube is used for the coolant. The remaining portion acts as an alternate path for heat removal in case the coolant flow fails. In that event, the heat would be conducted to the outer surface of the coolant tube. The radial fins serve as a conducting path to the outer surface of the facility where the heat can be dissipated to the surrounding D_2O and water. This safety path will prevent the converter tube from exceeding a safe temperature without coolant flow, even with a power generation rate over double that of the design value.

The possible hazards associated with operation of the facility are being evaluated, and it appears that the system is inherently safe for any credible accident involving criticality, coolant failure, or a reactor excursion.

It is expected that the facility will provide a region for sample irradiation 3 in. in diameter and 6 in. long with a uniform flux of 8×10^{11} cm^{-2} sec^{-1} in the fission spectrum. The temperature of the wall of the sample chamber will be below 60°C if the pool water is used for heat removal; the addition of a chilling system would permit this temperature to be reduced to 25°C.

Some neutrons reflected back from the moderator (moderated feedback) will also be present. Computer calculations,[29] which were based on an infinite-length cylinder with the same cross section as the facility, show that the increase in atomic displacements in the irradiated samples caused by the moderated feedback will be less than 7%.

PLASTIC DEFORMATION OF IRON AND ITS ALLOYS

(Fe-Si alloys; Fe; etch pits; electron microscopy; E)

S. M. Ohr

With the development of direct methods of observing lattice defects with the light and electron microscopes, the plastic properties of metals and alloys have been successfully studied in terms of the behavior of these lattice defects. The purpose of this program is the application of these direct methods to the study of the effect of irradiation on the mechanism of plastic deformation in iron and its alloys.

We have initiated with both vacuum-melted high-purity iron and Fe-Si alloy samples: (1) observation of the distribution of dislocations at the surface following plastic deformation and the measurement of dislocation mobility by etch-pit techniques, (2) direct observation and crystallographic analysis of dislocations and dislocation loops in thin foils by transmission electron microscopy and electron diffraction, and (3) mechanical tests performed at various temperatures and strain rates.

Figure 17.19*a* shows an optical micrograph of etch pits at dislocations in Ferrovac E iron, while Fig. 17.19*b* shows the same specimen observed by transmission electron microscopy. The sample, 5 mils thick, was deformed 2% in tension and was polished and etched for the observation of etch pits. The sample was then thinned electrolytically to approximately 1000 A for observation by transmission electron microscopy. Figure 17.19*a* reveals low-angle dislocation boundaries, as well as dislocations introduced by deformation. Figure 17.19*b* exhibits the same features, but at higher magnification; a grain boundary, low-angle boundaries consisting of parallel rows of dislocations, and complex tangles of dislocations and dislocation loops are shown.

The observations of plastic properties will be repeated on irradiated samples, and any changes in structure and in parameters that characterize yielding and deformation will be investigated. The nature of dislocation interactions at low temperature is to be correlated with the low-temperature brittleness of these bcc metals.

CRYSTALLOGRAPHY OF DISLOCATIONS AND DISLOCATION LOOPS IN DEFORMED IRON[30]

(electron microscopy; E/T)

S. M. Ohr D. N. Beshers[31]

Crystallographic analyses of dislocations and dislocation loops in deformed bcc iron observed in the electron microscope have been carried out by applying the electron diffraction theory of contrast at dislocations. Dislocations in deformed

[29]The flux calculations were performed by J. R. Knight, Oak Ridge Central Data Processing Division.

[30]Abstract of paper to be published in the *Philosophical Magazine*.

[31]Columbia University, New York.

UNCLASSIFIED
PHOTO 66008

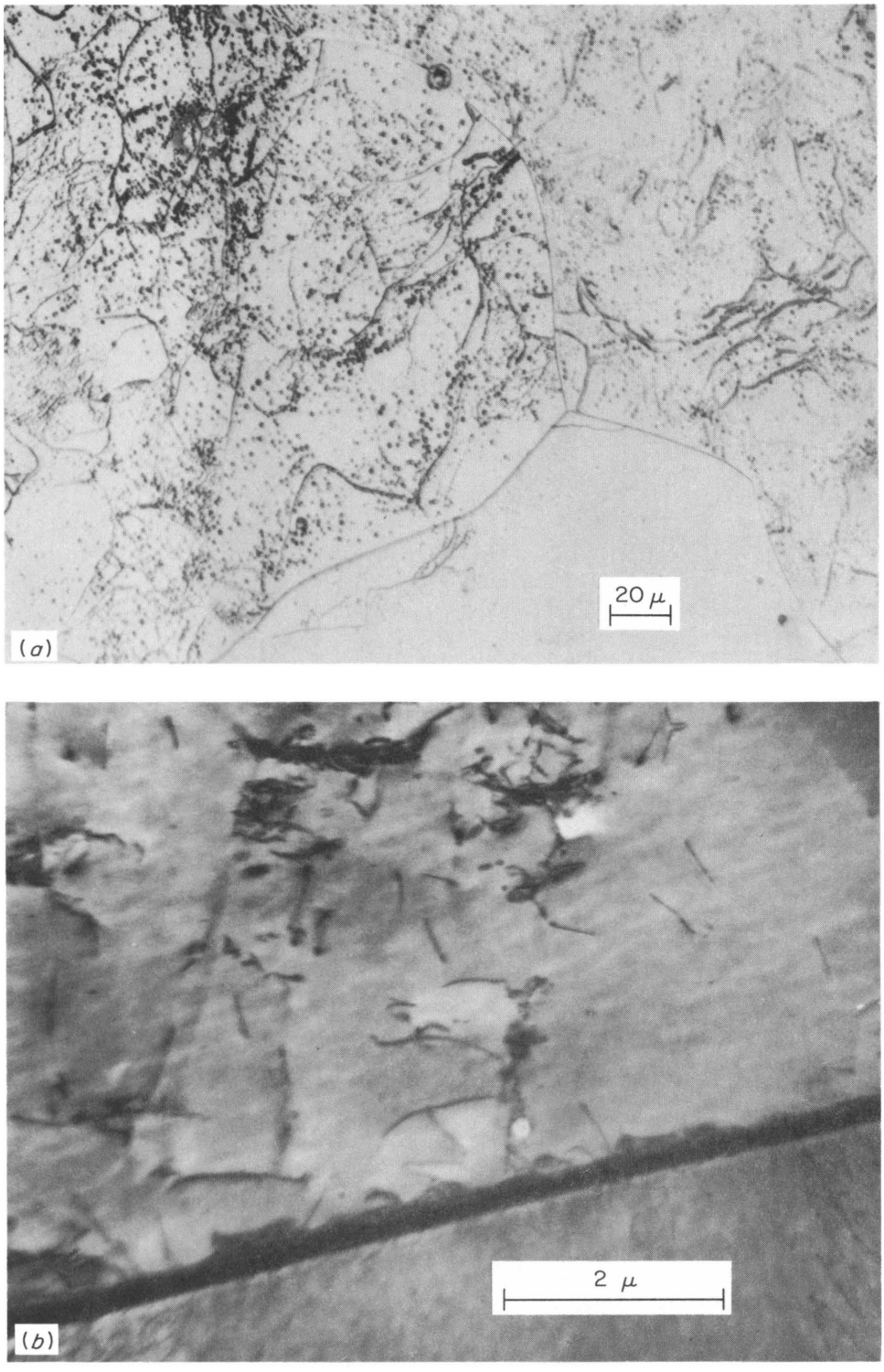

Fig. 17.19. (*a*) Optical Micrograph of Etch Pits at Dislocations; (*b*) Transmission Electron Micrograph from the Same Specimen of Ferrovac E Iron.

iron are in the form of tangles, with interspersed clusters of dislocation loops, from the very first stage of deformation. Crystallographic analyses show that the tangles consist of dislocations of two distinct Burgers vectors, in the ratio of approximately 2 to 1. The dislocations of the primary system are composed of segments of both signs, in roughly equal proportion. The Burgers vector of a majority of dislocation loops is identical to that of the primary dislocations; the rest of the loops belong to the secondary system. The loops are found to be pure edge prismatic dislocations lying in {111} planes and are identified as vacancy type. From a consideration of the elastic theory of defect interaction, it is concluded that the interactions of dislocations with dislocations of dissimilar Burgers vectors and the formation of a cluster of small loops around the dislocations and junctions are responsible for formation of dislocation tangles.

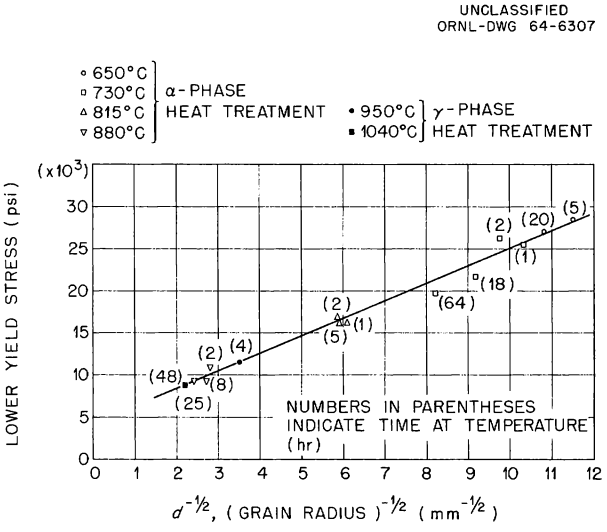

Fig. 17.20. Yield Stress vs Reciprocal Square Root Grain Radius for Ferrovac E with Various Heat Treatments. Strain rate: 0.02 min^{-1}.

IRRADIATION EFFECTS ON THE MECHANICAL PROPERTIES OF IRON AND IRON ALLOYS

(Fe; steels; yield stress; grain size; neutrons, fast or thermal; E)

N. E. Hinkle

A program is under way[32] to study the effect of irradiation on the tensile properties of iron and iron-base alloys of various grain sizes. The tensile properties are to be measured as a function of dose, dose rate, and irradiation temperature. Also, the separate effects of thermal- and fast-neutron fluxes are being investigated.

The dependence of yield stress on grain size has been measured for samples of Ferrovac E (a vacuum-melted high-purity iron) and Ferrovac 1020 steel (vacuum-melted iron alloy containing 0.2% C and 0.5% Mn). The various grain sizes are obtained by varying the times and temperatures of the prior heat treatments. The heat treatments employed and the dependence of lower yield stress on grain size are shown in Fig. 17.20 for Ferrovac E. The yield stress, σ_{YS}, is plotted vs the reciprocal square root of the grain radius, d, in accordance with the Cottrell-Petch relation,[33,34]

$$\sigma_{YS} = \sigma_0 + K_Y d^{-1/2} , \qquad (1)$$

where it is thought that σ_0 represents the lattice friction stress, and K_Y is proportional to the stress necessary to unpin a dislocation from its locking atmosphere. The data in Fig. 17.20 indicate agreement with Eq. (1) for Ferrovac E for samples heat-treated in the α phase (T <910°C) and in the γ phase (T >910°C). A typical photomicrograph showing the grain structure of a sample heat-treated in the α phase is given in Fig. 17.21. This is to be compared with the photomicrograph in Fig. 17.22 of a sample heat-treated in the γ phase. The gamma-treated sample exhibits considerable subcell formation within the grains. However, the values of yield stress as a function of grain size for the gamma-treated samples are consistent with those for the alpha-treated samples, as is seen in Fig. 17.20. It will be of interest to compare the effects of irradiation on samples given the two types of heat treatments.

For the vacuum-melted 1020 steel, subcritical heat treatments (T <723°C) produce a very fine grain structure containing spheroidized carbide particles. The yield-stress–grain-size relationship coincided with that for the Ferrovac E, indicating that the carbides have little or no effect

[32]N. E. Hinkle, *Solid State Div. Ann. Progr. Rept. May 31, 1963*, ORNL-3480, pp. 128–31.

[33]N. J. Petch, *J. Iron Steel Inst. (London)* **173**, 25 (1953).

[34]A. H. Cottrell, *Trans. Met. Soc. AIME* **212**, 192 (1958).

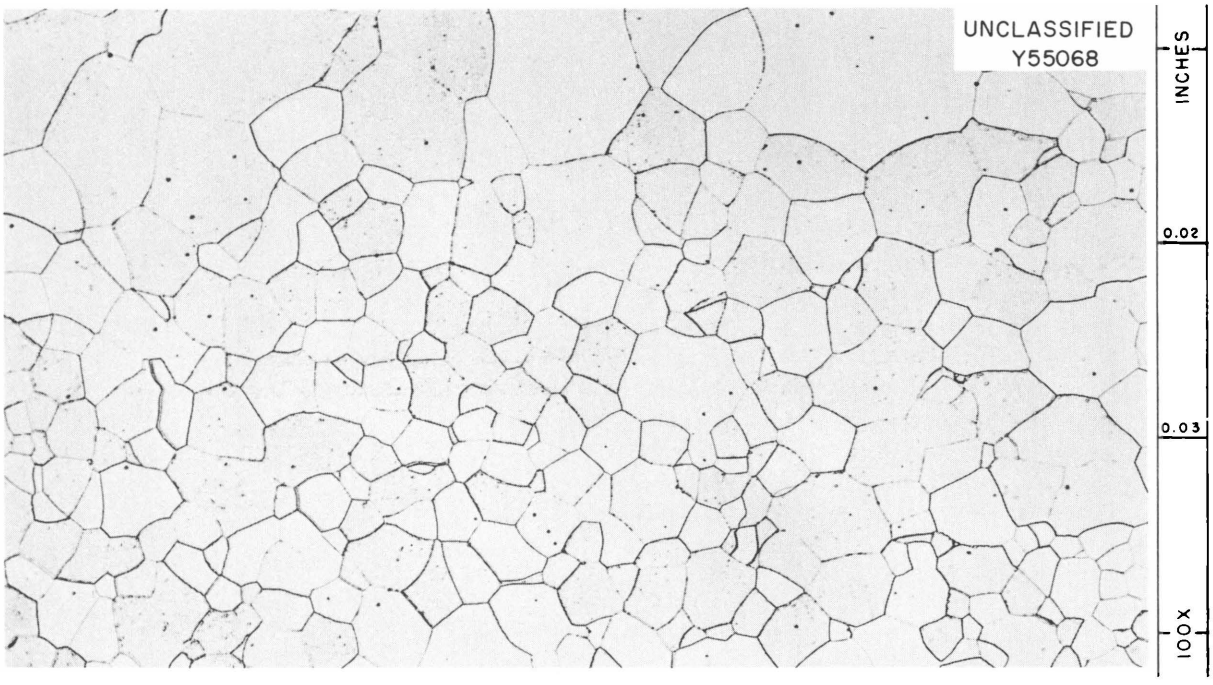

Fig. 17.21. Microstructure of Ferrovac E Heat Treated in the Alpha Phase. The sample was cold worked to about 95% reduction in area, annealed 2 hr in vacuum at 815°C, and furnace cooled. 100×.

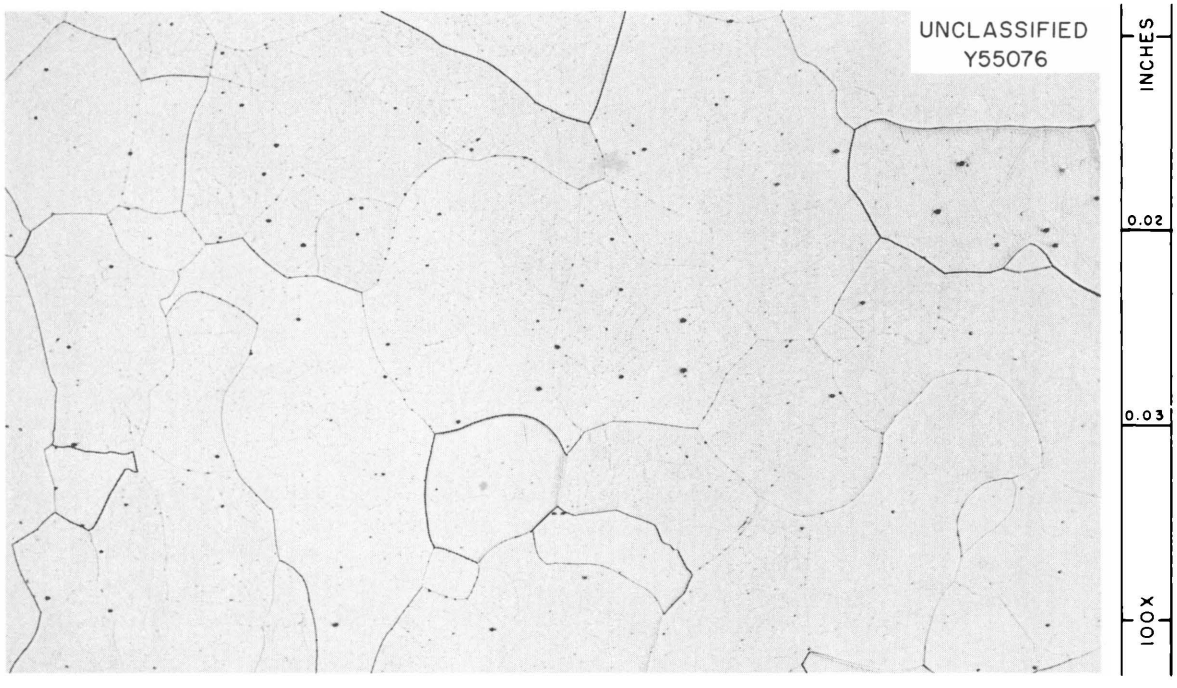

Fig. 17.22. Microstructure of Ferrovac E Heat Treated in the Gamma Phase. The sample was cold worked to about 95% reduction in area, annealed 4 hr in vacuum at 950°C, and furnace cooled. Note the subcell structure within the grains. 100×.

on the yield stress, as far as Eq. (1) is concerned. However, efforts to establish the yield-stress–grain-size relationship for the Ferrovac 1020 steel previously given supercritical heat treatments ($T > 840°C$) have thus far been unsuccessful.

The first of a series of irradiation assemblies containing iron and steel tensile specimens has been irradiated in a piggyback position of the ORR poolside facility. The tensile specimens in this assembly (ORR-56) were fabricated from Ferrovac E, Ferrovac 1020 steel, and an ASTM A-212 grade B pressure-vessel steel, each of various grain sizes. In addition, a few samples of an EGCR pressure-vessel heat of A-212B and an ASTM reference heat of A-212B were included for purposes of comparison with data of other investigations. The specimens were irradiated at 40 to 50°C and at 260°C.

As is shown in Fig. 17.23, for the low-temperature irradiation the samples were spring-loaded against a series of water-cooled tubes. For the elevated-temperature irradiations, the samples, with sheathed thermocouples attached, were placed in aluminum capsules filled with aluminum powder. The capsules were wrapped with sheathed heating elements and strapped together in a stringer arrangement as shown in Fig. 17.24. The completed irradiation assembly prior to enclosure in a welded aluminum can is shown in Fig. 17.25.

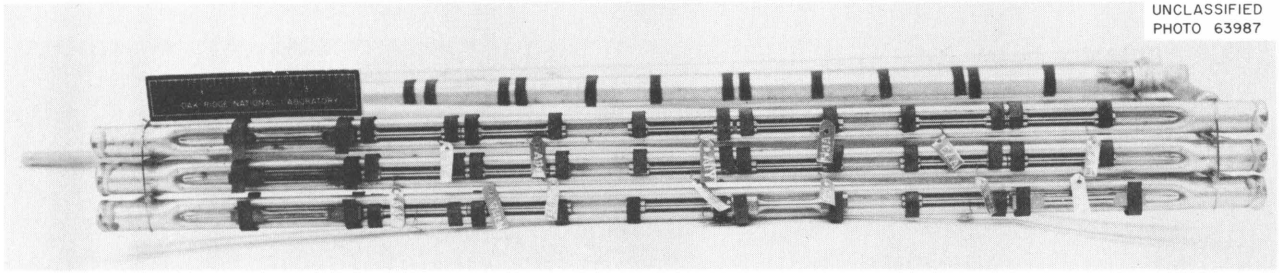

Fig. 17.23. Partial Assembly of ORR-56, Showing the Tensile Samples Spring-Mounted Against the Water-Cooled Tubes.

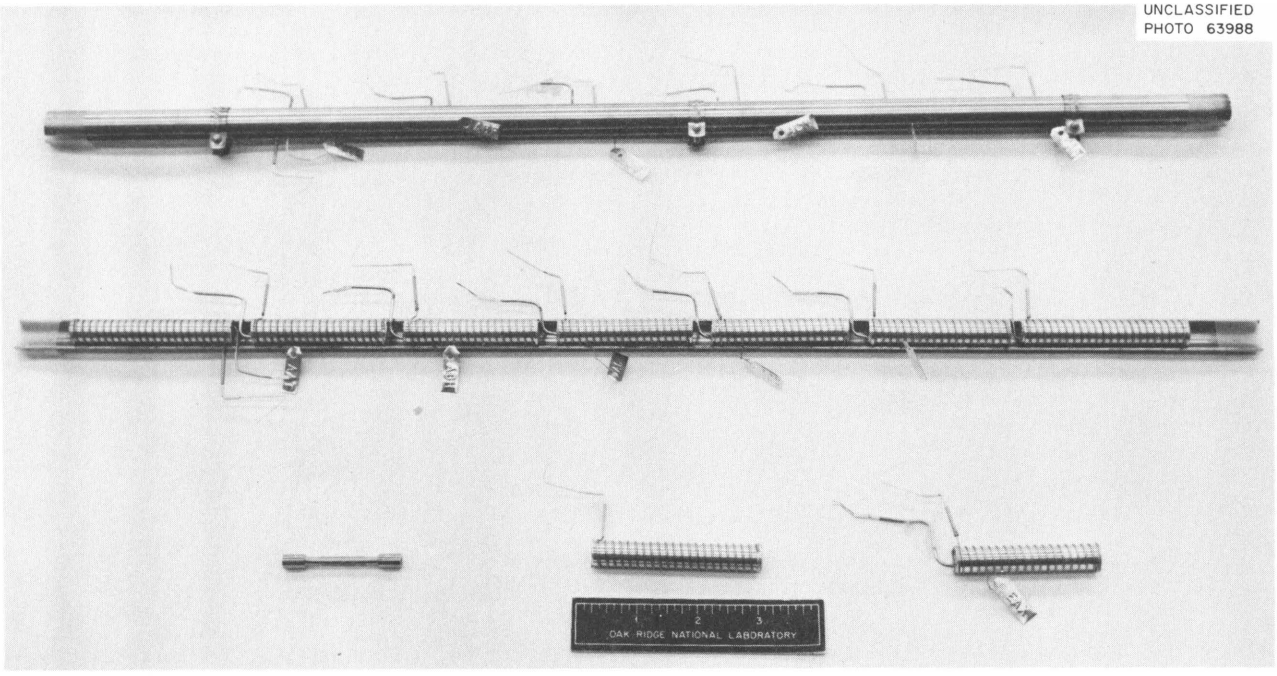

Fig. 17.24. Elevated-Temperature Capsules and Stringer Prior to Placing in ORR-56 Assembly.

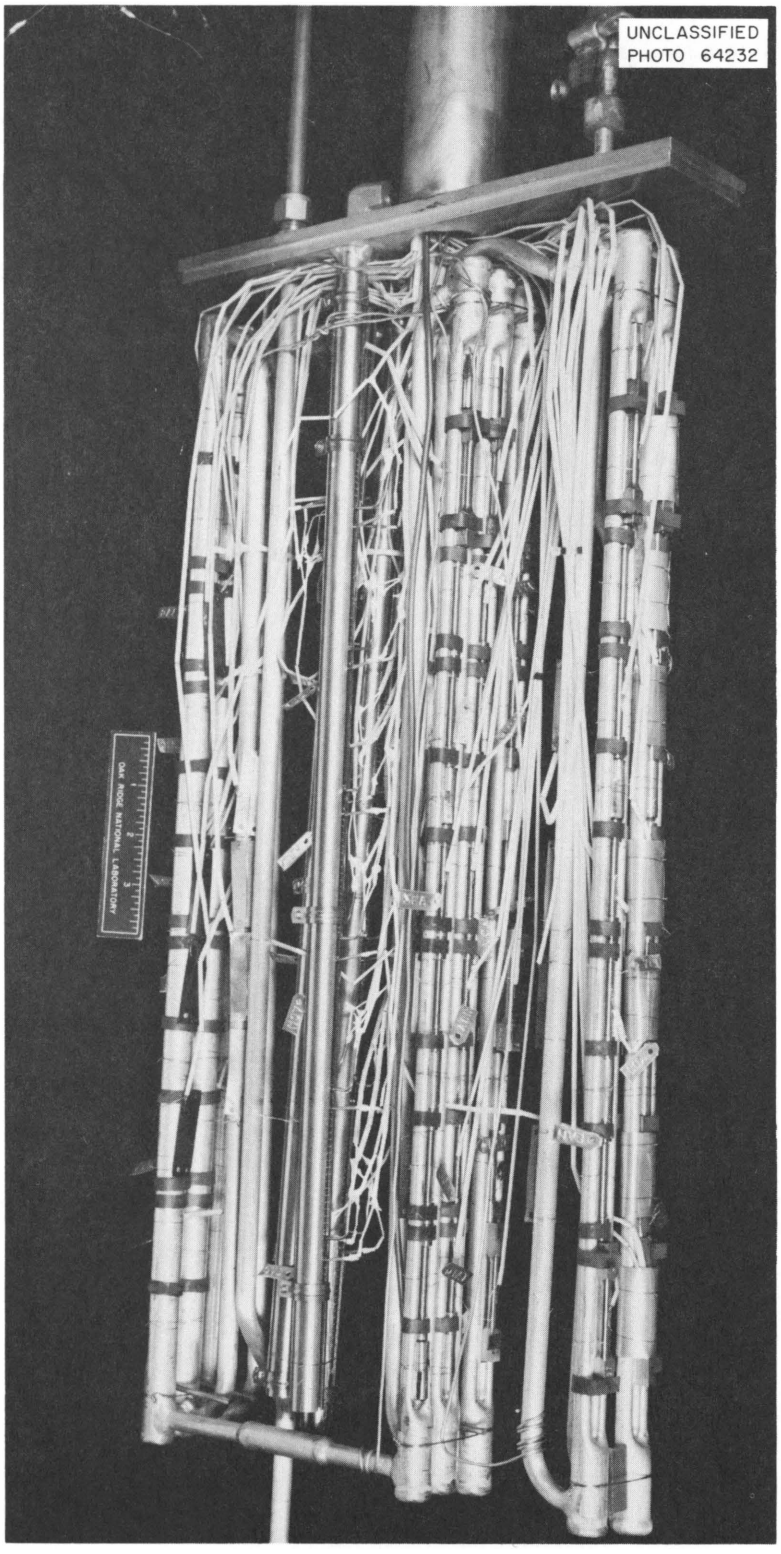

Fig. 17.25. Completed Assembly of ORR-56 Prior to Enclosure. The column of samples adjacent to the scale at the left was positioned toward the reactor face.

The in-reactor operation proved that the experiment design was satisfactory; thus future piggyback irradiation assemblies will use the same basic design. Hot-cell disassembly of the experiment has been completed, and testing of the tensile specimens will start soon.

A major objective of this work is to determine the specific influence of dose rate, in addition to the total dose. For this reason, it is especially important that careful measurements of the neutron flux be made. Experiment ORR-56 contained flux monitors of nickel, iron, and cobalt. The nickel flux monitors, cadmium-shielded, are used to determine the neutron flux greater than 2.9 Mev, assuming an effective threshold cross section of 0.39 barn for the reaction $^{58}Ni\ (n,p)\ ^{58}Co$, which corresponds to a mean fission-spectrum cross section (averaged over the entire fission spectrum) of 0.10 barn.[35] The cadmium shielding is needed to minimize the thermal-neutron burnup of the ^{58}Co isotope. Unshielded iron monitors are used to determine the neutron flux greater than 4.0 Mev, assuming an effective threshold cross section of 0.60 barn for the reaction $^{54}Fe\ (n,p)\ ^{54}Mn$. This value corresponds to 0.060 barn[35] for the mean fission-spectrum cross section. The calculations are made using the relationship

$$\phi = \frac{A}{N_0\sigma(1 - e^{-\lambda t_i})\,(e^{-\lambda t_d})}, \qquad (2)$$

where

A = activity, in disintegrations per second, of radioactive isotope per gram of monitor,

N_0 = number of atoms of reacting isotope per gram of monitor,

σ = effective threshold cross section for fast-neutron monitors or capture cross section for cobalt,

$\lambda = 0.693/T_{1/2}$ where $T_{1/2}$ is the half-life of the radioactive isotope,

t_i = irradiation time, and

t_d = decay time after reactor shutdown.

The cobalt monitors are used to determine the thermal-neutron flux by the reaction $^{59}Co\ (n_{th},\gamma)\ ^{60}Co$. The activity of unshielded cobalt monitors is due to both thermal and epithermal neutrons. Therefore, cadmium-shielded cobalt monitors are also included in order to determine the amount of activity due to epithermal neutrons. The disintegration rate of the cadmium-shielded cobalt monitors in experiment ORR-56 was less than 5% of the disintegration rate of the bare cobalt monitors. Therefore, the thermal-neutron flux with errors of less than a few percent is calculated by Eq. (2) using the disintegration rates of the bare cobalt monitors. The neutron flux for experiment ORR-56, calculated as outlined above, is shown in Fig. 17.26.

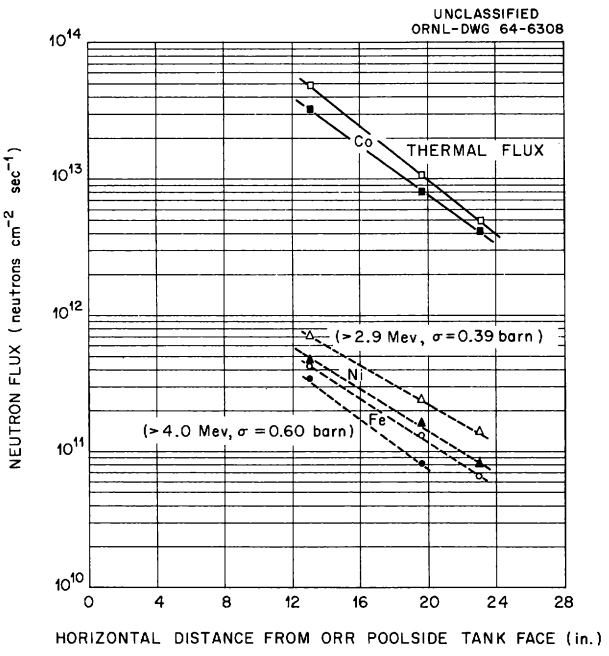

Fig. 17.26. Neutron Flux vs Horizontal Distance from ORR Poolside Tank Face for Experiment ORR-56. The curves refer to the maximum and minimum fluxes along the vertical section occupied by a column of samples.

REACTOR PRESSURE-VESSEL MATERIALS[36]

(E)

M. S. Wechsler R. G. Berggren

The characteristics of nuclear reactor pressure vessels are described, and a discussion is given of the use of prestressed concrete, stainless steel, ferritic steel, and low-alloy high-strength steel as materials of construction.

[35] T. O. Passell, "The Use of Nickel-58 and Iron-54 as Integrators of Fast-Neutron Flux," p. 501 in *Neutron Dosimetry*, vol. I, International Atomic Energy Agency, Vienna, 1963.

[36] Abstract of paper to be published in *Nuclear Safety*.

EGCR PRESSURE-VESSEL SURVEILLANCE PROGRAM

(E)

R. G. Berggren W. J. Stelzman T. N. Jones

Continuing assistance has been given the Gas-Cooled Reactor Project in the implementation of the EGCR pressure-vessel surveillance program. This program was established to monitor the ductile-brittle characteristics of the EGCR pressure vessel during service exposure to radiation. This is to be accomplished by placing notch-impact and tensile test samples adjacent to the inner wall of the pressure vessel and removing portions of the samples for testing after prescribed periods of time. The samples were machined from the same heats of ASTM A-212 grade B steel as were used in the fabrication of the EGCR pressure vessel, and in many cases they were machined from material trimmed from the actual plates used in this pressure vessel. The weld-metal samples were machined from a special weldment prepared by the Baldwin-Lima-Hamilton Corporation. The weldment was fabricated from an extra plate of heat A-2110 and duplicates, insofar as possible, the welding materials and procedures used in the equator of the pressure vessel (Fig. 17.27). Synthetic heat-affected-zone samples were prepared at Rensselaer Polytechnic Institute.

The locations and the heat numbers of the shell plates for the cylindrical section of the EGCR pressure vessel are shown in Fig. 17.27. Additional heats were employed for the hemispherical heads, and they are also included in the surveillance program.

The EGCR pressure-vessel surveillance schedule is summarized in Table 17.1. The schedule provides for a greater quantity of data for the materials employed in the cylindrical portion of the vessel, which includes the region of highest neutron flux. In addition to the 484 Charpy V-notch impact samples and 92 tensile samples to be installed in the EGCR, an equal number of control samples have been prepared and will be retained for testing at the same time as the surveillance samples are tested. Additional specimens will be given accelerated radiation exposures in the ORR.

Charpy V-notch impact samples, drop-weight samples, and tensile samples have been tested to determine the preirradiation properties of these heats of ASTM A-212 grade B steel. The results of these tests are presented in Table 17.2. The drop-weight tests were conducted by the U.S. Naval Research Laboratory. The Charpy V-notch impact tests on synthetic heat-affected-zone samples were conducted at both Rensselaer Polytechnic Institute and ORNL. Table 17.2 shows that the nil-ductility transition (NDT) temperatures determined in the drop-weight tests varied only slightly among the heats of EGCR steel. Following determination of the NDT temperatures, additional Charpy V-notch impact tests were conducted at the NDT temperatures. The average fracture energy for Charpy impact tests at the NDT temperature is termed the "correlation energy." Charpy V-notch correlation energies for the EGCR steel heats varied over the rather wide range of 15 to 38 ft-lb. It was also noted that fracture energies for individual specimens varied as much as ±50% for the steel heats that gave the higher correlation energies. These were also the steel heats for which the sample stock consisted entirely of relatively small pieces of scrap metal which had been flame-cut from the steel plates during fabrication of the EGCR pressure vessel.

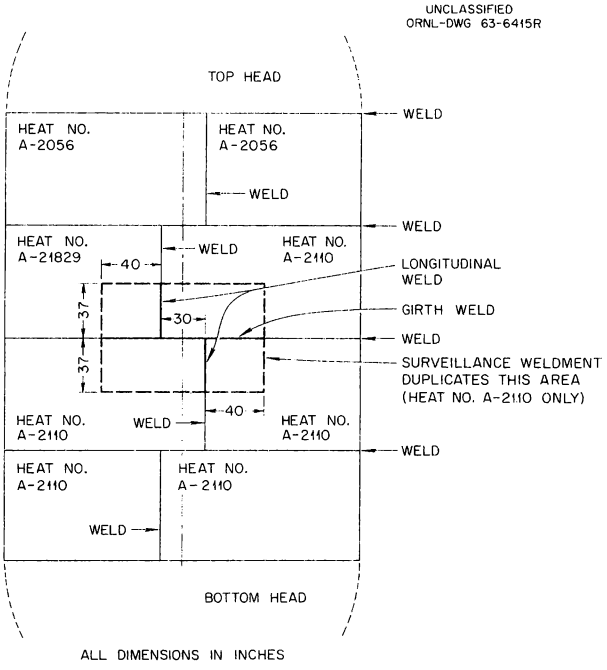

Fig. 17.27. Diagram of EGCR Pressure Vessel, Showing Location of Shell Plates of Different Heats of ASTM A212 Grade B Steel.

It is improbable that these variations of fracture energy were due to test procedure or inaccuracies of the testing machine (see later discussion of Charpy impact machine calibration); it is more likely that the scatter in fracture energies (and possibly the higher correlation energies) is due to inhomogeneity in the steel samples. While care was exercised not to take surveillance specimens from the vicinity of the flame-cut edges of the sample stock, it appears that inhomogeneity of properties may have been introduced by the flame-cutting operation to a depth that affected the Charpy V-notch impact test results. These same heats showed the greatest variations in tensile properties. Metallographic examination of these steels is planned. These observations indicate the great care that is required in obtaining samples representative of an engineering structure.

Table 17.1. EGCR Pressure-Vessel Surveillance Schedule

Each group of 3 containers contains 10 Charpy V-notch impact specimens and 2 tensile specimens, except containers 13–15 of strings 1 and 8 which contain 12 Charpy V-notch impact specimens. Tensile specimens are of the same material as are the Charpy specimens except where heat numbers for the tensile specimens are given in brackets.

Key: A-2110 indicates heat A-2110; no suffix indicates base-plate material.
WL indicates weld metal from a longitudinal weld.
WG indicates weld metal from a girth weld.
H2 indicates synthetic heat-affected-zone material, 2400°F peak temperature and thermal cycle for 95,800 joules/in. weld.
H3 indicates synthetic heat-affected-zone material, 2400°F peak temperature and thermal cycle for 145,500 joules/in. weld.

String No.	Exposure Period (years)	Material					
		Containers 1–3	Containers 4–6	Containers 7–9	Containers 10–12	Containers 13–15	Containers 16–18
1	2	A-2110	A-21829	A-2056	A-2056H3 (Ref. A-212B)[a]	A-2056H2	A-2110WL
2	5	A-2110	A-21829	A-2110H3 [A-2056]	A-2110H2 (Ref. A-212B)	A-22193	A-2110WG
3	10	A-2110	A-21829	A-2056	A-2056H2 (Ref. A-212B)	A-21822	A-2110WL
4	15	A-2110	A-21829	A-2056	A-2056H3 (Ref. A-212B)	A-2061	A-2110WG
5	20	A-2110	A-21829	A-2110H3 [A-2056]	A-2110H2 (Ref. A-212B)	A-19216	A-2110WL
6	*b*	A-2110	A-21829	A-2056	A-2056H2 (Ref. A-212B)	A-23965	A-2110WG
7	*b*	A-2110	A-21829	A-2110H3 [A-2056]	A-2110H2 (Ref. A-212B)	A-2106	A-2110WL
8	*b*	A-2110	A-21829	A-2056	A-2056H2 (Ref. A-212B)	A-2056H3	A-2110WG

[a]Reference A-212B is material from a plate of ASTM A-212 grade B steel provided by the United States Steel Corp. and used in a number of radiation effects programs for intercomparison of results.

[b]Exposure periods to be determined later on the basis of previous tests. Some of these specimens may be used for annealing experiments.

Table 17.2. Mechanical Properties of EGCR Pressure-Vessel Steels: ASTM A-212 Grade B and E-7016 Weld Metal

Heat No.	Material Condition	Charpy V-Notch (20 ft-lb) Transition Temperature (°F)	Drop-Weight NDT (°F)	Charpy V-Notch Correlation Energy (ft-lb)	Yield Strength (psi)	Ultimate Tensile Strength (psi)	Total Elongation (%)	Reduction of Area (%)
Normalized Base Plate								
A-2056	*a*	36	0	16	47,800	73,900	28.0	57.5
A-2110	*a*	12	−10	15	49,200	72,300	27.6	57.4
A-2061	*b*	−10	0	22	41,000	74,100	28.4	68.3
A-2106	*b*	−15	0	23	43,100	75,300	26.6	66.0
A-19216	*b*	−42	−10	36	47,800	76,600	26.9	67.0
A-21822	*b*	−40	0	34	43,500	77,200	26.9	72.0
A-21829	*b*	−10			42,600	81,000	25.8	62.4
A-22193	*b*	−20	0	38	46,600	74,500	28.2	71.6
A-23965	*b*	−36	−10	27	46,400	75,100	26.7	70.5
Deposited Weld Metal								
Girth weld, S.R.	*c*	−62			56,800	74,700	19.1	69.5
Longitudinal weld, S.R.	*c*	−112			55,600	72,800	20.3	70.8
Synthetic Heat-Affected Zones								
A-2056	*d*	110						
A-2056	*e*	80 to 100						
A-2056	*f*	100						
A-2056	*g*	82 to 106						
A-2110	*d*	48						
A-2110	*e*	28						
A-2110	*f*	65						
A-2110	*g*	25 to 50						

[a]Normalized at 1650°F for 1 hr per inch of thickness and cooled in air.

[b]Fabrication scrap from EGCR pressure vessel.

[c]Stress relieved at 1150°F for 4 hr.

[d]Heat-affected zone synthetically prepared for a weld energy input of 95,800 joules/in. with a peak temperature of 2400°F and a cooling rate of 18.4°F/sec at 1000°F.

[e]Prepared as in footnote *d* and stress relieved for 4 hr at 1150°F.

[f]Same as *d* except with energy input of 145,500 joules/in. and cooling rate of 9.3°F/sec at 1000°F.

[g]Prepared as in footnote *f* and stress relieved 4 hr at 1150°F.

The Charpy V-notch impact test results for EGCR pressure-vessel weldments, Table 17.2 and Fig. 17.28, indicate that the transition temperature of the stress-relieved weld metal is significantly lower than that of the base-plate material.

A critical region in welded structures may be the heat-affected zone adjacent to the welds. This is indicated in the present results (Table 17.2) by the higher Charpy V-notch transition temperatures exhibited by the synthetic heat-affected-zone samples. Unfortunately, this region is usually quite localized, and it is difficult to machine notch-impact samples from weldments that will be indicative of the mechanical properties of the heat-affected zone. For this reason, synthetic heat-affected-zone samples were prepared (under subcontract at Rensselaer Polytechnic Institute) on the basis of the welding parameters (arc current and voltage, travel speed, and preheat conditions) employed in the fabrication of the reactor pressure vessel. The samples were prepared by subjecting them to thermal histories corresponding to peak temperatures of 2400°F, preheat temperatures of 210 and 275°F, and energy inputs of 95,800 and 145,500 joules/in., which are conditions typical of the thermal histories experienced by the heat-affected zones in the EGCR pressure vessel. Microstructures of the synthetic samples were the same as for corresponding regions of weld heat-affected zones.

Charpy V-notch impact test curves are shown in Fig. 17.29 for the base plate of heat A-2110 and for synthetic heat-affected-zone samples of this heat for the 95,800 joules/in. energy input and for both the "as-welded" condition[37] and after stress-relief treatment at 1100°F. It is seen that there

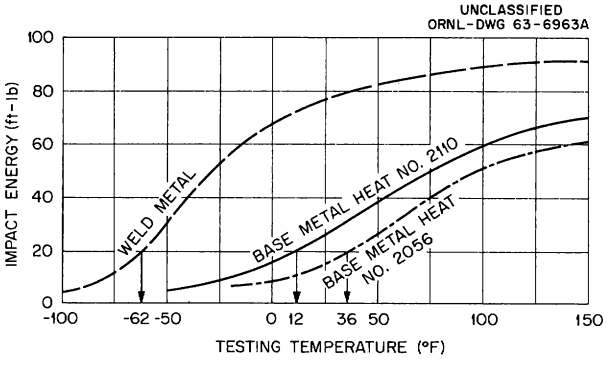

Fig. 17.28. Impact Energy Absorbed in Fracture vs Test Temperature for Base-Plate and Weld-Metal Charpy V-Notch Impact Samples of EGCR Steel.

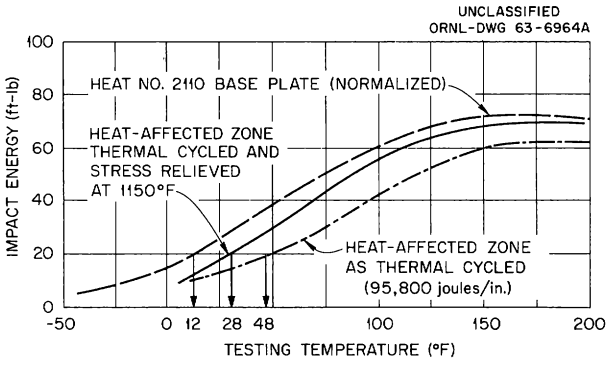

Fig. 17.29. Impact Energy Absorbed in Fracture vs Test Temperature for Base-Plate and Synthetic Heat-Affected-Zone Samples of EGCR Steel. Curves are shown for the synthetic heat-affected-zone samples as thermal cycled to produce a microstructure characteristic of a heat input of 95,800 joules/in. and for similar samples stress relieved at 1150°F.

was a reduction in notch ductility due to thermal cycling, and the stress-relief treatment produced some recovery of the original notch ductility.

The results presented in Table 17.2 show that the heat-affected-zone samples of heat A-2056 had higher notch-impact transition temperatures than those of heat A-2110. After metallographic examination, the poorer properties of heat A-2056 were attributed[37] to a continuous network of proeutectoid ferrite surrounding the prior austenite grains. In this case, the stress-relief treatment is ineffective in restoring notch ductility. For the heat-affected-zone samples of heat A-2110, less proeutectoid ferrite was observed, and the decrease in notch ductility upon thermal cycling was attributed to the formation of martensitic products.[37] In this case, the stress-relief treatment had a beneficial effect.

SM-1 PRESSURE-VESSEL SURVEILLANCE PROGRAM

(E)

R. G. Berggren L. D. Schaffer[38]

Subsize Izod impact samples of ASTM A-212 grade B steel are being used for the pressure-

[37]W. F. Savage and F. C. Breimeister, *A Further Study of the Weld Heat-Affected-Zone in A-212-B Steel*, Rensselaer Polytechnic Institute, Troy, N.Y. (January 1964).

[38]Reactor Division.

vessel surveillance program of the SM-1 reactor at Fort Belvoir, Virginia. The results of impact tests on the samples from the two capsules removed thus far from the reactor were described in a previous report.[39] The analysis of these results has been hampered by uncertainties in the neutron fluxes experienced by the samples and by the comparison of these fluxes with those at the pressure-vessel beltline. On the basis of more recent flux information,[40] a reexamination of the impact tests results has been made,[41] which indicates that one of the notches on the subsize Izod samples (notch 3) is being exposed to fast neutrons at a rate nearly equal to that of the pressure vessel. Therefore, the data obtained upon testing notch 3 of the test bars in surveillance capsules as they are removed from the SM-1 should give a good indication of the change in the ductile-brittle transition temperature of the SM-1 pressure-vessel steel.

Six capsules remain in the SM-1. The removal of the next capsule, capsule III, is planned for late 1964.

The transition from a ductile fracture at high temperatures to a brittle fracture at low temperatures in notch-impact tests may be correlated with the amount of shear or cleavage failure in the fracture path. The regions of shear or cleavage failure may be deduced from the appearance of the fracture surface. A dull, fibrous appearance indicates shear failure, whereas bright, crystalline regions suggest cleavage. The present work was undertaken in the attempt to correlate observations of this type with a microscopic examination of the cross section of the fractured region.

Metallographic examinations were performed on the broken Izod specimens from capsule I. The specimens were nickel-plated to preserve the edge detail of the cross section and were sectioned as shown in Fig. 17.30. The fracture cross sections were treated metallographically, and a series of photomicrographs (250×) were taken to show the entire length of the fractured path. The assembled montages are presented in Figs. 17.31 and 17.32. The nickel plate is seen as a continuous white area on the fracture surface. The root of the notch appears at the left in the figures. The fracture started at the root, propagated from left to right, and ended at the back of the specimen at the right in the figures. The white regions in the microstructure are ferrite, and the gray-to-black regions are pearlite. Cleavage failure in ferrite grains is identified by a straight or flat fracture path, often containing several steps. Shear failure in ferrite grains is indicated by an irregular fracture path; strain markings frequently appear near the fracture face. A cleavage facet is often distorted after fracture by shear strain in adjacent grains. Portions of the fracture path are difficult to classify; this is particularly true of regions where the fracture path passes through pearlite colonies. Also, ferrite grains sometimes show characteristics of both cleavage and shear modes of fracture.

The results of this analysis are given in Table 17.3. This type of study has been conducted on only a few specimens, and the results should not be considered adequate for drawing any general conclusions. However, these limited results indicate that the amount of cleavage failure in a fracture in the irradiated steel is very nearly that found in the unirradiated steel tested at the same temperature rather than being that found in the unirradiated steel yielding the same fracture energy

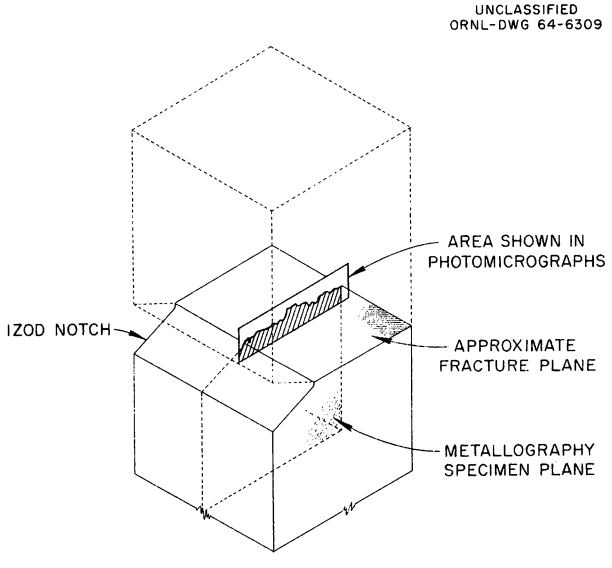

Fig. 17.30. Geometry of the Metallographic Section Used for Fracture Profiles in Figs. 17.31 and 17.32.

[39] R. G. Berggren *et al., Solid State Div. Ann. Progr. Rept. Aug. 31, 1962,* ORNL-3364, pp. 147–49.

[40] F. G. Moote *et al., Fast Neutron Flux in a Mockup of SM-1A Core and Vessel,* ACNP-63586 (August 1963).

[41] R. G. Berggren and L. D. Schaffer, *Army Reactors Program Ann. Progr. Rept. Oct. 31, 1963,* to be published.

UNCLASSIFIED
PHOTO 66009

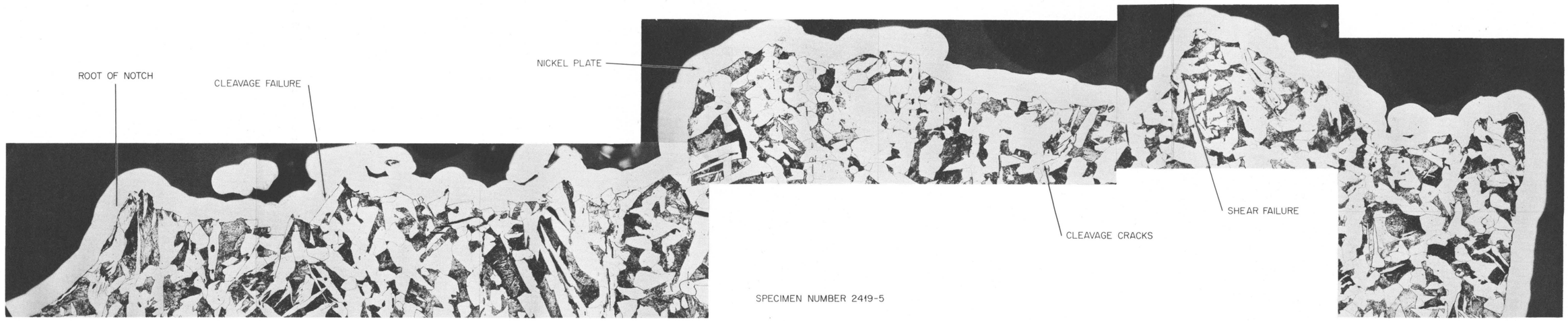

Fig. 17.31. Fracture Profile of Unirradiated SM-1 Subsize Izod Impact Samples. Tested at $-40^{\circ}F$; energy absorbed in fracture, 2.1 ft-lb. 250×.

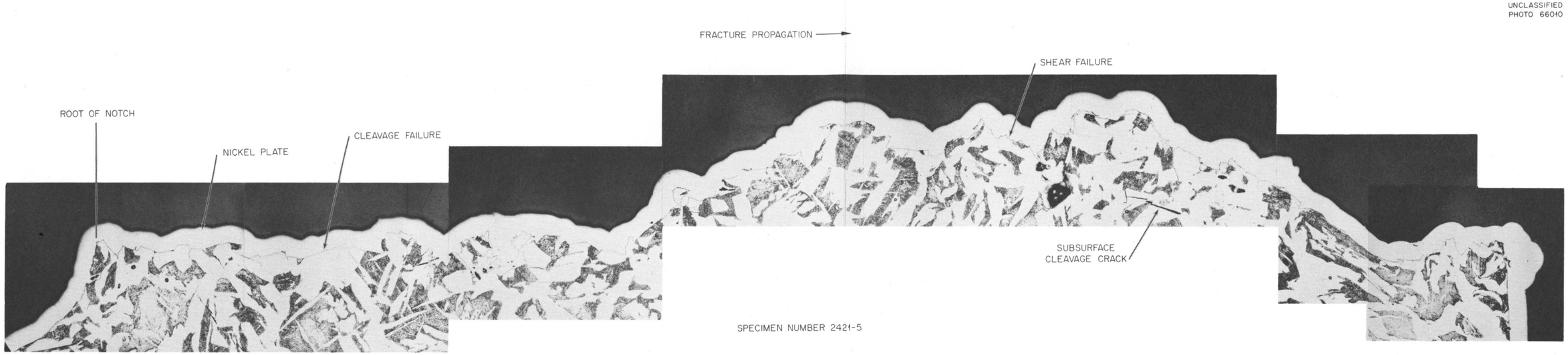

Fig. 17.32. Fracture Profile of Irradiated SM-1 Subsize Izod Surveillance Sample. Irradiated in SM-1 after 16.4 Mwyr of reactor operation. Tested at 5°F; energy absorbed in fracture, 2.4 ft-lb. 250×.

Table 17.3. Fracture Analysis Results

	Specimen No.			
	2419-5[a]	2419-2	2419-4	2421-5[b]
Irradiation	None	None	None	16.4 Mwyr
Test temperature, °F	−40	−5	+20	+5
Fracture energy, ft-lb	2.1	1.5[c]	4.2	2.4
Cleavage fracture, %	46	39	25	26
Shear fracture, %	47	56	74	65
Unclassified fracture, %	8	5	1	9

[a]Fig. 17.28.
[b]Fig. 17.29.
[c]Value probably in error.

value (at a lower temperature). This observation appears to be in direct opposition to earlier correlations of fracture energy with percent "crystallinity." Further study of this question is planned.

ACCELERATED IRRADIATIONS OF PRESSURE-VESSEL STEELS

[550°F (282°C); notch impact; E]

R. G. Berggren W. J. Stelzman T. N. Jones

It is known that the mechanical properties of heat-affected-zone regions of the steel in welded steel structures may be of critical importance. This is indicated by the higher ductile-brittle transition temperatures shown in Table 17.2 and Fig. 17.29 for the synthetic heat-affected-zone samples as compared to the base-plate and weld-metal samples. In the application of low-carbon steels to reactor pressure vessels, attention must be given to the possibility that the heat-affected-zone areas will undergo further reduction in notch ductility when they are irradiated. In an earlier study[42] of the effect of irradiation on base-plate and simulated heat-affected-zone samples of ASTM A-212 grade B steel, it was found that the increase in transition temperature was roughly the same for the two materials, despite the higher initial transition temperature for the heat-affected zones. For a neutron exposure of about 9×10^{18} neutrons/cm^2 ($E>1$ Mev) at about 120°F, the increase in transition temperature was somewhat greater than 200°F.

To extend the study of irradiation effects on the notch-impact transition temperature of heat-affected-zone materials to elevated exposure temperatures, two irradiation experiments were installed in the poolside facility of the ORR during the year. The experiments contained Charpy V-notch impact samples of both base-plate and synthetic heat-affected-zone materials. The design of the irradiation capsule is shown in Fig. 17.33. For both experiments, the desired irradiation temperature of 550°F was exceeded. In the first experiment, the stainless steel leaf springs relaxed during the elevated-temperature exposure, changing the heat flow characteristics of the experiment, and premature heater failures were experienced. In the second experiment, leaf springs of Inconel

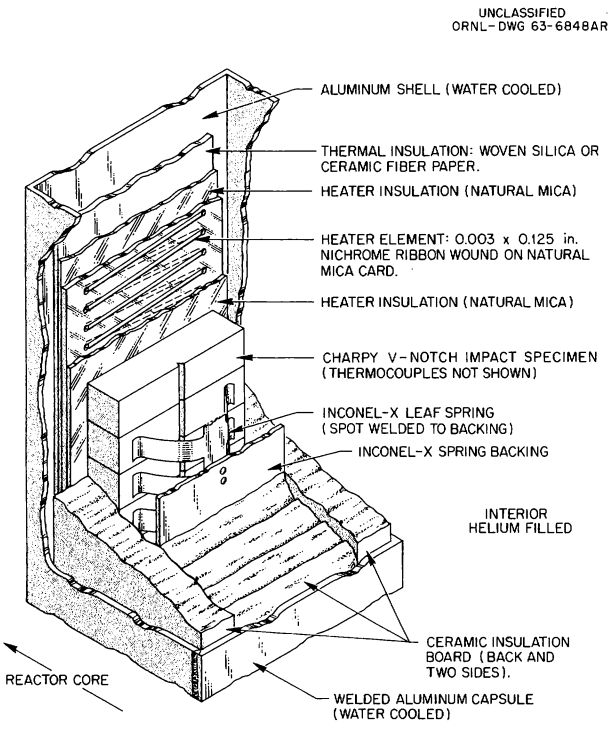

Fig. 17.33. Capsule for Elevated-Temperature Irradiations of Charpy V-Notch Impact Samples.

[42]R. G. Berggren, M. S. Wechsler, and T. N. Jones, *Solid State Div. Ann. Progr. Rept. Aug. 31, 1961*, ORNL-3213, pp. 39–42.

X and ceramic fiber thermal insulation were used. In this case, the thermal barrier presented by the ceramic fiber paper was greater than expected, and the operating temperature of the experiment was about 900°F. Again, premature heater failures were experienced. An improved irradiation capsule is being prepared for installation in the ORR during June 1964. The heater elements in this apparatus are swaged wire elements, sheathed with stainless steel and insulated with MgO.

CHARPY IMPACT MACHINE CALIBRATION

(E)

R. G. Berggren W. J. Stelzman T. N. Jones

Efforts to meet the stringent Charpy test calibration standards of this program have met with only partial success. The Charpy impact testers used in this program satisfy the ASTM standards. However, attempts to calibrate the machines using calibration specimens provided by the Army Materials Research Agency (AMRA) have revealed errors arising from the dynamic characteristics of the machines. These errors have been reduced, but not yet to AMRA requirements. The testing machine vendor is presently modifying one of our machines to meet AMRA calibration standards, and acceptance tests are scheduled for June 1964. If successful, our second machine will be similarly modified and calibrated.

To determine the probable error of previously reported results, impact specimens of an ASTM A-212 grade B steel of a type previously tested in our two machines were tested in calibrated impact-testing machines at AMRA and at Rensselaer Polytechnic Institute. The fracture energies obtained on these calibrated machines were in good agreement with energies obtained on our machines. Thus it appears that the AMRA calibration specimens, of heat-treated SAE-4340 steel, are more sensitive to testing-machine variables than is the ASTM A-212 grade B steel. This apparent anomaly, of differing results for calibration specimens and agreement of results for the mild steel, is probably a consequence of the very different microstructures and fracture behavior of the two steels. Therefore, the data obtained for mild steels tested in our machines are considered quite reliable. In addition, reported radiation-induced shifts of impact transition temperature are considered valid since machine errors will tend to cancel out when comparing unirradiated with irradiated specimens.

Part VI. Technology

18. Solid State Division's ^{60}Co and ^{137}Cs Gamma Sources

J. W. Cleland L. C. Templeton

The Solid State Division's ^{60}Co gamma source facility No. 2 was initially installed[1] in 1959. During the past year the source tubes were removed and transferred to a new facility (No. 3) located in Building 2000. Source 2 was then reloaded on August 7, 1963, with ~9000 curies of ^{137}Cs. Each source tube contains one 4-in. pellet of compacted ^{137}Cs with a specific activity of 25 to 27 curies/g, and the photon intensity was determined on September 12, 1963, as 1.5×10^6 r/hr or 1.22×10^{12} (0.667-Mev) photons cm^{-2} sec^{-1}.

Figures 18.1 and 18.2 and Table 18.1 summarize temperature and dose-rate information obtained during the last few years for the sources. At present, source 1 in Building 3025 and source 3 in Building 2000 are loaded with ^{60}Co, which has a half-life of 5.27 years. Source 2 in Building 3025 is loaded with ^{137}Cs; its half-life is 30 years. In addition to the ^{137}Cs in source 2, there is some ^{134}Cs, which has a half-life of 2.1 years. It is estimated that initially 5% of the activity is due to the ^{134}Cs. In Figs. 18.1 and 18.2, each curve was drawn parallel to the line determined by the half-life of the particular isotope used. An exception is the curve for ^{137}Cs (source 2) at the bottom of Fig. 18.1. The curve was steepened to an extent necessary to account for the effect of the ^{134}Cs.

For measuring the dose rates, two materials have been used, ceric sulfate and RADIPOL capsules. Upon exposure to an appropriate dose

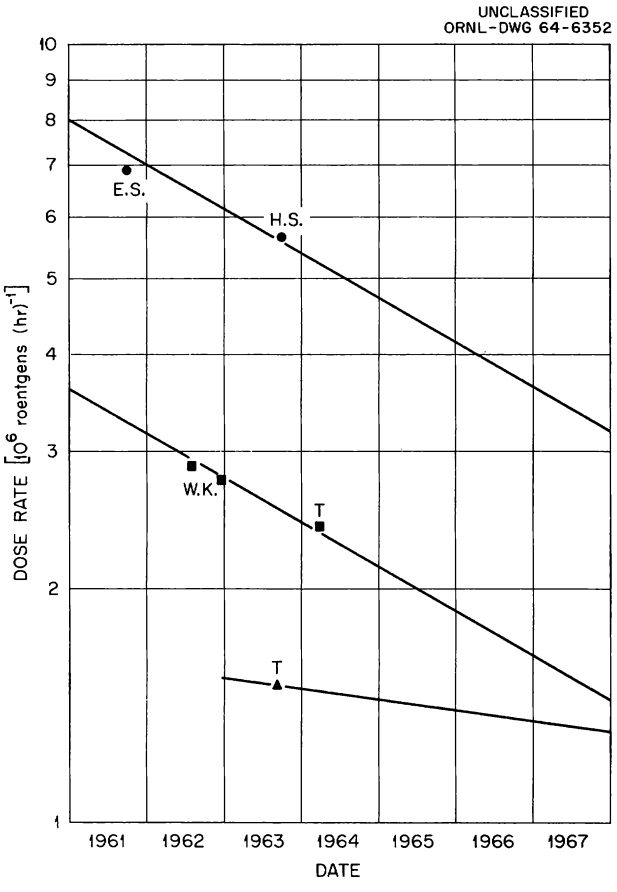

Fig. 18.1. Dose Rates on Various Dates for ^{60}Co Gamma Source No. 1 and for ^{137}Cs Gamma Source No. 2. The top curve is for the central hole of source No. 1; the middle curve is for the larger of the holes surrounding the central hole. The bottom curve is for source No. 2. The letters near each point indicate the person who made the measurement for that point. E. S. = E. Sonder; H. S. = H. Saito; W. K. = W. K. Kirkland, and T. = L. C. Templeton.

[1] J. W. Cleland, *Solid State Div. Ann. Progr. Rept. Aug. 31, 1961*, ORNL-3213, p. 74.

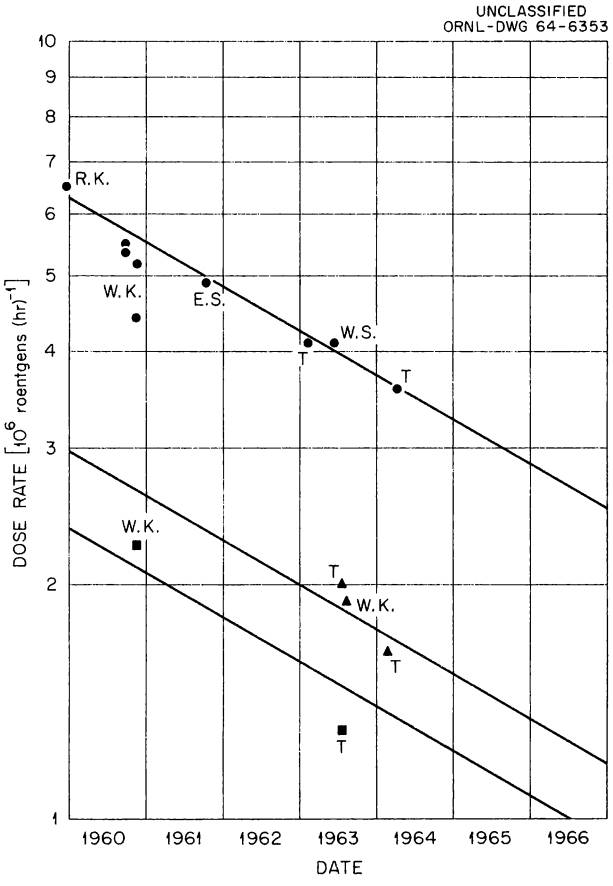

Fig. 18.2. Dose Rates on Various Dates for ^{60}Co Gamma Source No. 3. The top curve is for the central hole; the middle curve is for the larger of the holes which surround the central hole; and the bottom curve is for the smaller of the surrounding holes (about June 3, 1963, source No. 3, a new facility, was loaded with ^{60}Co which was taken from source No. 2. Measurements made prior to that date were, therefore, made in facility No. 2). The letters near each point indicate the person who made the measurement for that point. R. K. = R. H. Kernohan; E. S. = E. Sonder; T. = L. C. Templeton; W. S. = W. A. Sibley; and W. K. = W. K. Kirkland.

Table 18.1. Temperatures of Gamma Sources

Date	No. and Source	Hole	Thermocouple Placement[a]	Temperature (°C)
10/59	1 ^{60}Co	Center	A	37
			W	39
12/60	2 ^{60}Co	Side ($11\frac{1}{2}$)	A	15
12/60	2 ^{60}Co	Center	A	18
11/62	2 ^{60}Co	Center	H	29
6/63	3 ^{60}Co[b]	Center	H	39[c]
12/63	3 ^{60}Co	Center	H	32[d]
1/64	3 ^{60}Co	Center	H	34[e]
5/64	2 ^{137}Cs	Center	H	23

[a] A — thermocouple placed in contact with a silicon sample which was fastened to an aluminum stick; W — same as A except that a wood stick was used; H — thermocouple embedded in a KCl sample, the latter placed inside a brass holder.

[b] Cobalt was moved from source 2 to identical source 3 in 1963.

[c] Measured in summer.

[d] Measured in winter.

[e] With cooling water controlled at 15.1°C.

some, but not all, of the ceric sulfate is converted into cerous sulfate. The RADIPOL capsules contain a liquid which is polymerized by gamma radiation. The liquid is transformed into a solid by a given dose. The data indicate good agreement between the dose rates obtained by use of the two materials. When using ceric sulfate, it is important that the container be tightly sealed in order to prevent loss of liquid by vaporization.

Temperatures in the sample exposure holes are given in Table 18.1. It will be noted that, unless the temperature of the water used for cooling the source is controlled, the temperature may differ by more than 5°C from summer to winter.

19. Solid State Division's Thermal-Neutron Irradiation Facility

J. W. Cleland J. T. Howe

The express need for a high-dose-rate thermal-neutron irradiation facility at ORNL has long been recognized. A convenient experimental method for a determination of the ratio of the thermal-neutron flux to the resonance flux is that of the cadmium ratio of a $1/v$ detector, where this value is about 33 within the active lattice of a graphite-moderated reactor. This means that the flux in any energy decade, such as 1–10 ev or 10–100 ev, is about one-seventh the thermal-neutron flux for such a cadmium ratio, and one can, therefore, conveniently express the ratio of the thermal to the fast (damaging) neutron flux in any experimental locale by measuring the cadmium ratio. There is no known locale in the ORR or the LITR wherein the cadmium ratio is in excess of about 300. The cadmium ratio was in excess of 10^5 in the biological thermal-neutron treatment chamber of the ORNL Graphite Reactor; however, the actual thermal-neutron dose rate was only about 10^9 cm^{-2} sec^{-1} in this facility. The cadmium ratio in the vertical graphite thimbles outside the heavy-water region in the Argonne CP-5 reactor has been measured as being in excess of 10^4, and the actual thermal-neutron dose rate is in excess of 10^{12} cm^{-2} sec^{-1} in these locales.

Van der Walt and Colomb[1] have calculated the design requirements for a facility of high thermal-neutron flux in the absence of both fast neutrons and gamma rays for the BSR, and certain members of the Neutron Physics, Analytical Chemistry, and Solid State Divisions have discussed the design of a thermal-neutron irradiation facility of general usage. This facility consists of a $46 \times 30 \times 32$ in. aluminum tank containing 1750 lb of heavy water. Vertical sample tubes (2 in. ID) are located 19, 29, and 40 in. from the reactor face. One of the three tubes at 29 in. from the reactor has an inside diameter of $2\frac{3}{4}$ in. and is shielded from gamma rays by a $14 \times 8 \times 8$ in. thin-walled aluminum container filled with bismuth. It has been estimated[1] that the irradiation intensity in this primary sample tube would be 9×10^{11} thermal neutrons cm^{-2} sec^{-1}, with a thermal- to fast-neutron dose ratio of 4×10^{11} and a thermal-neutron to gamma-ray dose ratio of 2.9×10^{11}. Note that these calculated ratios would correspond to a cadmium ratio of 10^9 to 10^{10} and a gamma dose rate that would be essentially negligible. The tank has been constructed and leak tested and is ready for installation.

[1] R. van der Walt and A. L. Colomb, *A Facility of High Thermal Neutron Flux in the Absence of Fast Neutrons and Gamma Rays*, ORNL-TM-399 (Oct. 17, 1962); see also R. C. von Borstel *et al.*, *Exposure of Biological Specimens to High Fluxes of Thermal Neutrons*, ORNL-TM-489 (Feb. 18, 1963).

20. Phase Modulation of Injected Carriers

(transistor amplifier; Ge; E)

J. C. Pigg C. C. Robinson

The analogy between the triode and the transistor has been long recognized both from a conceptual and an operational standpoint. In each case there is a source of carriers which can be controlled so as to vary the current through a circuit which is in series with the controlled component. One might also expect that it would be possible to construct a component analogous to the klystron, in which the current is phase modulated rather than amplitude modulated. Experiments have shown that it is possible to construct such a device which will amplify a signal.

The configuration of the samples discussed is shown in Fig. 20.1. A voltage impressed across the sample so as to bias the junction in a forward direction will cause injection of minority carriers. These injected carriers will then drift down the sample under the influence of the applied electric field. An ac voltage applied to one set of contacts, such as contacts 1 and 2, will produce an ac voltage across another pair of subsequent contacts, such as contacts 3 and 4. An ac voltage across contacts 3 and 4 will result in a negligible ac voltage across a preceding set, such as contacts 1 and 2. Such behavior would be expected by analogy with klystron-type behavior.

A *p*-type sample with an *n*-type injecting barrier will be discussed, although samples have been made using *n*-type material. Both *n*- and *p*-type samples behave in a similar manner. An antimony-alloyed junction was used. An apparatus has been constructed which permits fusing of contacts on both sides of the sample at the same time that the junction is made. The contacts and current lead contact on the *p*-type material are composed of indium.

The rectification properties of the junction are illustrated in Fig. 20.2. It is clear from the reverse characteristic that there is considerable leakage current. Consequently, the efficiency of the barrier is reduced. The injected current occurs when the barrier is biased in the forward direction. A plot of forward current as a function of voltage bias is shown in Fig. 20.3 for three samples. Samples *B* and *C* showed amplification, while sample *A* did not. Consequently, it can be concluded that the characteristic of the forward current does not, in itself, determine the concentration of injected carriers at a distance from the barrier. A more promising parameter appears to be the fractional change of conductivity as a function of forward current.

Since the current is a function of electric field and of the gradient of the excess carrier concentration, both of which are functions of distance

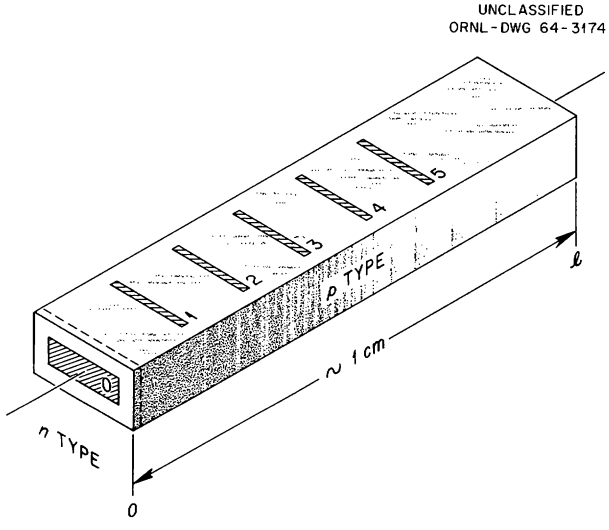

Fig. 20.1. Sample Configuration.

along the sample, the measured conductance is an integrated value of conductance between two points. It can, however, be expressed as two terms, one of which is the original bulk conductance and the second of which is proportional to the excess carrier concentration. The fractional change of conductance is thus proportional to the excess carrier concentration and may be expressed as fractional change in conductivity since the factors arising from the sample dimensions cancel. A plot of $\Delta\sigma/\sigma_0$ for measurements taken at various points along the sample is shown in Fig. 20.4. The subscripts indicate the numbered contacts between which the voltage was measured. It is clear from Fig. 20.4 that the injecting current produces a measurable excess carrier concentration throughout the sample.

The current through the sample is the sum of the charge drift due to the electric field and the diffusion arising from the gradient of the excess charge concentration. The latter contribution may be studied by producing an excess charge concentration and measuring the change of voltage

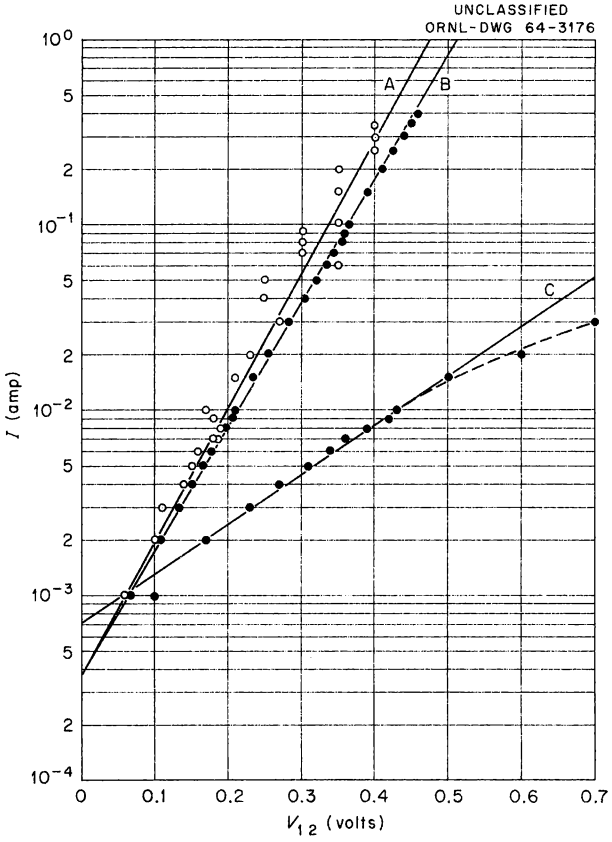

Fig. 20.3. Forward Current as a Function of Bias.

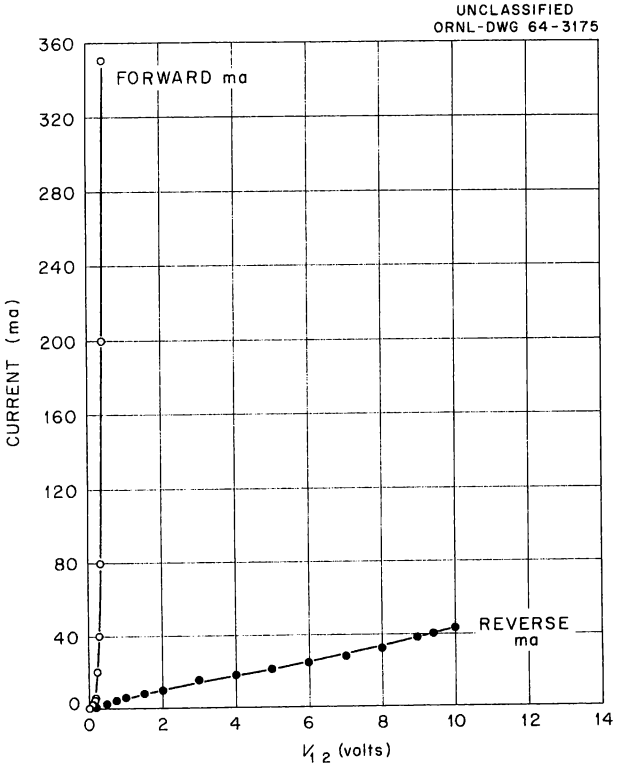

Fig. 20.2. Rectification Properties of the Injecting Contact.

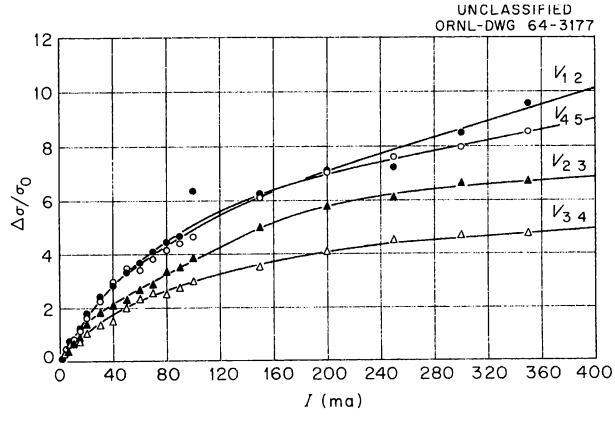

Fig. 20.4. Fractional Change of Conductivity as a Function of Forward Current.

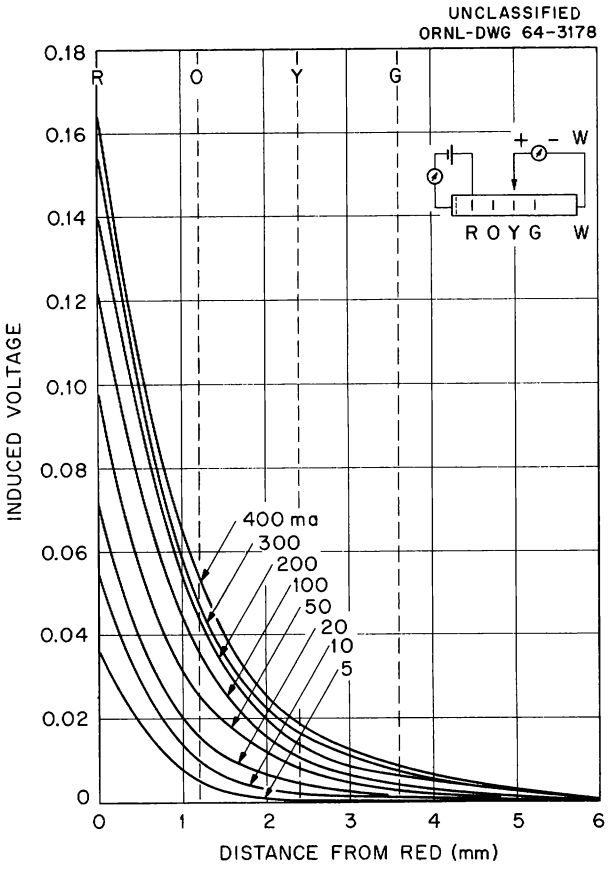

Fig. 20.5. Diffusion of Excess Carrier Concentration.

along the sample. One method of studying the diffusion of excess carriers is illustrated in Fig. 20.5. A bias is applied between the junction contact and the first set of sample contacts. The excess carrier concentration remaining at sample contacts will produce a concentration gradient between the sample contacts and the end of the sample. A potential gradient will be produced such as to make the current zero in the sample between the R and W contacts. The resulting electric field is a measure of the concentration gradient and, thus, the excess carrier concentrations. An effective diffusion length may be defined as the distance at which the concentration falls to 1/e of its initial value. This diffusion length is slightly dependent upon the injected carrier concentration and varies from 0.5 to 0.7 of the distance used between contacts.

The ac measurements were made with the circuit shown in Fig. 20.6a. When a shorting jumper is connected between contacts 0 and 1, the equivalent circuit shown in Fig. 20.6b is obtained. The value of the signal across R_{23} is given by

$$v_{23} = v_{12} \frac{R_{23}}{R_{23} + R_{36} + R_{61}}.$$

Hence, v_{23} is always smaller than v_{12}. When an injecting current is present in the sample, the value of v_{23} increases as the excess carrier concentration increases. The gain of the device, v_{23}/v_{12}, is shown in Fig. 20.7 as a function of excess carrier concentration. Both the absolute value of v_{23}/v_{12} and the value corrected for the zero-current reading are shown. Since R_{23} decreases with increased current through the sample,

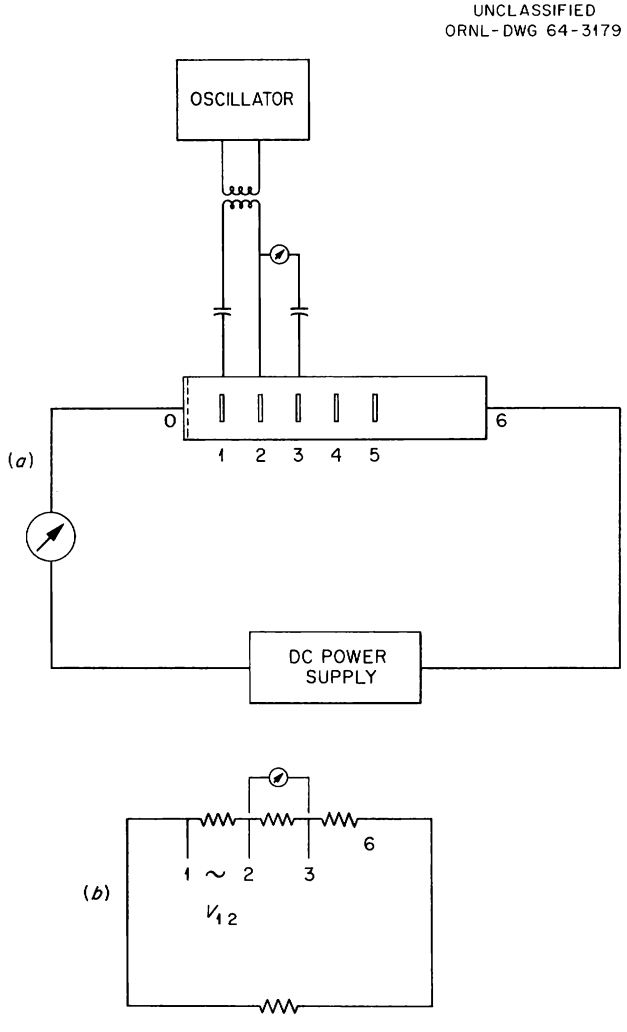

Fig. 20.6. Sample Circuit.

the high-current correction should be less than the zero-current correction. The values plotted assume a constant value for the correction. Hence, the contribution due to the injected current is, in reality, larger than that shown for high currents.

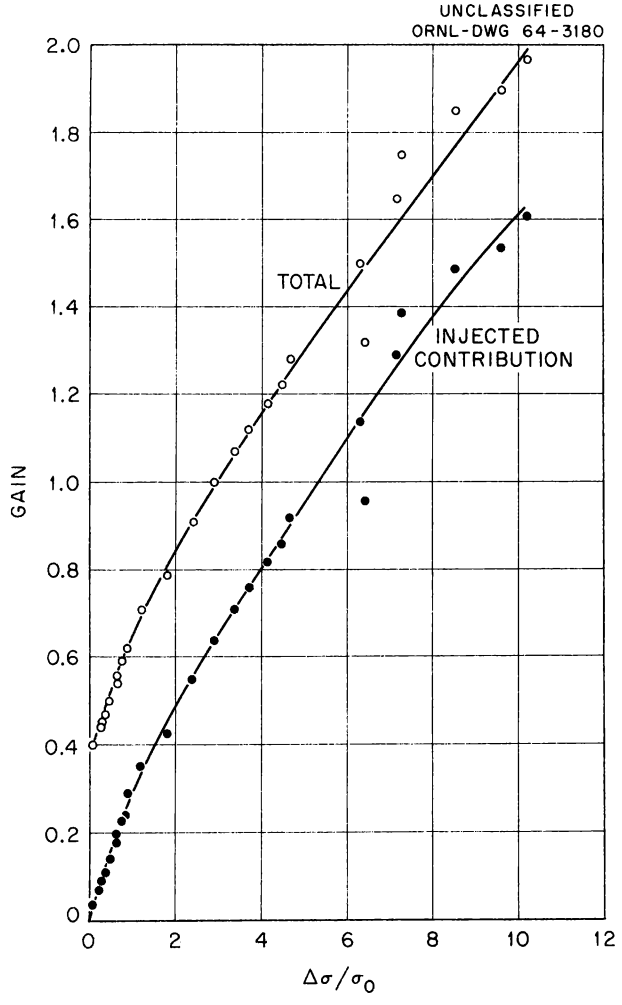

Fig. 20.7. Amplification as a Function of Excess Carrier Concentration.

The dependence of amplification on frequency is shown in Fig. 20.8 for two samples. The frequency dependence is a function of the contact spacing, diffusion constant, impurity concentration, and other factors not as yet determined. The two samples shown in Fig. 20.8 are from the same ingot, and the contact spacing is the same, but the junction characteristics differ. The designations B and C refer to the same samples designated B and C in Fig. 20.3.

The amplification of the device is a function of the excess carrier concentration injected into the sample, the effective diffusion length, the contact spacing, and the signal frequency. The power gain is slightly larger than the voltage gain discussed here. If the various parameters can be adequately understood and controlled, the phase modulation of excess carrier concentration constitutes a potentially useful electronic technique.

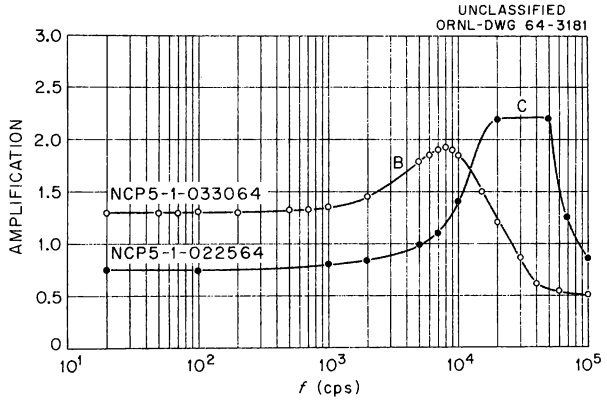

Fig. 20.8. Amplification Dependence on Frequency.

21. Pure Materials Program

PURE MATERIALS PROGRAM

J. W. Cleland

The purpose of this program is to develop the necessary techniques for the production of research-quality materials needed in selected areas of materials research. Progress in understanding the fundamental behavior of and ultimate range of properties possessed by many materials demands research specimens with both a high degree of purity and perfection. The choice of materials for consideration in the program has been made, for the most part, on the basis of the potential gain to a fundamental understanding of solids. Most materials of commercial interest, for example, the elemental semiconductors, are not being actively considered, since reasonable specimens are usually available from commercial suppliers. Certain research materials that have not been investigated previously are now being produced, and techniques of purification and crystal growth have had to be extended to these new types of materials.

This program involves a number of research divisions at ORNL and the special skills of a number of other AEC installations and AEC contractors. Many of the actual crystal-growth techniques have been performed by groups in the Reactor Chemistry[1] and the Metals and Ceramics[2] Divisions and have been separately discussed in their annual reports. The Analytical Chemistry Division has provided special techniques such as mass spectral analysis, neutron activation analysis, and microspectroanalysis. Also, a variety of physical property measurements have been made by research groups at ORNL and at other AEC installations that have aided in an analysis of the purity and perfection of selected samples.

Included in this report are only those materials being grown or evaluated by the Solid State Division.

RESEARCH MATERIALS INFORMATION CENTER

T. F. Connolly

One of the continuing needs in the field of solid-state or materials research is information on the availability of high-quality research specimens whose purity or composition is precisely known. Although a large number of interesting materials are produced by commercial, government, and university laboratories, the open-literature publications or sales catalogs seldom indicate the source and purity of starting materials, methods of further purification, crystal growth, and assay of the end product. Moreover, it is even more difficult to ascertain who has experience in preparation of any but the more common or "fashionable" materials of current interest.

The Research Materials Information Center was, therefore, established as a part of the Pure Materials Program of the Solid State Division to collect and provide information on the purification, production, characterization, and availability of research-quality materials to both producers and users. A companion listing is also made of those materials that are not currently available but are

---

[1] Isotopic LiF, UO_2, MgO, and CaF_2; see *Reactor Chem. Div. Ann. Progr. Rept. Jan. 31, 1964*, ORNL-3591, p. 231.

[2] BeO, ThO_2, HfO_2-SiO_2, $3BeO \cdot Al_2O_3 \cdot 6SiO_2$ (beryl), SnO_2, UAl_3, UAl_4, $ErMnO_3$, KCl (calcium doped), iron-substituted sodium-based micaceous materials, synthesized $Cs_2O \cdot Fe_2O_3 \cdot 4SiO_2$, and Al_2O_3; see *Metals and Ceramics Div. Ann. Progr. Rept. May 31, 1964*, ORNL-3670.

desired by various investigators. The primary emphasis is on high-purity, inorganic research materials (usually single-crystal) such as metals, alloys, semiconductors, refractory or insulating compounds, laser and optical materials, and magnetic materials. Structural materials, devices, and radioisotopes are not included, since these are covered by the Defense Metals Information Center at Battelle Memorial Institute and the Isotopes Information Center at ORNL.

The main reason for the existence of the Center is to collect and provide information to the scientific community on the availability of specific, requested materials. The primary mechanism is a completed data sheet. These sheets may be obtained from T. F. Connolly, Research Materials Information Center, Oak Ridge National Laboratory, P.O. Box X, Oak Ridge, Tennessee 37831. Interested participants should file such data sheets for each material, indicating that it is available or desired, and should carefully specify the research purpose, minimum purity and dimensions, desired dopant or specific impurities not tolerated, and other special characteristics such as physical, optical, electrical, and magnetic properties.

An aperiodic bulletin (newsletters containing selected articles on materials preparation and evaluation, and current lists of available and desired materials) is published and distributed to all participants in the program. No purchases, loans, or exchanges are arranged or handled directly; however, recipients of information are asked to notify the Center of any subsequent results on any specific materials in order that its records can be adjusted accordingly. General searches of the entire collection for the purpose of reviews may be made on occasion, and the collection and searching mechanism is also available for use by visitors to the Laboratory.

Equipment has been installed that will conduct an automatic search for coded entries that have been placed on film. More than 1500 data sheets on a wide variety of research materials have already been received from about 600 individuals representing more than 100 research groups. These data sheets have been filmed and the data encoded as to material, form, dimensions, orientation, impurity content, method of growth, final analysis, intended use, special characteristics, and availability for external distribution. Any future change or improvement in any of these properties can be coded into a later section of the film. Any requested materials for which no information is available is also encoded; hence, the requestor of a desired material will be notified if such a material becomes available at a later date.

Background information on materials is also being collected and encoded. A thesaurus of more than 300 coding terms has been established under such general categories as (1) type and form of material, (2) crystal structure, (3) growth techniques, etc., and each such category can be further divided into additional coding terms. Open-literature publications, company reports, sales catalogs, abstracts, and preprints have been collected and coded as received. The collection now contains about 9000 documents on 30 reels (100 ft each) of 16-mm film; each reel can be searched for a particular set of coding terms in about 15 sec of machine time.

One of the prime advantages of this retrieval system is that the searcher can select his own coding terms from the thesaurus (i.e., AlSb, single crystal, *p*-type, 100 orientation, float-zone growth) and can scan each data sheet, abstract, title page, or entire document as the machine searches. He can then obtain a hard copy of any of the above directly from the machine if the information is of particular interest.

It should be emphasized that close cooperation is required between the Center and those who analyze, grow, characterize, and use research-quality materials. The most immediate and continuing need of the Center is for completed data sheets from all producers of such materials and for rapid notification of any significant new result or development via internal reports, preprints, or personal communication.

GROWTH OF SINGLE-CRYSTAL HgS

(phase transformation; E)

O. E. Schow

Investigation of methods for the production of HgS research specimens is being continued. Preliminary measurements have been made on the pressure dependence of the sublimation temperature and the meta-cinnabar–cinnabar phase transformation for pressures from 0 to 10 atm (absolute). Materials for the studies have been

purified by fractional sublimation in sealed systems and by vacuum fractional sublimation above and below the transformation temperature.

GROWTH OF SINGLE-CRYSTAL CdTe

(Stockbarger method; E)

O. E. Schow

The Pure Materials Program of the Solid State Division has undertaken the preparation of research specimens of single-crystal CdTe. Several polycrystals weighing ~80 g each have been produced by using only reagent-grade cadmium and tellurium and the Stockbarger technique. The grain size was too small to furnish crystals for semiconductor studies but quite adequate for studies of the chemistry of the impurities. The results of the analysis of the impurity segregation indicate a factor of 10 decrease in the impurity level of the first centimeter, compared with the level of the last centimeter of a 15-cm-long polycrystal for the elements silver, copper, iron, and lead. The cadmium-tellurium ratio was measured by x-ray fluorescence, and to the limit of experimental accuracy the ingot was homogeneous in this respect. There was no increase in the cadmium at the grain boundaries or any crystal defects, even though there was an excess of cadmium in the crystal as a whole. Work will be continued with 99.9999% cadmium and 99.9999% tellurium after the impurity studies have been finished and the crystal-growing techniques have been perfected.

MAGNETIC SUSCEPTIBILITY OF Er_2GeMoO_8

[k (300°K) = 0.85×10^{-3} cgs unit/cm^3; E]

E. Sonder G. W. Clark A. T. Chapman

Crystals of Er_2GeMoO_8 tend to orient in a magnetic field contrary to their shape anisotropy. Since this behavior suggests interesting magnetic properties, we measured the temperature dependence of the magnetic susceptibility of this material, using the equipment on hand in the Solid State Division. This equipment was not designed to measure strongly paramagnetic samples; therefore, the determination was made with small amounts of the compound in the form of powder placed in a relatively massive, diamagnetic silica cup. Two separate Er_2GeMoO_8 samples were used – samples 1 and 2, which weighed 1.7 and 0.35 mg respectively. The magnetic field dependence of the room-temperature susceptibility indicated that sample 2 was slightly contaminated with a ferromagnetic impurity, the data being consistent with the presence of about 10^{-10} g of iron. Nevertheless, by extrapolating the susceptibility to infinite field, the room-temperature value of the susceptibility of Er_2GeMoO_8 could be calculated. The value obtained was k (300°K) = 0.85×10^{-3} cgs unit/cm^3; the value found for sample 1 was 0.90×10^{-3}. These values are in agreement with the value (0.84×10^{-3}) obtained on a larger single crystal with different equipment.

The temperature dependence of the susceptibility is shown in Fig. 21.1. It is clear that between 50 and 400°K, Er_2GeMoO_8 acts like a normal, paramagnetic substance. There is no indication of any unusual behavior in the range studied. Since such small samples had to be used in conjunction with a massive, diamagnetic silica cup, and since there seemed to be slight ferromagnetic contamination, we felt that the data were not precise enough to permit determination of a Weiss constant. Depending on the treatment of corrections, plots of $1/k$ vs T intersect the abscissa in the range −35 to −5°K; this indicates that any

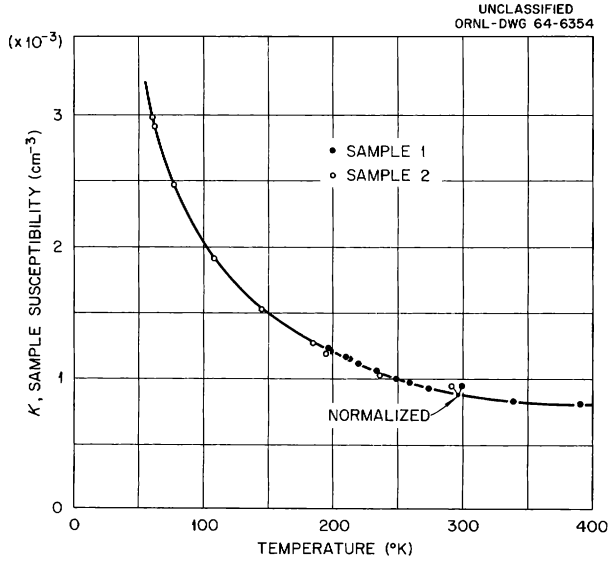

Fig. 21.1. Susceptibility of Er_2GeMoO_8 Between 60 and 400°K.

interaction present between the spins is of an antiferromagnetic nature.

MAGNETIC SUSCEPTIBILITY OF Cu_2O

(heat-treatment effects; E)

M. J. Smith E. Sonder

Cuprous oxide is probably one of the earliest semiconductors to be identified and used commercially. It has a forbidden gap of about 1.5 ev and is normally *p* type, with local levels lying 0.3 to 0.5 ev above the valence band. The reason for the *p*-type behavior is that the compound contains excess oxygen that depends upon the partial pressure of the ambient gas during preparation or high-temperature annealing. A considerable amount of work on this subject,[3-5] both theoretical and experimental, has been published. It is generally accepted that the cuprous oxide is oxidized according to the reaction

$$2Cu_2O + O_2 \rightleftharpoons 4CuO + 4\square .$$

It is necessary to include the copper vacancies (□) in the balance; they are a necessary consequence of the reaction taking place in a fixed lattice. Introduction of vacancies increases the entropy in the same way as does the introduction of another chemical entity. The equilibrium constant can be written

$$K = \frac{[\square]^4[CuO]^4}{[Cu_2O]^2 P(O_2)} ,$$

where the square brackets indicate concentration, and $P(O_2)$ is the partial pressure of oxygen gas. The concentration of the base material, Cu_2O, is essentially constant; the concentration of the vacancies is equal to that of the Cu^{2+} ions. Thus, the Cu^{2+} concentration should vary as the $\frac{1}{8}$ power of the oxygen pressure. It is assumed that the divalent copper ions or the vacancies act as acceptors.

[3] G. F. J. Garlick, *Handbuch der Physik*, 19th ed., p. 377, Springer-Verlag, Berlin, 1956.

[4] R. S. Toth, R. Kilkson, and D. Trivich, *Phys. Rev.* **122**, 482 (1961).

[5] M. O'Keeffee, Y. Ebisuzaki, and W. J. Moore, *J. Phys. Soc. Japan* **18**, 131 (1963); also, references given therein.

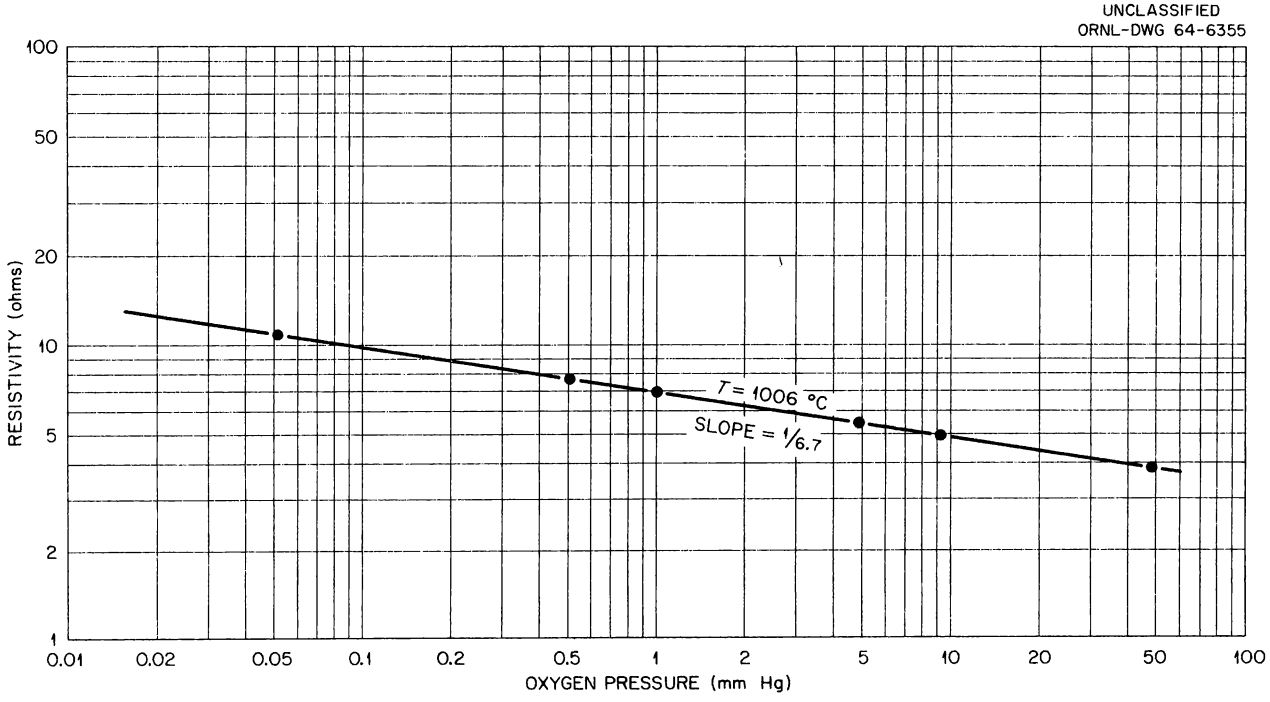

Fig. 21.2. Change of Resistivity of High-Purity Cu_2O with Ambient Pressure of Oxygen. The temperature of 1006°C shown on the curve was that of treatment and measurement.

Experimental determinations of the relationship between oxygen pressure and conductivity have been made. The conductivity varies as the $\frac{1}{7}$ power of the oxygen pressure. The data shown in Fig. 21.2 agree with this dependence for one of the samples used in this laboratory. Since the conductivity depends upon the mobility of the current carriers as well as their number, it is of interest to determine whether the different exponent found in the oxygen pressure dependence of the conductivity and that expected from simple theoretical considerations for the acceptor concentration is due to a change of mobility with oxygen pressure or whether a modification of the simple theory is required.

Since the Cu^{2+} has an unpaired electron, measurements of the temperature dependence of the magnetic susceptibility can yield accurate enough values of the cupric concentration to permit an experimental determination of the exponent in the power relationship between oxygen pressure and acceptor concentration.

A number of low-temperature susceptibility measurements alternating with high-temperature oxygen treatments were performed on two samples of Cu_2O produced by the Virginia Institute for Scientific Research in connection with the Pure Materials Program. Typical curves for one sample of the paramagnetic contribution to the susceptibility, κ_p, vs inverse temperature are presented in Fig. 21.3. It is clear that between 4 and 20°K, κ_p varies linearly with $1/T$, as one would expect from the formula $\kappa_p = N(Cu^{2+})\beta^2/kT$, where $N(Cu^{2+})$ is the number of cupric ions per cubic centimeter in the material, and β is the Bohr magneton. It is also clear that the slope is different after different treatments. However, it was found that the slopes of the curves were not simply related to the oxygen pressures used in the high-temperature treatments. Although the number of magnetic centers, as measured from the slopes of Fig. 21.3, tended to be larger when the sample had been treated with higher oxygen pressures, a lack of reproducibility was found

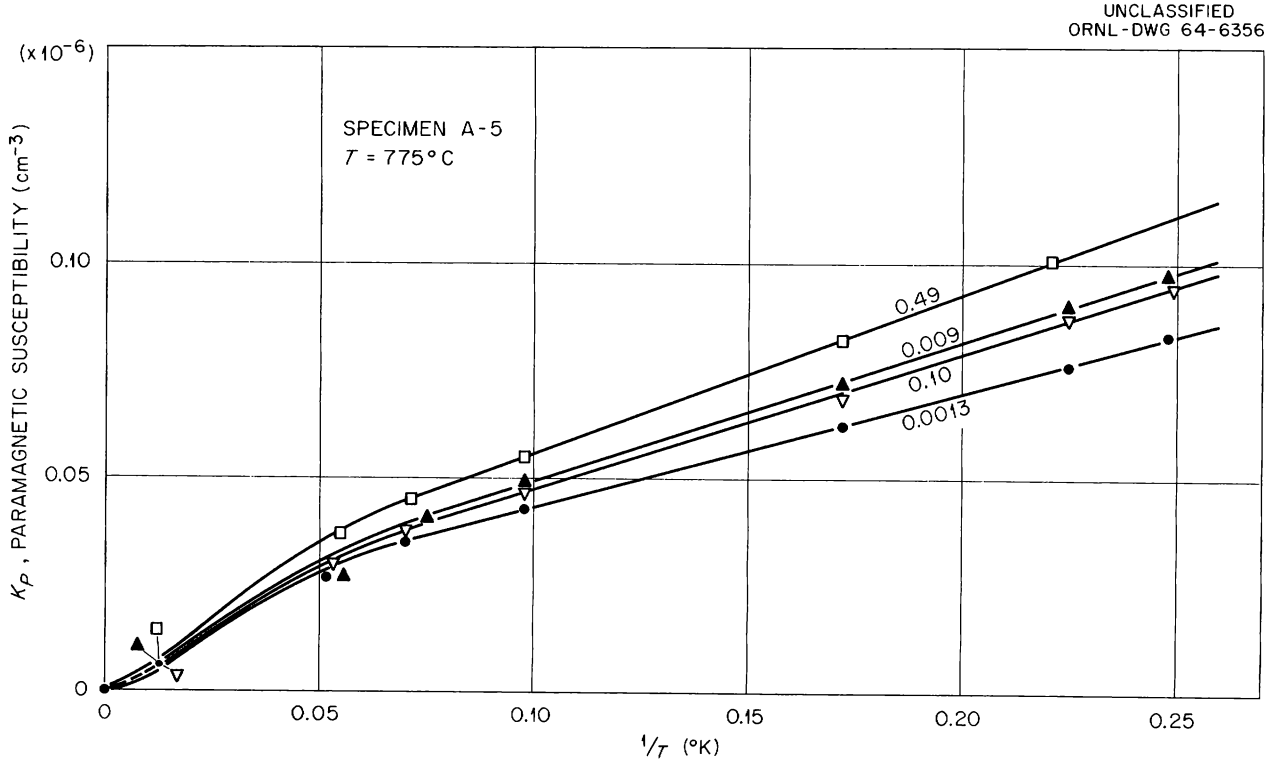

Fig. 21.3. Paramagnetic Contribution to the Magnetic Susceptibility vs Reciprocal Temperature. The numbers written next to the four curves give the pressure of oxygen gas in mm Hg used at 775°C for the heat treatments of the sample. The curvature apparent below $1/T = 0.05$ is not expected for a simple paramagnet and is not explained.

after the sample had been treated at different oxygen pressures repeatedly. The possibility that the particular samples used for the measurements shown in Fig. 21.3 were atypical was eliminated by the fact that very similar results were obtained on a sample from a different ingot.

It is unlikely that the poor reproducibility observed is due to incomplete freezing-in of the high-temperature Cu_2O-O_2 equilibrium. Using resistance measurements, we made an extensive study of the rate of approach of equilibrium at different temperatures. At the temperature of 775°K used in the treatments in question, the time constant for the reaction involving oxygen was about 1 min. The quench was accomplished in about 1 sec with gas containing oxygen at a partial pressure equal to the pressure of oxygen used in the treatment.

Contamination of the Cu_2O during the oxygen reaction cannot be eliminated as a possible cause for the erratic results. On the other hand, it is not clear how the levels of the two entities, the divalent copper ion and the positive ion vacancy, are distributed in the forbidden gap or how their states of association vary with temperature. The fact that the curves of Fig. 21.3 do not go through the origin, that is, that there is an unexplained change in the susceptibility between 80 and 20°K, supports the conclusion that complications exist that are not accounted for by the simple ideas upon which the experiment was based.

POTASSIUM CHLORIDE SINGLE CRYSTALS

(starting-material purification; Kyropoulos)

C. T. Butler J. R. Russell

The major goals of the program for producing ultrapure KCl during the past year were twofold. First, it was desired to develop a set of routine growth procedures so that crystals of uniformly high quality and similar physical characteristics could be produced in moderate quantities for distribution to interested scientists. This aim has been largely accomplished, and several crystals have been furnished to members of the Solid State Division and to cooperating scientists at other laboratories for research purposes. Second, it was desired to standardize the type and treatment of the starting material so that the effects on the final crystal of crucible material, furnace atmospheres, etc., could be studied. The large variations in impurity content of commercial KCl powder prevented a careful study of these experimental parameters.

All starting material is now produced by R. B. Quincy of the Analytical Chemistry Division. Nearly all of the procedures for removal of various classes of impurities from reagent-grade KCl powder have been perfected, and an ORNL report on these will be issued. Analyses of the first few ingots are presented in Table 21.1. Here, and in Table 21.2, concentrations are given in micrograms per gram. The starting charges, which are supplied in the form of 300-g fused ingots sealed under vacuum in 54-mm-diam quartz tubes, are stored unopened until they are needed. When a new furnace charge is required, an ingot is opened in a glove box under an argon atmosphere and loaded into the crucible and furnace tube. The furnace tube is then capped before it is removed from the box to be assembled onto the Kyropoulos apparatus. With these and other precautions, the total impurity levels found in the finished crystals have been lowered, but variations of any specific impurity from crystal to crystal are still quite high. This effect is evident in Table 21.2.

Despite the precautions taken to exclude contamination, the amount of OH included in the crystals depends upon prevailing humidity conditions. During the winter months, when the relative humidity was often less than 20%, the amount of OH in the crystals stayed below about 50 ppb (0.2 μg/g). During spring and summer, however, when the humidity in the growing room often rose to 90% at 100°F or above (due to a failure of the air-conditioning system), the OH content of the crystals rose as high as 3.5 ppm (15 μg/g). Order-of-magnitude calculations which assume a monolayer surface coverage of the KCl charge and quartz pieces predict that a residual OH concentration of about 25 ppb should be expected, regardless of humidity conditions. Also, a similar calculation based upon in-leakage of water vapor at the measured leak rate of the furnace and 100% relative humidity at 100°F was within a factor of 5 of the maximum OH concentration found. As a result of this experience, the growing laboratory is being isolated from the building air conditioning, and a separate cooling and dehumidifying

unit is being installed. One of the two electrostatic precipitators used on the present ductwork will be adapted to the new unit. This alteration should also reduce further the calcium content of the crystals, since a major source of this element is cigarette smoke and chalk dust brought in by the building air supply. (The calcium content from dusting of the walls and ceiling was previously minimized by coating the room with a special, nondusting, plastic-base paint.)

The concentration of OH in the crystals was estimated by absorption spectrophotometry, using the relation[6,7]

$$[OH] = 2.5\alpha_{204},$$

[6]T. I. Gie and M. V. Klein, *Bull. Am. Phys. Soc.* **8**, 230 (1963).

[7]B. Fritz. F. Lüty, and J. Anger, *Z. Physik* **174**, 240 (1963).

Table 21.1. Analyses of Starting Ingots

Starting Ingot No.	Element Concentration (μg/g)														Corresponding Boule No.
	Br	Ca	Cs	Fe	I	Li	Mg	N	Na	P	Rb	S	Si	Sr	
2C	<3	<3		<0.4	<1	<2		10	4		<2	3.5	<0.2	<3	082163
3C	38	<2	<3	<1	7	<1	<5	8	4		<2	<1	<0.2	<3	112063
JM-1C	2	<2	<3	<0.3	3	<1	<5	16	2		<2	1		<3	121263
4C	4	<2			5	<0.3		<1	3			2			012064
JM-2C	9.8	<2	<3	0.15	<1	<0.3	<5	11	<2		<2			<3	020564
5C	1	<2	<3		2	<0.3	<5	10	3		<2	1		<3	021264
6C	15	<2	<3	<0.3	5	<0.3	<5	2	3	0.7	<2	5		<3	022764
7C	<1	<2		<0.2	4.5			<1.0	3	1.07	<2	<1		<3	030664
8C	2.8	<2	<3	<0.1	<1	<0.3	<5	12	<2	<0.5	<2	<1		<3	042764
9C	5	<2	<3	<1	<1	<0.3	<5	4	<2	<0.5	<2	<1		<3	043064
10C	21	<1		<1	2.8			3		<0.3	<2	<1		<1	050664

Table 21.2. Analyses of Single-Crystal Boules

Boule Number	Element Concentration (μg/g)																	
	Ag	Al	Br	Ca	Cu	Fe	I	Mg	N	Na	OH^-	P	Pb	Pt	Rb	S	Si	Sr
051763			31	<3	<1	<1	2.6		13	<2	<0.26	0.46	<0.001			<1		<5
082163			24	<2	<1	<2	1.8	<0.1	6	2	4	0.5	0.009		3	<2		<3
091663			26	<2	<1		<1	<0.1	4	2	<0.5		<0.002		<2	<1		<3
110663			13	<2	<4	3.6	<1		16	2		0.6			<2	<1	<0.5	<3
111463			1.6	<2	<0.1	<1	<1		6	2		<0.2			<2	<1	<0.2	<3
112063			8.3	<2	<0.1	<0.5	<1	<3	46	3	0.06	1.1			<2	8	<0.5	<3
121263			32	<2	<25	<3	15	<5	<1	<2	0.22	<10	<0.002		<2	<1	<5	<3
012064		<3	39	<2	<3	<50	13		5	<2	0.12	1.2	0.003		<2	<1	<2	<3
020564			<0.6	<2	<0.02	<1	3.8	<5	7	0.4	0.13	13.5	<0.01		<2	<1	<5	<3
021264	<1	<5	<0.9	<2	<0.4	<1	4	<5	24	<1		<5	0.02	<1	<2	<2	<2	<3

where [OH] is the concentration in OH ions per 10^6 K^+ sites, and α_{204} is the absorption coefficient in cm^{-1} measured at the peak of the 204-mμ absorption band.

A large, vertical zone-refining apparatus is being constructed. Much of the gain in purity obtained by zone refining is lost when a single crystal is grown by using normal Kyropoulos or Stockbarger techniques. The new apparatus will attempt to circumvent this problem by allowing a seed to be introduced directly into the molten zone after several zone passes have been made, but before the last zone pass. The equipment is finished and is being tested, but no attempts have been made to produce single crystals.

As one of the routine analysis procedures, curves of color-center growth at room temperature are being made on many of the crystals grown during the past two years. So far, the crystals have late-stage *F*-coloration heights which differ by less than 25%; the maximum difference in late-stage slopes is only about 10%. There is seldom a measurable first stage in these crystals with the 3.5×10^6-r/hr gamma-ray source used. All of this is in contrast to commercial crystals which may show late-stage slope and height differences over a 15:1 range,[8,9] and first-stage absorptions ranging from essentially zero to more than 30 cm^{-1}.

ANALYSIS FOR TRACE AMOUNTS OF LEAD IN KCl SINGLE CRYSTALS

(optical absorption; spectroscopy; E)

C. T. Butler

A search is constantly being made for more sensitive or simpler methods for analyzing KCl crystals for trace impurities. By analyzing a series of lead-doped KCl crystals both by atomic absorption spectroscopy[10] and by absorption spectrometry, Sibley, Sonder, and Butler[11] were able to establish that, over a range of concentrations from 0.05 to 200 lead ions per million potassium sites (ppm), the lead concentration is given by the relation

$$[Pb] = 0.67\alpha_{272},$$

where α_{272} is the absorption coefficient, in cm^{-1}, at the peak of the lead optical absorption band at 272 mμ, and [Pb] is the concentration in lead ions per million potassium sites. Figure 21.4 shows the data. There are indications that this linear relationship holds for values somewhat greater than the maximum value shown, and it presumably holds for values lower than the minimum shown. Thus, the time-consuming, expensive, and destructive method of atomic absorption spectroscopy for single-crystal analyses can be replaced by a quick, cheap, and often nondestructive optical absorption technique.

However, at least three possible difficulties exist for the optical absorption method. The lead may conceivably exist in the crystal in more than one physical state or in conjunction

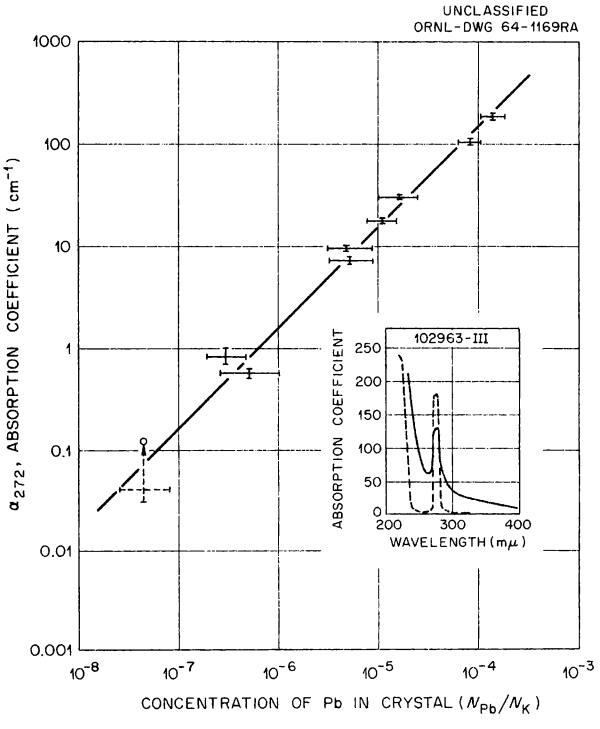

Fig. 21.4. Absorption Coefficient at the Peak of the Pb Absorption Band vs Measured Pb Concentration.

[8]C. T. Butler, W. A. Sibley, and E. Sonder, *J. Chem. Phys.* **39**, 242–43 (1963).

[9]C. T. Butler, W. A. Sibley, and E. Sonder, *Solid State Div. Ann. Progr. Rept. May 31, 1963*, ORNL-3480, pp. 97–98.

[10]The atomic absorption spectroscopy was performed by C. A. Pritchard of the Analytical Chemistry Division.

[11]Chap. 15, this report.

with one or more other impurity. Additionally, it may be undetectable because of an insufficient optical path length available in the crystal. That association or precipitation is unimportant for lead in KCl at these concentrations is indicated by the constant 45° slope of the line drawn through the data points in Fig. 21.4. For crystals grown by the Kyropoulos method at this laboratory, heat treatment for 10 min at 450°C followed by a rapid cooling caused no observable increase of the 272-mμ absorption peak, indicating that no appreciable chemical association occurs in these crystals. However, some commercial crystals containing lead at levels from 0.01 to 0.1 ppm and OH^- or other impurities to levels above 1 ppm showed an increase of the 272-mμ band by a factor of 2 to 3 when similarly treated. This probably indicates some chemical interaction between lead and other species in these relatively impure crystals. The lowest data point in Fig. 21.4 illustrates this effect for Optovac crystal 103C. Quenching this crystal brings the data point close to the proper line, as indicated by the arrow. The third difficulty with optical absorption analyses rests with the length of sample necessary to analyze for low concentrations of lead. After consideration of such things as the slope of the pure-crystal background absorption, interfering bands, etc., an absorbance of 0.05 may be chosen as the minimum reading acceptable for reliable determination of the lead content of a crystal. The relation predicts, then, that a crystal length of nearly 8 cm is necessary to detect 0.01 ppm of lead.

Having obtained the correlation of the lead absorption band with the measured content, and recognizing that luminescence is inherently a more sensitive tool than absorption, we attempted to relate the height of the lead luminescence at 341 mμ to the known lead content of the crystals. Blocks of KCl were excited with a narrow beam of ultraviolet radiation, and the luminescence was analyzed at right angles to the exciting light with a $\frac{1}{2}$-m Bausch and Lomb monochromator and a cooled EMI 9558Q multiplier phototube. The ultraviolet source was a 60-w deuterium lamp fitted with a Bausch and Lomb quartz-fluorite condenser and a holder for interference filters to cover the spectral range above 200 mμ. The sample chamber of the spectrometer was so constructed that samples ranging from entire Kyropoulos boules (4 × 4 × 8 cm) to blocks (1 × 1 × 0.5 cm) cleaved from the boules could be used interchangeably with only about a 10% variation in the recorded intensities. To remove opaque KCl films, boule sides were lightly water-polished by wiping with a damp Kleenex and drying with a flow of warm air.

Figure 21.5 shows the relation of the peak height of the lead emission for a series of crystals to their lead content as determined by optical absorption. A straight line with a slope of 45° has been drawn through the data points. Part of the observed scatter is due to the fact that the average lead concentration over the entire length of a boule is measured by the absorption method, while the 341-mμ emission is a measure of the average lead concentration in a small volume within the crystal. The exciting wavelength for the above data was 270 mμ – near the peak of the absorption band. No data points occur below about 4 ppb (0.004 ppm). This is considerably below the minimum concentration detectable by atomic absorption spectroscopy and probably represents the limit of the absorption technique for the boule lengths available. The luminescence limit of detection, on the other hand, should be well below 4 ppb if no interfering bands are present, with an appreciable contribution near 341 mμ.

At lead concentrations somewhere between 0.1 and 1 ppm, the luminescence begins to deviate from a linear relationship to the known lead concentration. Investigation indicates that the deviation appears to be due mainly to absorption of the exciting wavelength by the crystal. The reasons are actually unimportant, however, since the optical absorption method may be used with ease about 0.5 ppm, where the necessary sample thicknesses approach 1 mm. If, for some reason, it were desired to extend the upper limit for the luminescence technique, a better approach would seem to be in-line illumination of very thin specimens with light having an energy well above the absorption edge. Many of the usual errors associated with right-angle illumination of larger blocks would seemingly be removed by this technique.

It was found in this work that the same crystals which showed an increase in absorption after heat treatment also showed an increase in luminescence after such treatment. In Fig. 21.5, data points are shown for Optovac crystal 0217, both before and after quenching. The point for

the quenched specimen lies very close to the 45° line, while that for the untreated specimen is quite far removed. Thus, if luminescence is to be used to estimate reliably the amount of lead in a crystal of unknown origin, the crystal should be first quenched from an elevated temperature. In this sense, neither the optical absorption nor the emission methods are nondestructive, although the treated pieces are still useful for chemical analyses.

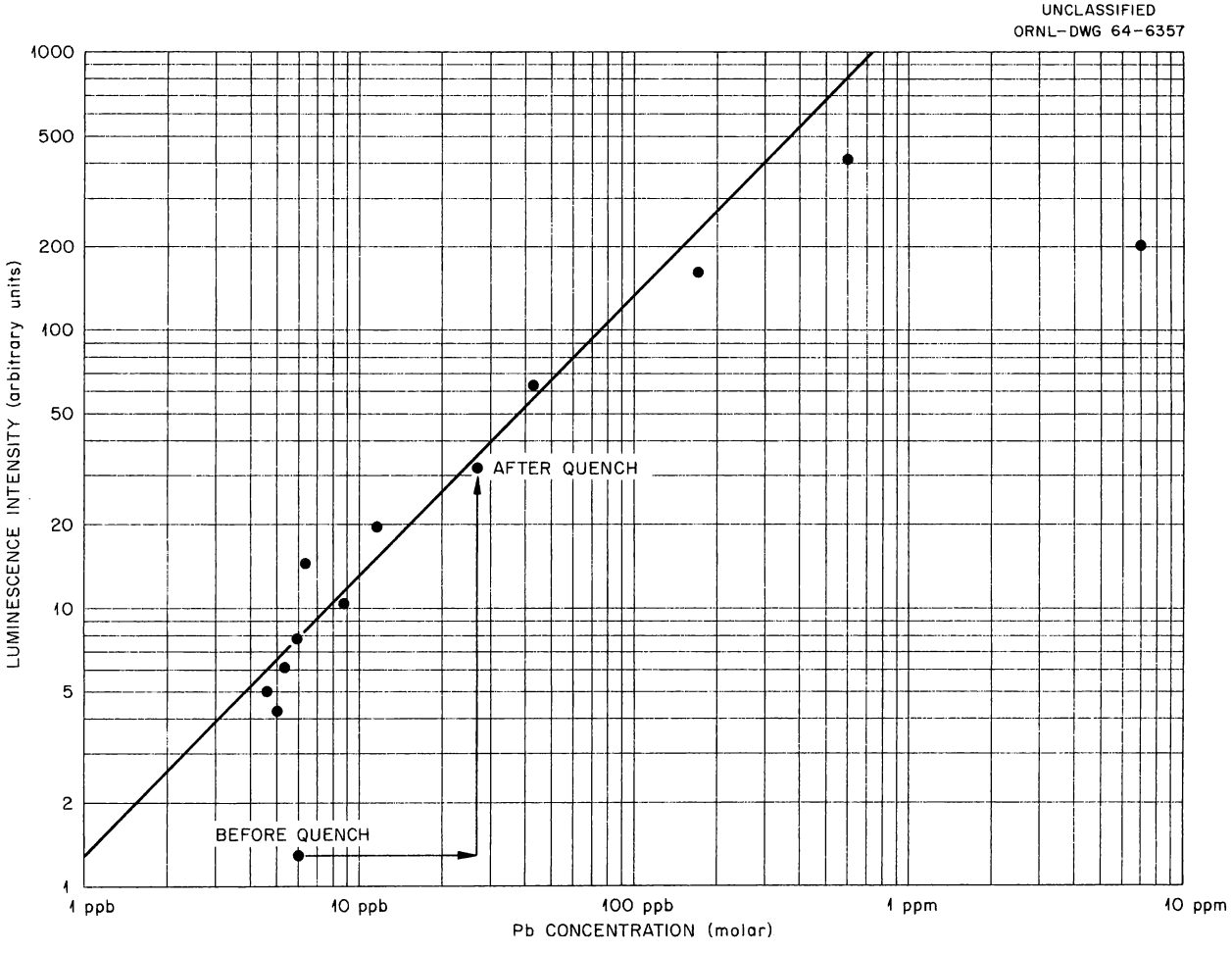

Fig. 21.5. Relative Intensity at the Peak of the Pb Luminescence Band vs Measured Pb Concentration.

Publications, Papers, and Seminars

Publications and Papers

JOURNAL ARTICLES

K. Akimoto and W. A. Sibley
"Hardening of Potassium Chloride Single Crystals by Quenching and Irradiation," *J. Appl. Phys.* **34**, 1767 (1963).

U. Bertocci, L. D. Hulett, and L. H. Jenkins
"On the Formation of Electrochemical Etch Pits on the (111) Face of Cu," *J. Electrochem. Soc.* **110**, 1190 (1963).

M. A. Breazeale and D. O. Thompson
"Finite-Amplitude Ultrasonic Waves in Aluminum," *Appl. Phys. Letters* **3**, 77 (1963).

C. T. Butler, W. A. Sibley, and E. Sonder
"Variation of Coloration Rates and Luminescence in Harshaw Potassium Chloride," *J. Chem. Phys.* **39**, 242 (1963).

H. R. Child, M. K. Wilkinson, J. W. Cable, W. C. Koehler, and E. O. Wollan
"Neutron Diffraction Investigation of the Magnetic Properties of Compounds of Rare-Earth Metals with Group V Anions," *Phys. Rev.* **131**, 922 (1963).

J. H. Crawford, Jr.
"Model for Radiation Equilibrium Between *F*- and *M*-Centers in KCl," *Phys. Rev. Letters* **12**, 28 (1964).

H.-D. Dietze
"Theory of Coercive Force for Randomly Distributed Lattice Defects and Precipitations," *Physik Kondensierten Materie* **2**, 117 (1964).

G. P. Felcher, J. W. Cable, and M. K. Wilkinson
"Magnetic Moment Distribution in Cu_2MnAl," *J. Phys. Chem. Solids* **24**, 1663 (1963).

R. Gwin and R. B. Murray
"Scintillation Process in CsI(Tl). I. Comparison with Activator Saturation Model," *Phys. Rev.* **131**, 501 (1963).

"Scintillation Process in CsI(Tl). II. Emission Spectra and the Possible Role of Self-Trapped Holes," *Phys. Rev.* **131**, 508 (1963).

C. Lehmann and G. Leibfried
"Long Range Channeling Effects in Irradiated Crystals," *J. Appl. Phys.* **34**, 2831 (1963).

C. Lehmann and M. T. Robinson
"Truncated Matching Potentials in the Classical Theory of Elastic Atomic Scattering," *Phys. Rev.* **134**, A37 (1964).

A. Meyer and R. F. Wood
"Electronic Structure of the *M* Center in LiCl and LiF," *Phys. Rev.* **133**, A1436 (1964).

M. T. Robinson and O. S. Oen
"Computer Studies of the Slowing Down of Energetic Atoms in Crystals," *Phys. Rev.* **132**, 2385 (1963).

W. A. Sibley
"Light Scattering in Alkali Halide Single Crystals," *Phys. Rev.* **132**, 2065 (1963).

"Effect of Plastic Deformation on the Production of *F* Centers, *M* Centers, and *V* Centers in KCl," *Phys. Rev.* **133**, A1176 (1964).

W. A. Sibley and E. Sonder
"Hardening of KCl by Electron and Gamma Irradiation," *J. Appl. Phys.* **34**, 2366 (1963).

H. G. Smith
"Molecular Motion in the Silver Perchlorate–Benzene Complex," *J. Chem. Phys.* **40**, 2412 (1964).

H. G. Smith and D. L. Holcomb
"Modified Polaroid Film Holder for X-Ray and Neutron Diffraction," *Rev. Sci. Instr.* **34**, 1441 (1963).

M. J. Smith
"Co^{60} γ-Radiation-Induced Point Defects in Bi_2Te_3," *J. Appl. Phys.* **34**, 2879 (1963).

E. Sonder and L. C. Templeton
"Gamma Irradiation of Silicon. II. Levels in *n*-Type Float-Zone Material," *J. Appl. Phys.* **34**, 3295 (1963).

D. Walton
"Comment on 'Formation Conditions of Thin Epitaxial Germanium Films on Single Crystal Substrates' by Billy W. Sloope and Calvin O. Tiller," *J. Appl. Phys.* **34**, 1827 (1963).

D. Walton, T. N. Rhodin, and R. W. Rollins
"Nucleation of Silver on Sodium Chloride," *J. Chem. Phys.* **38**, 2698 (1963).

M. C. Wittels
"Stored Energy in Reactor Materials," *Nucl. Safety* **4**(4), 40 (1963).

M. C. Wittels, F. A. Sherrill, and J. O. Stiegler
"Single Crystals Grown from Small Droplets," *Z. Krist.* **119**, 42 (1963).

M. C. Wittels, F. A. Sherrill, and F. W. Young, Jr.
"X-Ray Line Widths of Nearly Perfect Copper Crystals," *Phys. Letters* **5**, 183 (1963).

M. C. Wittels, J. O. Stiegler, and F. A. Sherrill
"Comments on the Letter by Adam and Cox," *J. Nucl. Energy: Pt. A and B* **17**, 436 (1963).

"An Investigation of Transmutation Effects in Crystalline Solids," *Phys. Status Solidi* **4**, 533 (1964).

R. F. Wood
"Excited States of the *F*-Center Electron," *Phys. Rev. Letters* **11**, 202 (1963).

BOOKS AND PROCEEDINGS

R. G. Berggren
"Radiation Effects on Metal Materials," p. 41 in *Advanced Technology Symposium*, SC-4920(M) (1963).

T. H. Blewitt, R. R. Coltman, and C. E. Klabunde
"Volume Changes Induced by Radiation in Copper and Aluminum," *J. Phys. Soc. Japan* **18** (suppl. III), 283 (1963).

"Energy Release in Irradiated Copper," *J. Phys. Soc. Japan* **18** (suppl. III), 288 (1963).

T. F. Connolly
"Author Participation in Indexing – From Primary Publication to Information Center," p. 35 in *Proceedings 26th Annual Meeting American Documentation Institute*, ed. by H. R. Luhn, American Documentation Institute, Washington, D.C., 1963.

J. H. Crawford, Jr.
"Radiation Effects in Diamond Lattice Semiconductors," *IEEE Trans. Nucl. Sci.* **NS-10**, 1 (1963).

"Investigations of Color Centers in Alkali Halides at Oak Ridge National Laboratory: Structure Sensitivity of Color Center Production in γ-Irradiated KCl," *J. Phys. Soc. Japan* **18** (suppl. III), 329 (1963).

N. E. Hinkle
"Effect of Neutron Bombardment on Stress Rupture Properties of Some Structural Alloys," p. 344 in *Radiation Effects on Metals and Neutron Dosimetry*, ASTM-STP-341, American Society for Testing and Materials, Philadelphia, 1962.

A. I. Schindler and R. H. Kernohan
"The Interaction Between Irradiation-Induced Defects and Magnetic Structure," *J. Phys. Soc. Japan* **18** (suppl. III), 314 (1963).

D. O. Thompson
"Evidence for Vacancy Clustering in Dislocations in Copper as Measured by Internal Friction Techniques," *J. Phys. Soc. Japan* **18** (suppl. I), 104 (1963).

M. S. Wechsler
"Fundamental Aspects of Radiation Effects on Diffusion-Controlled Reactions in Alloys," p. 86 in *Radiation Effects on Metals and Neutron Dosimetry*, ASTM-STP-341, American Society for Testing and Materials, Philadelphia, 1962.

M. S. Wechsler, J. M. Williams, and H. M. Otte
"Atomic Rearrangements in Deformed Cu-Si and Cu-Si-Mn Alloys," *J. Phys. Soc. Japan* **18** (suppl. II), 123 (1963).

R. A. Weeks and E. Sonder
"The Relation Between the Magnetic Susceptibility, Electron Spin Resonance, and the Optical Absorption of the E_1' Center in Fused Silica," p. 869 in *Paramagnetic Resonance*, vol. II, ed. by W. Low, Academic, New York, 1963.

F. W. Young, Jr.
"Etch Pit Studies of Dislocations in Copper Crystals Deformed by Bending: I. Annealed Crystals; II. Irradiated Crystals," *J. Phys. Soc. Japan* **18** (suppl. I), 1 (1963).

F. W. Young, Jr., and L. D. Hulett
"Role of Crystal Imperfections in the Chemical Reactivity of Copper Surfaces," p. 375, chap. 12, in *Metal Surfaces*, American Society for Metals, Novelty, Ohio, 1963.

THESES

T. Purcell
"Paramagnetic Centers in Germanium Dioxide Glass Produced by Electron and Gamma-Ray Irradiations," thesis, submitted to the Graduate Council of Vanderbilt University in partial fulfillment of the requirements for the M.S. degree, 1964.

PAPERS PRESENTED AT TECHNICAL MEETINGS

J. H. Barrett

"Theory of Radiation-Enhanced Diffusion," presented at American Physical Society March Meeting, Philadelphia, Mar. 23–26, 1964.

R. G. Berggren

"Some Features of Irradiation Capsules Used by Oak Ridge National Laboratory, Solid State Division," presented at AEC Symposium on Problems in Irradiated Capsule Experiments, Germantown, Md., Oct. 8–9, 1963.

C. T. Butler, E. Sonder, and W. A. Sibley

"Variation of Some Electronic Behavior of KCl Crystals from Different Sources of Supply," presented at American Physical Society Southeastern Meeting, Lexington, Ky., Nov. 7–9, 1963.

J. G. Castle, Jr., D. W. Feldman, and R. A. Weeks

"Spin-Lattice Relaxation of Defect Centers in GeO_2 Glass," presented at American Physical Society March Meeting, Philadelphia, Mar. 23–26, 1964.

J. W. Cleland, R. F. Bass, and J. H. Crawford, Jr.

"Fission-Neutron Lattice Defect Introduction Rates in Semiconducting Materials," presented at American Physical Society Southeastern Meeting, Lexington, Ky., Nov. 7–9, 1963.

"Photon- and Neutron-Induced Lattice Defect Introduction Rates in *n*-Type Silicon," presented at American Physical Society Annual Meeting, New York, Jan. 22–25, 1964.

J. H. Crawford, Jr.

"Radiation Effects in Defect Structures in Diamond Structure Semiconductors," presented at Summer School on Solid State Physics, Mol, Belgium, Aug. 12–30, 1963.

"Information for Materials Research," presented at Electrochemical Society Fall Meeting, 124th, New York, Sept. 29–Oct. 3, 1963.

O. L. Curtis, Jr.

"Annealing of Recombination Centers in Arsenic-Doped Germanium near Room Temperature," presented at American Physical Society March Meeting, Philadelphia, Mar. 23–26, 1964.

D. K. Holmes

"Radiation Damage in Non-Fissionable Metals," presented at Summer School on Solid State Physics, Mol, Belgium, Aug. 12–30, 1963.

"Range Calculations and Channeling," presented at Summer School on Solid State Physics, Mol, Belgium, Aug. 12–30, 1963.

"Radiation Damage in Solids," presented at Summer Meeting of Physicists, Hercegnovi, Yugoslavia, Sept. 1–15, 1963.

L. D. Hulett, Jr., and F. W. Young, Jr.

"A Test of the Kinematic Theory of Crystal Dissolution," presented at American Physical Society March Meeting, Philadelphia, Mar. 23–26, 1964.

L. H. Jenkins and U. Bertocci

"On the Structure and Electrochemical Properties of Copper Single Crystals," presented at Electrochemical Society Western Regional Conference, Trail, British Columbia, Sept. 12–14, 1963.

"On the Surface Structure of Single Crystalline Copper Electrodes," presented at Electrochemical Society Fall Meeting, 124th, New York, Sept. 29–Oct. 3, 1963.

H. W. Joy and R. F. Wood

"The Absorption and Emission Spectra of the *F* Center," presented at American Physical Society March Meeting, Philadelphia, Mar. 23–26, 1964.

W. C. Mallard, E. Sonder, and J. H. Crawford, Jr.
"Self-Trapped Hole-Production Rates in KCl:Pb and KCl:Tl," presented at American Physical Society Southeastern Meeting, Lexington, Ky., Nov. 7–9, 1963.

T. S. Noggle
"Fission Tracks in Single Crystals of UO_2," presented at Electron Microscope Society of America Meeting, Denver, Colo., Aug. 28–31, 1963.

"Electron Microscope Studies of Fission Fragment Damage in Molybdenum Trioxide," presented at American Physical Society Southeastern Meeting, Lexington, Ky., Nov. 7–9, 1963.

"Fission Fragment Damage in Molybdenum Trioxide," presented at American Physical Society March Meeting, Philadelphia, Mar. 23–26, 1964.

S. M. Ohr and D. N. Beshers
"Dislocations and Dislocation Loops in Deformed Iron," presented at American Physical Society March Meeting, Philadelphia, Mar. 23–26, 1964.

T. Purcell and R. A. Weeks
"Electron Spin Resonance of Defects in GeO_2 Glass," presented at American Physical Society March Meeting, Philadelphia, Mar. 23–26, 1964.

F. A. Sherrill and F. W. Young, Jr.
"Anomalous Transmission of X-Rays in Copper Crystals," presented at American Physical Society March Meeting, Philadelphia, Mar. 23–26, 1964.

W. A. Sibley, E. Sonder, and C. T. Butler
"The Effect of Pb as Impurity on the Late-Stage *F*-Center Coloration of Room-Temperature-Irradiated KCl Crystals," presented at American Physical Society March Meeting, Philadelphia, Mar. 23–26, 1964.

H. G. Smith and G. E. Bacon
"Neutron Study of the Phase Transitions in K_2ReCl_6," presented at the International Union of Crystallography Congress and Symposia, Rome, Italy, Sept. 9–18, 1963.

H. G. Smith and D. L. Holcomb
"A Modified Polaroid Film Holder for X-Ray and Neutron Diffraction Photographs," presented at the International Union of Crystallography Congress and Symposia, Rome, Italy, Sept. 9–18, 1963.

H. G. Smith and S. W. Peterson
"Anomalous Neutron Scattering of Slow Neutrons in Crystals," presented at the Conference on Neutron Scattering, Grenoble, France, September 1963.

M. J. Smith
"Determination of the Non-Stoichiometric Doping Mechanism of Bi_2Se_3," presented at American Physical Society Southeastern Meeting, Lexington, Ky., Nov. 7–9, 1963.

A. L. Southern
"Sputtering of Al and Au Monocrystals by Positive Argon Ions with Energies of 1 to 5 kev," presented at American Physical Society Spring Meeting, Washington, D.C., Apr. 27–30, 1964.

"The Assembly and Use of an Ionized Argon Beam System for Determining the Sputtering Yield of Gold," presented at Institute of Electrical and Electronic Engineers Region 3 Annual Meeting, Clearwater, Fla., May 4–6, 1964.

J. T. Stanley
"In-Reactor Measurements of the Precipitation of Nitrides in Alpha-Iron," presented at American Institute of Mechanical Engineers Annual Meeting, New York, Feb. 17–20, 1964.

"Precipitation of Nitrides in Irradiated α-Iron," presented at American Physical Society March Meeting, Philadelphia, Mar. 23–26, 1964.

D. O. Thompson and M. A. Breazeale

"Ultrasonic Waves of Finite Amplitude in Solids," presented at Acoustical Society of America Meeting, Ann Arbor, Mich., Nov. 6–9, 1963.

D. O. Thompson and V. K. Paré

"Dose Dependence of the Dislocation Breakaway Stress in Neutron Irradiated Copper as Measured by Amplitude Dependent Internal Friction," presented at American Institute of Mechanical Engineers Annual Meeting, New York, Feb. 17–20, 1964.

"Dose Dependence of the Dislocation Breakaway Stress in Neutron Irradiated Copper as Measured by Amplitude Dependent Internal Friction," presented at American Physical Society March Meeting, Philadelphia, Mar. 23–26, 1964.

D. Walton

"Phonon Scattering from *F*-Centers," presented at American Physical Society Southeastern Meeting, Lexington, Ky., Nov. 7–9, 1963.

"Phonon Scattering by the *F*-Center Electron," presented at American Physical Society March Meeting, Philadelphia, Mar. 23–26, 1964.

M. S. Wechsler

"The Radiation-Embrittlement of Metals and Alloys," presented at Summer School on Solid State Physics, Mol, Belgium, Aug. 12–30, 1963.

"Radiation-Enhanced Ordering in Cu-Al Alloys," presented at American Institute of Mechanical Engineers Annual Meeting, New York, Feb. 17–20, 1964.

R. A. Weeks

"Effects of Irradiation on Polarization Currents in Glass," presented at Dielectrics in Space Symposium, Pittsburgh, Pa., June 25, 1963.

"Defect Structures in Quartz and Silica," presented at 1963 Gordon Research Conference, Tilton, N.H., Aug. 26–30, 1963.

R. A. Weeks and M. Abraham

"Free Hydrogen in Synthetic Quartz Crystals," presented at American Physical Society March Meeting, Philadelphia, Mar. 23–26, 1964.

J. M. Williams, W. Schüle, and M. S. Wechsler

"Annealing of Copper-Nickel Alloys Following Irradiation and Deformation," presented at American Physical Society March Meeting, Philadelphia, Mar. 23–26, 1964.

M. C. Wittels, F. A. Sherrill, and A. C. Kimbrough

"A Vertically Rotating Double Crystal X-Ray Spectrometer," presented at 12th Annual Conference on Applications of X-Ray Analysis, Denver, Colo., Aug. 7–9, 1963.

R. F. Wood

"The Excited States of the *F* Center," presented at American Physical Society March Meeting, Philadelphia, Mar. 23–26, 1964.

F. W. Young, Jr.

"On the Relation of Impurities to the Chemical and Physical Properties of Copper Crystals," presented at Electrochemical Society Fall Meeting, 124th, New York, Sept. 29–Oct. 3, 1963.

"Growth of Copper Crystals of Low Dislocation Density," presented at American Institute of Mechanical Engineers Symposium on Crystal Growth, Cleveland, Oct. 21–25, 1963.

"X-Ray Observations of Dislocations in Nearly Perfect Copper Crystals," presented at American Physical Society Southeastern Meeting, Lexington, Ky., Nov. 7–9, 1963.

F. W. Young, Jr., and F. A. Sherrill

"Microstrain in Low Dislocation Density Copper Crystals as Investigated with Borrmann X-Ray Transmission, presented at American Institute of Mechanical Engineers Annual Meeting, Feb. 17–20, 1964, New York.

"Dislocations in Copper as Observed with Anomalous X-Ray Transmission," presented at American Physical Society March Meeting, Philadelphia, Mar. 23–26, 1964.

REPORTS ISSUED

T. Purcell

Paramagnetic Centers in Germanium Dioxide Glass Produced by Electron and Gamma-Ray Irradiation, ORNL-3635 (May 1, 1964).

M. T. Robinson

Tables of Classical Scattering Integrals for the Bohr, Born-Mayer, and Thomas-Fermi Potentials, ORNL-3493 (July 15, 1963).

Research Materials Information Center Bulletin

ORNL-RMIC-1 (June 1963).

Seminars

SOLID STATE SEMINARS AT ORNL

The following seminars were held during the period covered by this report. R. B. Murray is currently serving as Seminar Chairman.

1963	
June 13	R. H. Silsbee, Cornell University, Ithaca, N.Y. "Mössbauer-Light Transitions of Color Centers"
July 8	M. Abraham, Lawrence Radiation Laboratory, Berkeley, Calif. "Dynamic Nuclear Orientation by Electron Resonance"
July 11	D. Feldman, Westinghouse Research Laboratory, Pittsburgh, Pa. "Spin Lattice Relaxation of *F*-Centers in KCl"
July 12	F. Lüty, University of Illinois, Urbana, "The Kinetics of *F*-Center Aggregation"
July 15	W. D. Robertson, Yale University, New Haven, Conn. "The Effect of Elastic Anisotropy on the Growth of Cleavage Cracks"
August 1	R. O. Pohl, Cornell University, Ithaca, N.Y. "Phonon Scattering by Lattice Defects"

August 6	A. Halperin, Hebrew University, Jerusalem, Israel "Effects of Thermal Pretreatment on the Coloration Properties of Alkali Halides"
August 20	Alfred Seeger, Max Planck Institut für Metallforschung, Stuttgart, Germany "Work Hardening in Face-Centered Cubic Metals"
August 22	R. Douglas, University of Sheffield, England "Some Problems in Oxidation-Reduction Equilibria in Inorganic Glasses"
August 23	George Wilkinson, University of London, England "Solid State Spectroscopy – Intrinsic and Impurity"
September 16	A. Leadbetter, University of Bristol, England "Point Defects and Anharmonicity in Lead"
September 30	R. Sizmann, Technische Hochschule, Munich, Germany "The Radiation Damage Program at Munich"
October 4	C. G. Kuper, University of St. Andrews, Great Britain "Superconductivity of Lanthanum and Uranium"
October 9	M. W. Thompson, Atomic Energy Research Establishment, Harwell, England "Ion Bombardment of Metals"
October 11[a]	B. N. Cooper, Harvard University, Cambridge, Mass. "The Study of Spin Waves in Spiral Spin Structures by Magnetic Resonance"
October 17	A. D. B. Woods, Chalk River, Canada "Recent Inelastic Neutron Scattering Experiments at Chalk River"
October 28	Heinz Maier-Leibnitz, Technische Hochschule, Munich, Germany "Low Temperature Investigations of Radiation Damage Using the Munich Research Reactor"
November 5	Walter Marshall, Atomic Energy Research Establishment, Harwell, England "Evidence on Covalency Effects from Neutron Diffraction"
November 14	A. Gilbert, Battelle Memorial Institute, Columbus, Ohio "Dislocation Mobility and Fracture"
November 18[a]	Rene Pauthenet, Laboratoire D'Electrostatique et de Physique du Metal, Grenoble, France "Ferromagnetism in Ordered Fe-Ni Alloys"
November 22[a]	R. D. Lowde, Atomic Energy Research Establishment, Harwell, England "Some Current Work on Magnetism at Harwell"
November 29	Alan Crocker, RIAS, Inc., Baltimore, Md. "Dislocation Loops in Anisotropic Materials"
December 6	C. Kikuchi, University of Michigan, Ann Arbor "Vanadium Solid-State Chemistry"
December 17	B. W. Batterman, Bell Telephone Laboratories, Murray Hill, N.J. "Dynamical Diffraction and Fluorescence Scattering"
December 31[b]	William Hayes, Oxford University, England "Localized Vibrations of Light Impurities in Calcium Fluoride"

[a]Joint Physics and Solid State Divisions seminar.

[b]Joint Chemistry and Solid State Divisions seminar.

1964

January 7	D. O. Welch, University of Pennsylvania, Philadelphia "The Activation Energy of Motion for Point Defects in Elastic Fields"
January 16	Phillip Bray, Brown University, Providence, R.I. "Nuclear Resonance Studies of the Structure of Glasses"
January 23	Roland Schuttler, C.E.N., Fontenay-aux-Roses, France "Radiation Damage in Silicon by Fast Neutrons: Studies with PIN Junctions"
January 30	R. D. Birkhoff, Health Physics Division, ORNL "Studies of Solid State Plasma by Electron Beam and Optical Methods"
February 6	S. M. Ohr, Solid State Division, ORNL "Crystallography of Dislocations and Dislocation Loops in Deformed Iron"
February 10[c]	Raymond Pepinsky, Florida Atlantic University, Boca Raton, Florida "Crystallographic Data Information Center"
February 13	A. J. Sievers, Cornell University, Ithaca, N.Y. "Thermal Conductivity near Low Temperature Phase Transitions"
February 17	V. H. Ritz, Naval Research Laboratory, Washington, D.C. "*F*-Center Production Mechanisms at Low Temperature"
February 24	Geoffrey Dearnaley, Atomic Energy Research Establishment, Harwell, England "Channeling and Radiation Damage in Silicon"
March 2	John B. Birks, University of Manchester, England "The Scintillation Process in Organic and Inorganic Materials"
March 5	J. L. Beeby, University of Illinois, Urbana "Electronic Structure of the Transition Metal Alloys"
March 12	Joseph Ford, Georgia Institute of Technology, Atlanta "Irreversibility in Nonlinear Oscillator Systems"
April 9	L. D. Roberts, Physics Division, ORNL "A Correlation of the Residual Electrical Resistance with the Mössbauer Isomer Shift for Gold Alloys"
April 16	Bo Domeij, Nobel Institute of Physics, Stockholm, Sweden "Experimental Studies of the Ranges of kev Ions in Solids"
April 23	J. S. Faulkner, Metals and Ceramics Division, ORNL "Electronic States of Random Systems"
April 30	R. M. Nicklow, Solid State Division, ORNL "Lattice Vibrations and the Temperature Dependence of X-Ray Bragg Intensities"
May 7	R. H. Ritchie, Health Physics Division, ORNL "Volume and Surface Plasmons in Metals"
May 14	W. A. Arnold, Biology Division, ORNL "Photosynthesis and Delayed Light"
May 21	R. A. Weeks, Solid State Division, ORNL "Paramagnetism of Diamagnetic Insulating Solids"
May 28	M. E. Caspari, University of Pennsylvania, Philadelphia "Temporary Bleaching Effects in Additively Colored Alkali Halides"

[c]Joint Metals and Ceramics and Solid State Divisions seminar.

EDUCATIONAL LECTURES AND SEMINARS

A number of seminars and lectures were presented during the year by members of the Solid State Division, both in this country and abroad:

J. W. Cleland	National Bureau of Standards, Washington, D.C., June 17, 1963 Research Materials Coordination and Planning Meeting, Division of Isotopes and Development (AEC), Oak Ridge, Nov. 14, 1963 "Pure Materials Program" Southeastern Section, Society for Applied Spectroscopy, Oak Ridge, Sept. 7, 1963 "Pure Materials, Information, and Analysis" University of Michigan, Ann Arbor, Sept. 27, 1963 Rensselaer Polytechnic Institute, Troy, N.Y., Mar. 27, 1964 "Radiation Effects in Semiconducting Materials" Topical Conference on Semi-Metals, American Physical Society, Columbia University, New York, Jan. 21, 1964 "Research Materials Information Center"
C. Lehmann	Atomic Energy of Canada Limited, Chalk River, Ontario, Sept. 25, 1963 "Analytical Calculations of Channeling of Atoms in Crystals"
G. Leibfried	Atomic Energy of Canada Limited, Chalk River, Ontario, Sept. 25, 1963 "Channeling Effects in Crystals"
O. S. Oen	Atomic Energy of Canada Limited, Chalk River, Ontario, Sept. 25, 1963 "Monte Carlo Range Calculations in Solids for kev Atoms"
M. T. Robinson	Atomic Energy of Canada Limited, Chalk River, Ontario, Sept. 25, 1963 Sandia Corporation, Albuquerque, N.M., Jan. 22, 1964 "Computer Calculations of the Slowing Down of Atoms in Crystals"
H. C. Schweinler	ORINS-NSF Summer Institute on Modern Physics for Physics Teachers from Small Colleges, Oak Ridge, June 20—Aug. 7, 1963 (series of 35 lectures) "Quantum Mechanics"
W. A. Sibley	North American Aviation Science Center, Canoga Park, Calif., Oct. 5, 1963 "Coloration and Hardening of KCl Crystals"
E. Sonder	Emory University, Atlanta, Ga., May 19, 1964 "The Story of the *M*-Center"
M. S. Wechsler	Army Nuclear Science Seminar, Oak Ridge, Aug. 13, 1963 "Radiation and Radiation Effects" Battelle Memorial Institute, Geneva, Switzerland, Aug. 20, 1963 Brookhaven National Laboratory, Upton, N.Y., Oct. 1, 1963 "Radiation-Enhanced Diffusion in Cu-Al Alloys"

M. S. Wechsler	C.C.R.-Euratom, Ispra, Italy, Aug. 23, 1963 "Radiation Embrittlement of Metals and Alloys" Maryland Institute of Metals, Baltimore, Md., Apr. 14, 1964 "Radiation Effects on Metals and Alloys"
R. A. Weeks	Brown University, Providence, R.I., May 14, 1964 "Intrinsic Paramagnetic States of GeO_2 Glass" University of Michigan, Ann Arbor, Feb. 2, 1964 "Intrinsic Paramagnetic Defects of Quartz and Silica"
R. F. Wood	Biology Division, ORNL, Oct. 7, 9, and 11, 1963 "Application of Elementary Quantum Mechanics to Biology"
F. W. Young, Jr.	University of Virginia, Charlottesville, Feb. 18, 1964 "Anomalous Transmission of X-Rays Through Nearly Perfect Copper Crystals" National Bureau of Standards, Washington, D.C., May 13, 1964 "Observation of Dislocations in Copper Using Anomalous X-Ray Transmission"

Six members of the Division presented lectures under the auspices of the University Traveling Lecture Program sponsored by ORINS:

R. R. Coltman	Clemson College, Clemson, S.C., Mar. 20, 1964 "Radiation Effects in Metals"
R. B. Murray	University of Georgia, Athens, Jan. 30, 1964 "Mechanism of Scintillation Process in Alkali Halide Crystals"
V. K. Paré	Virginia Polytechnic Institute, Blacksburg, Jan. 14, 1964 Rice University, Houston, Tex., Mar. 13, 1964 "Studies of Point Defects in Metals Through Their Interaction with Dislocations, as Measured by Internal Friction and Modulus Changes"
D. Walton	University of Georgia, Athens, Mar. 5, 1964 "Low Temperature Lattice Thermal Conductivity"
M. K. Wilkinson	Rice University, Houston, Tex., Dec. 4, 1963 "Magnetic Properties of Rare-Earth Metals and Intermetallic Compounds" Texas Christian University, Fort Worth, Dec. 5, 1963 Texas A and M University, College Station, May 5, 1964 "The Role of Neutron Diffraction in Solid State Physics" Tulane University, New Orleans, La., May 4, 1964 "Techniques and Applications of Neutron Diffraction"
F. W. Young, Jr.	Wake Forest College, Winston-Salem, N.C., Dec. 5, 1963 "Studies of Dislocation Motion and Multiplication at Low Strains in Copper Crystals"

CONFERENCES

On November 18 and 19, 1963, a conference on Color Centers in Alkali Halides was held in Gatlinburg, Tennessee. This was a highly specialized topical conference devoted to the problem of the mechanism of defect production in alkali halides by ionizing radiation. The conference was organized by members of the Solid State Division, with some assistance from J. H. Shulman and C. C. Click of the Naval Research Laboratory. No formal papers were presented, but detailed discussions of recent work relating to this problem were conducted by about 30 scientists from both the United States and abroad.

ORNL-3676
UC-34 – Physics
TID-4500 (33rd ed.)

INTERNAL DISTRIBUTION

1. M. M. Abraham
2. T. O. Baldwin
3. J. H. Barrett
4. S. E. Beall
5. P. R. Bell
6. M. Bender
7. W. T. Berg
8. R. G. Berggren
9. U. Bertocci
10. J. O. Betterton, Jr.
11. D. S. Billington
12. E. P. Blizard
13. A. L. Boch
14. E. G. Bohlmann
15. C. J. Borkowski
16. G. E. Boyd
17. M. A. Breazeale (consultant)
18. M. A. Bredig
19. R. B. Briggs
20. F. R. Bruce
21. W. E. Brundage
22. C. T. Butler
23. N. Cabrera (consultant)
24. R. O. Chester
25. J. W. Cleland
26. T. F. Connolly
27. R. R. Coltman
28. W. D. Compton (consultant)
29. J. A. Cox
30. J. H. Crawford, Jr.
31. F. L. Culler
32. J. E. Cunningham
33. P. B. DeNee
34. J. L. Fowler
35. J. H. Frye, Jr.
36. J. L. Gabbard
37. H. A. Gersch (consultant)
38. G. Gilat
39. J. H. Gillette
40. J. J. Gilman
41. R. J. Gray
42. W. R. Grimes
43. N. E. Hinkle
44. A. Hollaender
45. D. K. Holmes
46. A. S. Householder
47. J. P. Howe (consultant)
48. J. T. Howe
49. L. D. Hulett
50. L. H. Jenkins
51. R. W. Johnson
52. R. J. Jones
53. W. H. Jordan
54. G. W. Keilholtz
55. C. P. Keim
56. F. J. Keller
57. M. T. Kelley
58. R. H. Kernohan
59. E. M. King
60. C. E. Klabunde
61. F. A. Kocur
62. J. S. Koehler (consultant)
63. J. A. Krumhansl (consultant)
64. E. J. Lee
65. G. Leibfried (consultant)
66. A. B. Lewis (consultant)
67. T. A. Lincoln
68. S. C. Lind
69. R. S. Livingston
70. H. G. MacPherson
71. C. J. McHargue
72. A. Meyer
73. A. J. Miller
74. E. C. Miller
75. J. W. Mitchell (consultant)
76. K. Z. Morgan
77. R. B. Murray
78. C. M. Nelson (consultant)
79. M. L. Nelson
80. R. M. Nicklow
81. T. S. Noggle
82. O. S. Oen
83. S. M. Ohr
84. V. Paré
85-86. R. B. Parker
87. J. C. Pigg
88. H. Pomerance
89. T. L. Purcell
90. M. E. Ramsey
91. T. A. Read (consultant)
92. J. K. Redman
93. C. C. Robinson

94. M. T. Robinson
95. A. F. Rupp
96. J. R. Russell
97. H. Saito
98. W. F. Schilling
99. O. E. Schow
100. H. C. Schweinler
101. H. E. Seagren
102. F. Seitz (consultant)
103. S. T. Sekula
104. F. A. Sherrill
105. E. D. Shipley
106. W. A. Sibley
107. R. H. Silsbee (consultant)
108. O. Sisman
109. M. J. Skinner
110. L. Slifkin (consultant)
111. G. P. Smith
112. H. G. Smith
113. A. H. Snell
114. E. Sonder
115. A. L. Southern
116. J. T. Stanley
117. E. E. Stansbury
118. W. J. Stelzman
119. C. D. Susano
120. J. A. Swartout
121. E. H. Taylor
122. L. C. Templeton
123. G. T. Trammell (consultant)
124. David Turnbull (consultant)
125. D. Walton
126. C. C. Webster
127. M. S. Wechsler
128. R. A. Weeks
129. A. M. Weinberg
130. E. P. Wigner (consultant)
131. M. K. Wilkinson
132. F. E. Williams (consultant)
133. G. C. Williams
134. J. M. Williams
135. W. R. Willis (consultant)
136. M. C. Wittels
137. E. O. Wollan
138. R. F. Wood
139. F. W. Young
140. Gale Young
141. W. H. Young
142. Biology Library
143-145. Central Research Library
146. Laboratory Shift Supervisor
147. Reactor Division Library
148-149. ORNL – Y-12 Technical Library Document Reference Section
150-199. Laboratory Records Department
200. Laboratory Records, ORNL R.C.

EXTERNAL DISTRIBUTION

201. W. W. Shaver, Corning Glass Works, Corning, New York
202. R. W. McNamee, Union Carbide Corporation, New York
203. Boeing Airplane Company
204. Research and Development Division, AEC, ORO
205. J. R. Johnson, Minnesota Mining and Manufacturing Co., St. Paul
206. A. E. Ruark, AEC, Washington
207. G. L. Stiehl, Convair Division of General Dynamics Corp., San Diego
208. R. O. Bolt, California Research Corp., Richmond
209. Benjamin Lax, Lincoln Laboratory, Lexington, Massachusetts
210. George H. Wagner, Linde Air Products Company, Tonawanda Laboratory, East Park Drive and Woodward Avenue, Tonawanda, New York
211. D. K. Stevens, Materials and Metallurgy Branch, Division of Research, U.S. Atomic Energy Commission, Washington, D.C.
212. R. I. Leininger, Battelle Memorial Institute, 505 King Avenue, Columbus, Ohio
213. Westinghouse Electric Corp., Research Laboratories, Pittsburgh, Pennsylvania
214. J. G. Castle, Jr., Physics Dept., Westinghouse Electric Corp., Research Laboratories, Pittsburgh, Pennsylvania
215. C. Kikuchi, University of Michigan, Willow Run Laboratory, Ann Arbor, Michigan
216. N. R. Beaudry, Office of Ordnance Research, Duke Station, Durham, North Carolina

217. J. Hitch, Office of Isotope Development, AEC, Washington, D.C.
218. P. W. McDaniel, Division of Research, USAEC, Washington, D.C.
219. H. Y. Fan, Solid State Physics Dept., Purdue University, Lafayette, Indiana
220. T. J. Turner, Department of Physics, Wake Forest College, Winston-Salem, North Carolina
221. J. B. Trice, Military Space Vehicle Department, General Electric Co., Philadelphia, Pennsylvania
222. T. H. Blewitt, Argonne National Laboratory, Chicago, Illinois
223. R. A. Charpie, Union Carbide Corporation, New York, New York
224. L. B. Emlet, Union Carbide Corporation, New York, New York
225. C. D. Yost, ARPA, Pentagon, Washington, D.C.
226. D. F. Cope, Reactor Division, Oak Ridge Operations Office
227. J. M. Simmons, Division of Reactor Development, AEC, Washington, D.C.
228. H. Shulman, Diamond Ordance Fuse Laboratory, Washington, D.C.
229. G. D. Watkins, General Electric Research Laboratories, Schenectady, New York
230. R. Street, Department of Physics, Monash University, P.O. Box 92, Clayton, Victoria, Australia
231. R. A. Young, Georgia Institute of Technology, Atalnta, Ga.
232. A. Merlini, Solid State Physics Department, C.C.R.-EURATOM, Ispra (Varese), Italy
233. S. Amelinckx, Solid State Physics Department, C.E.N., Mol-Donk, Belgium
234. A. Seeger, Max Planck Institut für Metallforschung, Seestrasse 75, Stuttgart N, Germany
235. J. Diehl, Max Planck Institut für Metallforschung, Seestrasse 75, Stuttgart N, Germany
236. P. Baruch, Laboratorie de Physique, Ecole Normale Superieure, Paris V, France
237. V. B. Bhanot, Physics Department, Panjab University, Chandigarh-3, India
238. C. Lehmann, KFA-Werkstoffinstitut, JüLich, Germany
239. W. M. Lomer, AERE, Harwell, England
240. W. Marshall, AERE, Harwell, England
241. A. B. Lidiard, AERE, Harwell, England
242. W. C. Mallard, Emory University, Atlanta, Georgia
243. H. D. Dietze, Lehrstuhl für Reaktorwerkstoffe, Technische Hochschule, Aachen, Germany
244. D. O. Thompson, North American Aviation Science Center, Thousand Oaks, Calif.
245. W. D. Manly, Union Carbide Corporation, New York
246. R. H. Gillette, European Research Associates, Brussels, Belgium
247. H. Brooks, Harvard University, Cambridge, Mass.
248. H. Huntington, Department of Physics, Rensselaer Polytechnic Institute, Troy, N.Y.
249. O. C. Simpson, Argonne National Laboratory, Argonne, Ill.
250. G. H. Vineyard, Brookhaven National Laboratory, Upton, Long Island, N.Y.
251. J. Friedel, Physique des Solides, Faculte des Sciences d'Orsay, Orsay, France
252. R. J. Schuttler, Service SEPP, CEN/FAR (Fort de Chatillon), Boite Postale 6, Fontenay-aux-Roses (Seine), France

253-897. Given distribution as shown in TID-4500 (33rd ed.) under Physics category (75 copies – CFSTI)

Reports previously issued in this series are:

ORNL-1025*	Period Ending January 31, 1951
ORNL-1095	Period Ending April 30, 1951
ORNL-1128*	Period Ending July 31, 1951
ORNL-1214*	Period Ending October 31, 1951
ORNL-1261*	Period Ending January 31, 1952
ORNL-1301*	Period Ending May 10, 1952
ORNL-1359*	Period Ending August 10, 1952
ORNL-1429*	Period Ending November 10, 1952
ORNL-1506*	Period Ending February 10, 1953
ORNL-1606	Period Ending August 31, 1953
ORNL-1677	Period Ending February 28, 1954
ORNL-1762*	Period Ending August 30, 1954
ORNL-1851*	Period Ending February 28, 1955
ORNL-1852	Period Ending February 28, 1955
ORNL-1944	Period Ending August 30, 1955
ORNL-1945	Period Ending August 30, 1955
ORNL-2051	Period Ending February 29, 1956
ORNL-2052*	Period Ending February 29, 1956
ORNL-2188	Period Ending August 30, 1956
ORNL-2189*	Period Ending August 30, 1956
ORNL-2413	Period Ending August 31, 1957
ORNL-2614	Period Ending August 31, 1958
ORNL-2829	Period Ending August 31, 1959
ORNL-3017	Period Ending August 31, 1960
ORNL-3213	Period Ending August 31, 1961
ORNL-3364	Period Ending August 31, 1962
ORNL-3480	Period Ending May 31, 1963

*Classified